



UNIVERSITÀ DEGLI STUDI DI MILANO  
DIPARTIMENTO DI CHIMICA

*Doctorate School of Chemical Sciences and Technologies  
PhD Course in Chemistry, XXVIII Cycle*

# **Asymmetric hydrogenation of industrially relevant substrates**

**Marc Renom Carrasco**

R10361

CHIM/06 Organic Chemistry

*Tutor:* Prof. Dr. Cesare Gennari

*Academic Co-Tutor:* Prof. Dr. Johannes G. de Vries (Leibniz-Institut für Katalyse, DE)

*Industrial Co-Tutor:* Dr. Laurent Lefort (DSM Innovative Synthesis BV, NL)

*Coordinator:* Prof. Dr. Emanuela Licandro

Milano, March 2016



**“Imagination is more important than knowledge.**  
For knowledge is limited, whereas imagination embraces the  
entire world, stimulating progress, giving birth to evolution.  
It is, strictly speaking, a real factor in scientific research.”

*A. Einstein*



# Table of contents

<b>Preface</b>	<b>7</b>
<b>Part A. Asymmetric Hydrogenation of Pyridines</b>	<b>11</b>
<b>Chapter I.</b> Overview on the Asymmetric Hydrogenation of <i>N</i> -Heteroarenes	13
<b>Chapter II.</b> Asymmetric Hydrogenation of 2-Substituted Pyridines	43
<b>Chapter III.</b> Asymmetric Hydrogenation of 3-Substituted Pyridines	63
<b>References</b>	93
<b>Part B. Tandem Olefin Metathesis–Asymmetric (Transfer) Hydrogenation</b>	<b>99</b>
<b>Chapter IV.</b> Overview on the Tandem Olefin Metathesis–(Transfer) Hydrogenation	101
<b>Chapter V.</b> Tandem Olefin Metathesis–Asymmetric Hydrogenation	113
<b>Chapter VI.</b> Tandem Olefin Metathesis–Asymmetric Transfer Hydrogenation	133
<b>References</b>	151
<b>Summary</b>	<b>155</b>
<b>List of publications</b>	<b>157</b>
<b>Acknowledgments</b>	<b>159</b>



# Preface

A chiral object is one that has a non-superimposable mirror image. This concept, easily exemplified with the hands, as they are mirror images but not superimposable one with the other, can be extended as well to molecules (Figure 1). In chemistry, each of the two images is known as enantiomer. This inherent property of some molecules has a dramatic effect on our existence and everyday life: DNA, proteins, amino acids, sugars, are all chiral entities. Probably the most famous example in our society is thalidomide, a drug prescribed to pregnant women during the 60's. In this unfortunate case, while one of the enantiomers had a sedative effect, the other was teratogenic, i.e. caused malformations to the fetus. Another interesting example is the different odor perceived for the two enantiomers of carvone. Since our olfactory receptors also contain chiral groups, we are able to differentiate (*R*)-carvone, with a spearmint leaves smell, from the (*S*)-carvone, which smells like caraway seeds.

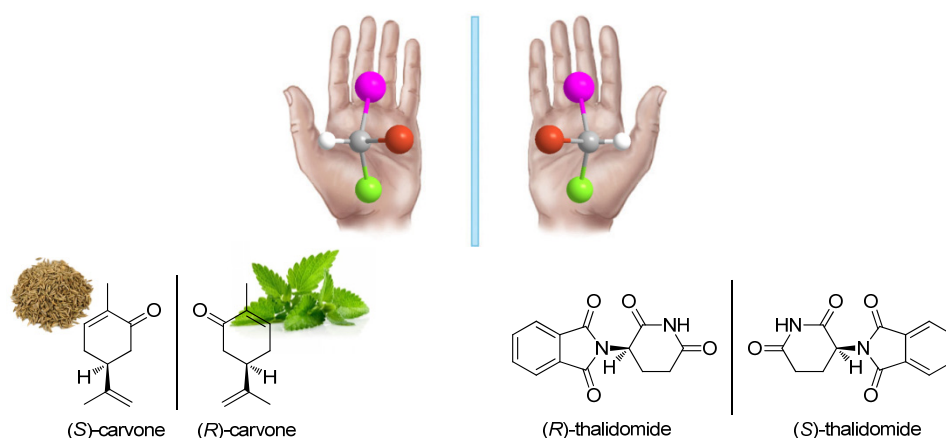
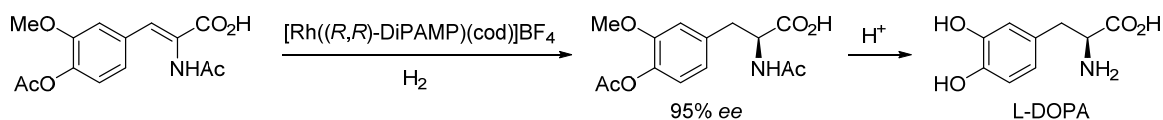


**Figure 1.** The two enantiomers of different chiral molecules.

Since Le Bel and van't Hoff, in 1874, proposed that a carbon with four different substituents in a tetrahedral disposition can exist as a pair of isomers (the so called enantiomers), scientist have been fascinated by the challenge to achieve full stereocontrol during chemical transformations starting from achiral compounds. This has led to the development of enantioselective synthesis, an important subfield in organic synthesis.

Catalysis is the increase in the rate at which a chemical reaction takes place by lowering the energy barrier between the reactants and the products. This is achieved by employing a substance, known as catalyst, which participates in the reaction but that is not consumed. In this way, ideally, a catalyst can catalyze a reaction an infinite number of times without being consumed. The field of catalysis has found many applications in our society: when we make cheese or beer, in the cars to reduce the emission of toxic chemicals or in the industry to synthesize drugs more efficiently. But catalysts are not a human invention, as enzymes are extremely highly efficient catalysts present in all organisms.

The application of catalysis to enantioselective synthesis led to the important field of asymmetric catalysis. Among all different enantioselective transformations that have been studied, catalytic asymmetric hydrogenation, consisting on the addition of molecular hydrogen to a compound in a stereoselective fashion, is by far the most industrially relevant. The first industrial application was the production of the amino acid L-DOPA (Figure 1), which had proven useful in the treatment of the Parkinson's disease.



**Scheme 1.** Industrial process for the synthesis of L-DOPA by Rh-catalyzed asymmetric hydrogenation.

Paradoxically, although this is an operationally simple 100% atom economic process, it has only been implemented in a limited number of industrial processes. Most of the hydrogenations are still performed in a non-enantioselective way and followed by a separation of the two enantiomers formed in a 50:50 ratio. This implies the disposal of half of the reacted material and elevated solvent wastes and energy consumption. There are three reasons that might explain this situation: (i) the lack of efficient methodologies for the asymmetric hydrogenation of challenging substrates, (ii) the high price of noble metals commonly used as catalysts (Rh, Ru, Ir, Pd, Pt...) and (iii) the time-to-market pressure, which does not allow sufficient time for the development of a catalytic process.

This thesis has aimed to overcome some of these limitations focusing on the development of new metal-catalyzed asymmetric hydrogenation methodologies.

In Part A (Chapters I to III), the studies on the asymmetric hydrogenation of substituted pyridines are described. These heteroaromatic compounds have proven very challenging to hydrogenate enantioselectively, however, the resulting chiral piperidines are of high industrial interest. In Chapter I, the state of the art and the mechanistic studies carried out on related *N*-heteroaromatic substrates are extensively discussed. In Chapter II, a new method for the asymmetric hydrogenation of 2-substitued pyridines is reported, together with complementary mechanistic studies that shed light on the origin of the enantioselectivity. In Chapter III, a method for the highly enantioselective hydrogenation of 3-substitued pyridines is disclosed.



Furthermore, a deep mechanistic study reveals how this high level of stereocontrol can be achieved on substrates where no good results had been reported until now.

Part B (Chapter IV to VI) is centered on the problems associated with the high prices of noble metals. Two different solutions have been envisioned in the scientific community to overcome this problem. The first one relies on the replacement of the more commonly used expensive metals for cheap and abundant 1<sup>st</sup> row transition metals, such as Fe, Co, Ni or Cu. The second approach consists in recycling or reusing the noble metals for more than one reaction. In this regard, tandem catalysis is a commonly applied methodology, where the same metal is used to catalyze at least two different reactions in one pot. In our case, we focused on developing an asymmetric version of the tandem olefin metathesis–hydrogenation. Chapter IV contains an introduction on the topic. In Chapter V and VI, the conversion of different Ru-olefin metathesis catalysts to efficient asymmetric hydrogenation and asymmetric transfer hydrogenation catalysts is described, respectively. These transformations have been subsequently applied to the tandem metathesis-asymmetric hydrogenation and to the metathesis-asymmetric transfer hydrogenation.

---

The work reported in this thesis has been carried out between DSM Innovative Synthesis (NL), for 18 months, and the University of Milan (IT), for 18 months more, within the “Marie Skłodowska Curie” EID-ITN Network “REDUCTO”, involving the mentioned industrial and academic partners. During the months spent at the University of Milan I have also been involved in a project aiming at the development of new chiral (cyclopentadienyl)iron complexes active in asymmetric hydrogenation of different prochiral substrates.







Part A.

# Asymmetric Hydrogenation of Pyridines

**Abstract:**

A general overview on the state of the art in the asymmetric hydrogenation of pyridines is discussed in Chapter I. This is accompanied by a review on the asymmetric hydrogenation of *N*-heteroarenes, which will set the basis for understanding the following investigations. In Chapter II and III, the results of the study towards the development of new systems for the asymmetric hydrogenation of 2- and 3-substituted pyridines are presented, respectively. Mechanistic studies on both systems allow for a deeper comprehension of the subject.



# CHAPTER I.

## OVERVIEW ON THE ASYMMETRIC HYDROGENATION OF *N*-HETEROARENES

---

Nitrogen-containing molecules are very common in nature and, besides, every single one of the 25 best-selling drugs in 2014 contains at least one nitrogen atom. Although many of these biologically active molecules are chiral and contain nitrogen heterocyclic moieties, the asymmetric hydrogenation (AH) of *N*-heteroaromatic compounds has been very little explored compared to other prochiral substrates, such as imines or enamides. There are few reasons that make *N*-heteroarenes a real challenge: (i) their high aromatic resonance stability requires elevated temperatures and pressures in hydrogenation, which adversely affects the enantioselectivity. (ii) The nitrogen atom has a strong tendency to coordinate and thus poison the metal catalyst. (iii) The lack of secondary coordinating groups which could interact with the metal center makes more difficult to achieve good enantioselectivities.

Among all *N*-heteroaromatic compounds, the hydrogenation of pyridines is of special interest for the industry, since enantiomerically pure piperidines are ubiquitous structural motifs in many biologically active compounds (Figure 1).

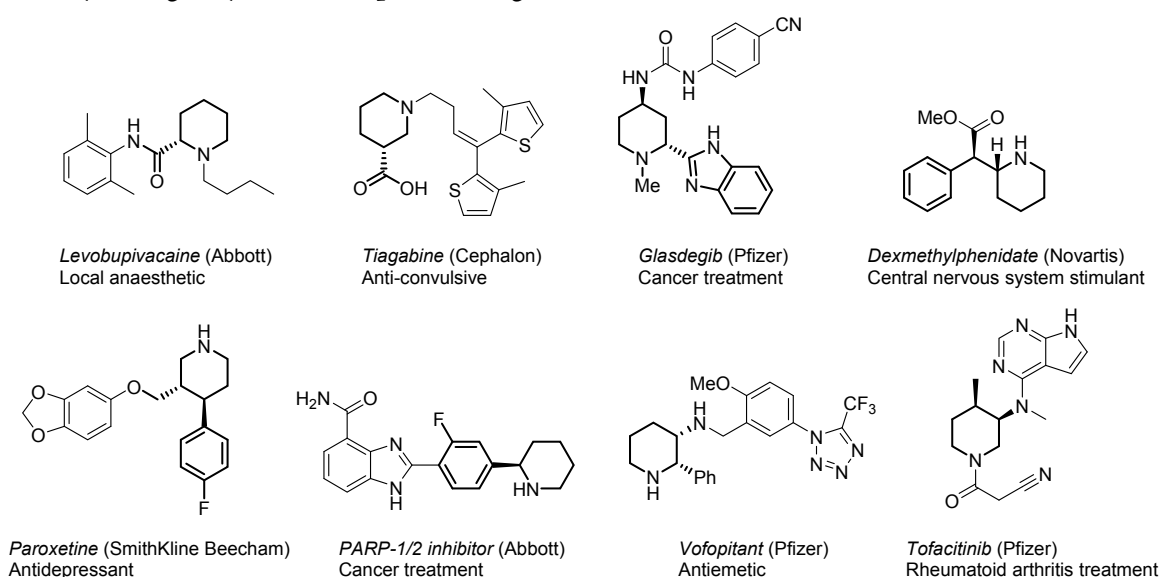


**Figure 1.** Selected chiral piperidine-containing drugs.

However, pyridines are also one of the most challenging substrates: they possess high aromatic stabilization energies (close to that of benzene)<sup>1</sup> and, in contrast to benzene-fused heteroarenes, they require the hydrogenation of three double bonds to afford the saturated piperidine products. This difficulty to enantioselectively hydrogenate pyridines can be easily deduced from the number of reports published regarding the enantioselective hydrogenation of pyridines (Figure 2). While the number of publications of enantioselective hydrogenation of *N*-heteroarenes has increased constantly during the last ten years, the number of reports about pyridines has remained constant.

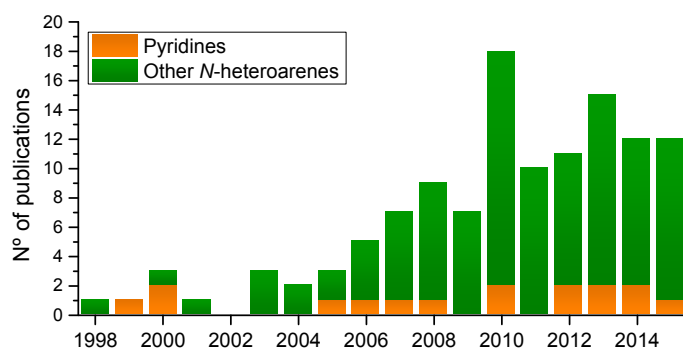
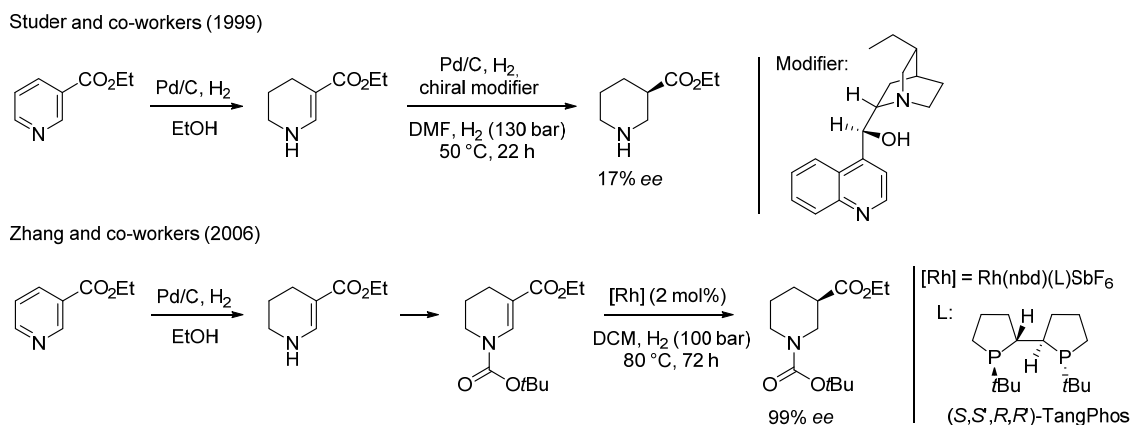


**Figure 2.** Number of publications regarding the enantioselective hydrogenation of pyridines and other *N*-heteroarenes. Source: SciFinder.

## I.1 ASYMMETRIC HYDROGENATION OF PYRIDINES – STATE OF THE ART

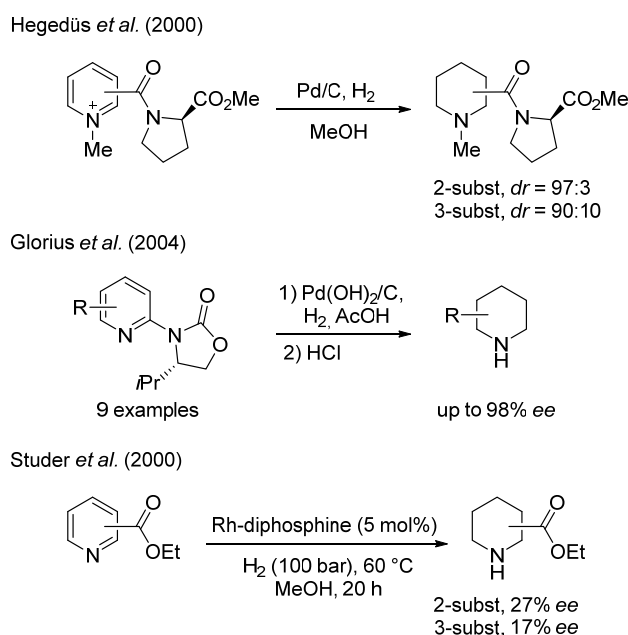
The first approach for the synthesis of chiral piperidines from pyridines was a two-step hydrogenation disclosed by Studer and co-workers in 1999 (Scheme 1). An initial partial hydrogenation of ethyl nicotinate with Pd/C furnished the corresponding 1,4,5,6-tetrahydropyridine. In the second step, employing Pd/C and 10,11-dihydrocinchonidine as chiral modifier under harsh hydrogenation conditions, they obtained ethyl nipecotinate with 17% *ee*.<sup>2</sup> In 2006, Zhang and co-workers proposed a modified version of this approach, using a chiral homogeneous catalyst for the second hydrogenation step (Scheme 1). Although the tetrahydropyridine had to be first protected as a carbamate, the final nipecotinate derivative was obtained with 99% *ee*.<sup>3</sup>



**Scheme 1.** Two-step methodologies for the hydrogenation of ethyl nicotinate.

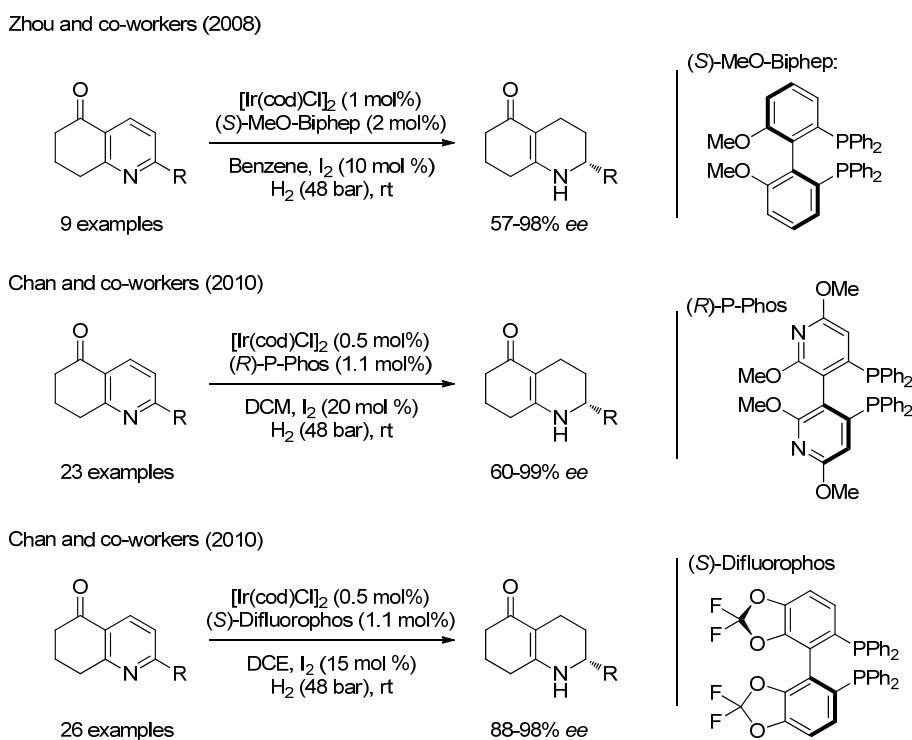
It was not until 2000 when the first examples of one-step asymmetric hydrogenation (AH) of pyridines were published. Johnson and co-workers achieved full hydrogenation of ethyl nicotinate with 17% *ee* using a Pd-diphenylphosphino-ferrocene catalyst anchored to mesoporous silica.<sup>4</sup> Hegedűs *et al.*, by means of a heterogeneous catalyst, were able to hydrogenate nicotinic and picolinic acids derivatized with (*S*)-proline, achieving diastereomeric ratios up to 97:3 (Scheme 2).<sup>5</sup> Some years later, three more diastereoselective procedures were published using a heterogeneous catalyst and a chiral auxiliary attached to the substrate. Two of them consisted in the hydrogenation of 2-methylnicotinic acid derivatives,<sup>6</sup> and the third one involved the hydrogenation of 2-oxazolidinonepyridines. In the latter example, reported by Glorius *et al.*, *ee*'s up to 98% were obtained (Scheme 2) and the chiral auxiliary could be removed by simple acidic work-up.<sup>7</sup>

More importantly, in a pioneering work by Studer *et al.*, the homogeneous AH of unprotected ethyl nicotinate and picolinate was reported to occur with *ee*'s up to 17% and 27%, respectively, using a Rh-diphosphine complex (Scheme 2).<sup>8</sup>



**Scheme 2.** Reports on the asymmetric homogeneous and heterogeneous hydrogenation of pyridines.

In 2008, Zhou and co-workers also reported the asymmetric partial hydrogenation of the pyridine derivative 7,8-dihydro-quinolin-5(6*H*)-one (Scheme 3). The most interesting feature of this system is that no activation of the pyridine was required. Using an iridium catalyst with (*S*)-MeO-Biphep as ligand, they were able to partially hydrogenate the mentioned pyridine derivatives substituted in the 2-position with *ee*'s up to 97%.<sup>9</sup> Two years later, Chan and co-workers published two more papers using exactly the same system, with the only variation of the ligand and the solvent. Comparable *ee*'s and a TON up to 960 in the case of (*S*)-Difluorophos were obtained.<sup>10</sup> Unfortunately, this methodology is restricted to this particular kind of substrates and no examples with other pyridine substrates were reported.



**Scheme 3.** Asymmetric partial hydrogenation of 7,8-dihydro-quinolin-5(6*H*)-one derivatives.

Apart from these latter examples, in the last years, almost all newly developed methodologies have relied on the activation of the pyridines by quaternization, i.e. the formation of a covalent bond with the pyridine nitrogen, to form the corresponding pyridinium derivative (Figure 3). This strategy overcomes all problems associated with the hydrogenation of *N*-heteroarenes: (i) the positive charge in the nitrogen destabilizes the aromaticity of the ring making it more reactive towards hydrogenation. (ii) The first hydrogenation step becomes irreversible. (iii) The quaternization of the pyridine eliminates completely its coordination ability and significantly reduces that of the product. (iv) The activating group might also act as a secondary coordinating unit, which by interaction with the metal center could improve the enantioselectivity of the reaction. Vidal-Ferran and co-workers recently published a review assessing the different activation strategies of *N*-heteroarenes.<sup>11</sup>

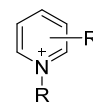
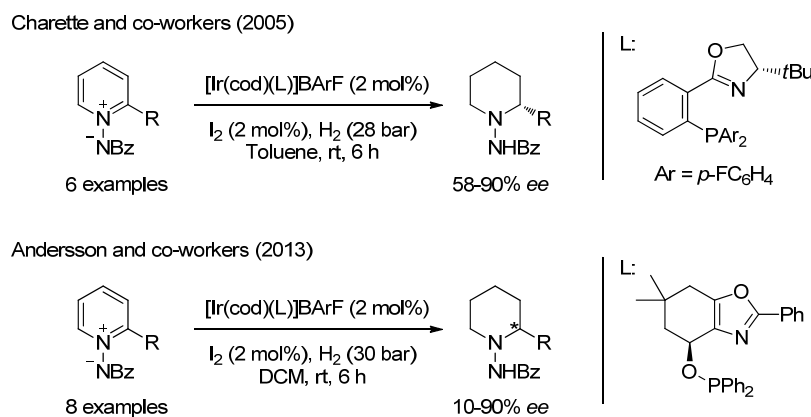


**Figure 3**

The activation of pyridines by acylation, alcoxycarbonylation or alkylation is a strategy that had already been extensively used in nucleophilic dearomatization reactions.<sup>12</sup> Nonetheless, it

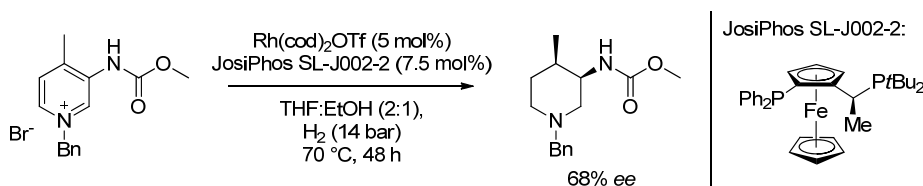


was not until 2005 when Charette and co-workers decided to apply a similar activation protocol for the asymmetric homogeneous hydrogenation of pyridines (Scheme 4). Converting pyridines into *N*-benzoyliminopyridinium ylides and using an Ir-phosphinooxazoline complex, they were able to hydrogenate a range of 2-alkyl-*N*-benzoyliminopyridinium ylides with good conversions and modest to high *ee*'s (54-90%).<sup>13</sup> More recently, Andersson and co-workers published an almost identical system, with the only difference of the ligand and the solvent (Scheme 4).<sup>14</sup>



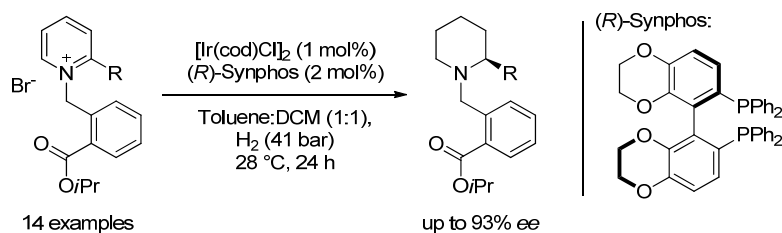
**Scheme 4.** Asymmetric hydrogenation of *N*-benzoyliminopyridinium ylides.

In 2007, Pfizer filed a patent on the synthesis of the drug Tofacitinib where one of the steps involved the hydrogenation of a 3-methoxycarbonylamino-4-methylpyridine (Scheme 5). The reported approach involved the activation of the pyridine by benzylation followed by AH with a Rh-JosiPhos catalyst, which led to 84% of the *cis* product with 68% *ee*.<sup>15</sup> The advantage of this strategy is that the benzyl group could be later removed by simple hydrogenation.



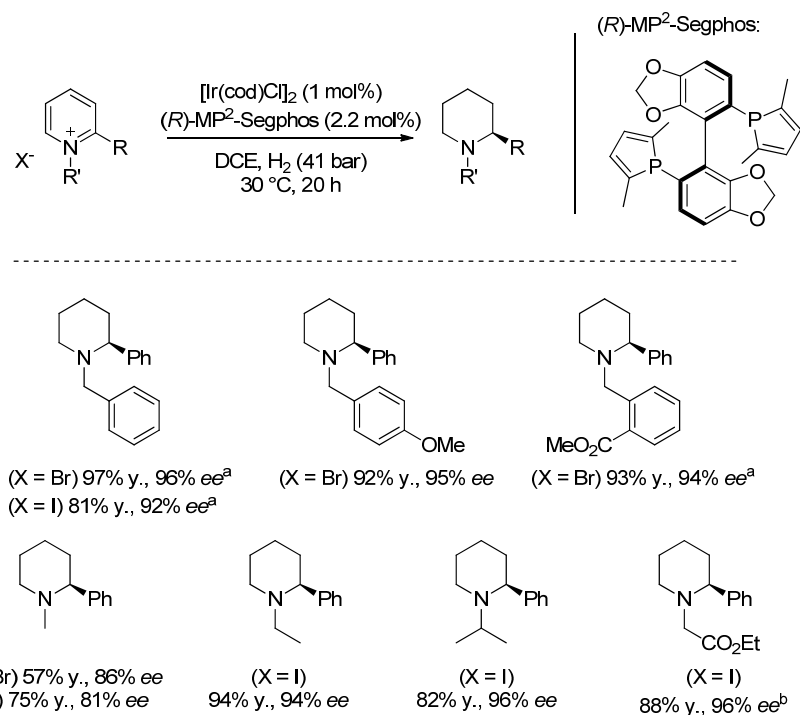
**Scheme 5.** Intermediate step in the synthesis of the drug Tofacitinib by Pfizer, involving the AH of the *N*-benzylated pyridinium salt.

Surprisingly, five more years passed until somebody used this convenient activation strategy to expand the scope. Zhou and co-workers found that *N*-benzyl-pyridinium salts were suitable substrates for AH employing an Ir-diphosphine catalyst (Scheme 6). After some solvent optimization and realizing that Br<sup>-</sup> was the only suitable counterion, they achieved the hydrogenation *N*-benzyl-2-phenylpyridinium bromide with 75% *ee*. To increase the enantioselectivity of the reaction they decided to modify the activating group. When introducing a methyl ester in the 2-position of the benzyl the *ee* increased to 89% – probably due to the directing effect of this new coordinating group – and when the isopropyl ester was used instead 92% *ee* was obtained as a result of the increased steric hindrance. Finally, after a fine tuning of the ligand, the substrate scope was assessed obtaining full conversion in almost all cases and excellent *ee*'s for the aromatic substituents.<sup>16</sup>



**Scheme 6.** Asymmetric hydrogenation of *N*-benzylated 2-substituted pyridinium salts.

As already discussed, *N*-benzylation might be one of the best activation strategies since the final piperidine can be easily deprotected. Nevertheless, an efficient and flexible method to hydrogenate *N*-alkylpyridinium salts would be of interest also when the target compounds is *N*-alkylated, avoiding in this way the protection/deprotection steps. This is what Zhang and co-workers reported in 2014, where by means of  $[\text{Ir}(\text{cod})\text{Cl}]_2$  and an uncommon chiral phosphole-based ligand, they hydrogenated a wide range of *N*-alkyl-2-arylpyridinium salts improving substantially the results from Zhou. With this system they were able to obtain higher *ee*'s without the need of a directing group in the benzylic moiety. The use of iodide as counterion was also tolerated and, even more remarkably, high enantioselectivities could be obtained using different *N*-benzyl or *N*-alkyl activating groups (Scheme 7). Finally, it was demonstrated that this robust system can hydrogenate *N*-benzyl-2-phenylpyridinium bromide with a catalyst loading as low as 0.25 mol%.<sup>17</sup>

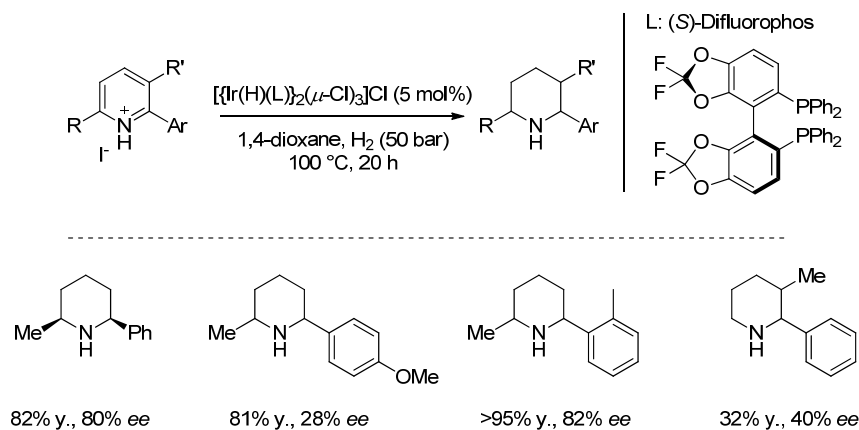


**Scheme 7.** Asymmetric hydrogenation of different *N*-substituted 2-phenylpyridinium bromides or iodides.

a) 1,2-dichloroethane/acetone (1:1) as solvent. b) 1,2-dichloroethane/acetone (5:1) as solvent. y. = yield.

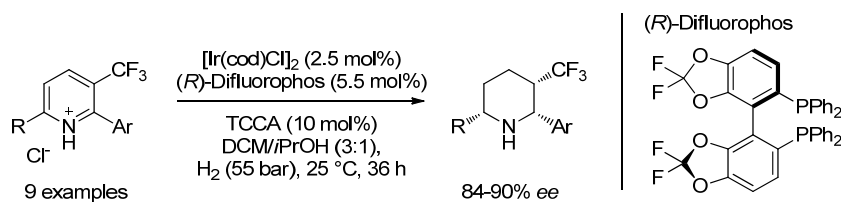
Recently, two more papers were published in the AH of multisubstituted pyridines and in both cases pyridines were activated as hydrohalide salts. Mashima and co-workers used a halogen-bridged iridium dinuclear complex developed in their group for the hydrogenation of

different 2,6- and 2,3-disubstituted pyridinium iodides with good yields, high diastereoselectivities ( $dr >95:5$ ) and enantioselectivities ranging from modest to good (28-82%  $ee$ ) (Scheme 8).<sup>18</sup>



**Scheme 8.** Asymmetric hydrogenation of disubstituted pyridinium iodides. y. = yield.

The most recent one was published by Zhou and co-workers in 2015. Using  $[\text{Ir}(\text{cod})\text{Cl}]_2$  and also Difluorophos as ligand, they succeeded in hydrogenating different multisubstituted 3-trifluoromethylpyridinium chlorides with excellent yields, diastereoselectivities and enantioselectivities (Scheme 9).<sup>19</sup>



**Scheme 9.** Asymmetric hydrogenation of multisubstituted 3-trifluoromethylpyridinium chlorides. TCCA: trichloroisocyanuric acid.

As it has been shown, metal-catalyzed AH is the most common strategy to reduce pyridines enantioselectively. Other reduction methodologies, such as the metal-catalyzed asymmetric transfer hydrogenation, are still underexploited, as only one non-enantioselective example has been reported so far.<sup>20</sup> Moreover, the metal free hydrogenations are starting to gain importance, like the partial hydrogenation of pyridines developed by Rueping *et al.*, where a catalytic amount of phosphoric acid and stoichiometric amounts of Hantzsch ester are used to achieve  $ee$ 's up to 92%.<sup>21</sup> More recently, a metal-free borane-catalyzed diastereoselective hydrogenation of pyridines was published by Du and co-workers, where  $dr$ 's up to 98:2 are obtained.<sup>22</sup>

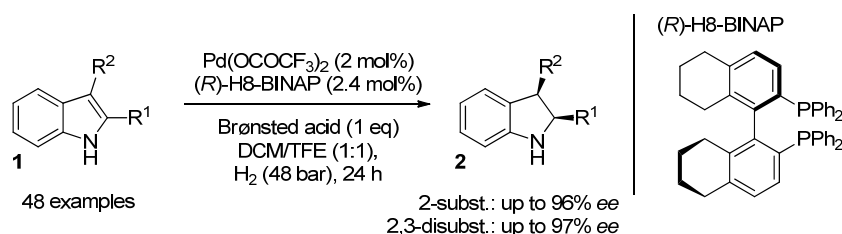
## I.2 REVIEW: MECHANISTIC STUDIES ON THE ASYMMETRIC HYDROGENATION OF *N*-HETEROARENES

In this section, a review on all mechanistic studies performed for the asymmetric hydrogenation (AH) of *N*-heteroarenes will be presented. As no such investigations have been

disclosed for the AH of pyridines so far, the aim of it is to facilitate the comprehension of the mechanistic studies discussed in Chapter II and III.

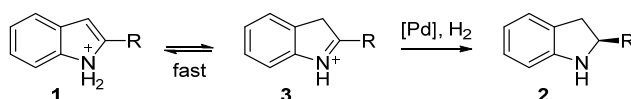
## INDOLE

Facile access to chiral indolines can be achieved by AH of substituted indoles. Indolines are interesting molecules since they occur in many natural products and biologically active compounds.<sup>23</sup> Numerous systems have been described for the AH of protected and unprotected indoles using Ir,<sup>24</sup> Rh,<sup>25</sup> Ru<sup>26</sup> or Pd<sup>27</sup> catalysts. Unfortunately, only the group of Zhou has put some effort into understanding the mechanism of the Pd catalyzed hydrogenation of unprotected indoles. In their initial work,<sup>27a</sup> later expanded with a full paper,<sup>27b</sup> 2- and 2,3-substituted indoles were hydrogenated with the combination of Pd(OCOCF<sub>3</sub>)<sub>2</sub> and (*R*)-H<sub>8</sub>-BINAP using a strong Brønsted acid as activator (Scheme 10).

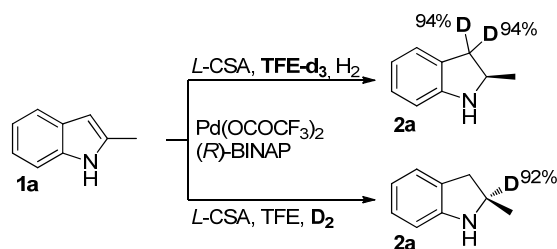


**Scheme 10.** Asymmetric hydrogenation of unprotected indoles.

The proposed mechanism can be seen in Scheme 11. Initially the protonated indole **1** would tautomerize to the iminium intermediate **3**, whose presence was confirmed by NMR and MS. Once the aromaticity of the indole is broken, the iminium intermediate would be prone to react with the Pd-hydride species in an enantioselective fashion to furnish indoline **2**. To get further insight into the mechanism, two isotopic labeling experiments were performed (Scheme 12). The first one, conducted in deuterated 2,2,2-trifluoroethanol (TFE-*d*<sub>3</sub>) and H<sub>2</sub>, showed that two deuterium atoms had been incorporated in the 3-position, suggesting an enamine-iminium equilibrium faster than the hydrogenation. The complementary experiment, where non-deuterated TFE and D<sub>2</sub> were employed, showed the incorporation of one deuterium in the 2-position, confirming the addition of the Pd hydride species to the iminium intermediate.

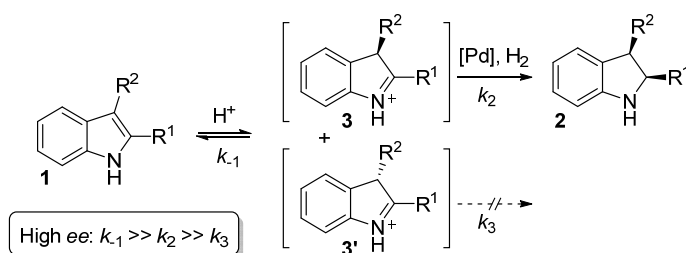


**Scheme 11.** Proposed mechanism for AH 2-substituted indoles.



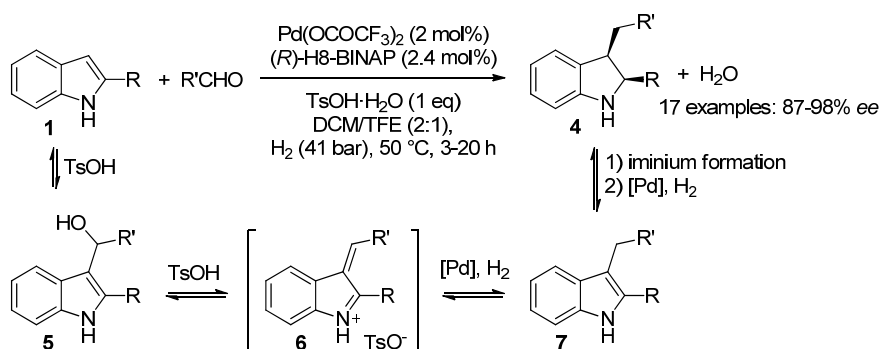
**Scheme 12.** Isotopic labeling experiments for the AH of 2-substituted indoles.

In the case of 2,3-disubstituted indoles, the enantioselectivity depends on the enamine-iminium equilibrium and the subsequent hydrogenation. It is in fact a dynamic kinetic resolution (DKR) where two different enantiomers of the iminium intermediate are formed, one being preferentially hydrogenated by the chiral catalyst (Scheme 13). This places the reaction under Curtin-Hammett control. To obtain high *ee*'s, the enamine-iminium equilibrium should be much faster than the hydrogenation step, which is indeed something that was proven in the first deuterium experiment. This latter concept was also proven experimentally when, by increasing the temperature (to accelerate the equilibrium) and decreasing the pressure (to slow down the hydrogenation), a higher *ee* was obtained.



**Scheme 13.** Proposed mechanism for the hydrogenation of 2,3-disubstituted indoles via dynamic kinetic resolution.

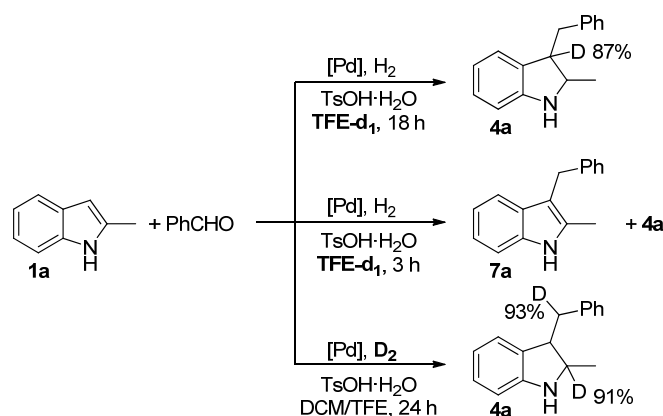
Zhou and co-workers carried out a similar mechanistic study for the tandem reductive alkylation-AH of 2-substituted indoles.<sup>27d</sup> The reaction process was initiated by a Brønsted acid-promoted Friedel-Crafts reaction of an aldehyde with indole **1** to furnish the corresponding 3-( $\alpha$ -hydroxyalkyl)indole **5**. Then, a dehydration followed by a 1,4-addition of the Pd-hydride to the generated vinylogous imine **6** would lead to the 2,3-disubstituted indole **7**, which was subsequently hydrogenated to indoline **4** via dynamic kinetic resolution (DKR), as previously shown in Scheme 13. Indeed, the conversion of **5** to indoline **4** had been already explored and optimized in a previous publication.<sup>27c</sup>



**Scheme 14.** Tandem reductive alkylation-AH of 2-substituted indoles and proposed mechanism.

To find more evidences about the mechanism, isotopic labeling experiments with deuterium gas or deuterated solvents were carried out (Scheme 15). The reaction performed in TFE-*d*<sub>1</sub> showed the incorporation of one deuterium in the 3-position of **4a**, arising from the tautomerization of enamine **7a** to the corresponding iminium form. When the same conditions were used, but stopping the reaction after 3 h, intermediate **7a** could be isolated with no

deuterium incorporation. Finally, running the reaction with  $D_2$ , instead of  $H_2$ , showed the incorporation of one deuterium at the 2-position and at the benzylic position of indoline **4a**, clearly indicating the positions where the hydride additions take place.

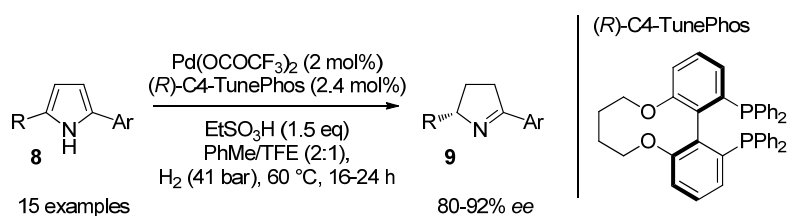


**Scheme 15.** Isotopic labeling experiments for the tandem reductive alkylation-AH of indoles **1a**.

## PYRROLE

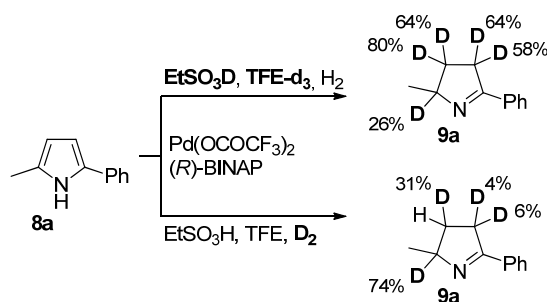
The enantioselective hydrogenation of substituted pyrroles to chiral pyrrolidines was first described using heterogeneous catalysts and a chiral auxiliary covalently attached to the pyrrole ring.<sup>28</sup> Some years later Kuwano *et al.* disclosed a system for the AH of *N*-Boc protected 2,3,5-trisubstituted pyrroles with a Ru catalyst.<sup>29</sup>

In 2011, using a similar system to that employed for indoles, Zhou and co-workers developed an enantioselective partial hydrogenation of unprotected 2,5-disubstituted pyrroles (Scheme 16).<sup>30</sup>



**Scheme 16.** Asymmetric hydrogenation of unprotected 2,5-disubstituted pyrroles.

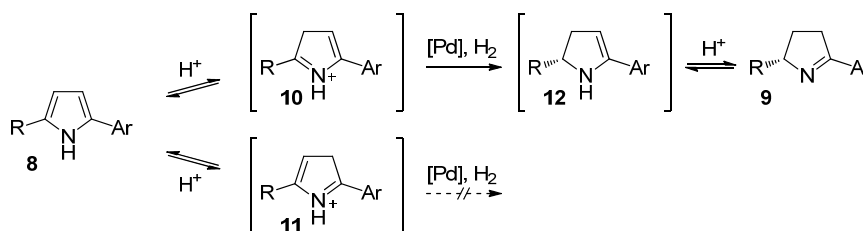
Isotopic labeling experiments were conducted in order to get a deeper insight into the reaction mechanism (Scheme 17).



**Scheme 17.** Isotopic labeling experiments for the AH of 2,5-disubstituted pyrroles.

When deuterated ethanesulfonic acid and TFE- $d_3$  were used, deuterium incorporation was observed mainly in the 3- and 4- positions of imine **9a** due to the enamine-imine equilibrium. When the same experiment was conducted using deuterium gas, the incorporation was mainly observed in the 2-position, arising from the enantioselective hydride addition to the iminium intermediate.

Based on the mechanistic studies previously performed for the AH of indoles, the isotopic labeling experiments and the NMR identification of the iminium salts **10** and **11**, they proposed the mechanism shown in Scheme 18. The unprotected pyrrole in presence of a strong Brønsted acid is in equilibrium with the two iminium salts, but only **10** is hydrogenated to enamine **12**. In this acidic media, the enamine isomerizes to the more stable imine **9**, which does not further react. The observed selectivity was studied by density functional theory calculations (DFT). Results showed that iminium **11** is more stable due to the conjugation with the aromatic group and the delocalization of the positive charge, making it more unreactive than iminium **10**.

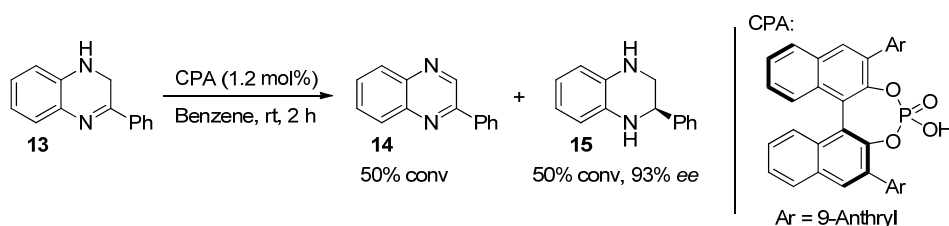


**Scheme 18.** Proposed mechanism for the AH of 2,5-disubstituted pyrroles.

## QUINOXALINE

The hydrogenation of quinoxalines to furnish biologically active tetrahydroquinoxalines<sup>23b,31</sup> can be formally seen as a double imine hydrogenation. This is probably the reason why many systems applied for imine AH are also tested with quinoxalines. Metal-catalyzed hydrogenations with Ir,<sup>32</sup> Ru<sup>33</sup> or Fe,<sup>34</sup> and also organocatalysts,<sup>35</sup> have been reported for the asymmetric reduction of these substrates.

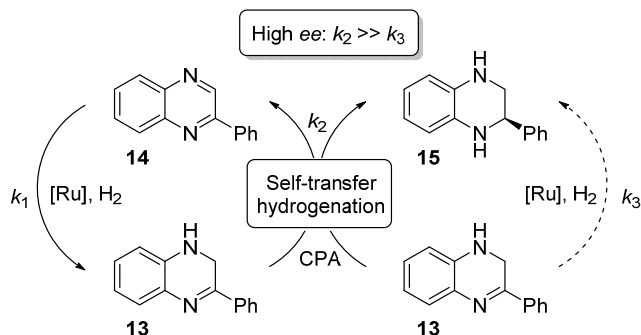
Zhou and co-workers studied a particular case of AH of quinoxalines.<sup>36</sup> By serendipity, they found out that dihydroquinoxaline **13** was disproportionating into quinoxaline **14** and tetrahydroquinoxaline **15** via a self-transfer hydrogenation. The presence of a chiral phosphoric acid (CPA) made this process faster and enantioselective (Scheme 19).



**Scheme 19.** Self-transfer hydrogenation of dihydroquinoxalines.

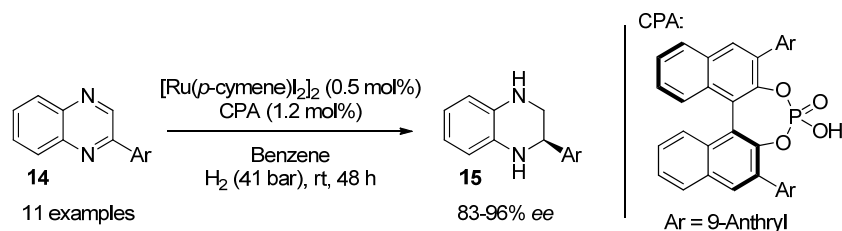
In the view of these results, they decided to establish a protocol for the AH of quinoxalines to tetrahydroquinoxalines (Scheme 20). For that, they selected an achiral Ru catalyst able to

hydrogenate quinoxaline **14** to dihydroquinoxaline **13** ( $k_1$ ), but that was not very efficient in the hydrogenation to tetrahydroquinoxaline **15** ( $k_3$ ). In this way, if the self-transfer hydrogenation ( $k_2$ ) was faster than  $k_3$ , the production of **15** would take place via the highly enantioselective pathway.



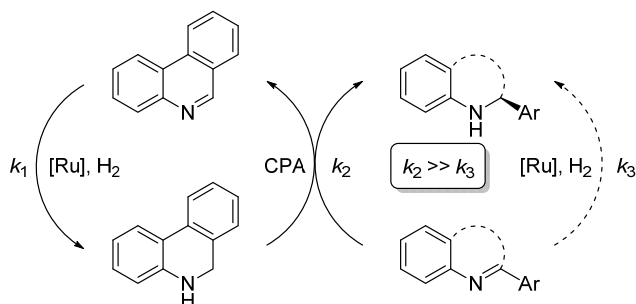
**Scheme 20.** Proposed mechanism for the AH of quinoxalines.

Applying the designed protocol, they were able to hydrogenate a wide range of 2-arylquinoxalines with excellent yields and enantioselectivities (Scheme 21). Unexpectedly, they observed a reverse enantioselectivity compared to the one obtained by Rueping and co-workers when using the same enantiomer of the CPA but Hantzsch esters as stoichiometric reductant.<sup>35b</sup> The authors ascribed this fact to the different steric demands present in the transition state of the hydride transfer. While Hantzsch esters do a 1,4-hydride transfer, dihydroquinoxalines go via a 1,2-hydride transfer pathway. DFT calculations supported this latter hypothesis.



**Scheme 21.** Asymmetric hydrogenation of 2-arylquinoxalines.

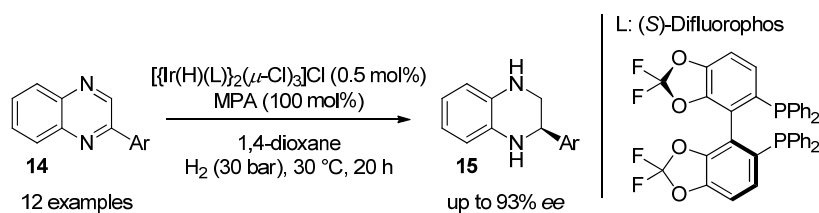
This same concept was later expanded by using 9,10-dihydrophenanthridine as a regenerable hydrogen source, in combination with a chiral phosphoric acid, for the AH of quinoxalines, benzoxazinones, benzoxazines, and quinolines (Scheme 22).<sup>37</sup>



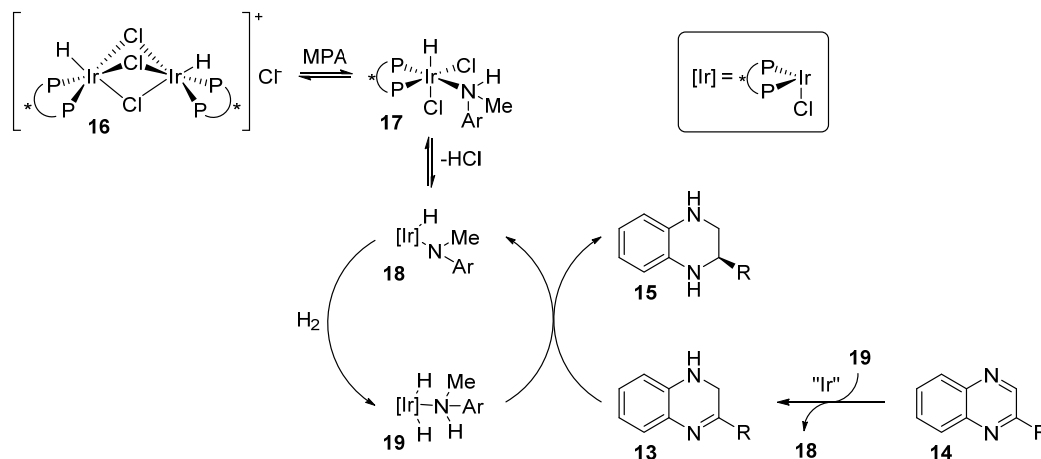
**Scheme 22.** 9,10-dihydrophenanthridine as a transfer hydrogenation catalyst.



Mashima and co-workers used a completely different system for the hydrogenation of 2-arylquinoxalines, consisting of a chiral halide-bridged dinuclear iridium complex in the presence of a stoichiometric amount of *N*-methyl-*p*-anisidine (MPA) (Scheme 23).<sup>32a</sup>



Numerous experiments were performed to gain insight on the reaction mechanism, the role of the base and the active species involved. The dinuclear iridium complex **16** was reacting *in situ* with MPA to form the mononuclear species **17**, which after releasing HCl, led to the Ir-hydride **18**. The authors propose an outer-sphere mechanism, where catalytic species **18**, after reacting with H<sub>2</sub>, would hydrogenate quinoxaline **14** or dihydroquinoxaline **13**. It is noteworthy that the base not only acts as a non-innocent ligand in the hydrogenation process, but it also quenches the *in situ* generated HCl during the activation of the catalyst. It was found that the generated traces of HCl could promote the non-enantioselective disproportionation of dihydroquinoxaline **13**, as shown by Zhou.<sup>36</sup> As expected, quinoxalines and the other intermediates are also able to coordinate the catalyst, forming less active and enantioselective species than those formed with MPA. For this reason, an important amount of MPA is needed for the reaction to take place with high enantiomeric excess. Isotopic labeling experiments using D<sub>2</sub> showed the insertion of one deuterium in the 2- and 3-positions, as expected for the two hydride additions.



In further experiments the authors serendipitously found out that the analogous catalytic system featuring Josiphos SL-J001-1 instead of (*S*)-Difluorophos, had a superior performance in the enantioselective hydrogenation of 2-phenylquinoxaline, allowing to achieve full conversion and 96% *ee*.

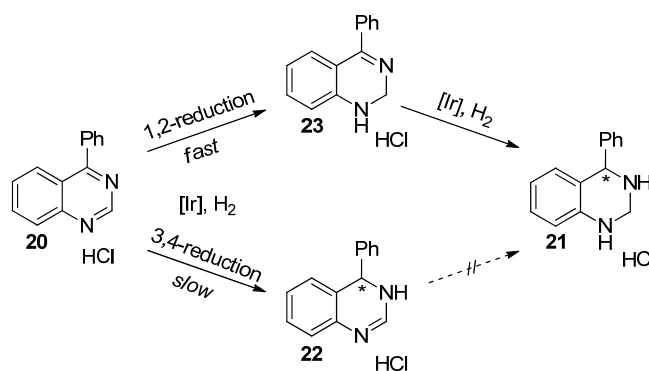
## QUINAZOLINE

Only one AH of quinazolines has been disclosed so far. Mashima and co-workers used the halide-bridged dinuclear iridium complex that had proven efficient for other *N*-heteroaromatic substrates to enantioselectively hydrogenate 2-arylquinazolinium salts (Table 1).<sup>38</sup>

**Table 1.** Asymmetric hydrogenation of 4-arylquinazolinium salts.

#	R	yield of <b>21</b> (%)	ee of <b>21</b> (%)	yield of <b>22</b> (%)	yield of <b>23</b> (%)
1	Ph	89	99	11	-
2	2-MeC <sub>6</sub> H <sub>4</sub>	Trace	-	2	89
3	4-MeC <sub>6</sub> H <sub>4</sub>	81	97	8	2
4	4-OMeC <sub>6</sub> H <sub>4</sub>	66	98	14	20
5	4-CF <sub>3</sub> C <sub>6</sub> H <sub>4</sub>	82	99	6	10

To get some insight into the reaction mechanism, a time-course study of the reaction following the distribution of the different intermediates was performed. Within the first 5 hours, the quinazolinium hydrochloride was almost completely consumed to give the 1,2-reduction product **23**, which was then gradually enantioselectively hydrogenated to the tetrahydroquinazoline **21** (Scheme 25). Simultaneously, some 3,4-reduction product **22** was also slowly formed, reaching an 11% conversion at the end of the reaction. This latter product was not hydrogenated, probably due to the stability of its hydrochloride salt.



**Scheme 25.** Proposed stepwise hydrogenation of quinazolinium hydrochlorides.

## ISOQUINOLINE

1,2,3,4-Tetrahydroisoquinolines motifs are widely spread in nature and have found many applications in pharmaceutical products.<sup>39</sup> However, together with pyridines, isoquinolines are one of the most challenging substrates for AH. Only a few methods have been reported, all of them based on Ir catalysts,<sup>40</sup> except one example of Ru catalysis in ionic liquids.<sup>41</sup> Even so, interesting mechanistic studies have been reported by the groups of Zhou and Mashima regarding the enantioselective hydrogenation of isoquinolines.

In 2013, Zhou and co-workers disclosed the AH of *N*-benzylated isoquinolinium salts, applying the same strategy that had previously given successful results for pyridines.<sup>16</sup> Using an Ir-diphosphine complex they were able to hydrogenate a wide range of 1- and 3-substituted isoquinolinium salts with excellent yields and good to excellent enantioselectivities (Table 2).<sup>40c</sup>

**Table 2.** Asymmetric hydrogenation of 1- and 3-substituted isoquinolinium salts.

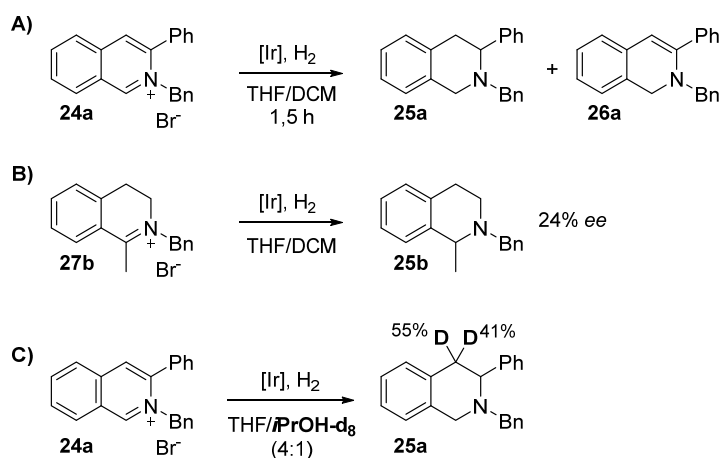
14 examples

(*R*<sub>ax</sub>, *S*, *S*)-C3\*-TunePhos

#	R <sup>1</sup>	R <sup>2</sup>	yield (%)	ee (%)
1	Ph	H	99	96
2	4-OMeC <sub>6</sub> H <sub>4</sub>	H	99	94
3	4-CF <sub>3</sub> C <sub>6</sub> H <sub>4</sub>	H	96	93
4 <sup>[a]</sup>	Me	H	99	70
5	H	Ph	94	85
6	H	4-OMeC <sub>6</sub> H <sub>4</sub>	99	80
7	H	<i>i</i> Pr	99	43

[a] Ar = phenyl

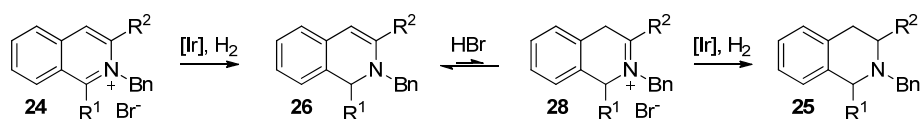
To shed light into the reaction mechanism, some experiments were carried out. Initially, in order to detect some intermediates, the reaction was stopped after 1.5 h. In the case of *N*-benzyl-1-phenylisoquinolinium bromide, only starting material and final product were observed, instead when 3-phenyl derivative **24a** was used, 1,2-dihydroisoquinoline **26a** could be identified (Scheme 26A), indicating that the 1,2-reduction occurs first. When the latter intermediate was isolated and subjected to hydrogenation in the absence of HBr, no conversion was obtained, underscoring the need of the *in situ* generated HBr for the reaction to proceed. Furthermore, when *N*-benzyl-1-methyl-3,4-dihydroisoquinoline **27b** was enantioselectively hydrogenated, **25b** was obtained only with 24% *ee* (Scheme 26B, in contrast with the 70% *ee* from Table 2, entry 4), excluding in this way a mechanism involving an initial C3-C4 hydrogenation.



**Scheme 26.** Mechanistic studies on the AH of isoquinolines.

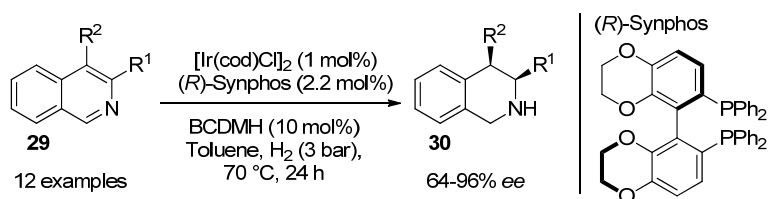
Finally, an isotopic labeling experiment showed the incorporation of almost one deuterium atom in the 4-position of **25a** (Scheme 26C), suggesting that the enamine intermediate tautomerizes to the corresponding iminium and then it is promptly hydrogenated.

Based on the above evidences, the proposed mechanism would be initiated by a 1,2-hydride addition to isoquinolinium **24** to give the 1,2-dihydropyridine **26**, which would be subsequently isomerized to the iminium salt **28** and readily hydrogenated to the final 1,2,3,4-tetrahydroisoquinoline **25** (Scheme 27). According to this mechanism, while for the 1-substituted isoquinolines the enantiodetermining step would be the first hydride addition, for the 3-substituted it should be the second. As the authors remark, a 1,4-reduction as a first step of the mechanism leading directly to iminium **28** cannot be ruled out.



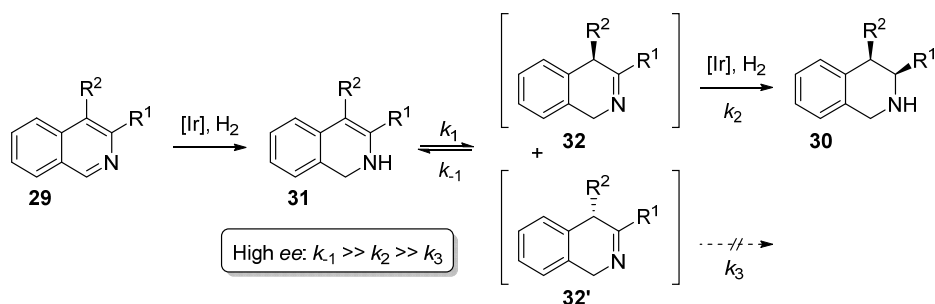
**Scheme 27.** Proposed mechanism for the AH 1- and 3-substituted isoquinolines.

In another publication from the same group, the AH of unprotected 3,4-disubstituted isoquinolines is disclosed. By using an Ir-diphosphine complex and 1-bromo-3-chloro-5,5-dimethyl-hydantoin (BCDMH) as additive, the corresponding tetrahydroisoquinolines were obtained with good to excellent yields, diastereoselectivities and *ee*'s (Scheme 28).<sup>40b</sup>



**Scheme 28.** Asymmetric hydrogenation of unprotected 3,4-disubstituted isoquinolines.

With shorter reaction times, they were able to isolate the intermediate from the 1,2-reduction **31**. When this isolated 1,2-dihydroisoquinoline was hydrogenated under the optimized conditions, the final tetrahydroisoquinoline **30** was obtained with the same conversion and *ee*. Furthermore, increasing the temperature and decreasing the pressure led to a higher enantioselectivity, suggesting that a dynamic kinetic resolution was involved in the process.



**Scheme 29.** Proposed mechanism for the hydrogenation of 2,3-disubstituted isoquinolines via dynamic kinetic resolution.

The proposed mechanism would go as follows (Scheme 29): initially, a 1,2-hydride addition to the less sterically hindered carbon would give the enamine intermediate **31**. This enamine would be in fast equilibrium (due to the high temperature) with the two enantiomers of the imine form (**32** and **32'**) and one of the two would be preferentially hydrogenated to the final tetrahydroisoquinoline.

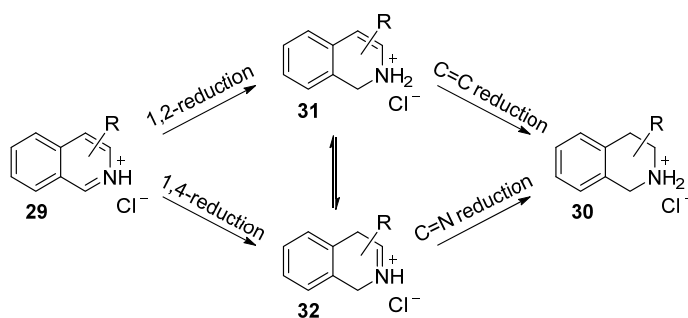
More recently, Mashima's group also studied the AH of isoquinolinium chlorides with their dinuclear iridium complex. In a first publication of 2013, this new system is described with a couple of mechanistic experiments,<sup>40e</sup> but the full mechanistic investigation was published two years later.<sup>40f</sup> All possible substitution patterns in the heteroaromatic cycle were tested (Table 3), obtaining excellent yields and very high enantioselectivities for 1-, 3-, and 1,3-substituted isoquinolines. More problematic were the substrates with substituents in the 4-position (Table 3, entries 7, 11 and 12), giving poor *ee*'s or diastereoselectivities.

**Table 3.** Substrate scope for the AH of isoquinolinium chlorides.

#	R <sup>1</sup>	R <sup>2</sup>	R <sup>3</sup>	yield (%)	<i>ee</i> (%)
1	Ph	H	H	99	96
2	4-OMeC <sub>6</sub> H <sub>4</sub>	H	H	99	99
3	4-CF <sub>3</sub> C <sub>6</sub> H <sub>4</sub>	H	H	99	98
4	Cy	H	H	99	79
5 <sup>[a]</sup>	H	Ph	H	99	96
6 <sup>[a]</sup>	H	Cy	H	99	79
7	H	H	Ph	99	5
8	Ph	Ph	H	98	98
9	Cy	Ph	H	87	97
10	Ph	<i>n</i> Hex	H	80	98
11 <sup>[b]</sup>	Ph	H	Ph	99	90
12 <sup>[c]</sup>	H	Ph	Ph	99	43

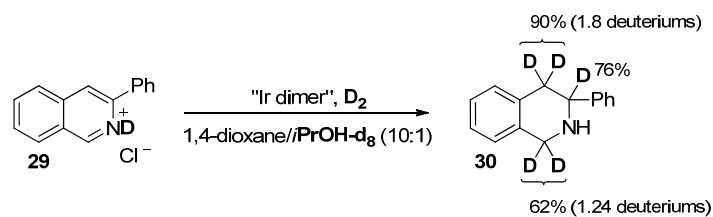
[a] Reaction performed at 30 °C. [b] *syn:anti* = 4:1. [c] *syn:anti* = 20:1.

To start exploring the mechanism of this reaction, the different possible pathways shown in Scheme 30 were proposed. Three different mechanism can be postulated for the first reduction, among which 1,2- and 1,4-reduction seem the more plausible, while 3,4-reduction was excluded based on the fact that Ir complexes are more prone to hydrogenate C=N bonds rather than C=C bonds.<sup>42</sup> The two resulting dihydroisoquinolinium salts **31** and **32** would be in equilibrium through an enamine-iminium tautomerization. Finally, these two intermediates could be hydrogenated via a C=C enamine hydrogenation or a C=N iminium hydrogenation. However, as already observed with other substrates,<sup>27b,30,40b</sup> the AH of unprotected enamines proceeds via an enamine-iminium tautomerization and subsequent hydride addition to the iminium ion.



**Scheme 30.** Plausible pathways for the hydrogenation of isoquinolinium salts.

To gain insight into the reaction mechanism, an isotopic labeling experiment was performed using  $D_2$ , deuterated solvent and 3-phenylisoquinolinium chloride as substrate (Scheme 31). The first thing to observe is that more than one deuterium was incorporated in the 1-position, suggesting that the first step is reversible. Also in the 4-position, the initial hydrogen atom was almost completely replaced for deuterium as a result of a fast enamine-iminium tautomerization. The same conclusions could be drawn from a parallel experiment performed using 1-phenylisoquinolinium chloride as substrate. Although the final hydrogenation of the dihydroisoquinoline is generally accepted to proceed via the iminium intermediate, an additional experiment using  $D_2$  and undeuterated solvent would have confirmed it.



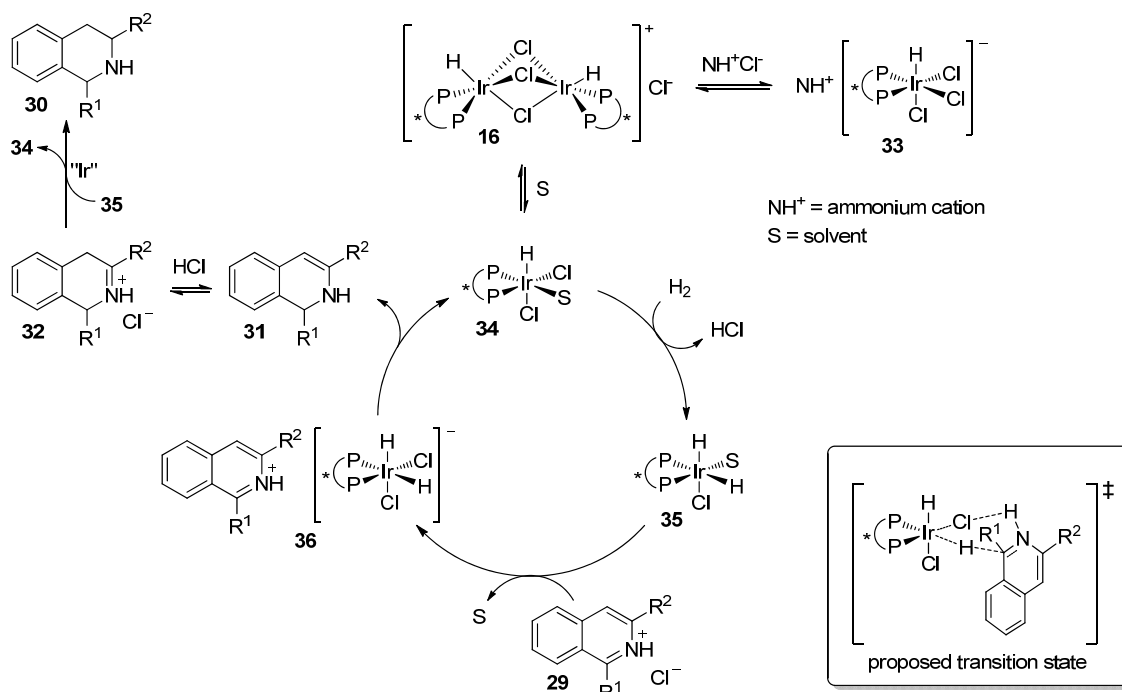
**Scheme 31.** Deuterium labeling experiment for 3-phenylisoquinolinium chloride

Additionally, two more experiments were performed and monitored by NMR. When the AH of the 3-phenylisoquinolinium salt was carried out under atmospheric pressure of  $H_2$ , the iminium intermediate was formed and slowly converted into the final tetrahydroisoquinoline. Instead, when 1- or 4- substrates were used, no reaction took place. According to the authors, these results lend credit to the 1,4-reduction pathway rather than the 1,2-reduction, since the substituents in the 1- and 4-positions clearly retarded the reaction.

Two years later, the same authors disclosed the full investigation about the mechanism of this reaction<sup>40f</sup> expressing a different point of view on the controversial 1,2-/1,4-hydride addition in the first step. In this study, different interactions of the possible reaction intermediates with the active iridium catalyst were investigated. One of the intermediate Ir species of the catalytic cycle was identified as the anionic complex **36** with an isoquinolinium derivative as a counterion (Scheme 32). The dihydride iridium complex **36** was postulated as the responsible of the reductions through a proposed 6-membered cyclic transition state, that implying that only the 1,2-reduction is possible. This has not been unambiguously demonstrated yet, but these apparently contradictory results are just reflecting how difficult is to investigate which one of the two paths is leading to the dihydroisoquinoline.

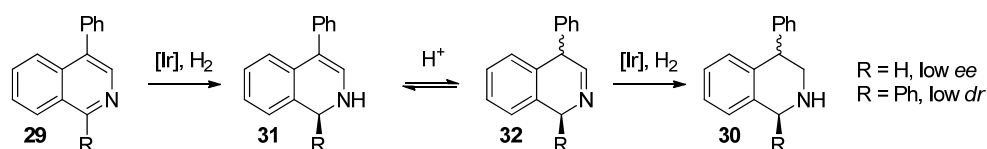
In addition, Mashima and co-workers demonstrated that the salt formation of the substrate was crucial for the high yields and enantioselectivities. The coordination of unprotonated substrate or product led to less enantioselective catalysts or to the formation of inactive iridium dimers, which could be reactivated by addition of isoquinolinium chloride salts. Moreover, it was found that an Ir dihydride complex was involved in the catalytic cycle.

Thus, the final catalytic cycle would be the one represented in Scheme 32. The iridium dimer **16**, in equilibrium with the ionic form **33**, dissociates to the Ir-monohydride **34**. Upon reaction with H<sub>2</sub>, the Ir-dihydride **35** is formed, and after displacement of the solvent by a chloride from the isoquinolinium salt the ionic complex **36** is generated. Finally, the hydride addition, via the proposed outer-sphere 6-membered ring transition state, would regenerate complex **34** and form the corresponding dihydroisoquinoline. The second reduction would take place in a similar manner.



**Scheme 32.** Proposed catalytic cycle and transition state for the AH of isoquinolinium salts.

The poor stereoselectivities mentioned before for isoquinolines with substituents in the 4-position are also in agreement with the proposed mechanism. In the case of 4-substituted isoquinolines, the enamine-iminium isomerization generates a racemic stereocenter at C4 leading to a poor 5% *ee* (Scheme 33). This interpretation holds true also for 1,4-disubstituted isoquinolines: the initial highly enantioselective 1,2-reduction gives the 1,2-dihydroisoquinoline which, after the enamine tautomerization and subsequent hydrogenation, generates the two diastereomers with low diastereoselectivity (*syn:anti* = 4:1), but with very high *ee* from the first hydrogenation step (*syn*: 90% *ee*, *anti*: 97% *ee*). Finally, for the 3,4-disubstituted isoquinoline, a dynamic kinetic resolution could be expected as has been previously proposed for other substrates (analogous to Scheme 29), but probably the system would require further optimization to achieve an *ee* higher than 43%.

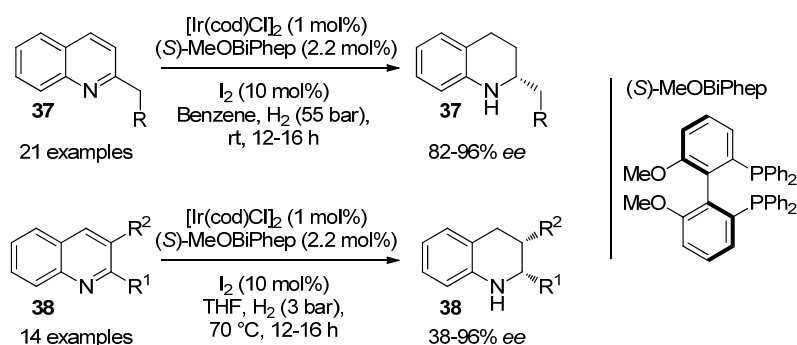


**Scheme 33.** Proposed mechanism for the lack of stereoselectivity in 4- and 1,4-substituted isoquinolines.

## QUINOLINE

Besides being an ubiquitous motif in natural products, 1,2,3,4-tetrahydroquinolines have found many applications in pharmaceutical and agrochemical synthesis.<sup>43</sup> That might be the reason why quinolines are, by far, the most well studied *N*-heteroarene substrates in AH. A wide range of systems employing homogeneous chiral catalysts have been reported: hydrogenations with Ir,<sup>10,32g,40a,44,45</sup> Pd<sup>46</sup>, Ru;<sup>37,41,47</sup> transfer hydrogenations with Ir,<sup>48</sup> Ru<sup>49</sup> and Rh;<sup>49,50</sup> exploiting the concept of Frustrated Lewis Pair;<sup>51</sup> or employing Hantzsch esters as hydride source in combination with catalytic amounts of chiral anions (generally chiral phosphates).<sup>52</sup>

Zhou and co-workers were the first ones to perform mechanistic studies on the AH of these substrates. They developed a system for the reduction of 2-substituted and 2,3-disubstituted quinolines employing an Ir-diphosphine catalyst with I<sub>2</sub> as additive (Scheme 34).<sup>45a</sup>

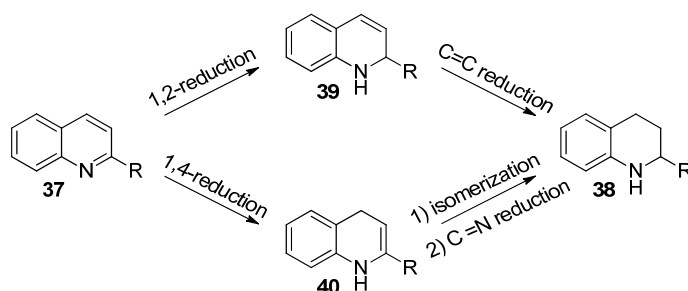


**Scheme 34.** Asymmetric hydrogenation of 2-substituted and 2,3-disubstituted quinolines

The first aspect they investigated was the role of I<sub>2</sub>. Two functions were proposed: substrate activation or catalyst activation. When 2-methylquinoline was allowed to react with I<sub>2</sub> in toluene for 24 h, a yellow complex was formed, which upon hydrogenation under the optimized conditions did not lead to any product. Instead, when the catalyst was stirred for 12 h in DCM in the presence of I<sub>2</sub>, a mixture of complexes was observed by <sup>31</sup>P-NMR (due to the coexistence of chloride and iodide) which was able to hydrogenate 2-methylquinoline with 93% *ee*. These results, and the fact that without I<sub>2</sub> no reaction occurs, reveal that the catalyst is indeed activated by iodine.

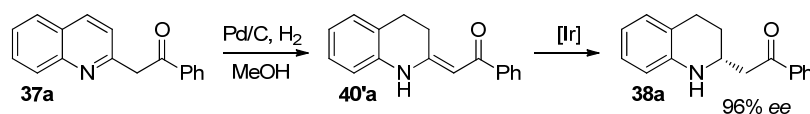
Two possible hydrogenation pathways were proposed (Scheme 35): on the one hand, a 1,2-hydride addition followed by C=C reduction; on the other hand, a 1,4-addition followed by isomerization and C=N reduction. Contrary to what happens with isoquinolines, the products of 1,2- and 1,4-hydride addition are not tautomers.





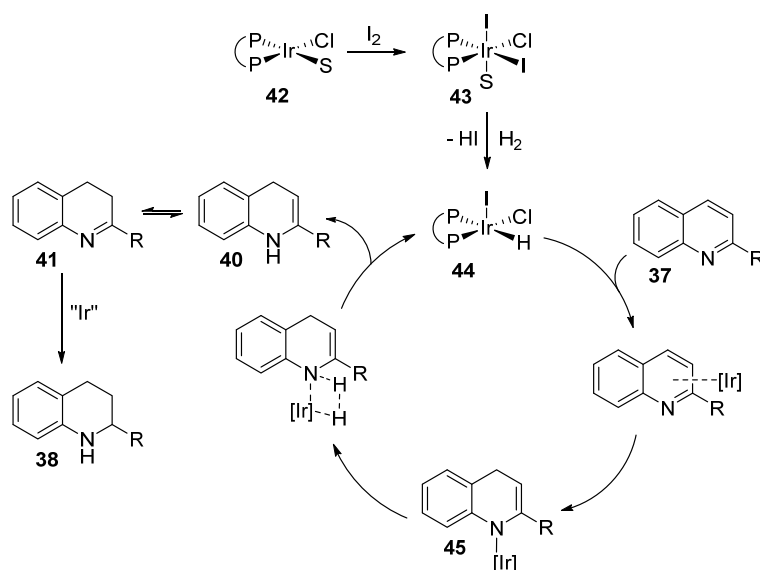
**Scheme 35.** Proposed pathways for the hydrogenation of quinolines.

To demonstrate which was the most probable pathway, the product of 1,2-addition **39** was synthesized. Unfortunately, in presence of the Ir catalysts this product was rapidly dehydrogenated to give the original quinoline. Thus, the synthesis of the product of 1,4-addition to 1-phenyl-2-(quinolin-2-yl)ethanone **37a** was attempted by using Pd/C and H<sub>2</sub> in MeOH. The more stable product **40'a** with the conjugated double bond was obtained instead but, when the latter was submitted to hydrogenation conditions, the desired product **38a** was obtained with 96% *ee* (Scheme 36). This same intermediate **40'a** was also detected when running the hydrogenation of the quinoline at lower pressures and shorter reaction times. DFT calculations on the thermodynamic values for the hydride addition to 2-methylquinoline showed a more favorable 1,4-addition rather than 1,2-addition.



**Scheme 36.** Synthesis and hydrogenation of intermediate enamine **40'a**.

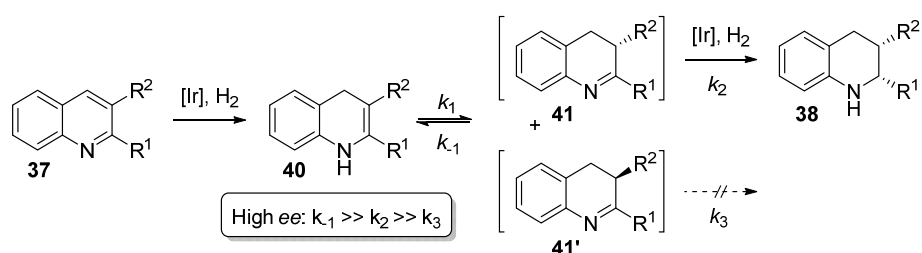
Based on these data, an inner-sphere mechanism was proposed by the authors (Scheme 37). Initially the active catalyst would be formed via an oxidative addition of I<sub>2</sub> followed by a heterolytic cleavage of hydrogen, with hydrogen iodide formation.



**Scheme 37.** Proposed mechanism for the Ir-catalyzed AH quinolines.

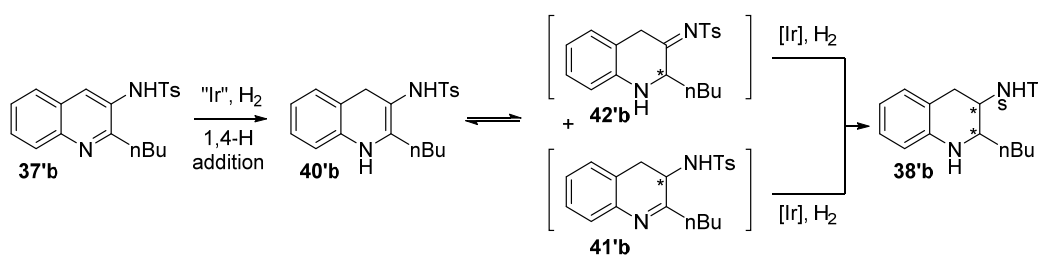
The quinoline could coordinate to the Ir species **44**, and the subsequent 1,4-hydride addition would afford intermediate **45**, which via heterolytic cleavage of H<sub>2</sub>, would regenerate **44** and form the 1,4-dihydroquinoline **40**. After isomerization, the formed imine **41** would be hydrogenated according to an analogous catalytic cycle, involving an enantioselective 1,2-hydride transfer to give the final tetrahydroquinoline **38**. It is also worth mentioning that the same Ir-diphosphine catalyst was able to catalyze the dehydrogenation of the tetrahydroquinoline in boiling xylene releasing H<sub>2</sub> and affording the corresponding quinoline.

Regarding the AH of 2,3-disubstituted quinolines, the dynamic kinetic resolution proposed for other substrates seemed also valid in this case. Based on the proposed mechanism for the hydrogenation of quinolines, the enantioselectivity would depend on the final 1,2-hydride addition to the fast-equilibrating imine enantiomers **41** and **41'**, which would be selective for one of the two dihydroquinoline (Scheme 38). This is also supported by the increase of enantiomeric excess when the reaction was run at higher temperatures and lower pressures. Hydrogenation of 2,3-dimethylquinoline at 25 °C and 48 bar of H<sub>2</sub> gave 5% *ee*, instead, when performed at 70 °C and 3 bar the *ee* increased to 73%.



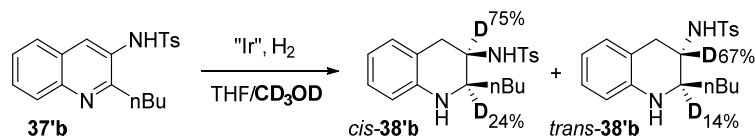
**Scheme 38.** Proposed mechanism for the AH of 2,3-disubstituted quinolines.

Some years later, the same group provided more evidences for supporting this mechanism during the optimization of the AH of 2-substituted quinoline-3-amines.<sup>45b</sup> While trying to find the more suitable protecting group for the hydrogenation of 2-butylquinolin-3-amines, they realized that in all cases the diastereomeric ratios were rather low. They suspected that this poor diastereoselectivities could be attributed to a competition between two different possible enamine-imine isomerizations (Scheme 39). Once enamine **40'b** is formed by 1,4-hydride addition, it is in equilibrium with the exocyclic imine **42'b** and with the endocyclic imine **41'b**. The hydrogenation of those two imines may lead to different diastereoselectivities.



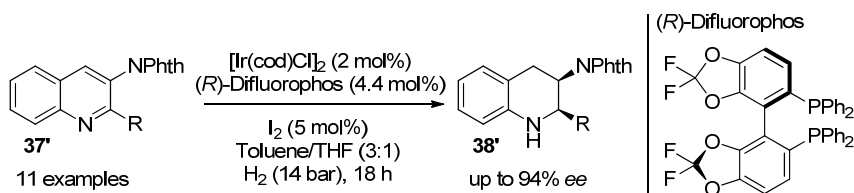
**Scheme 39.** Proposed mechanism responsible for the poor diastereoselectivities obtained.

This hypothesis was supported by isotopic labeling experiments using deuterated MeOH as co-solvent (Scheme 40). Deuterium incorporation was observed in the 2-position (during the tautomerization to the exocyclic imine) and 3-position (tautomerizing to the endocyclic imine).



**Scheme 40.** Deuterium labeling experiments in the AH of 2-butylquinolin-3-amine.

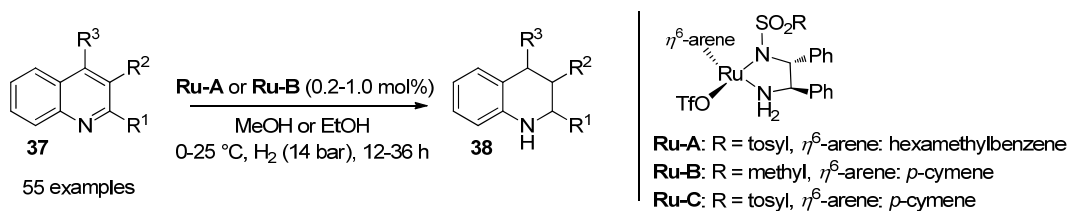
The authors foresaw that the isomerization could be impeded by double protecting the amino group. Thus, by using the phthaloyl (Phth) group and after some optimization of the reaction conditions and ligands, they were able to hydrogenate these aromatic amines with excellent yields, diastereoselectivities and enantioselectivities (Scheme 41).



**Scheme 41.** Asymmetric hydrogenation of 2-substituted quinoline-3-amines.

Fan and co-workers disclosed a Ru-catalyzed AH of quinolines reaching *ee*'s up to 99% and TON up to 5000 (Table 4).<sup>47c</sup> This system proved very efficient for a very wide range of substrates: 2- and 2,3-disubstituted quinolines were smoothly hydrogenated with excellent enantioselectivities. Unfortunately, when 3-substituted quinolines were used, the racemic product was obtained and no reaction was observed when employing 4-substituted substrates.

**Table 4.** Substrate scope for the AH of quinolines.

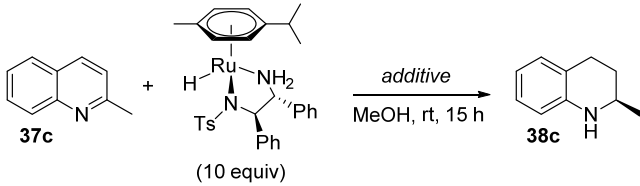


#	R <sup>1</sup>	R <sup>2</sup>	R <sup>3</sup>	yield (%)	<i>ee</i> (%)
1	Me	H	H	100	99
2	Bn	H	H	100	>99
3	Ph	H	H	94	92
4	2-OMeC <sub>6</sub> H <sub>4</sub>	H	H	91	95
5 <sup>[a]</sup>	styryl	H	H	100	99
6	COOMe	H	H	0	-
7	<i>n</i> Bu	Me	H	100	97 ( <i>syn</i> ) <sup>[b]</sup>
8	-(CH <sub>2</sub> ) <sub>4</sub> -		H	100	17 ( <i>syn</i> ) <sup>[c]</sup>
9	H	Me	H	100	0
10	H	Ph	H	100	0
11	H	H	Me	0	-
12	Me	H	Me	0	-

[a] Double bond also hydrogenated [b] *dr* = 46:54. [c] *dr* > 20:1.

Additionally, a thorough mechanistic study was performed by the authors. Initially, the need of activation of the quinolines by protonation was investigated. Performing a stoichiometric reaction between 2-methylquinoline (**37c**) and an excess of the Ru-hydride species (the expected active species) in the absence of H<sub>2</sub> led to no conversion (Table 5, entry 1). Instead, when the protonated substrate was used 44% conversion was obtained (entry 2), and when another equivalent of acid was added the conversion increased to 96%, with 96% *ee* in both cases (entry 3). These results, which had already been observed when performing the reaction in ionic liquid,<sup>47a</sup> demonstrated that the quinoline should be activated by protonation prior to the hydride addition.

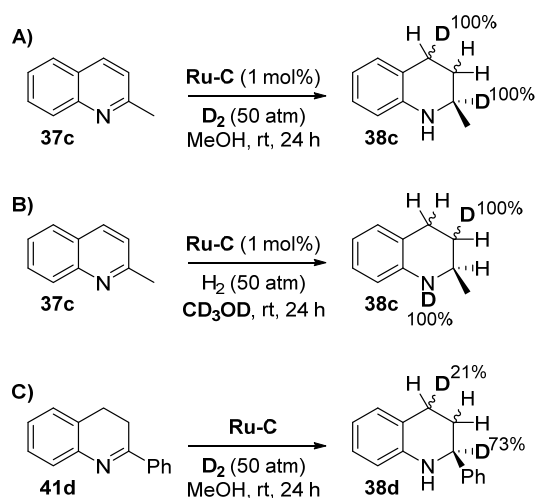
**Table 5.** Stoichiometric reaction between 2-methylquinoline and Ru-hydride species.



#	Substrate	Additive	yield (%)	<i>ee</i> (%)
1	<b>37c</b>	none	0	-
2	<b>37c</b> ·TfOH	none	44	96
3	<b>37c</b> ·TfOH	R <sub>2</sub> NH·TfOH (1 equiv)	96	96

Next, the authors investigated which one of the two possible pathways for the hydrogenation of quinolines (Scheme 35) is more likely to take place. On the one hand, the product of 1,2-addition was synthesized but, as already observed by Zhou,<sup>45a</sup> it rapidly underwent dehydrogenation in presence of the Ru catalyst. To overcome this problem, the 1,2-dihydropyridine was *N*-benzoyl-protected, forming a stable compound which was inactive under hydrogenation conditions, suggesting that the unpolarized C3=C4 bond could not be reduced by this Ru catalyst. On the other hand, the synthesis of the intermediate arising from the 1,4-hydride addition and subsequent isomerization was aimed at investigating the other hydrogenation pathway. Considering the instability of 2-alkyl-3,4-dihydroquinolines, the more stable 2-phenyl-3,4-dihydroquinoline (**41d**) was synthesized and hydrogenated under the optimized conditions, giving full conversion and the same *ee* as the direct hydrogenation of 2-phenylquinoline. Although some dehydrogenation of **41d** was observed, direct hydrogenation did also occur, as proven by the isotopic labeling experiments (see below). Furthermore, intermediate **41d**, together with the initial quinoline and the final product, was detected by <sup>1</sup>H-NMR and ESI-HRMS analysis after 5 min of reaction. All these experimental data supported a pathway involving a 1,4-hydride addition followed by isomerization and 1,2-reduction.

To further reinforce this mechanism, an isotopic labeling experiment was carried out. According to it, hydrides should be incorporated in the 2- and 4-positions, and protons in the 1- and 3-positions. This outcome was indeed observed when the hydrogenation of 2-methylquinoline (**37c**) was performed either using D<sub>2</sub> or deuterated methanol (Scheme 42A and B).

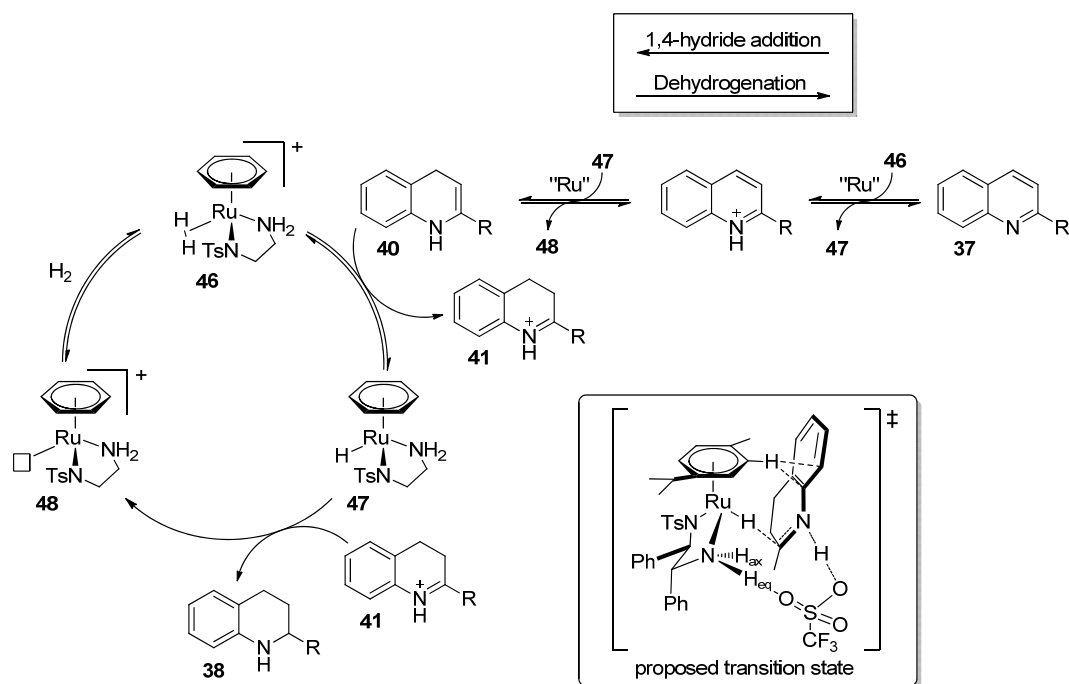


**Scheme 42.** Deuterium labeling experiments for the Ru-catalyzed hydrogenation of quinolines.

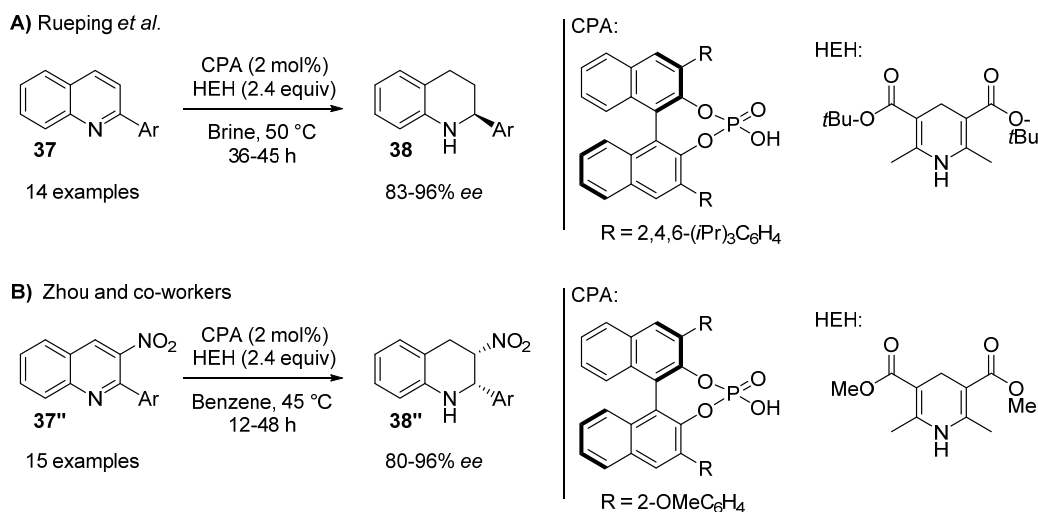
Moreover, the presence of a background transfer hydrogenation was investigated by using deuterated isopropanol and a 16e Ru complex recognized as possible active species in the transfer hydrogenation of aromatic ketones. No evidences were found for this pathway, which hence was excluded.

Finally, to close up the catalytic cycle, the reversibility of the hydrogenation was studied. Although the dehydrogenation of 1,2,3,4-tetrahydroquinolines had been observed using Ir catalysts, this Ru system was unable to catalyze the 1,2-dehydrogenation reaction of tetrahydroquinolines, thus making the C=N hydrogenation an irreversible step. Instead, when 2-phenyl-3,4-dihydroquinoline (**41d**) was hydrogenated with D<sub>2</sub>, deuterium incorporation was observed in the 4-position (Scheme 42C). Besides, less than one deuterium was introduced in the 2-position, since some of the hydrogen atoms derived from the dehydrogenation were also incorporated in that position. This outcome confirms that the initial 1,4-hydride addition is reversible.

According to these evidences, an ionic outer-sphere mechanism, where the hydrogen addition undergoes a stepwise H<sup>+</sup>/H<sup>-</sup> transfer process, was proposed (Scheme 43). The Ru complex **48** can accommodate a molecule of H<sub>2</sub> which, by reaction with quinoline, is heterolytically split to give the quinolinium salt and the Ru-hydride species **47**. The subsequent 1,4-addition gives the 1,4-dihydropyridine and regenerates complex **48**. These steps are reversible and can regenerate the initial quinoline by a dehydrogenation process. The enamine intermediate also acts as a base to split another molecule of H<sub>2</sub> and isomerize to the iminium cation **41**. Finally, an irreversible and enantioselective 1,2-hydride addition affords the final tetrahydroquinoline **38**. According to DFT calculations, this last hydride addition takes place via a cyclic 10-membered transition state with participation of the TfO<sup>-</sup> anion. The enantioselectivity arises from a CH/π interaction between the fused phenyl ring of the dihydroquinoline and a hydrogen of the η<sup>6</sup>-arene ligand.

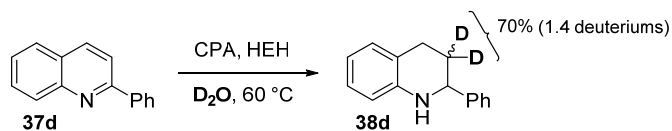


Mechanistic studies on the organocatalytic reduction of 2- and 2,3-substituted quinolines have been carried out respectively by Rueping *et al.* (Scheme 44A)<sup>52d</sup> and by Zhou and co-workers (Scheme 44B).<sup>52g</sup> In both cases the reduction was carried out with stoichiometric amounts of Hantzsch ester derivatives (HEH) and a chiral phosphoric acid (CPA) as catalyst.



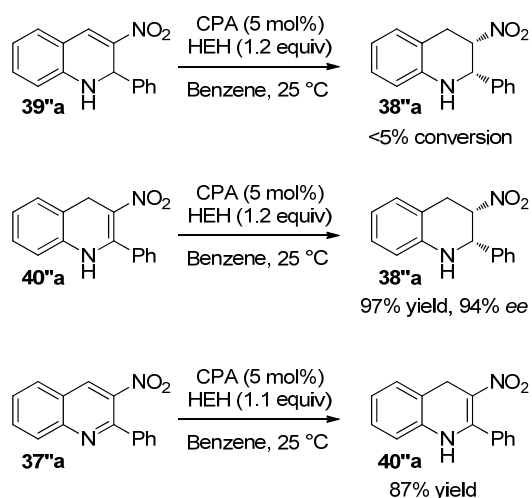
**Scheme 44.** Organocatalytic asymmetric reduction of quinolines.

Rueping performed an isotopic labeling experiment using D<sub>2</sub>O to find out which was the source of protons during the enamine-imine tautomerization step (Scheme 45). The analysis of the product **38d** showed that more than one deuterium had been incorporated in the 3-position, which suggests that water is the proton source and that the tautomerization is faster than the hydride addition, assuming the same mechanism proposed for the metal-catalyzed reactions.



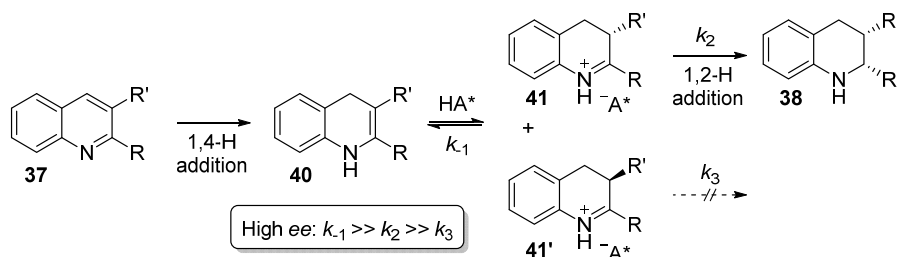
**Scheme 45.** Deuterium labeling experiments for the organocatalytic reduction of quinolines.

In Zhou's investigations, the possible intermediates arising from a 1,4- or a 1,2-hydride addition were isolated and submitted to hydrogenation under the optimized conditions (Scheme 46). In the case of the 1,2-dihydroquinoline **39''a** derivative no reaction took place. Instead, when the 1,4-dihydroquinoline **40''a** intermediate was used as substrate, the final tetrahydroquinoline **38''a** was obtained with the same conversion and *ee* than when the 3-nitro-2-phenylquinoline (**37''a**) was used. Finally, the hydrogenation of the latter quinoline with only one equivalent of hydride, led to the corresponding 1,4-dihydroquinoline as a major product.



**Scheme 46.** Mechanistic studies on the asymmetric reduction of quinolines.

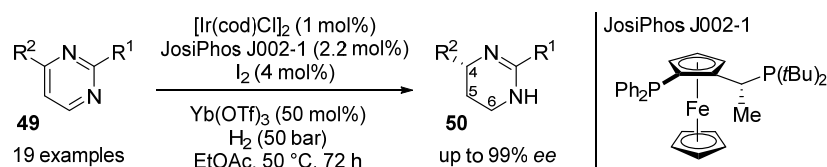
Both studies seem to point towards the same mechanism (Scheme 47). Initially, through a 1,4-hydride addition, the 1,4-dihydroquinoline **40** would be formed. This one would be in fast equilibrium with the imine forms **41** and **41'**, as proven by the deuteration experiment shown in Scheme 45. Finally, the AH of the iminium salt with a chiral counterion would give the final tetrahydroquinoline **38**.



**Scheme 47.** Proposed mechanism for the asymmetric reduction of 2,3-disubstituted quinolines, generalizable to 2-substituted.

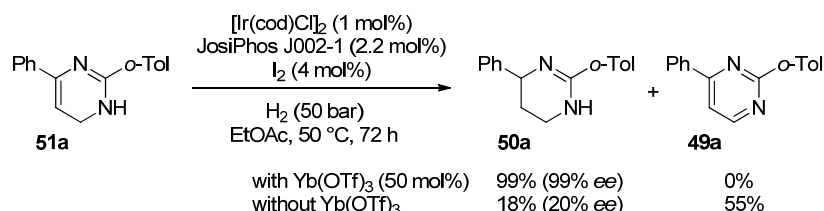
## PYRIMIDINE

The partial AH of pyrimidines gives direct access to chiral amidines, which are recurrent motifs in the nature and in pharmaceutical compounds.<sup>53</sup> Recently, Kuwano *et al.* disclosed the first partial AH of pyrimidines using the well-known Ir-diphosphine-I<sub>2</sub> catalytic system and Yb(OTf)<sub>3</sub> as activator. With this methodology they were able to hydrogenate a series of 2,4-disubstituted pyrimidines into the corresponding 1,4,5,6-tetrahydropyrimidines with high conversion and enantioselectivities (Scheme 48).<sup>54</sup>



**Scheme 48.** Asymmetric hydrogenation of 2,4-disubstituted pyrimidines.

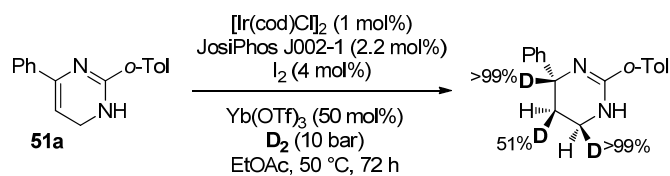
During the hydrogenation process, 1,6-dihydropyrimidine **51a** was observed, suggesting that the reduction proceeds via a stepwise hydrogenation of N1=C6 and C4=C5. When this intermediate was isolated and submitted to the optimized reaction conditions, the final 1,4,5,6-tetrahydropyrimidines **50a** was obtained with full conversion and high *ee*. Instead, if Yb(OTf)<sub>3</sub> was not used, the conversion and *ee* dropped significantly and an important amount of dehydrogenation product **49a** was observed (Scheme 49). This indicates that the Lewis acid is not only required for the initial dearomatization of the pyrimidine, but also for the hydrogenation of intermediate **51a** and to achieve high *ee*'s.



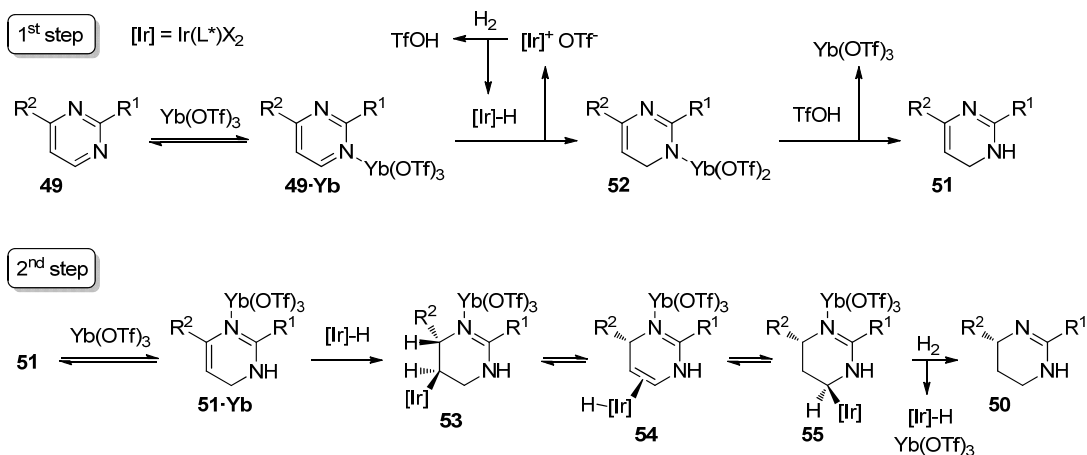
**Scheme 49.** Asymmetric hydrogenation of the 1,6-dihydropyrimidine intermediate.

To gain more insight into the hydrogenation pathway, intermediate **51a** was hydrogenated using D<sub>2</sub> (Scheme 50). Surprisingly, the pro-*S* hydrogen of the 6-position was completely replaced by deuterium. As full deuteration was also observed in the 4-position, the authors proposed that the C4=C5 reduction (Scheme 51, 2<sup>nd</sup> step) proceeds via an initial iridium-catalyzed enantioselective isomerization, to give dihydropyrimidine **51**, followed by C5=C6 hydrogenation. This mechanism is also in agreement with the partial deuteration observed at the 5-position. If the hydrogenation would take place without isomerization, the pro-*R* hydrogen in the 5-position should be fully deuterated. On the contrary, during the migration the deuteride on iridium in intermediate **54** can be replaced by a hydride, leading to this observed partial deuteration in the isotopic labeling experiment. Finally, the Ir complex in intermediate **55** would be released by a  $\sigma$ -bond metathesis with H<sub>2</sub> or by a sequential oxidative addition and reductive elimination. The conversion of pyrimidine **49** to dihydropyrimidine **51** takes places via an initial coordination of the Yb(OTf)<sub>3</sub> to N1 and a hydride addition of the hydridoiridium(III) species.





**Scheme 50.** Isotopic labeling experiment for the AH of 1,6-dihydropyrimidine intermediate.



**Scheme 51.** Proposed mechanism for the AH of 2,4-disubstituted pyrimidines.

### I.3 CONCLUSIONS

Many systems have been developed in the last years for the AH of pyridines, but still, we are far from a highly active and enantioselective system which can be successfully implemented in the industry. The costs of these methodologies are still very high and further investigations have to be conducted in order to improve the current systems.

The best way to rationally design more efficient catalysts for the hydrogenation of pyridines is to understand the different steps that take place during their hydrogenation, where up to three double bonds have to be hydrogenated. Since no mechanism for the AH of pyridines has been reported yet (the only mechanistic study on non-enantioselective transfer hydrogenation of pyridines is a deuterium experiment from Xiao and co-workers)<sup>20</sup> our prior knowledge was mainly based on the studies performed on similar *N*-heteroarenes. Analyzing all mechanistic studies described in this introduction some common facts could be observed:

- All substrates are activated prior to the hydride addition. The substrate is quaternized beforehand by alkylation, acylation or protonation, which in some cases is arising from the acid generated *in situ* during the catalyst activation. In this latter case, it might be also a heterolytic H<sub>2</sub> splitting assisted by the *N*-heteroarene itself. The only exception being the system developed by Mashima and co-workers for the AH of quinoxalines.<sup>32a</sup>
- All hydride additions take place when the substrate is in the imine/iminium form, this involving sometimes a preliminary tautomerization from the enamine form. No enamine or enaminium hydrogenation can be proposed from the experimental data obtained in these

studies. In the cases where only partial hydrogenation is observed, this outcome is ascribed to the high stability of the intermediate formed.

- The latter point implies that, if the enamine intermediate of a *N*-heteroarene substituted only in the  $\beta$ -position is formed, its hydrogenation will lead to very poor *ee*'s, since the enamine-imine tautomerization will create a racemic stereocenter in that position.
- $\alpha,\beta$ -Disubstituted *N*-heteroarenes can be hydrogenated with high enantioselectivities via a dynamic kinetic resolution. Experimentally, this process is optimized at high temperatures, to favor a fast equilibration of the two iminium enantiomers, and at lower pressures, to slow down the hydrogenation step.
- For some substrates it is difficult to determine and to generalize if the first hydrogenation step takes place via a 1,2- or a 1,4-hydride addition. Which pathway is followed seems to depend on both electronic and steric effects.
- The possibility of dehydrogenation processes involved in the mechanism should never be excluded. This competitive process complicates even more the mechanistic studies.

Summarizing, it can be observed that all these mechanisms consist of basically two types of reactions: (i) enamine-imine/iminium tautomerizations and (ii) hydride additions to the imines or iminium ions (either 1,2- or 1,4-additions).

Although consistent efforts have been made to understand these reactions, more mechanistic insight is crucial for further development of the field. Special attention should be given to the mode of enantioinduction in the enantiodetermining step, to the influence of other activating methods and to the mechanism governing the AH of more challenging substrates, such as pyridines. The first part of this thesis accounts for my efforts in this sense.

## CHAPTER II.

# ASYMMETRIC HYDROGENATION OF 2-SUBSTITUTED PYRIDINES

---

### II.1 INTRODUCTION

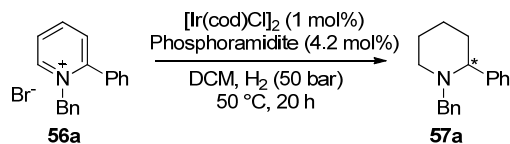
Several efficient approaches have been disclosed for the highly enantioselective hydrogenation of 2-substituted pyridines over the last 10 years. However, they are still far from becoming industrially viable processes. The reports by Charette<sup>13</sup> and by Zhou<sup>16</sup> require very specific pyridine activations, either as *N*-benzoyliminopyridinium ylides (Scheme 4) or as *N*-(2-(isopropoxycarbonyl)benzyl)pyridinium bromide (Scheme 6), respectively. The approach from Zhang,<sup>17</sup> is much more versatile, since many different quaternization strategies can be employed (Scheme 7), but it requires the use of an uncommon chiral phosphole-based ligand.

Although bidentate ligands are generally considered superior to monodentate ones, during the last 15 years monodentate phosphines, phosphonites, phosphoramidites and phosphites have shown to be good competitors. Excellent results have been obtained in the asymmetric hydrogenation (AH) of  $\alpha$ - and  $\beta$ -dehydroamino acids, itaconic acid derivatives, and enamides.<sup>42a,55</sup> Among them, monodentate phosphoramidites are especially appealing because they are cheap, air stable and can be prepared in parallel synthesis, allowing for an easy preparation of structurally diverse chiral phosphoramidite libraries.<sup>56</sup> More recently, they have also been applied in the AH of substituted *N*-protected indoles,<sup>25e</sup> quinoxalines<sup>32c</sup> and quinolines.<sup>44o</sup>

Our goal was set to find a method for the hydrogenation of 2-substituted pyridines employing monodentate phosphoramidites and a simple pyridine quaternization as *N*-benzylpyridinium salts, which could be easily deprotected afterwards. Furthermore, since no mechanistic studies have been performed for the AH of pyridines, we decided to perform a study of the reaction which could help to understand the overall hydrogenation process.

### II.2 RESULTS AND DISCUSSION

For an initial screening of different phosphoramidites available in house, iridium was chosen as metal, since it is the metal of choice for almost all examples of AH of pyridines. Hydrogenation of *N*-benzyl-2-phenylpyridinium bromide was conducted in DCM at 50 °C and under 50 bar of H<sub>2</sub> in a Premex 96er Multireaktor® (Figure 4), where up to 96 hydrogenations can be performed simultaneously.



	1	2	3
<b>A</b>			
<b>B</b>			
<b>C</b>			
<b>D</b>			
<b>E</b>			
<b>F</b>			
<b>G</b>			
<b>H</b>			

Yield (%):

	1	2	3
<b>A</b>	99	63	49
<b>B</b>	99	92	99
<b>C</b>	99	93	29
<b>D</b>	99	23	86
<b>E</b>	33	85	18
<b>F</b>	99	51	89
<b>G</b>	99	70	31
<b>H</b>	18	38	43

0% 100%

ee (%):

	1	2	3
<b>A</b>	21	21	52
<b>B</b>	9	1	20
<b>C</b>	20	15	30
<b>D</b>	30	1	35
<b>E</b>	8	39	13
<b>F</b>	19	6	28
<b>G</b>	7	11	25
<b>H</b>	18	30	1

0% 100%

**Figure 4.** Screening of monodentate phosphoramidites for the AH of *N*-benzyl-2-phenylpyridinium bromide. Reaction conditions: **56a** (0.05 mmol), [Ir(cod)Cl]<sub>2</sub> (1 mol%), phosphoramidite (4.2 mol%), DCM (1 mL), 50 °C, 50 bar H<sub>2</sub>, 20 h. Yield and *ee* (in absolute values) determined by chiral GC with dodecane as internal standard.

Although no highly enantioselective hydrogenation was achieved in the initial screening, some leads could be identified. Looking at the 1,1'-binaphthol backbone, it can be observed that substituents in the 3,3'-positions had a negative effect in the enantioselectivity (Figure 4, A1 vs B1 and D2; D1 vs E1). Similarly, other backbone substitutions, such as the octahydrobinaphthol or the taddol derivative, were not successful in this regard, leaving the 1,1-binaphthol as the best backbone choice. On the other hand, bulky amino groups gave the best performance in this reaction, achieving enantioselectivities up to 52% when using the bis(1-phenylethylamine) **PA2** (Figure 4, A3). Thus, we selected three of them (**PA1**, **PA2** and **PA3**) for the subsequent screening.

A mixed ligand approach is commonly employed when using monodentate ligands. It has been shown that the combination of two different monodentate ligands can sometimes improve the results obtained using those same ligands individually.<sup>44f,57</sup> Hence, the three selected phosphoramidites were screened in presence of an array of achiral alkyl or aryl phosphines or phosphites (Figure 5).

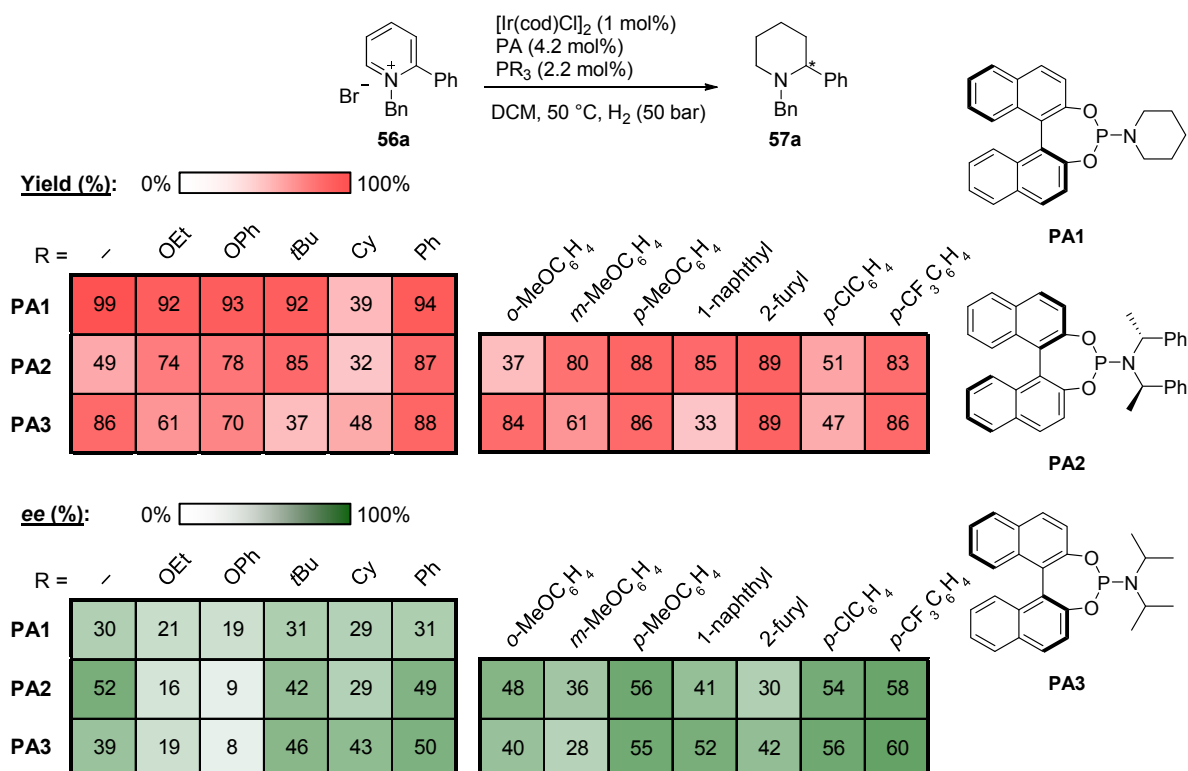


**Figure 5.** Screening of different achiral phosphines and phosphites in combination with three different chiral phosphoramidites for the asymmetric hydrogenation of **56a**. Reaction conditions: **56a** (0.05 mmol), [Ir(cod)Cl]<sub>2</sub> (1 mol%), phosphoramidite (4.2 mol%), phosphine/phosphite (2.2 mol%), DCM (1 mL), 50 °C, 50 bar H<sub>2</sub>, 20 h. Yield and *ee* (in absolute values) determined by chiral GC with dodecane as internal standard. **PA2** gave in all cases the opposite enantiomer than **PA1** and **PA3**.

Surprisingly, diverse behaviors were obtained for the different phosphoramidites. When using **PA1** in combination with an achiral phosphine or phosphite, no major changes were observed in the outcome of the reaction. When **PA2** was employed, the best results were obtained with PPh<sub>3</sub>, which increased substantially the yield without affecting the *ee*. Instead, the combination **PA3** and PPh<sub>3</sub> did not improve the yield, although it slightly increased the enantiomeric excess. Considering these results, **PA2** and **PA3** were screened with a range of electronically and sterically different aromatic phosphines. In both cases, *para*-substituted aromatic phosphines gave the best results, the combination **PA3** and tris(4-trifluoromethylphenyl)phosphine being the best performing (86% yield and 60% *ee*).

Next, we investigated the optimal equivalents of phosphoramidite and phosphine per atom of iridium (Table 6). Initially, only using **PA3** as ligand (entries 1-3), we observed that 2 equivalents were optimal. If more equivalents were used, both activity and *ee* decreased substantially, probably due to saturation of the coordination sites of Ir. When employing only the achiral phosphine, P(*p*-CF<sub>3</sub>C<sub>6</sub>H<sub>4</sub>)<sub>3</sub>, almost no conversion was observed. This means that, although achiral Ir complexes might be formed, they are not active in the hydrogenation of **56a**, and thus no erosion of the *ee* arising from an achiral complex takes place in this case.

**Table 6.** Equivalents of phosphoramidite and phosphine per Ir.

#	<b>PA3</b> (equiv./Ir)	<b>P(<i>p</i>-CF<sub>3</sub>C<sub>6</sub>H<sub>4</sub>)<sub>3</sub></b> (equiv./Ir)	yield (%)	<i>ee</i> (%)
1	1	-	60	17
2	2	-	86	39
3	4	-	31	2
4	-	1	3	-
5	-	2	2	-
6	-	4	0	-
7	1	1	100	76
8	1	1.5	100	77
9	1	2	71	77
10	1	5	33	75
11	1.5	1	100	77
12	2	1	86	60
13	2.5	1	23	38

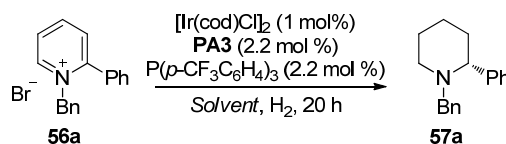
*Reaction conditions:* **56a** (0.05 mmol), [Ir(cod)Cl]<sub>2</sub> (1 mol%), **PA3**, P(*p*-CF<sub>3</sub>C<sub>6</sub>H<sub>4</sub>)<sub>3</sub>, DCM (1 mL), 50 °C, 50 bar H<sub>2</sub>, 20 h. Yield and *ee* determined by chiral GC with dodecane as internal standard.

Then, different phosphoramidite/phosphine ratios were screened. The best results were obtained with ratios of 1:1, 1.5:1 or 1:1.5 (entries 7, 8 and 11), which leads to think that, in the most active and enantioselective catalyst, Ir probably bears one phosphoramidite and one phosphine coordinated. When the amount of phosphine was increased, keeping the equivalents of phosphoramidite constant to one, the enantioselectivity of the reaction was not affected, but

the activity decreased considerably (entries 8-10). This is in agreement with the fact that achiral complexes are not active, so no erosion of the *ee* is observed, but big amounts of ligands saturate the coordination sites of the Ir complex making it less active. Instead, when the amount of phosphine was kept constant and the equivalents of phosphoramidite were increased, both the activity and the *ee* decreased substantially (entries 11-13). This fact is in agreement with the previously observed poor enantioselectivity of the Ir-bis(phosphoramidite) complex. Also in this case an excess of ligands quenches the activity of the catalyst.

Since the obtained results (100% yield, 77% *ee*) were still far from optimal, we tried to optimize other reaction parameters, such as the solvent, the pressure and the temperature (Table 7). Changing the solvent led in all cases to lower yields and lower *ee*'s (entries 1-6). When decreasing the pressure of H<sub>2</sub>, the *ee* remained constant but the yield was slightly affected (entries 7 and 8). Instead, when decreasing the temperature, the enantioselectivity rose to 83% *ee*, but the activity decreased considerably (entries 9 and 10).

**Table 7.** Screening of different solvents and pressure and temperature optimization.



#	Solvent	T (°C)	P <sub>H<sub>2</sub></sub> (bar)	yield (%)	<i>ee</i> (%)
1	DCM	50	50	100	77
2	CF <sub>3</sub> CH <sub>2</sub> OH	50	50	1	43
3	<i>i</i> PrOH	50	50	95	68
4	MeOH	50	50	39	5
5	CH <sub>3</sub> CN	50	50	22	54
6	Toluene	50	50	47	67
7	DCM	50	22	89	77
8	DCM	50	5	85	77
9	DCM	25	22	47	83
10	DCM	25	5	7	81

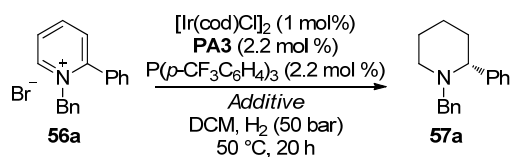
Reaction conditions: **56a** (0.05 mmol), [Ir(cod)Cl]<sub>2</sub> (1 mol%), **PA3** (2.2 mol%), P(*p*-CF<sub>3</sub>C<sub>6</sub>H<sub>4</sub>)<sub>3</sub> (2.2 mol%), solvent (1 mL), H<sub>2</sub>, 20 h. Yield and *ee* determined by chiral GC with dodecane as internal standard.

The effect of the counterion of the pyridinium salt was also assessed. **56a** was reacted for 10 min with AgBF<sub>4</sub>, AgOTf or AgSbF<sub>6</sub> in DCM to exchange the counterion. After filtering off the generated AgBr, the catalyst was added and the hydrogenation was carried out normally. In the three cases, worse yields and *ee*'s were obtained than when using bromide as counterion. Apparently, the presence of bromide is crucial to achieve good results, as Zhou and co-workers demonstrated with their system.<sup>16</sup>

In our last attempt to improve the enantiomeric excess, a few additives were tested. The addition of piperidine hydrochloride showed a positive effect in the hydrogenation of quinoxalines and quinolines with Ir-phosphoramidite catalysts.<sup>32c,44o</sup> Unfortunately, it did not

have any effect in our case, probably because our substrate is already quaternized, while in the mentioned reports the acid might have the role of activating the unprotected quinolines and quinoxalines. The addition of I<sub>2</sub> to an Ir<sup>I</sup> precursor in the presence of a diphosphine ligand has proven to be highly beneficial for the iridium-catalyzed AH of imines and *N*-heteroarenes.<sup>14,9,10b,32b,44e,y,45a,b</sup> After the investigations by Osborn and co-workers, where they showed that Ir<sup>III</sup>-complexes bearing a chelating diphosphine and iodo ligands are active catalyst for the AH of imines, it was proposed that I<sub>2</sub> was oxidatively added to Ir<sup>I</sup> to form the catalytically active Ir<sup>III</sup> complexes.<sup>58</sup> In our system, the addition of I<sub>2</sub> had a negative effect in the activity and the enantioselectivity. Finally, the effect of water in the reaction was assessed, not because we expected an improvement, but because pyridinium salts are very hygroscopic substrates. Fortunately, the results showed that the presence of water had little effect on the reaction outcome.

**Table 8.** Effect of different additives.

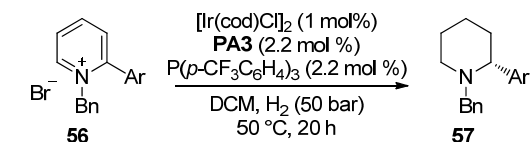


#	Additive (mol%)	yield (%)	ee (%)
1	Piperidine · HCl (10)	100	75
2	Piperidine · HCl (100)	100	75
3	Piperidine · HCl (200)	100	75
4	I <sub>2</sub> (4)	21	17
5	I <sub>2</sub> (8)	8	4
6	H <sub>2</sub> O (1000)	100	73

*Reaction conditions:* **56a** (0.05 mmol), [Ir(cod)Cl]<sub>2</sub> (1 mol%), **PA3** (2.2 mol%), P(*p*-CF<sub>3</sub>C<sub>6</sub>H<sub>4</sub>)<sub>3</sub> (2.2 mol%), DCM (1 mL), 50 °C, 50 bar H<sub>2</sub>, 20 h. Yield and *ee* determined by chiral GC with dodecane as internal standard.

Since we were not able to further optimize the reaction, we decided to perform a small substrate screening, to proof that this system was applicable to other aromatic substituted pyridines (Table 9). Actually the system was not very sensitive to the different electronics of the substituents, since full conversion was obtained in almost all cases and the enantioselectivities obtained ranged from 70 to 82% *ee*, with the exception of the 2-naphthyl substituted which gave only 58% *ee* (entry 7). Furthermore, an experiment performed on a 500 mg scale of substrate gave the expected enantiomeric excess with an isolated yield of 92% (entry 1).



**Table 9.** Asymmetric hydrogenation 2-substituted pyridinium salts.

#	Ar	yield (%)	ee (%)
1	Ph ( <b>56a</b> )	>99 (92) <sup>[a]</sup>	77 (R)
2	4-MeC <sub>6</sub> H <sub>4</sub> ( <b>56b</b> )	>99	71 (+)
3	4-MeOC <sub>6</sub> H <sub>4</sub> ( <b>56c</b> )	>99	82 (+)
4	3,5-diMeOC <sub>6</sub> H <sub>3</sub> ( <b>56d</b> )	99	70 (+)
5	4-CF <sub>3</sub> C <sub>6</sub> H <sub>4</sub> ( <b>56e</b> )	97	74 (+)
6	4-ClC <sub>6</sub> H <sub>4</sub> ( <b>56f</b> )	>99	74 (+)
7	2-naphthyl ( <b>56g</b> )	>99	58 (-)

Reaction conditions: **56** (0.1 mmol), [Ir(cod)Cl]<sub>2</sub> (1 mol%), **PA3** (2.2 mol%), P(*p*-CF<sub>3</sub>C<sub>6</sub>H<sub>4</sub>)<sub>3</sub> (2.2 mol%), DCM (2 mL), 50 °C, 50 bar H<sub>2</sub>, 20 h. Yield and *ee* determined by chiral GC, HPLC or SFC with dodecane as internal standard. [a] Isolated yield of a 500 mg scale experiment.

Even though the obtained enantiomeric excesses are not excellent, this methodology allowed to undertake, for the first time, a mechanistic study on the AH of 2-substituted pyridines, which might be then extrapolated to other Ir-diphosphine systems. Initially, to gain some understanding on the reaction, we monitored the yield and *ee* of different reaction species over time (Figure 6). We observed that after six hours the pyridinium salt **56a** had been almost totally converted to the chiral piperidine **57a**, the *ee* of this latter being constant all along the reaction course.

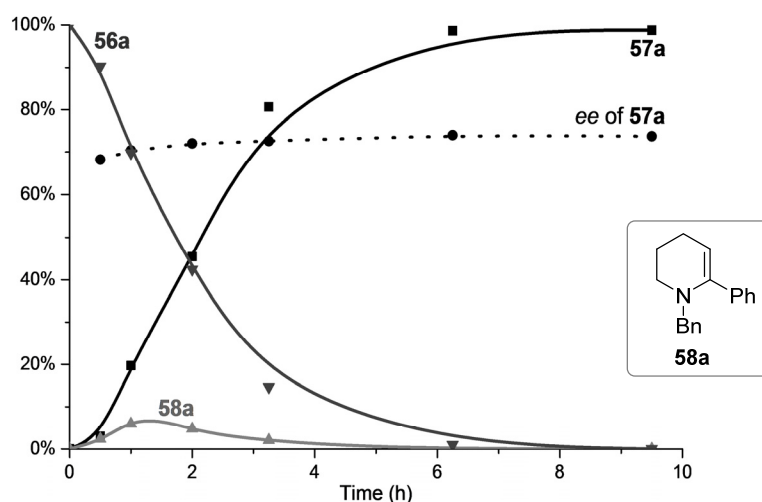


**Figure 6.** Evolution of the yield and *ee* of different reaction species over time. Reaction conditions: **56a** (1.5 mmol), [Ir(cod)Cl]<sub>2</sub> (1 mol%), **PA3** (2 mol%), P(*p*-CF<sub>3</sub>C<sub>6</sub>H<sub>4</sub>)<sub>3</sub> (2 mol%), DCM (30 mL), 50 °C, 50 bar H<sub>2</sub>, 20 h. Yield and *ee* of **57a** and the tetrahydropyridine **58a** determined by chiral GC with dodecane as internal standard. Disappearance of **56a** monitored by NMR with dimethyl terephthalate as internal standard.

During the first two hours another compound was formed, which was then slowly consumed, with a kinetic profile typical of a reaction intermediate. Indeed, as expected, this compound was identified by GC-MS as a tetrahydropyridine ( $m/z = 249$ ). Furthermore, during the screening of phosphoramidites, some of the reactions that were not completed contained a substantial amount of tetrahydropyridine **58a**, which was observable by NMR, along with **56a**, **57a** and other impurities. Although **58a** could not be isolated, consistently with the known instability of these kind of enamines,<sup>59</sup> NMR analysis of the crude (after basic work-up) gave enough evidences to identify **58a** as *N*-benzyl-6-phenyl-1,2,3,4-tetrahydropyridine (Figure 7): the triplet at 4.98 ppm (corresponding to C3)<sup>†</sup> coupling with the triplet-doublet at 2.08 (corresponding to C4) cannot be assigned to any other tetrahydropyridine than the mentioned one. The protons in C6 and the ones in the benzylic position are also observed. Instead, the C5 protons, expected between 1 and 2 ppm, overlap with the piperidine protons. Furthermore, all the observable geminal protons are homotopic, suggesting that no stereogenic center is present in the molecule, which fits with the proposed tetrahydropyridine.

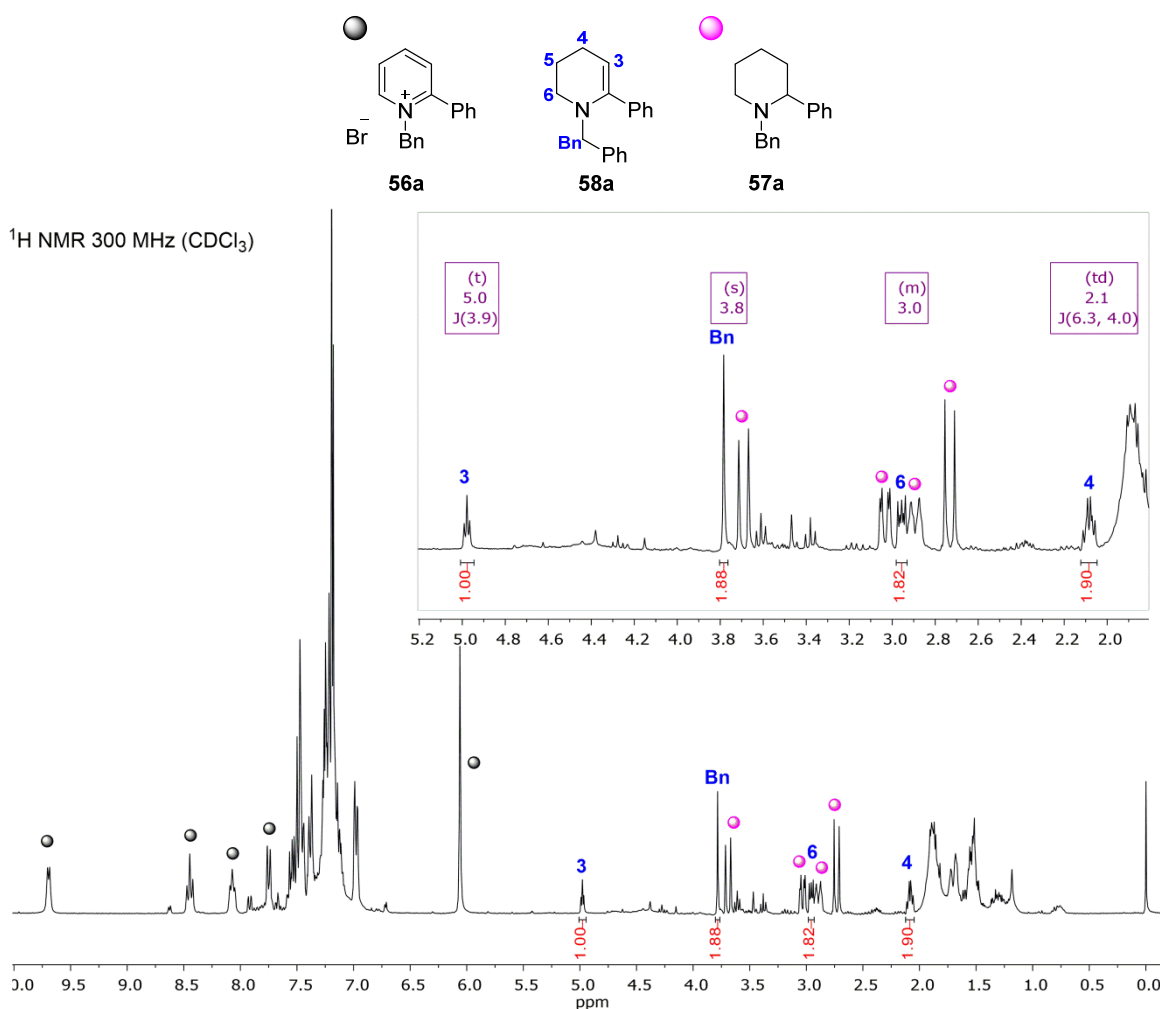


**Figure 7.** Identification of tetrahydropyridine **58a** by  $^1\text{H}$  NMR analysis of a crude mixtures.

<sup>†</sup> For clarity, the carbon numbering on the tetrahydropyridine **58a** follows the same numbering than the final piperidine **57a** and the initial pyridinium salt **56a** and not the IUPAC rules.

In all sampled points, the sum of **56a**, **57a** and **58a** is almost 100%, which suggests that the consumption of the dihydropyridine intermediate is very fast and that the bottleneck of the reaction is the consumption of the tetrahydropyridine.

To further investigate the steps **1a** → **TH** and **TH** → **2a**, isotopic labeling experiments were performed. The assignment of all protons of **57a** was not easy, as all hydrogen atoms in the piperidine ring are diastereotopic. Thus, to be able to ascertain the extent of deuterium incorporation in all positions it was necessary to record the <sup>1</sup>H NMR in two different solvents (CD<sub>3</sub>OD and toluene-d<sub>8</sub>). In each of these solvents, different protons were separated from the rest, allowing for an accurate integration, and the assignment of the chemical shift of each proton was done by multidimensional NMR analysis. Geminal protons were differentiated knowing that in 6-membered rings the axial protons are upfield of the equatorial ones. This shift effect is based on the anisotropy cone of C-C single bonds, as shown in Figure 8. While equatorial protons reside in the deshielding region (+δ), axial protons are in the -δ region.

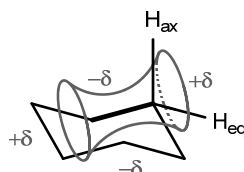
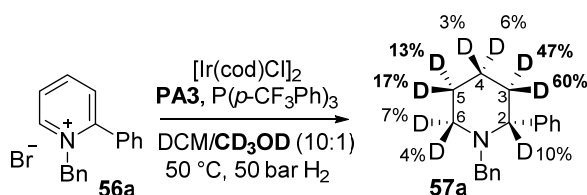


**Figure 8.** Anisotropy cone of a C-C single bond in a cyclohexyl ring.

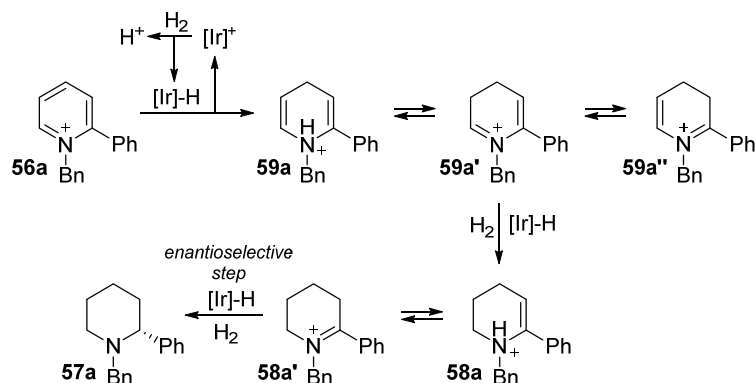
When the optimized reaction was carried out in presence of 10% CD<sub>3</sub>OD (Scheme 52), most of the deuterium was incorporated in C3 (1.07 deuteriums) and C5 (0.30 deuteriums), compared to the other carbons (<0.12 deuteriums each). This observation suggests that two enamine-iminium tautomerizations take place during the reaction, incorporating in this way the deuterium in the β-position of the nitrogen atom. Furthermore, the hydride addition is probably occurring in the iminium form, as previously reported for other *N*-heteroaromatic substrates.<sup>40b,c,f;45a,b;47c;54</sup>



**Scheme 52.** Isotopic labeling experiment in the AH of **56a** with CD<sub>3</sub>OD.

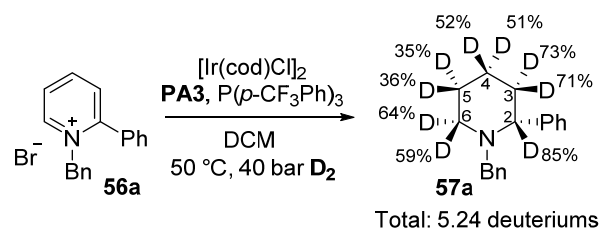
This deuteration pattern leads to hypothesize a mechanism as the one shown in Scheme 53. An initial formation of *N*-benzyl-2-phenyl-1,4-dihydropyridine intermediate (**59a**) via a 1,4-hydride addition to **56a** is consistent with the low deuterium incorporation at C4. Dihydropyridine **59a** would be in equilibrium with the two iminium ions **59a'** and **59a''**, as suggested by deuterium incorporation in C3 and C5 after H/D exchange with CD<sub>3</sub>OD. Moreover, the subsequent hydride addition to **59a'** occurs faster than to **59a''**, whose iminium carbon is more sterically hindered due to the presence of the phenyl substituent, and thus the detected tetrahydropyridine **58a** would be the formed intermediate. Finally, another enamine-

iminium tautomerization of **58a**, with further deuterium incorporation in C3, and subsequent 1,2-hydride addition would lead to the formation of piperidine **57a**.



**Scheme 53.** Proposed mechanism for the formation of **57a** from **56a**.

A second isotopic labeling experiment was carried out in presence of  $D_2$  instead of  $H_2$ . In this case, all the ring positions were deuterated, with a total amount of five deuterium atoms incorporated (Scheme 54). From here we deduced that, when the reaction is performed without protic solvents, the protons formed during the  $H_2$  or  $D_2$  splitting are the ones inserted in the C3 and C5 positions. Moreover, the fact that no ring-face preference is observed for the deuterium incorporation in any of the carbons suggests that the stereogenic center in C2 is not formed until the last step. Otherwise, the presence of a stereocenter in an early reaction intermediate would direct the hydride attacks preferentially to one of the two faces of the heterocycle.



**Scheme 54.** Isotopic labeling experiment in the AH of **56a** with  $D_2$ .

Altogether, the above-discussed isotopic labeling experiment suggests that an initial 1,4-hydride addition to **56a** probably takes place, forming the dihydropyridine **59a**. The latter is readily hydrogenated to **58a**, which is the only reaction intermediate detected by NMR and GC. Finally, the enantioselective 1,2-hydride addition to the iminium **58a'** would lead to the final piperidine **57a**, as shown in the proposed mechanism in Scheme 53.

## II.3 CONCLUSIONS

To sum up, we have been able to develop a new system for the asymmetric hydrogenation of *N*-benzyl-2-arylpyridinium bromides using an iridium catalyst and a mixed ligand system, containing a chiral phosphoramidite and an achiral phosphine. Although only *ee*'s up to 82% were

achieved, this approach demonstrates that the use of cheap and easy to prepare monodentate ligands is also suitable for this challenging transformation. Furthermore, the performed mechanistic study sheds light on the pyridine hydrogenation pathway, and shows that the enantioselective step does not occur until the very last step. This will hopefully allow for a better understanding of the system and the rational design of more active and enantioselective systems.

## II.4 EXPERIMENTAL SECTION

Dry DCM was obtained using an MBraun SPS system. Dry MeOH, EtOH, *i*PrOH and toluene (over molecular sieves in bottles with crown cap) were purchased from Sigma Aldrich and stored under nitrogen. 2,2,2-trifluoroethanol (TFE) was dried over molecular sieves. Commercially available reagents (from TCI Chemicals, ACROS, Sigma Aldrich, Strem) were used as received, without any further purification.

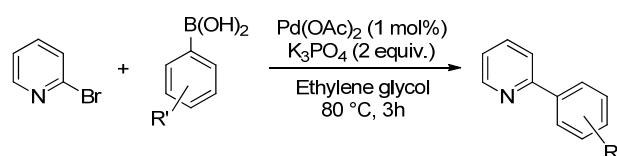
Flash column chromatography was performed using Grace Reveleris® X2 Flash Chromatography System (silica gel cartridges with particle size 40  $\mu\text{m}$ ). Gas chromatography was performed on an Agilent Technologies 7890A equipped with a flame ionization detector. HPLC analyses were performed using a Waters HPLC with a dual  $\lambda$  absorbance detector working at 210 and 254 nm. SFC analyses were performed using a THAR SFC.

$^1\text{H}$ -NMR spectra were recorded using two different spectrometers operating at 400 or 500 MHz. Proton chemical shifts are reported in ppm ( $\delta$ ) with the solvent reference relative to tetramethylsilane (TMS) employed as the internal standard ( $\text{CDCl}_3$   $\delta$  = 7.26 ppm;  $\text{CD}_2\text{Cl}_2$   $\delta$  = 5.32 ppm,  $\text{CD}_3\text{OD}$   $\delta$  = 3.31 ppm, toluene- $d_8$   $\delta$  = 7.09, 7.01, 6.97 and 2.08).  $^{13}\text{C}$ -NMR spectra were recorded on a 400 MHz spectrometer operating at 101 MHz, with complete proton decoupling. Carbon chemical shifts are reported in ppm ( $\delta$ ) relative to TMS with the respective solvent resonance as the internal standard ( $\text{CDCl}_3$ ,  $\delta$  = 77.16 ppm,  $\text{CD}_2\text{Cl}_2$   $\delta$  = 53.84 ppm,  $\text{CD}_3\text{OD}$   $\delta$  = 49.00 ppm).  $^{19}\text{F}$ -NMR spectra were recorded on a 300 MHz spectrometer operating at 282 MHz, with complete proton decoupling. Fluorine chemical shifts are reported in ppm ( $\delta$ ) relative to external  $\text{CFCl}_3$  at 0 ppm (positive values downfield). The following abbreviations are used to describe spin multiplicity: s = singlet, d = doublet, t = triplet, q = quartet, m = multiplet, dd = doublet-doublet, ddd = doublet-doublet-doublet, dt = doublet-triplet, td = triplet-doublet. Coupling constant values are given in Hz.

Optical rotation signs were determined on an automatic polarimeter with a 1 dm cell at the sodium D line ( $\lambda$  = 589 nm). High resolution mass spectra (HRMS) were performed on a Fourier Transform Ion Cyclotron Resonance (FT-ICR) Mass Spectrometer APEX II & Xmass software (Bruker Daltonics) – 4.7 T Magnet (Magnex) equipped with ESI source. Infrared spectra were recorded on a standard FT/IR spectrometer.

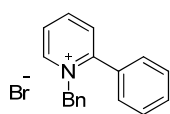
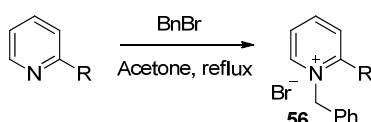
### General procedure for the synthesis of 2-arylpyridines

A mixture of 2-bromopyridine **63** (1 ml, 9.9 mmol), the boronic acid (14.9 mmol, 1.5 equiv.), Pd(OAc)<sub>2</sub> (22 mg, 0.1 mmol), K<sub>3</sub>PO<sub>4</sub> (4.2 g, 19.8 mmol) and 75 mL of ethylene glycol were stirred at 80 °C for 5 h. Once the reaction was completed, the reaction mixture was poured into 150 mL of brine and extracted with 150 mL of Et<sub>2</sub>O. NaOH (7.5 g) was added to the ethereal phase and the mixture was stirred for 15 min. Then it was poured into 150 mL of brine, the ethereal phase was again separated and stirred in the presence of NaOH (7.5 g). After 15 min more, the mixture was poured one last time into 150 mL of brine and the ethereal phase was separated, dried over Na<sub>2</sub>SO<sub>4</sub>, filtered and concentrated several times in the presence of MeOH. The obtained 2-arylpyridine was used in the next step without any further purification.



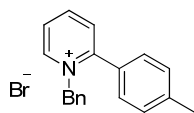
### General procedure for the benzylation of pyridines

Pyridinium salts **56** were prepared according to known literature methods.<sup>16,60</sup> A mixture of 2-arylpyridine (12.9 mmol), benzyl bromide (15.5 mmol, 1.2 equiv.) and 5.0 mL acetone were stirred under reflux temperature for 18-48h. If the product precipitated, it was filtered, washed several times with acetone and dried under high vacuum. If the product did not precipitate, the solvent was removed and the resulting sticky oil was recrystallized from MeOH/AcOEt (9:1). The desired products were obtained with yields ranging from 42-95% yield.



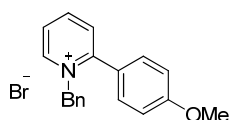
#### **N-Benzyl-2-phenylpyridinium bromide (56a):**

Known compound. Spectroscopic data are superimposable to those reported in the literature.<sup>61</sup>

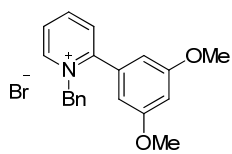


#### **N-Benzyl-2-(p-tolyl)pyridinium bromide (56b):** White solid; m.p. = 172 °C;

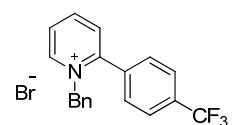
<sup>1</sup>H NMR (400 MHz, MeOD) δ 9.15 (dd, <sup>3</sup>J(H,H) = 6.3 Hz, <sup>4</sup>J(H,H) = 0.7 Hz, 1H), 8.67 (td, <sup>3</sup>J(H,H) = 7.9 Hz, <sup>4</sup>J(H,H) = 1.3 Hz, 1H), 8.16 (td, <sup>3</sup>J(H,H) = 7.0 Hz, <sup>4</sup>J(H,H) = 1.3 Hz, 1H), 8.05 (dd, <sup>3</sup>J(H,H) = 7.9 Hz, <sup>4</sup>J(H,H) = 0.8 Hz, 1H), 7.45 – 7.37 (m, 4H), 7.35 – 7.27 (m, 3H), 7.02 – 6.95 (m, 2H), 5.83 (s, 2H), 2.47 (s, 3H); <sup>13</sup>C NMR (101 MHz, MeOD) δ 157.9, 147.4, 143.4, 134.8, 132.3, 131.0, 130.3, 130.3, 130.2, 130.1, 129.0, 128.3, 63.3, 21.5; IR (film): ν = 3079.8, 3035.4, 1622.8, 1496.5, 1455.0 cm<sup>-1</sup>; MS (ESI+): m/z 246.2 [M]<sup>+</sup> (calcd. for C<sub>19</sub>H<sub>18</sub>N: 260.14).



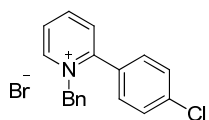
**N-Benzyl-2-(4-methoxyphenyl)pyridinium bromide (56c):** White solid; m.p. = 162 °C;  $^1\text{H}$  NMR (400 MHz, MeOD)  $\delta$  9.13 (dd,  $^3J(\text{H,H}) = 6.3$  Hz,  $^4J(\text{H,H}) = 0.9$  Hz, 1H), 8.65 (td,  $^3J(\text{H,H}) = 7.9$  Hz,  $^4J(\text{H,H}) = 1.4$  Hz, 1H), 8.13 (ddd,  $^3J(\text{H,H}) = 7.7$  Hz,  $^3J(\text{H,H}) = 6.4$  Hz,  $^4J(\text{H,H}) = 1.5$  Hz, 1H), 8.05 (dd,  $^3J(\text{H,H}) = 8.0$  Hz,  $^4J(\text{H,H}) = 1.1$  Hz, 1H), 7.49 – 7.42 (m, 2H), 7.35 – 7.30 (m, 3H), 7.16 – 7.09 (m, 2H), 7.03 – 6.95 (m, 2H), 5.86 (s, 2H), 3.90 (s, 3H);  $^{13}\text{C}$  NMR (101 MHz, MeOD)  $\delta$  163.6, 157.9, 147.4, 147.3, 134.9, 132.4, 132.0, 130.3, 130.3, 129.0, 128.0, 125.0, 115.8, 63.2, 56.2; IR (film):  $\nu = 3068.2, 3006.5, 1621.8, 1608.3, 1495.5, 1456.0, 1255.4, 1182.2$   $\text{cm}^{-1}$ ; MS (ESI+):  $m/z$  276.2  $[\text{M}]^+$  (calcd. for  $\text{C}_{19}\text{H}_{18}\text{NO}$ : 276.14).



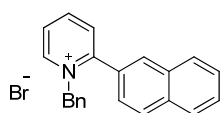
**N-Benzyl-2-(3,5-dimethoxyphenyl)pyridinium bromide (56d):** Orange solid; m.p. = 69 °C;  $^1\text{H}$  NMR (400 MHz, MeOD)  $\delta$  9.18 (d,  $^3J(\text{H,H}) = 5.9$  Hz, 1H), 8.70 (t,  $^3J(\text{H,H}) = 7.6$  Hz, 1H), 8.20 (t,  $^3J(\text{H,H}) = 6.6$  Hz, 1H), 8.09 (d,  $^3J(\text{H,H}) = 7.7$  Hz, 1H), 7.42 – 7.32 (m, 3H), 7.09 – 6.99 (m, 2H), 6.72 (m, 1H), 6.62 (t,  $^3J(\text{H,H}) = 1.9$  Hz, 2H), 5.85 (s, 2H), 3.78 (s, 6H);  $^{13}\text{C}$  NMR (101 MHz, MeOD)  $\delta$  161.5, 156.1, 146.2, 146.1, 133.6, 133.0, 130.7, 129.0, 128.9, 127.6, 127.3, 106.8, 102.9, 62.2, 55.0; IR (film):  $\nu = 3093.3, 1626.7, 1603.5, 1455.0, 1424.2, 1206.3, 1159.0$   $\text{cm}^{-1}$ ; MS (ESI+):  $m/z$  306.2  $[\text{M}]^+$  (calcd. for  $\text{C}_{20}\text{H}_{20}\text{NO}_2$ : 306.15).



**N-Benzyl-2-(4-(trifluoromethyl)phenyl)pyridinium bromide (56e):** White solid; m.p. = 185 °C;  $^1\text{H}$  NMR (400 MHz, MeOD)  $\delta$  9.28 (d,  $^3J(\text{H,H}) = 5.7$  Hz, 1H), 8.77 (td,  $^3J(\text{H,H}) = 7.9$  Hz,  $^4J(\text{H,H}) = 1.3$  Hz, 1H), 8.27 (ddd,  $^3J(\text{H,H}) = 7.7$  Hz,  $^3J(\text{H,H}) = 6.3$  Hz,  $^4J(\text{H,H}) = 1.4$  Hz, 1H), 8.13 (dd,  $^3J(\text{H,H}) = 7.9$  Hz,  $^4J(\text{H,H}) = 1.1$  Hz, 1H), 7.87 (d,  $^3J(\text{H,H}) = 8.3$  Hz, 2H), 7.73 (d,  $^3J(\text{H,H}) = 8.2$  Hz, 2H), 7.38 – 7.24 (m, 3H), 6.97 (d,  $^3J(\text{H,H}) = 7.0$  Hz, 2H), 5.86 (s, 2H);  $^{13}\text{C}$  NMR (101 MHz, MeOD)  $\delta$  155.8, 148.0, 147.9, 136.7 (q,  $^4J(\text{C,F}) = 1.6$  Hz), 134.4, 134.0 (q,  $^2J(\text{C,F}) = 32.8$  Hz), 132.3, 131.3, 130.3, 129.2, 129.1, 127.2 (q,  $^3J(\text{C,F}) = 3.7$  Hz), 125.0 (q,  $^1J(\text{C,F}) = 272.0$  Hz), 63.9;  $^{19}\text{F}$  NMR (282 MHz, MeOD)  $\delta$  -64.9; IR (film):  $\nu = 3057.6, 2967.9, 1623.8, 1616.1, 1458.9, 1323.9, 1169.6, 1123.3, 1071.3, 849.5$   $\text{cm}^{-1}$ ; MS (ESI+):  $m/z$  314.1  $[\text{M}]^+$  (calcd. for  $\text{C}_{19}\text{H}_{15}\text{F}_3\text{N}$ : 314.12).



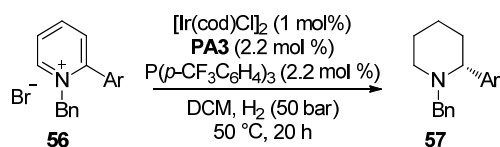
**N-Benzyl-2-(4-chlorophenyl)pyridinium bromide (56f):** White solid; m.p. = 101 °C;  $^1\text{H}$  NMR (400 MHz,  $\text{CDCl}_3$ )  $\delta$  9.56 (dd,  $^3J(\text{H,H}) = 6.2$  Hz,  $^4J(\text{H,H}) = 0.8$  Hz, 1H), 8.61 (td,  $^3J(\text{H,H}) = 7.8$  Hz,  $^4J(\text{H,H}) = 1.2$  Hz, 1H), 8.19 (ddd,  $^3J(\text{H,H}) = 7.7$  Hz,  $^3J(\text{H,H}) = 6.4$  Hz,  $^4J(\text{H,H}) = 1.4$  Hz, 1H), 7.82 (dd,  $^3J(\text{H,H}) = 7.9$  Hz,  $^4J(\text{H,H}) = 1.3$  Hz, 1H), 7.55 – 7.47 (m, 2H), 7.47 – 7.37 (m, 2H), 7.29 – 7.13 (m, 3H), 6.99 – 6.87 (m, 2H), 5.98 (s, 2H);  $^{13}\text{C}$  NMR (101 MHz,  $\text{CDCl}_3$ )  $\delta$  154.7, 147.5, 146.3, 138.1, 133.0, 130.8, 130.5, 129.8, 129.8, 129.5, 129.5, 128.5, 128.1, 62.7; IR (film):  $\nu = 3068.2, 3039.3, 1621.8, 1483.0, 1455.0, 1090.6$   $\text{cm}^{-1}$ ; MS (ESI+):  $m/z$  280.1  $[\text{M}]^+$  (calcd. for  $\text{C}_{18}\text{H}_{15}\text{ClN}$ : 280.09).



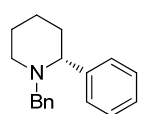
**N-Benzyl-2-(naphthalen-2-yl)pyridinium bromide (56g):** White solid; m.p. = 175 °C;  $^1\text{H}$  NMR (400 MHz, MeOD)  $\delta$  9.24 (dd,  $^3J(\text{H,H}) = 6.3$  Hz,  $^4J(\text{H,H}) = 1.0$  Hz, 1H), 8.72 (td,  $^3J(\text{H,H}) = 7.8$  Hz,  $^4J(\text{H,H}) = 1.4$  Hz, 1H),

8.20 (ddd,  $^3J(\text{H,H}) = 7.8$  Hz,  $^3J(\text{H,H}) = 6.3$ ,  $^4J(\text{H,H}) = 1.5$  Hz, 1H), 8.11 (dd,  $^3J(\text{H,H}) = 7.9$  Hz,  $^4J(\text{H,H}) = 1.3$  Hz, 1H), 8.08 – 8.01 (m, 2H), 7.98 (d,  $^3J(\text{H,H}) = 7.6$  Hz, 1H), 7.93 (d,  $^3J(\text{H,H}) = 7.6$  Hz, 1H), 7.69 – 7.53 (m, 3H), 7.29 – 7.15 (m, 3H), 6.92 (d,  $^3J(\text{H,H}) = 7.3$  Hz, 2H), 5.88 (s, 2H);  $^{13}\text{C}$  NMR (101 MHz, MeOD)  $\delta$  157.4, 147.5, 135.2, 134.5, 133.8, 132.4, 131.0, 130.3, 130.2, 130.2, 130.1, 129.8, 129.5, 129.0, 129.0, 128.7, 128.5, 125.9, 63.4; IR (film):  $\nu = 3055.7$ , 1619.9, 1573.6, 1498.4, 1455.0, 1273.8, 1159.0  $\text{cm}^{-1}$ ; MS (ESI+):  $m/z$  296.2  $[\text{M}]^+$  (calcd. for  $\text{C}_{22}\text{H}_{18}\text{N}$ : 296.14).

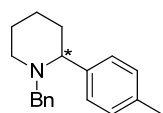
### General procedure for the asymmetric hydrogenation of pyridinium salts



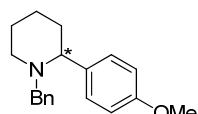
A solution of  $[\text{Ir}(\text{cod})\text{Cl}]_2$  (0.001 mmol), **PA3** (0.0022 mmol) and  $\text{P}(p\text{-CF}_3\text{C}_6\text{H}_4)_3$  (0.0022 mmol) in DCM (1 mL) was stirred at 45 °C for 30 min. The preformed catalyst was added to a 5 mL vial containing a solution of the corresponding *N*-benzyl-2-arylpyridinium bromide (0.1 mmol) in DCM (1 mL). The vial was capped with a PTFE septum, removed from the glovebox and placed into a Premex 96er Multireaktor<sup>®</sup>. After flushing it 5 times with  $\text{N}_2$  and 5 times with  $\text{H}_2$ , it was pressurized to 50 bar of  $\text{H}_2$  and stirred at 50 °C for 18 h.



**(R)-(+)-*N*-Benzyl-2-phenylpiperidine (57a)**: Known compound. Spectroscopic data are superimposable to those reported in the literature.<sup>20</sup> Absolute configuration assigned by comparison of the sign of the optical rotation with literature data.<sup>62</sup> Yield and enantiomeric excess determined by GC: CP-Chirasil-Dex CB (25m x 0.25mm, 0.25 $\mu\text{m}$ ); carrier: helium; gas flow: 2.7 bar; isotherm at 150 °C:  $t_s = 27.3$  min.,  $t_R = 27.8$  min.,  $t_{\text{TH}} = 38.5$  min. Alternative enantiomeric excess determination by SFC: Lux Cellulose-3 (250 x 4.6 mm); 200 Bar; 254 nm; 40 °C; isocratic  $\text{CO}_2/\text{MeOH}$  with 25 mM DEA = 9:1, 4 mL/min:  $t_R = 2.0$  min.,  $t_S = 2.3$  min.

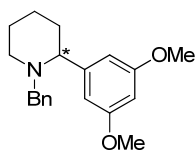


**(+)-*N*-Benzyl-2-(4-tolyl)piperidine (57b)**: Known compound. Spectroscopic data are superimposable to those reported in the literature.<sup>17</sup> Yield determined by GC: CP-Chirasil-Dex CB (25m x 0.25mm, 0.25 $\mu\text{m}$ ); carrier: helium; gas flow: 2.7 bar; oven temperature: isotherm at 160 °C:  $t_{57b} = 25.1$  min. Enantiomeric excess determined by SFC: Lux Cellulose-3 (250 x 4.6 mm); 200 Bar; 254 nm; 40 °C; isocratic  $\text{CO}_2/\text{MeOH}$  with 25 mM DEA = 9:1, 4 mL/min:  $t_{(+)} = 1.7$  min.,  $t_{(-)} = 2.1$  min.

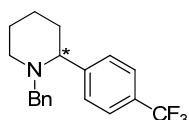


**(+)-*N*-Benzyl-2-(4-methoxyphenyl)piperidine (57c)**: Known compound. Spectroscopic data are superimposable to those reported in the literature.<sup>17</sup> Yield determined by GC: CP-Chirasil-Dex CB (25m x 0.25mm, 0.25 $\mu\text{m}$ ); carrier: helium; gas flow: 2.7 bar; oven temperature: isotherm at 170 °C:  $t_{57c} = 31.1$  min. Enantiomeric excess determined by HPLC: Lux Cellulose-3 (250 x 4.6 mm); 254 nm; isocratic Hexane/*i*PrOH/DEA 98:2:0.05, 0.7 mL/min:  $t_{(+)} = 8.2$  min.,  $t_{(-)} = 9.3$  min.

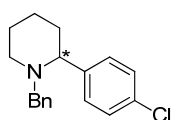




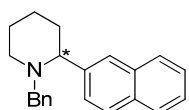
**(+)-N-Benzyl-2-(3,5-dimethoxyphenyl)piperidine (57d):**  $^1\text{H}$  NMR (400 MHz,  $\text{CD}_2\text{Cl}_2$ )  $\delta$  7.33 – 7.23 (m, 4H), 7.18 (m, 1H), 6.65 (s, 2H), 6.32 (m, 1H), 3.79 (m, 6H), 3.06 (d,  $J = 10.8$  Hz, 1H), 2.92 (d,  $J = 11.6$  Hz, 1H), 2.80 (d,  $J = 13.6$  Hz, 1H), 1.93 (td,  $J = 11.4, 2.2$  Hz, 1H), 1.82 – 1.72 (m, 2H), 1.67 – 1.48 (m, 4H), 1.37 (m, 1H);  $^{13}\text{C}$  NMR (101 MHz,  $\text{CD}_2\text{Cl}_2$ )  $\delta$  161.4, 149.0, 140.6, 129.0, 128.4, 126.9, 105.7, 99.2, 69.9, 60.1, 55.7, 53.7, 37.2, 26.5, 25.6; IR (film):  $\nu = 2933.2, 2852.2, 1607.4, 1594.8, 1454.1, 1427.1, 1203.4, 1154.2, 1061.6$   $\text{cm}^{-1}$ ; HRMS (ESI+):  $m/z$  312.19643  $[\text{M}+\text{H}]^+$  (calcd. for  $\text{C}_{20}\text{H}_{26}\text{NO}_2$ : 312.19581). Yield determined by GC: CP-Chirasil-Dex CB (25m x 0.25mm, 0.25 $\mu\text{m}$ ); carrier: helium; gas flow: 2.7 bar; oven temperature: 170  $^\circ\text{C}$  (60 min), 20  $^\circ\text{C}/\text{min}$ , 190  $^\circ\text{C}$  (10 min):  $t_{57d} = 61.7$  min. Enantiomeric excess determined by SFC: Lux Cellulose-3 (250 x 4.6 mm); 200 Bar; 254 nm; 40  $^\circ\text{C}$ ; isocratic  $\text{CO}_2/\text{MeOH}$  with 25 mM DEA = 9:1, 4 mL/min:  $t_{(-)} = 1.6$  min.,  $t_{(+)} = 1.8$  min.



**(+)-N-Benzyl-2-(4-(trifluoromethyl)phenyl)piperidine (57e):**  $^1\text{H}$  NMR (400 MHz,  $\text{CD}_2\text{Cl}_2$ )  $\delta$  7.65 – 7.56 (m, 4H), 7.31 – 7.23 (m, 4H), 7.20 (m, 1H), 3.67 (d,  $J = 13.6$  Hz, 1H), 3.22 (dd,  $J = 11.0, 2.9$  Hz, 1H), 2.95 (m, 1H), 2.84 (d,  $J = 13.6$  Hz, 1H), 1.97 (td,  $J = 11.6, 3.3$  Hz, 1H), 1.85 – 1.71 (m, 2H), 1.67 – 1.50 (m, 3H), 1.40 (m, 1H);  $^{13}\text{C}$  NMR (101 MHz,  $\text{CD}_2\text{Cl}_2$ )  $\delta$  150.8, 140.0, 129.0, 128.5, 128.3, 127.1, 125.9 (q,  $^3J(\text{C},\text{F}) = 3.7$  Hz), 124.9 (q,  $^1J(\text{C},\text{F}) = 273.9$  Hz), 69.2, 60.3, 53.6, 37.5, 26.4, 25.5;  $^{19}\text{F}$  NMR (282 MHz,  $\text{CD}_2\text{Cl}_2$ )  $\delta$  -63.1; IR (film):  $\nu = 2935.1, 2855.1, 2793.4, 1324.9, 1162.9, 1124.3, 1067.4, 834.1$   $\text{cm}^{-1}$ ; HRMS (ESI+):  $m/z$  320.16295  $[\text{M}+\text{H}]^+$  (calcd. for  $\text{C}_{19}\text{H}_{21}\text{NF}_3$ : 320.16206). Yield determined by GC: CP-Chirasil-Dex CB (25m x 0.25mm, 0.25 $\mu\text{m}$ ); carrier: helium; gas flow: 2.7 bar; oven temperature: isotherm at 150  $^\circ\text{C}$ :  $t_{57e} = 29.7$  min. Enantiomeric excess determined by HPLC: Lux Cellulose-3 (250 x 4.6 mm); 254 nm; isocratic Hexane + 0.05% DEA, 0.7 mL/min:  $t_{(+)} = 8.7$  min.,  $t_{(-)} = 8.9$  min.



**(+)-N-Benzyl-2-(4-chlorophenyl)piperidine (57f):** Known compound. Spectroscopic data are superimposable to those reported in the literature.<sup>17</sup> Yield determined by GC: CP-Chirasil-Dex CB (25m x 0.25mm, 0.25 $\mu\text{m}$ ); carrier: helium; gas flow: 2.7 bar; oven temperature: 150  $^\circ\text{C}$  (60 min), 20  $^\circ\text{C}/\text{min}$ , 190  $^\circ\text{C}$  (10 min):  $t_{57f} = 63.2$  min. Enantiomeric excess determined by SFC: Lux Cellulose-3 (250 x 4.6 mm); 200 Bar; 254 nm; 40  $^\circ\text{C}$ ; isocratic  $\text{CO}_2/\text{MeOH}$  with 25 mM DEA = 9:1, 4 mL/min:  $t_{(+)} = 2.2$  min.,  $t_{(-)} = 2.4$  min.



**(-)-N-Benzyl-2-(naphthalen-2-yl)piperidine (57g):** Known compound. Spectroscopic data are superimposable to those reported in the literature.<sup>17</sup> Yield determined by GC: CP-Chirasil-Dex CB (25m x 0.25mm, 0.25 $\mu\text{m}$ ); carrier: helium; gas flow: 2.7 bar; oven temperature: isotherm at 190  $^\circ\text{C}$ :  $t_{57g} = 36.7$  min. Enantiomeric excess determined by SFC: Lux Cellulose-3 (250 x 4.6 mm); 200 Bar; 254 nm; 40  $^\circ\text{C}$ ; isocratic  $\text{CO}_2/\text{MeOH}$  with 25 mM DEA = 9:1, 4 mL/min:  $t_{(+)} = 5.1$  min.,  $t_{(-)} = 5.8$  min.

**Monitoring of the reaction over time:**

A solution of  $[\text{Ir}(\text{cod})\text{Cl}]_2$  (10.3 mg, 0.015 mmol), **PA3** (14.0 mg, 0.034 mmol) and  $\text{P}(p\text{-CF}_3\text{C}_6\text{H}_4)_3$  (15.8 mg, 0.033 mmol) in DCM (15 mL) was stirred at 45 °C for 30 min. The preformed catalyst was added to a 50 mL vial containing a solution of the corresponding *N*-benzyl-2-phenylpyridinium bromide **1a** (503.38 mg, 1.53 mmol), dodecane (420.00 mg) and dimethyl terephthalate (145.98 mg) in DCM (15 mL). The autoclave was closed and taken out of the glovebox. After flushing it 5 times with  $\text{N}_2$ , it was pressurized to 50 bar of  $\text{H}_2$  and stirred at 50 °C for 10 h with sampling at different times. All samples were analyzed by chiral GC and NMR (results shown in Table 10).

**Table 10.** Yield and ee of different species involved in the AH of 60a to 61a.

Time (h)	<b>56a</b> (%) <sup>[a]</sup>	<b>57a</b> (%) <sup>[b]</sup>	<i>ee</i> of <b>57a</b> (%) <sup>[b]</sup>	<b>TH</b> (%) <sup>[b]</sup>
0	100	0	-	0
0.5	90	3	68	2
1	70	20	70	6
2	42	46	72	5
3.25	15	81	73	2
6.25	1	99	74	0
9.5	0	99	74	0

[a] Determined by NMR with dimethyl terephthalate as internal standard.

[b] Determined by GC analysis with CP-Chirasil-Dex CB column with dodecane as internal standard. Positive values of *ee* correspond to *S* configuration.

**Isotopic labeling experiments:**

**With  $\text{CD}_3\text{OD}$ .** Inside a glovebox, a solution of  $[\text{Ir}(\text{cod})\text{Cl}]_2$  (0.0015 mmol), **PA3** (0.0033 mmol) and  $\text{P}(p\text{-CF}_3\text{C}_6\text{H}_4)_3$  (0.0033 mmol) in DCM (1 mL) was stirred at 45 °C for 30 min. The preformed catalyst was added to a 5 mL vial containing a solution of the corresponding *N*-benzyl-2-arylpyridinium bromide (0.15 mmol) in DCM (2 mL) and  $\text{CD}_3\text{OD}$  (0.3 mL). The vial was capped with a PTFE septum, removed from the glovebox and placed into a Premex 96er Multireaktor®. After flushing it 5 times with  $\text{N}_2$  and 5 times with  $\text{H}_2$ , it was pressurized to 50 bar of  $\text{H}_2$  and stirred at 50 °C for 18 h. The crude mixture was washed with saturated aqueous solution of  $\text{Na}_2\text{CO}_3$  and extracted with DCM. The organic extracts were dried, concentrated and purified by flash column chromatography Hexane/EtOAc (from 99:1 to 95:5).

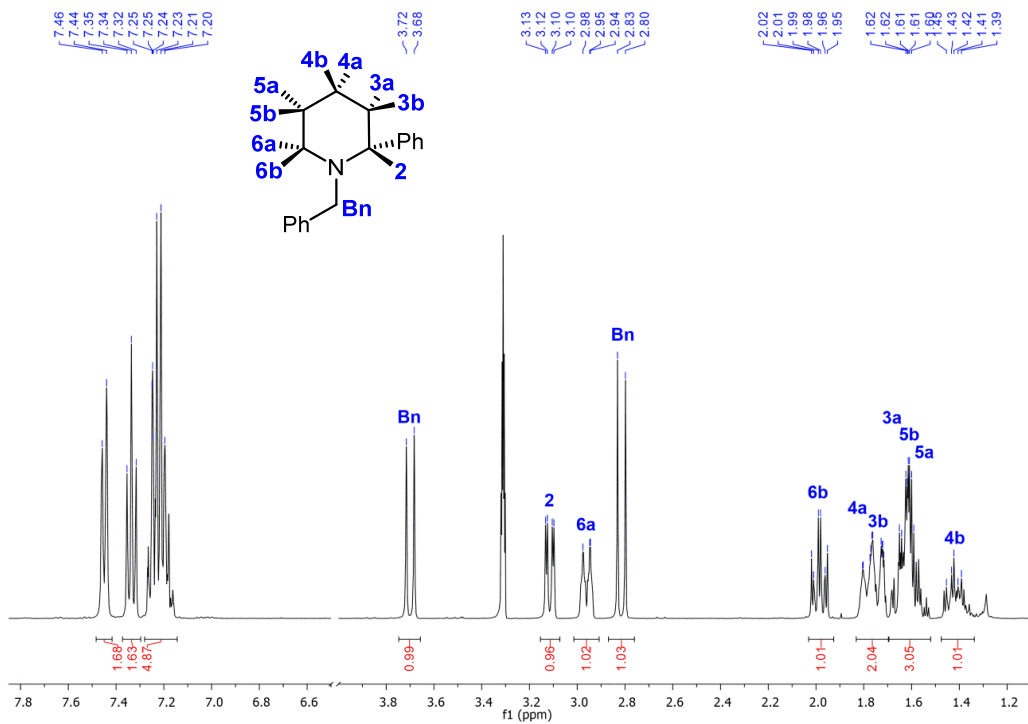
**With  $\text{D}_2$ .** Inside a glovebox, a solution of  $[\text{Ir}(\text{cod})\text{Cl}]_2$  (0.0015 mmol), **PA3** (0.0033 mmol) and  $\text{P}(p\text{-CF}_3\text{C}_6\text{H}_4)_3$  (0.0033 mmol) in DCM (1 mL) was stirred at 45 °C for 30 min. The preformed catalyst was added to a 5 mL vial containing a solution of the corresponding *N*-benzyl-2-arylpyridinium bromide (0.15 mmol) in DCM (2 mL). The vial was capped with a PTFE septum, removed from the glovebox and placed into a Premex 96er Multireaktor®. After flushing it 5 times with  $\text{N}_2$  and 5 times with  $\text{H}_2$ , it was pressurized to 40 bar of  $\text{D}_2$  and stirred at 50 °C for 18 h. The crude mixture was washed with saturated aqueous solution of  $\text{Na}_2\text{CO}_3$  and extracted

with DCM. The organic extracts were dried, concentrated and purified by flash column chromatography Hexane/EtOAc (from 99:1 to 95:5).

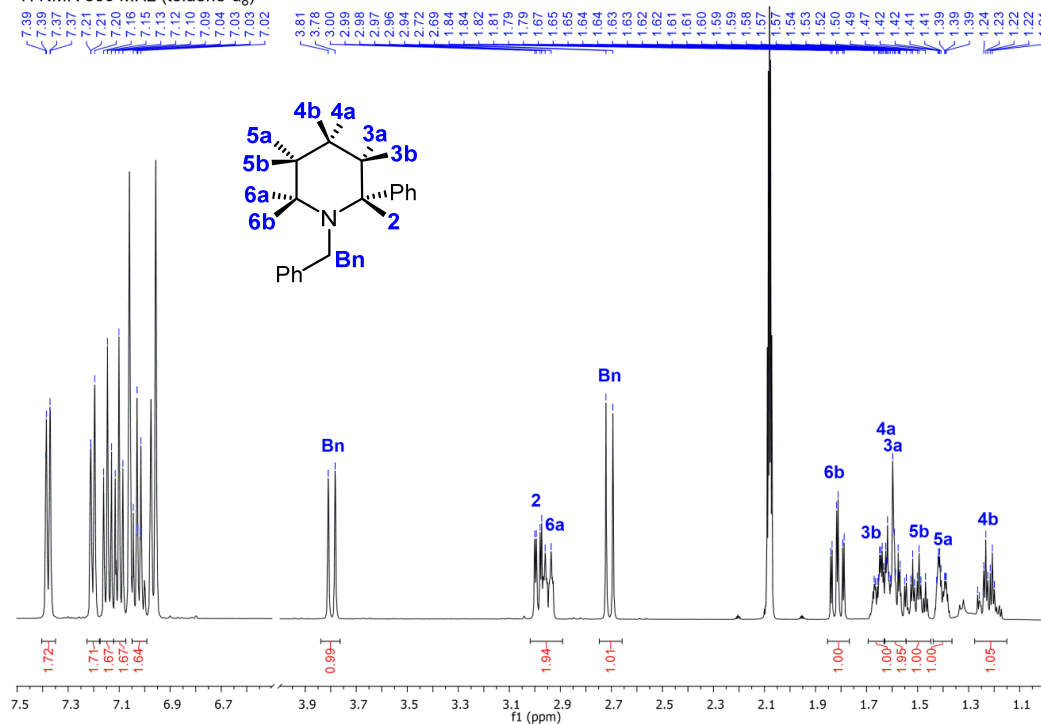
- Quantitative  $^1\text{H}$  NMR spectra of **57a** in  $\text{CD}_3\text{OD}$  and toluene- $d_8$  are shown below for a standard experiment and the two isotopic labeling experiments.

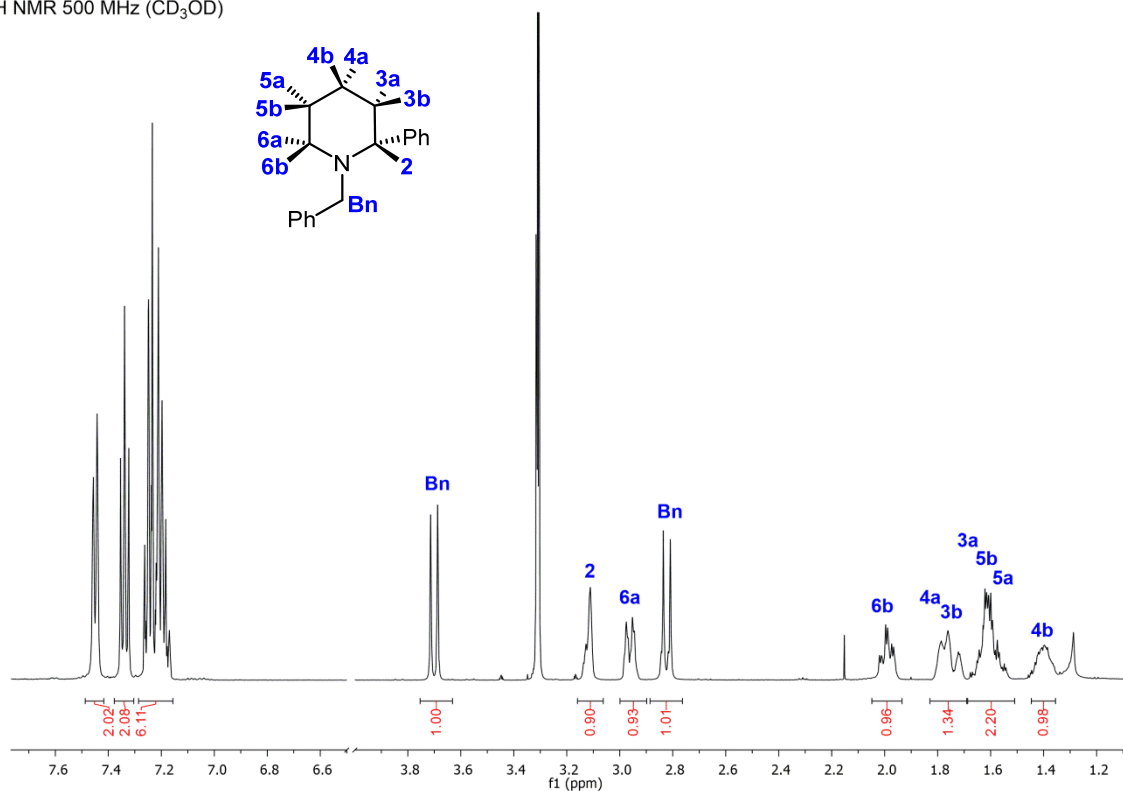
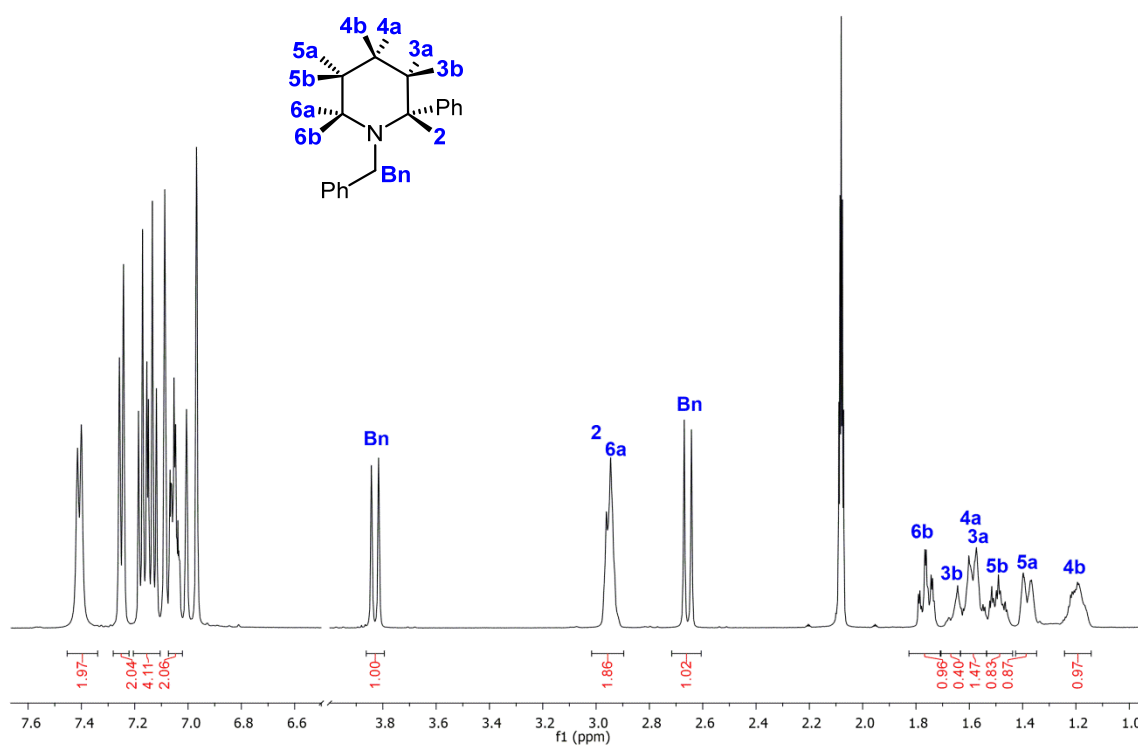
### Standard experiment:

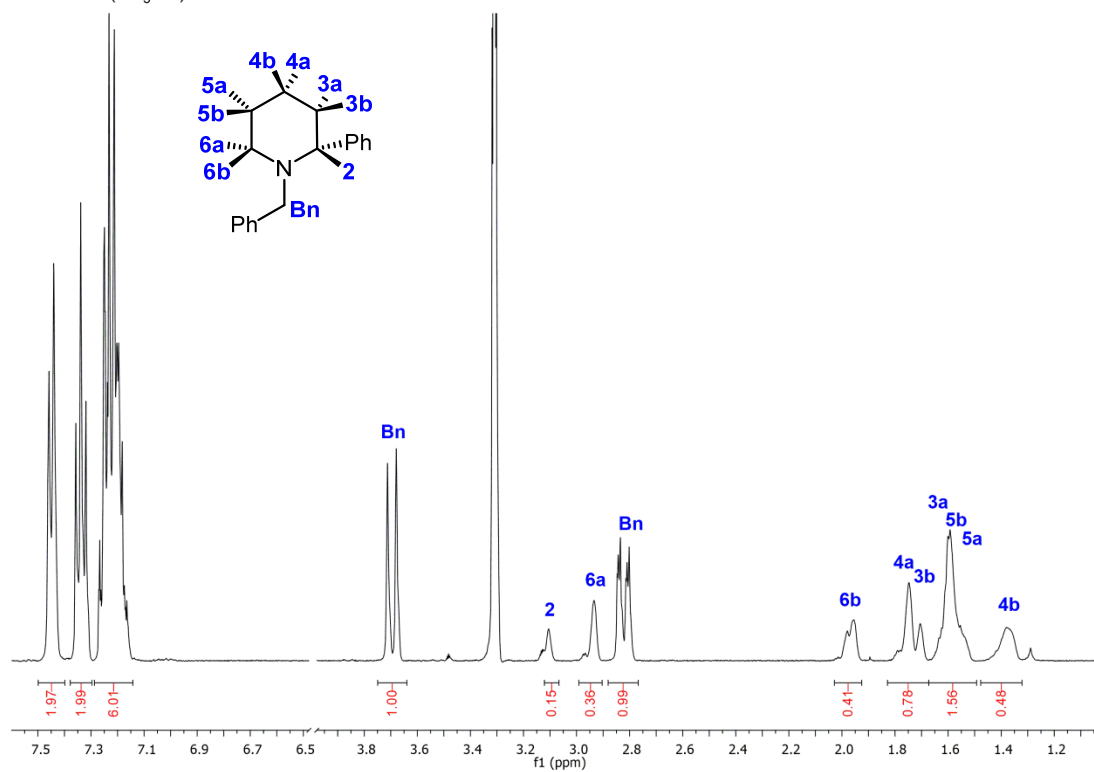
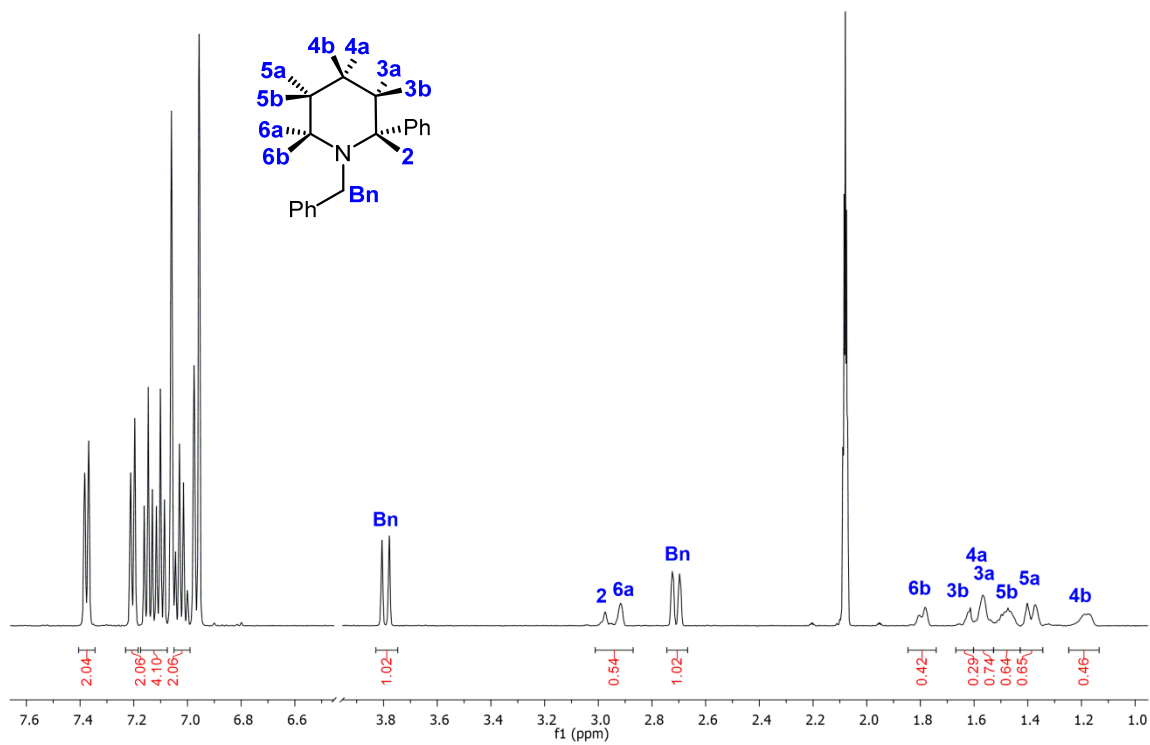
$^1\text{H}$  NMR 500 MHz ( $\text{CD}_3\text{OD}$ )



$^1\text{H}$  NMR 500 MHz (toluene- $d_8$ )



Isotopic labeling experiment with CD<sub>3</sub>OD:<sup>1</sup>H NMR 500 MHz (CD<sub>3</sub>OD)<sup>1</sup>H NMR 500 MHz (toluene-d<sub>8</sub>)

Isotopic labeling experiment with D<sub>2</sub>:<sup>1</sup>H NMR 500 MHz (CD<sub>3</sub>OD)<sup>1</sup>H NMR 500 MHz (toluene-d<sub>8</sub>)



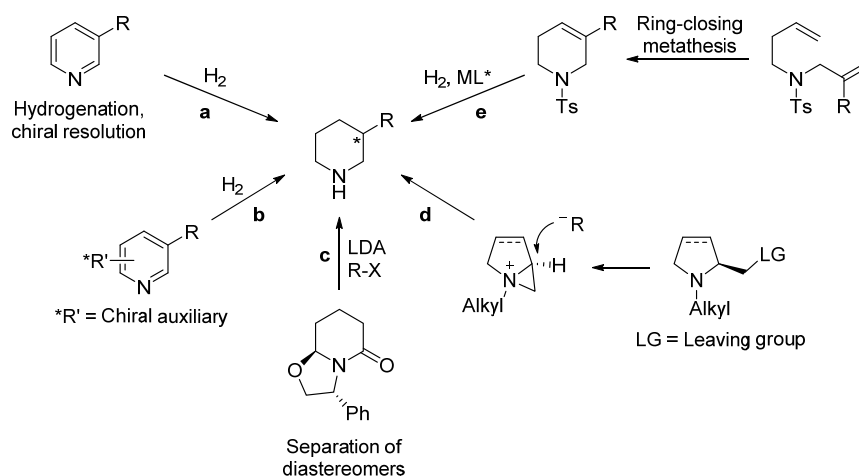
# CHAPTER III.

## ASYMMETRIC HYDROGENATION OF 3-SUBSTITUTED PYRIDINES

---

### III.1 INTRODUCTION

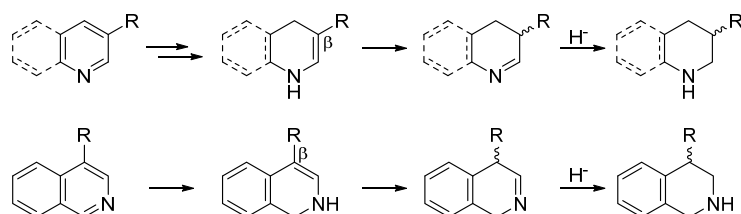
Among chiral piperidines, the 3-substituted ones are particularly challenging to obtain in enantiomerically enriched form. Although several approaches have been developed for their preparation, there is still no efficient method for their synthesis. The most common ways to obtain these 3-substituted piperidines (Scheme 55) are the following: (a) hydrogenation of 3-substituted pyridines and subsequent resolution, either by formation of diastereomeric salts<sup>63</sup> or by chemoenzymatic resolution;<sup>64</sup> (b) hydrogenation of 3-substituted pyridines bearing chiral auxiliaries with heterogeneous catalysts;<sup>64</sup> (c) alkylation and reduction of oxazolopiperidones;<sup>65</sup> (d) ring expansion via an aziridinium salt;<sup>66</sup> (e) ring closing-metathesis to form a prochiral tetrahydropyridine, which is subsequently hydrogenated enantioselectively.<sup>67</sup>



**Scheme 55.** Methods to prepare chiral 3-substituted piperidines.

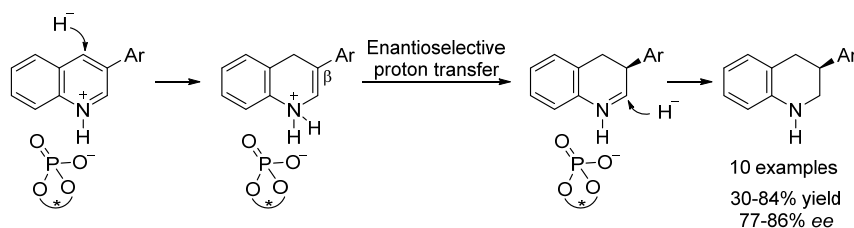
All these methods require either a separation of the stereoisomers after the reaction or several steps for the synthesis of the piperidine precursor. In contrast, the asymmetric hydrogenation (AH) of 3-substituted pyridines would be of great importance, since the preparation of these substrates is much easier and many of them are commercially available. Unfortunately, no highly enantioselective hydrogenation has been reported yet.

Attempts to enantioselectively hydrogenate 3-substituted pyridines or related 6-membered *N*-heteroaromatics, such as 3-substituted quinolines or 4-substituted isoquinoline, led in all cases to very poor enantioselectivities, between 0-17% *ee*.<sup>8,40e,47c,68</sup> All these substrates share a common mechanistic pathway, which involves a enamine-imine tautomerization before the hydride addition, generating a racemic stereocenter in the  $\beta$ -carbon of the nitrogen atom (Scheme 56).



**Scheme 56.** Accepted mechanistic pathway responsible for the racemization of the  $\beta$ -carbon.

However, Rueping and co-workers found a way to overcome this problem in the organocatalytic reduction of 3-substituted quinolines.<sup>52c</sup> The combination of Hantzsch esters as reductant with catalytic amounts of chiral phosphoric acids promoted an enantioselective enamine-iminium tautomerization. The chiral phosphate counterion induced the proton transfer preferentially from one of the faces of the dihydroquinoline ring, thus generating 3-substituted tetrahydroquinolines with *ee*'s up to 86% (Scheme 57).



**Scheme 57.** Proposed mechanism for the enantioselective proton transfer in the AH of 3-substituted quinolines.

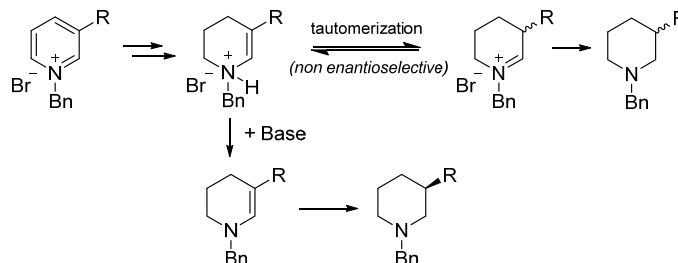
Regarding pyridines, the most similar example is the AH of 2,3,6-trisubstituted pyridines, recently reported by Zhou and co-workers, where enantioselectivities up to 90% *ee* are obtained (see Chapter I, Scheme 9).<sup>19</sup> In this particular example, the substituent in the 3-position is always a trifluoromethyl group, and the mechanism that allows to obtain high enantioselectivities is a dynamic kinetic resolution, which is the accepted path for all the reported cases of  $\alpha,\beta$ -disubstituted *N*-heteroarenes. Unfortunately, in the case of only 3-substituted pyridines, this mechanism is not observed or is less effective.

## III.2 RESULTS AND DISCUSSION

After having gained some knowledge about the mechanism of hydrogenation of 2-substituted pyridines (Chapter II), and taking in account all the mechanisms that have been proposed for *N*-heteroaromatic substrates, we decided to focus our efforts on the development of a highly enantioselective hydrogenation of 3-substituted pyridines.



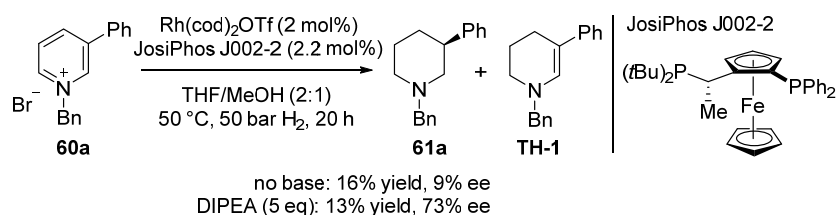
Since the low enantioselectivity was most probably arising from the enaminium-iminium tautomerization, we wondered if it was possible to avoid this tautomerization by addition of a base, which would quench the generated HBr, and find a catalyst able to hydrogenate the resulting enamine (Scheme 58).



**Scheme 58.** Proposed pathways for the AH of 3-substituted pyridines in presence or absence of a base.

Unfortunately, the examples about AH of enamines are rather limited, and even more if we speak about  $\beta$ -substituted enamines.<sup>69</sup> Much effort has been put on the AH of enamides, where a secondary coordination of the *N*-acyl moiety with the metal is crucial for achieving high enantioselectivities.<sup>70</sup>

However, we decided to test if the base would affect somehow the outcome of the reaction. Rh has been widely used in the AH of enamines and enamides<sup>69a,70a-g</sup> and JosiPhos J002-2, a ferrocene derived ligand,<sup>71</sup> has proved very effective in the AH of 2,4-disubstituted pyrimidines<sup>54</sup> and 3,4-disubstituted pyridinium salts.<sup>15</sup> Thus, this combination of Rh-JosiPhos was selected together with diisopropylethylamine (DIPEA), a bulky base which might have difficulties to coordinate to the catalyst. Finally, a mixture of THF and MeOH was chosen to solubilize the catalyst and the *N*-benzyl-3-phenylpyridinium bromide (**60a**), which was selected as model substrate. The hydrogenation was carried out at 50 °C under 50 bar of H<sub>2</sub> in the absence and in the presence of DIPEA, for comparison (Scheme 59). As expected, when no base was added, (*S*)-*N*-benzyl-3-phenylpiperidine (**61a**) was obtained with only 9% *ee*. Instead, when DIPEA was used, the enantioselectivity rose to 73% *ee*, but **TH-1** was observed as side product.

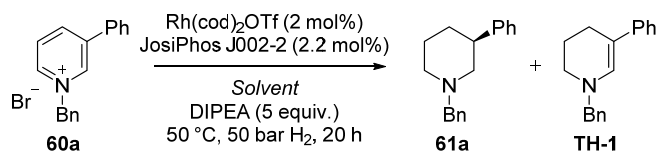


**Scheme 59.** Initial attempt for the AH of *N*-benzyl-3-phenylpyridinium bromide.

Encouraged by the dramatic effect of the base, we directed our efforts to optimize the reaction conditions. Initially, the solvent effect was investigated in order to increase the yield and *ee* of the piperidine **61a** and lower the amount of **TH-1** formed (Table 11). When the reaction was carried out in pure MeOH (entry 2), the final piperidine was obtained in high yield but low *ee*. Instead, in pure THF very low yield and the opposite enantiomer was obtained (entry 3). Testing different alcohols (entries 4-6) we observed that the more acidic the alcohol the higher

was the obtained *ee* (2,2,2-trifluoroethanol (TFE) > MeOH > EtOH > *i*PrOH) and the lower the amount of **TH-1**. Checking different ratios of THF/TFE (entries 6-8), the ratio 2:1 was a good compromise between yield and enantiomeric excess. Other solvent mixtures, such as DCM/TFE or toluene/TFE gave lower enantioselectivities (entries 10 and 11).

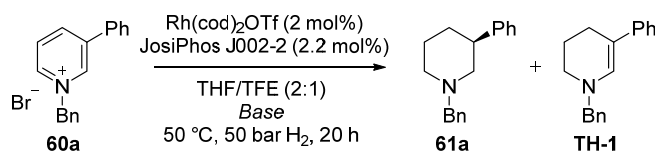
**Table 11.** Solvent screening.



#	Solvent	yield of <b>61a</b> (%)	<i>ee</i> of <b>61a</b> (%)	yield of <b>TH-1</b> (%)
1	THF/MeOH (2:1)	13	73	34
2	MeOH	81	13	9
3	THF	5	-59 <sup>[a]</sup>	41
4	THF/EtOH (2:1)	10	63	50
5	THF/IPA (2:1)	6	34	48
6	THF/TFE (2:1)	27	83	17
7	THF/TFE (1:1)	40	68	2
8	THF/TFE (1:2)	40	52	2
9	DCM/TFE (2:1)	40	63	3
10	Toluene/TFE (2:1)	35	67	10

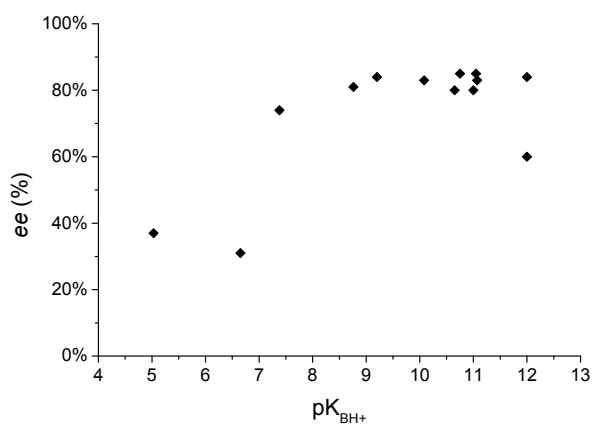
*Reaction conditions:* **60a** (0.025 mmol), Rh(cod)<sub>2</sub>OTf (2 mol%), JosiPhos J002-2 (2.2 mol%), DIPEA (5 equiv.), solvent (1.5 mL), 50 °C, 50 bar H<sub>2</sub>, 20 h. Yield and *ee* determined by chiral GC with dodecane as internal standard. [a] *R* configuration was obtained in this case.

Next we focused on the optimization of the base (Table 12). As already observed before, the absence of base led to a poor yield and enantiomeric excess (entry 1). Screening different amines (entries 2-14) it was noticed that the more basic the amine the higher was the enantiomeric excess. While alkyl amines gave enantioselectivities ranging from 74 to 85% *ee*, less basic amines, such as *p*-ethylaniline or 2,6-lutidine, led only to 37% and 31% *ee*, respectively (see Figure 9 for a complete correlation). The correlation with the yields of **61a** is not straightforward, and other factors apart from electronics might be involved. Other inorganic bases (entries 15 and 16) and phosphazene bases (entry 17) did not achieve as high enantioselectivities and produced important amounts of **TH-1**. It is noteworthy that non-bulky tertiary amines and even secondary amines were well tolerated. To check if the amines were coordinating to the catalyst, two enantiomers of a chiral secondary amine were tested (entries 18 and 19). In both cases the same enantiomeric excess was obtained, thus suggesting that there is no coordination of the ligand to the catalyst, at least during the enantiodetermining step. Finally, the equivalents of base were tested (entries 20-23). As long as more than one equivalent was used, the amount of base had little effect on the outcome of the reaction.

**Table 12.** Screening of bases.

#	Base	pK <sub>BH<sup>+</sup></sub> (in H <sub>2</sub> O)	yield of <b>61a</b> (%)	ee of <b>61a</b> (%)	yield of <b>TH-1</b> (%)
1	-	-	5	23	0
2	DIPEA	11.07	27	83	17
3	Et <sub>3</sub> N	10.75	57	85	20
4	Proton Sponge <sup>®</sup>	12	39	84	21
5	( <i>n</i> Pr) <sub>3</sub> N	10.65	62	80	16
6	( <i>i</i> Pr) <sub>2</sub> NH	11.05	37	85	11
7	DMAP	9.2	23	84	13
8	2,6-lutidine	6.65	98	31	0
9	<i>p</i> -ethylalaniline	5.03	18	37	0
10	DBU	12	23	60	49
11	<i>N</i> -methylmorpholine	7.38	40	74	6
12	Bn <sub>2</sub> NH	8.76	45	81	18
13	<i>N</i> -methylpiperidine	10.08	51	83	15
14	Quinuclidine	11	56	80	17
15	Cs <sub>2</sub> CO <sub>3</sub>	10.32	40	48	32
16	KOMe	15.54	54	48	23
17	BEMP	16.2	27	72	28
18 <sup>[a]</sup>	( <i>R</i> )- <i>N</i> -benzyl-1-phenylethanamine	≈ 9	97	59	4
19 <sup>[a]</sup>	( <i>S</i> )- <i>N</i> -benzyl-1-phenylethanamine	≈ 9	94	60	4
20	Et <sub>3</sub> N [0.5 equiv.]		40	76	9
21	Et <sub>3</sub> N [1 equiv.]		54	85	16
22	Et <sub>3</sub> N [3 equiv.]		60	81	17
23	Et <sub>3</sub> N [10 equiv.]		58	78	16

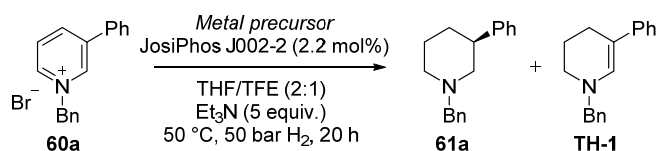
Reaction conditions: **60a** (0.025 mmol), Rh(cod)<sub>2</sub>OTf (2 mol%), JosiPhos J002-2 (2.2 mol%), base (5 equivalents, unless otherwise stated), THF/TFE (2:1, 1.5 mL), 50 °C, 50 bar H<sub>2</sub>, 20 h. Yield and ee determined by chiral GC with dodecane as internal standard. [a] Reaction performed at 70 °C.

**Figure 9.** Acidity of the protonated amines vs obtained ee.

We then decided to investigate whether a different metal precursor or ligand could improve the results. The enantiomeric excesses were found to be highly dependent on the metal precursor

(Table 13). The best results were obtained with  $\text{Rh}(\text{cod})_2\text{OTf}$ , the  $\text{Rh}^{\text{I}}$  complex that we had been using for all prior optimizations (entry 1). Surprisingly, similar results were achieved with  $\text{Rh}^{\text{II}}$ -carboxylate precursors (entries 2 and 3). Other Rh complexes did not show the same efficiency regardless of having coordinating or non-coordinating anions (entries 4-7). Interestingly, the same positive effect of the addition of base is observed when using iridium as metal – 5% *ee* in absence of base and 62% *ee* in presence of  $\text{Et}_3\text{N}$  (entry 9 *vs* 8) –.

**Table 13.** Screening of metal precursors.



#	Metal precursor	yield of 61a (%)	<i>ee</i> of 61a (%)	yield of TH-1 (%)
1	$\text{Rh}(\text{cod})_2\text{OTf}$	57	85	20
2	$[\text{Rh}(\text{OAc})_2]_2$	65	84	5
3	$[\text{Rh}(\text{CF}_3\text{CO}_2)_2]_2$	50	77	7
4	$\text{Rh}(\text{cod})_2\text{BF}_4$	55	38	13
5	$\text{Rh}(\text{cod})(\text{acac})$	51	16	9
6	$[\text{Rh}(\text{cod})\text{Cl}]_2$	53	39	10
7	$[\text{Rh}(\text{Cp}^*)\text{Cl}]_2$	65	56	3
8	$[\text{Ir}(\text{cod})\text{Cl}]_2^{[\text{a}]}$	12	62	18
9	$[\text{Ir}(\text{cod})\text{Cl}]_2^{[\text{b}]}$	4	5	0

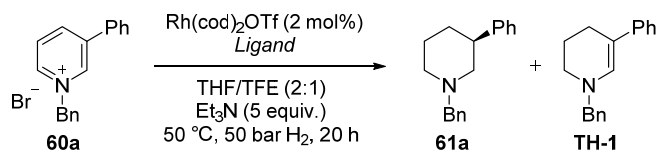
*Reaction conditions:* **60a** (0.025 mmol), metal precursor (2 mol% for monomers, 1 mol% for dimers), JosiPhos J002-2 (2.2 mol%),  $\text{Et}_3\text{N}$  (5 equiv.), THF/TFE (2:1, 1.5 mL), 50 °C, 50 bar  $\text{H}_2$ , 20 h. Yield and *ee* determined by chiral GC with dodecane as internal standard. [a] Performed in THF/MeOH (2:1). [b] Performed without base in THF/MeOH (2:1).

Next, a ligand screening was carried out to try to identify a better performing ligand than JosiPhos SL-J002-2 (Table 14). Very diverse ligands were selected, such as aryl or alkyl bidentate phosphines with different kinds of stereogenic units (stereocenters at carbon and/or phosphorus, stereoaxis, stereogenic plane), phosphinooxazolines or even monodentate phosphoramidites. Unfortunately no ligand outperformed JosiPhos, being another ferrocene derivative, WalPhos, the best among the rest (38% *ee*, entry 12). Therefore, we decided to explore different JosiPhos derivatives available in house to compare other possible electronic or steric effects (Table 15). Again, the best performing ligand turned out to be JosiPhos SL-J002-2 (57% yield, 85% *ee*). Replacing its phenyl substituent for 4-methoxy-3,5-dimethylphenyl had minor effects on the enantioselectivities (entry 1 *vs* 4), but when exchanging it for other alkyl or aryl substituents the enantiomeric excess decreased dramatically (entries 3, 5 and 6). Much more sensitive to variations is the other phosphine of the ligand: replacing the *tert*-butyl substituents for cyclohexyl caused a drop of the enantioselectivity from 85% to 45% *ee* (entry 1 *vs* 2). Exchanging it for an aromatic ring was even more detrimental for the *ee* (entry 4 *vs* 7).

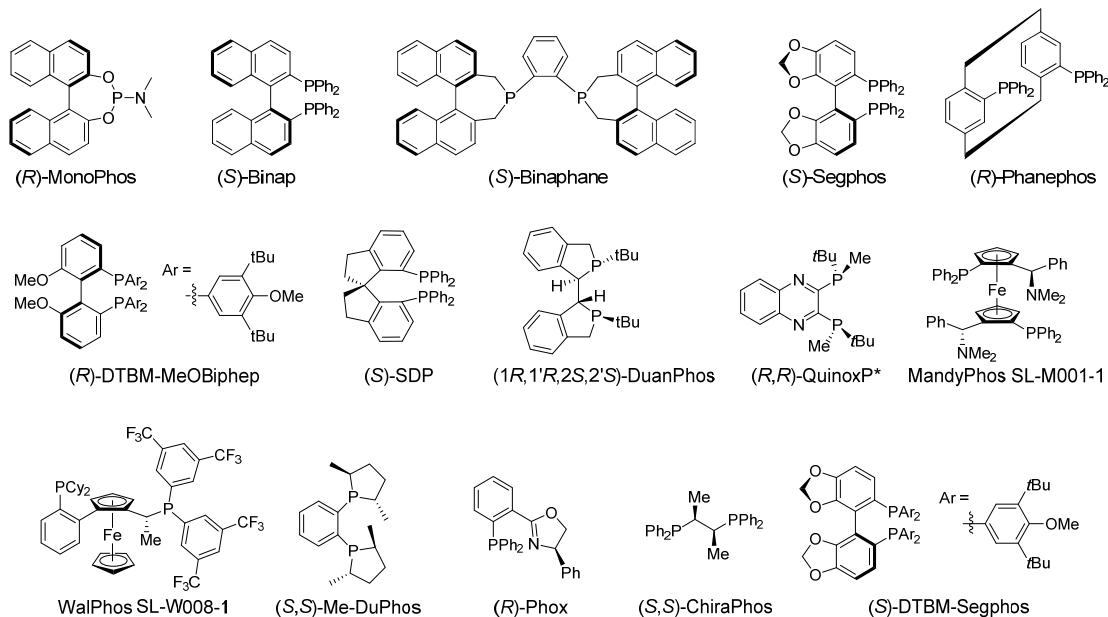
Increasing the temperature from 50 to 70 °C led to higher yields (74%), but lower enantioselectivities (70% *ee*). Small variations of the substrate concentration did not affect either

the yield or the *ee*, but decreasing the catalyst loading led to lower yields, without affecting the enantiomeric excess (36% yield with 1 mol% catalyst and 25% yield with 0.5 mol% catalyst). Surprisingly, when the reaction time was decreased from 20 h to 16 h, the enantioselectivity increased in expenses of the yield (50% yield, 90% *ee*), suggesting an erosion of the *ee* with time.

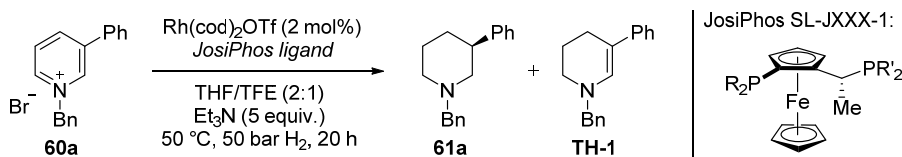
**Table 14.** Screening of ligands.



#	Ligand	yield of <b>61a</b> (%)	<i>ee</i> of <b>61a</b> (%)	yield of <b>TH-1</b> (%)
1	Josiphos SL-J002-2	57	85	20
2	( <i>R</i> )-MonoPhos	27	0	18
3	( <i>S</i> )-Binap	15	-10	26
4	( <i>S</i> )-Binaphane	50	-10	2
5	( <i>S</i> )-Segphos	35	-6	19
6	( <i>R</i> )-DTBM-MeOBiphep	42	2	33
7	( <i>R</i> )-Phanephos	16	10	45
8	( <i>S</i> )-SDP	72	14	1
9	(1 <i>R</i> ,1' <i>R</i> ,2 <i>S</i> ,2' <i>S</i> )-DuanPhos	25	-12	8
10	( <i>R,R</i> )-QuinoxP*	57	2	13
11	MandyPhos SL-M001-1	8	-5	47
12	WalPhos SL-W008-1	21	38	33
13	( <i>S,S</i> )-Me-DuPhos	26	0	6
14	( <i>R</i> )-Phox	55	0	12
15	( <i>S,S</i> )-Chiraphos	36	2	8
16	( <i>S</i> )-DTBM-Segphos	63	3	19



**Reaction conditions:** **60a** (0.025 mmol), Rh(cod)<sub>2</sub>OTf (2 mol%), ligand (2.2 mol% for bidentate, 4.2 mol% for monodentate), Et<sub>3</sub>N (5 equiv.), THF/TFE (2:1, 1.5 mL), 50 °C, 50 bar H<sub>2</sub>, 20 h. Yield and *ee* determined by chiral GC with dodecane as internal standard.

**Table 15.** Screening of JosiPhos ligands.

#	JosiPhos	R	R'	yield of 61a (%)	ee of 61a (%)	yield of TH-1 (%)
1	J002-2 <sup>[a]</sup>	Ph	<i>t</i> Bu	57	85	20
2	J001-1	Ph	Cy	23	-45	15
3	J009-1	Cy	<i>t</i> Bu	13	-37	15
4	J013-1	4-MeO-3,5-diMeC <sub>6</sub> H <sub>2</sub>	<i>t</i> Bu	60	-78	20
5	J212-1	1-furyl	<i>t</i> Bu	25	-56	56
6	J216-1	1-naphthyl	<i>t</i> Bu	60	-4	9
7	J425-1	4-MeO-3,5-diMeC <sub>6</sub> H <sub>2</sub>	<i>o</i> -tolyl	12	-5	12
8	J502-1	<i>t</i> Bu	Ph	21	41	60
9	J505-1	<i>t</i> Bu	<i>o</i> -tolyl	97	21	0

Reaction conditions: **60a** (0.025 mmol), Rh(cod)<sub>2</sub>OTf (2 mol%), JosiPhos ligand (2.2 mol%), Et<sub>3</sub>N (5 equiv.), THF/TFE (2:1, 1.5 mL), 50 °C, 50 bar H<sub>2</sub>, 20 h. Yield and *ee* determined by chiral GC with dodecane as internal standard. [a] JosiPhos SL-J002-2 is the enantiomer of SL-J002-1

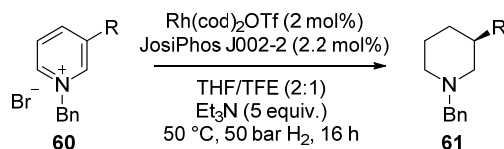
Before exploring the mechanism of the reaction, a substrate scope was performed with a variety of functional groups in the 3-position under the optimized conditions. The aim of it was to observe if the positive effect of the base was independent of the substituent (Table 16). While in absence of base only *ee*'s up to 40% were obtained, in presence of Et<sub>3</sub>N the enantioselectivities ranged from 32-90% *ee*. The yield did also increase in most of the cases. The best enantioselectivities were obtained with aromatic substituents, 75-90% *ee* (entries 1 and 4-7), but also considerable enantiomeric excesses were obtained with alkyl, esters and protected amines as substituents (entries 8-12). The best yields were obtained with electron donating groups, like *para*-methoxyphenyl (52% yield, entry 5). On the contrary, lower yields were obtained in the presence of electron withdrawing substituents (entries 4, 9 and 11).

Gratifyingly, when the reaction was scaled up to 0.5 g, comparable results were obtained (entry 3). When the bromide counterion was exchanged for a non-coordinating anion like BArF<sup>-</sup>, the enantiomeric excess dropped from 90% to 50% *ee* (entry 1 *vs* 2), thus highlighting one more time the importance of the counterion in these systems.<sup>16</sup> The best results were obtained with substrates bearing aromatic substituents: since the reaction optimization had been carried out using a phenyl-substituted model substrate. As it is well-known, every substrate requires a dedicate optimization, but as a matter of example, in the initial tests when the reaction was not yet optimized (DIPEA as base and 2:1 THF/MeOH as solvent), the hydrogenation of **60h** afforded the corresponding piperidine with 70% *ee*, instead of the 50% *ee* obtained in this conditions (entry 10).

Although this optimized protocol is not directly extrapolable to any kind of substituent in the pyridine, it demonstrated that the positive effect of the base is applicable to all of them. Moreover, in the cases where the absolute configuration could be determined, it was observed

that the substituent was always on the same face of the piperidine ring. These two facts suggest that all these substrates are hydrogenated via the same mechanism.

**Table 16.** Asymmetric hydrogenation of 3-substituted pyridinium salts in presence or absence of base.



#	R =	With Et <sub>3</sub> N		Without Et <sub>3</sub> N	
		yield of <b>61</b> (%)	<i>ee</i> of <b>61</b> (%)	yield of <b>61</b> (%)	<i>ee</i> of <b>61</b> (%)
1	Ph ( <b>60a</b> )	50	90 ( <i>S</i> )	5	23 ( <i>S</i> )
2	Ph ( <b>60a</b> ) <sup>[a]</sup>	66	50 ( <i>S</i> )	3	2 ( <i>S</i> )
3	Ph ( <b>60a</b> ) <sup>[b]</sup>	57(52) <sup>[c]</sup>	84 ( <i>S</i> )		
4	4-CF <sub>3</sub> C <sub>6</sub> H <sub>4</sub> ( <b>60b</b> )	20	83 (–)	12	14 (–)
5	2-MeC <sub>6</sub> H <sub>4</sub> ( <b>60c</b> )	50	75 (–)	7	30 (–)
6	4-MeOC <sub>6</sub> H <sub>4</sub> ( <b>60d</b> )	52	90 (–)	8	40 (–)
7	2-naphthyl ( <b>60e</b> )	42	86 (–)	21	20 (–)
8	Me ( <b>60f</b> )	36	57 ( <i>R</i> )	<1%	nd
9	CO <sub>2</sub> Et ( <b>60g</b> )	2	33	3	-17 <sup>[d]</sup>
10	NHBoc ( <b>60h</b> )	24	55 ( <i>R</i> )	25	27 ( <i>R</i> )
11	CF <sub>3</sub> ( <b>60i</b> )	2	41	2	11
12	<i>n</i> Bu ( <b>60j</b> )	43	32 (–)	<1%	nd

*Reaction conditions:* **60** (0.025 mmol), Rh(cod)<sub>2</sub>OTf (2 mol%), JosiPhos J002-2 (2.2 mol%), Et<sub>3</sub>N (5 equiv.), THF/TFE (2:1, 1.5 mL), 50 °C, 50 bar H<sub>2</sub>, 16 h. Yield and *ee* determined by chiral GC with dodecane as internal standard. [a] Br<sup>-</sup> counterion was exchanged for BARF<sup>-</sup> using AgBARF (silver tetrakis[3,5-bis(trifluoromethyl)phenyl]borate). [b] Reaction performed on 500 mg scale (1.53 mmol) for 20 h. [c] In parenthesis, isolated yield. [d] The opposite enantiomer was obtained.

As already done with 2-substituted pyridines (Chapter II), a mechanistic study was initiated monitoring the reaction over time (Figure 10). More than 90% of the pyridinium salt **60a** was consumed within the first 4 hours. Simultaneously, the piperidine **61a** was formed along with several *N*-benzylated tetrahydropyridines. Nevertheless, it should be noted that the sum of the products does not make up for the consumed starting material, suggesting that other intermediates or decomposition products are not observed by GC.

**TH-1** was formed at high rates during the first 3 hours of reaction and then its amount decreased very slowly. This side-product of the reaction could be isolated and fully characterized despite the reported instability of similar enamines.<sup>59</sup> **TH-2** was formed in very small amounts (less than 3%) and remained more or less constant during the course of the reaction. It was also identified as a tetrahydropyridine and was isolated at the end of the reaction. An alternative way to prepare this intermediate consists on reacting the pyridinium salt with an excess of NaBH<sub>4</sub> in MeOH. A third compound, which is formed in appreciable amounts during the first 5 hours of reaction and then consumed during the next 10 hours, was also observed. This intermediate was identified also as an *N*-benzylated tetrahydropyridine by GC-MS (*m/z* = 249). Although it was not possible to isolate or synthesize by other methods, when injected in a chiral GC it split in two

peaks, suggesting that it contains a stereocenter and therefore it should correspond either to **TH-3** or **TH-4**. Furthermore, this tetrahydropyridine showed a very high and constant enantiomeric excess (93% *ee*) during all the reaction. Remarkably, the enantiomeric excess of piperidine **61a** suffered important variations during the reaction course. It increased sharply during the first 10 hours of reaction and then it slowly decreased.

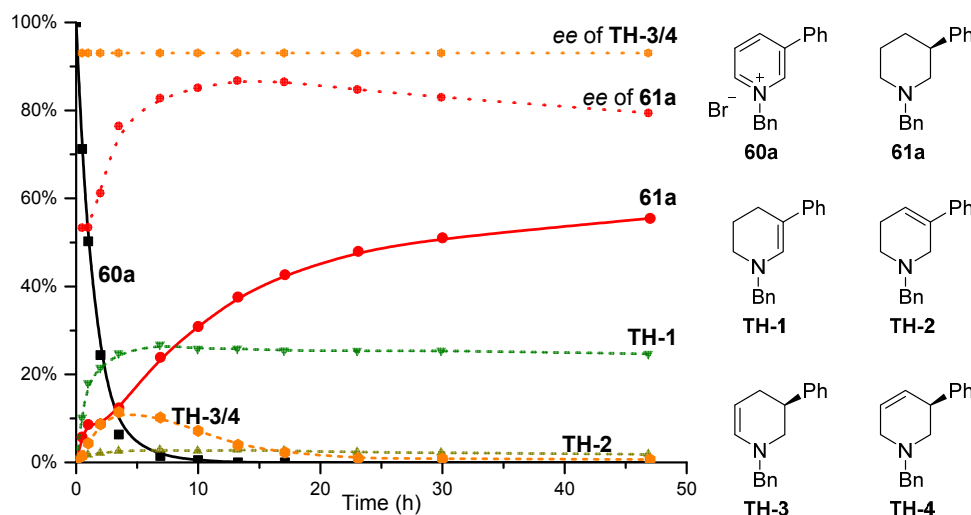


**Figure 10.** Monitoring the reaction over time. Reaction conditions: **60a** (1.53 mmol), Rh(cod)<sub>2</sub>OTf (2 mol%), JosiPhos J002-2 (2.2 mol%), Et<sub>3</sub>N (5 equiv.), THF/TFE (2:1, 27 mL), 50 °C, 50 bar H<sub>2</sub>. Consumption of **60a** determined by NMR with dimethyl terephthalate as internal standard. Yield and *ee* of **61a** and the different tetrahydropyridines monitored by chiral GC with dodecane as internal standard.

While monitoring the disappearance of the starting material by NMR, it was noted that exactly one equivalent of triethylammonium salt was formed after the complete consumption of **60a** (Figure 11). This is in agreement with the postulated idea that the added base would quench the generated HBr.

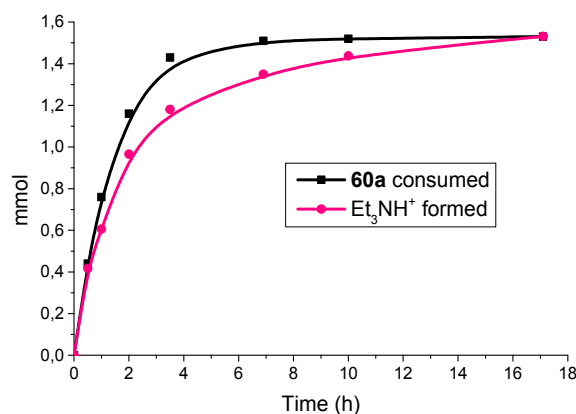
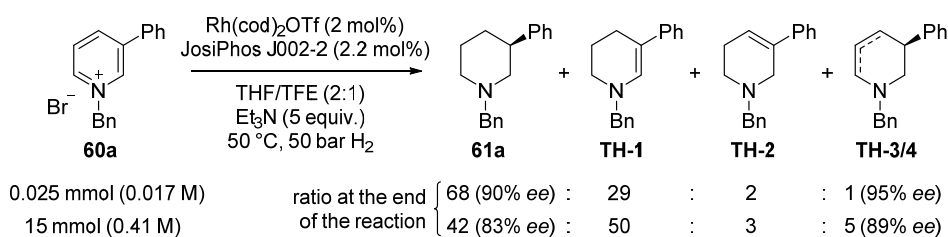


**Figure 11.** Comparison between the consumption rate of **60a** and the formation rate of triethylammonium.

To gain more information about the reaction intermediates, especially of some possible dihydropyridines, a parallel reaction was monitored by *in situ* FTIR spectroscopy. To do so, an ATR Diamond probe inserted into the autoclave was used and a chromatogram was recorded every minute during a 22 h reaction. All the acquired chromatograms were analyzed by a software



performing multivariate data analysis, which consists in: (i) determining the absorbance variation at every wavelength; (ii) grouping all the wavelengths that increase or decrease simultaneously (which can correspond to a single compound or a linear combination of compounds); (iii) plotting the variation of each of these groups with the reaction time. To be able to detect variations in the IR spectra, the concentration of the substrate had to be increased 24 times (from 0.017 M to 0.41 M), which affected the ratio of the different intermediates at the end of the reaction (Scheme 60).



**Scheme 60.** Ratio of products at the end of the reaction with the optimized conditions (0.017 M) and with the concentration used for the *in situ* FTIR experiment (0.41 M).

The superimposition of all the spectra acquired during the reaction can be seen in Figure 12A. Although initially it seems difficult to determine the variations, when plotting the variation of some selected wavelengths with time, the picture becomes more clear (Figure 12B). Some wavelengths, such as 727 (maroon) and 762  $\text{cm}^{-1}$  (purple), sharply decrease during the first hour. Others increase and then decrease, with a maximum at three hours, like 1032 (dark blue), 848 (orange) and 803  $\text{cm}^{-1}$  (yellow). The observed noise suggests that the technique is not sensitive enough for the concentration used, but when trying to perform the reaction at higher concentrations the obtained results were not comparable, probably because in those cases  $\text{Et}_3\text{N}$  becomes the main solvent. An added difficulty for the IR interpretation can be attributed to the similarity of the spectra of the different tetrahydropyridines and final piperidine.

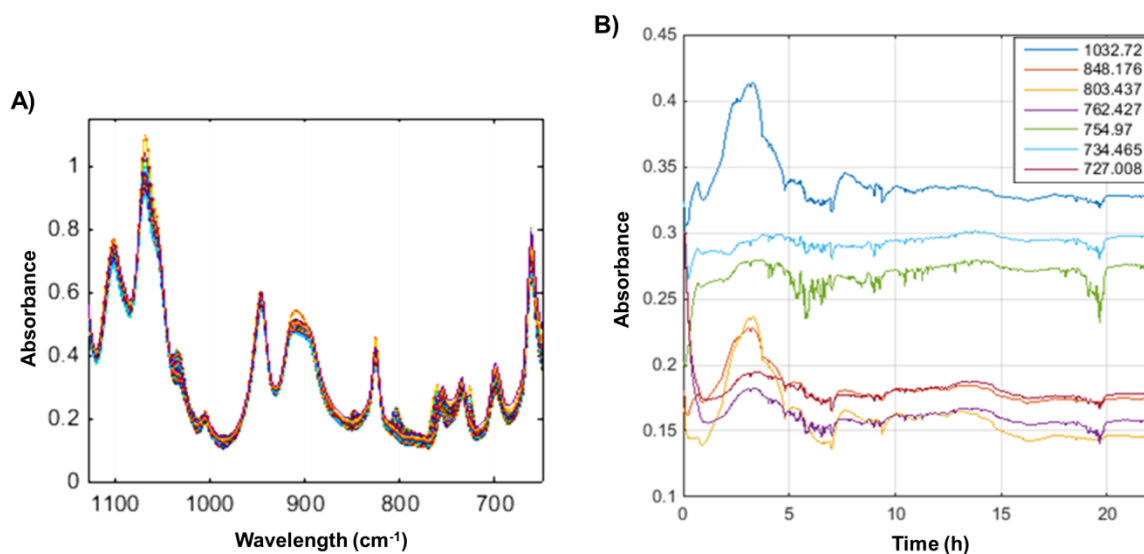


**Figure 12.** A) Superimposed spectra recorded during 22 hours of reaction. B) Variation of the absorbance with time of selected wavelengths.

Analyzing all wavelength variations, the software is able to show the spectra of different compounds or linear combination of compounds (named from **I-IV**, Figure 13A and B). The first three (**I** - purple, **II** - yellow and **III** - orange) could be intermediates of the reaction, which we were not able to assign. However, it was impossible to assign them to a specific dihydropyridine without having a reference. With respect to **IV** (blue), it disappears during the first hour and it is not further observed. Initially, it was thought that this plot corresponded to the disappearance of **60a**, but comparing the graph with the experimental IR spectra (Figure 13A.IV vs **60a** in Figure 13C), it can be seen that it is not exactly the same. Actually, **IV** corresponds to the simultaneous disappearance of **60a** and triethylamine, which forms triethylammonium bromide.

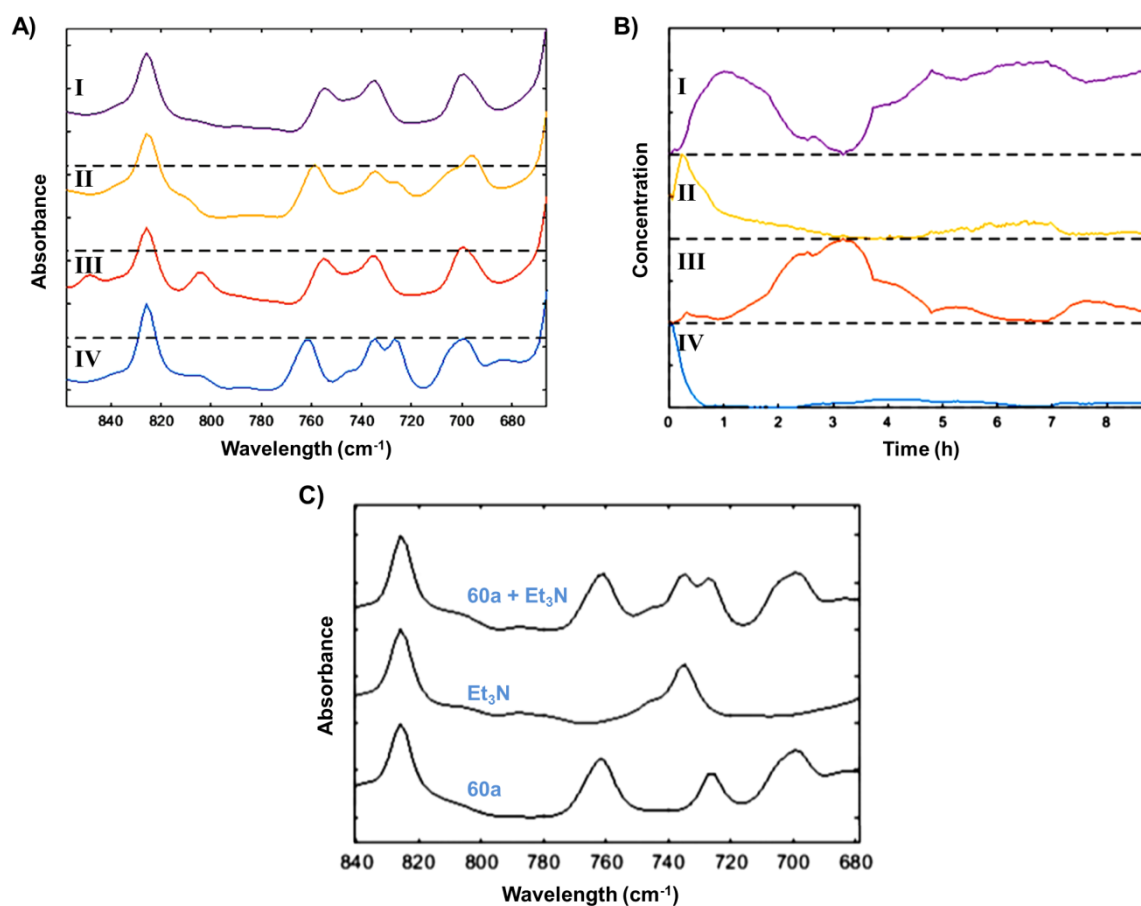


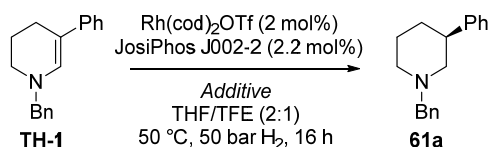
**Figure 13.** A) Generated IR spectra of different compounds or group of compounds identified by the software during the first 9 h. B) Evolution of these species with time. C) Experimental IR spectra of **60a**, **Et<sub>3</sub>N** and **60a + Et<sub>3</sub>N** (all measured in THF/TFE).

Thus, despite not being able to identify any dihydropyridine intermediate due to the complexity of the system, we were able to find more evidences proving the fast disappearance of **60a** with concomitant formation of ammonium salts.

Identifying all these tetrahydropyridines and their evolution with time gave us a good perspective of what was going on, but it was still not clear which one of them was leading to the highly enantioenriched piperidine **61a**. Since two of them could be isolated (**TH-1** and **TH-2**), they were submitted to the optimized hydrogenation conditions.

Under the exact conditions used to perform the hydrogenation of **60a** (Table 17, entry 1), only 7% of **TH-1** was converted into the racemic piperidine **61a**. Increasing the acidity of the system (entries 2 and 3) also increased the conversion, but the hydrogenation always took place in a non-enantioselective way. This is in agreement with the proposed mechanism for this kind of enamines which, by catching a  $H^+$  from the medium, tautomerize to the iminium form and then are hydrogenated: since the tautomerization is not enantioselective, **61a** is obtained as racemate.

**Table 17.** Hydrogenation of **TH-1** with different additives.

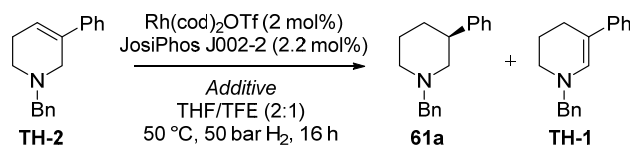


#	Additive	Remaining TH-1 (%)	yield of 61a (%)	ee of 61a (%)
1	Et <sub>3</sub> N [5 equiv.]	93	7	0
2	-	57	43	0
3	Et <sub>3</sub> N·HCl [5 equiv.]	12	88	0

*Reaction conditions:* **TH-1** (0.025 mmol), Rh(cod)<sub>2</sub>OTf (2 mol%), JosiPhos J002-2 (2.2 mol%), additive, THF/TFE (2:1, 1.5 mL), 50 °C, 50 bar H<sub>2</sub>, 20 h. Conversion and *ee* determined by chiral GC.

Similar experiments were performed with **TH-2** and, surprisingly, it was found that it could isomerize to **TH-1** under the reaction conditions (Table 18). Actually, Rh-diphosphine complexes are known to promote allylamine-enamine isomerizations.<sup>72</sup> Different amounts of base were tested (entries 1-3), even in the presence of pyridinium salt **60f** to try to reproduce the reaction conditions (entry 4). Again, the more acidic the media, the higher was the conversion. The fact that **61a** was obtained with some enantiomeric excess proves that **TH-2** can be enantioselectively hydrogenated, without the need to isomerize to **TH-1**. Unfortunately, the obtained *ee*'s are far from those obtained in the direct hydrogenation of **60a**.

**Table 18.** Hydrogenation of **TH-2** with different additives.



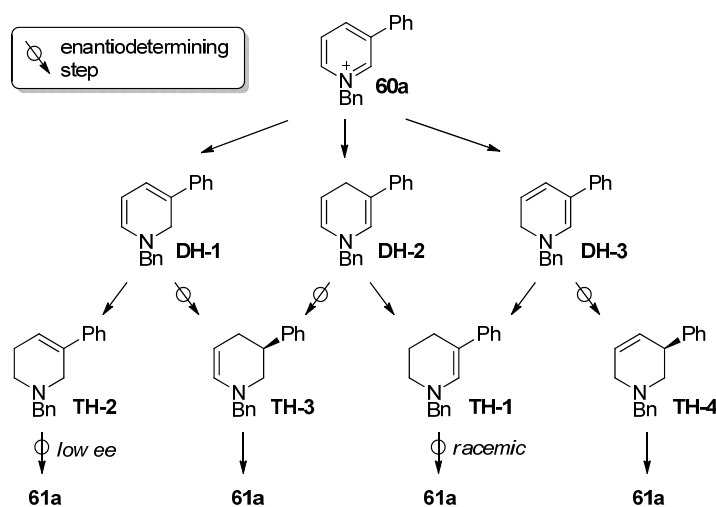
#	Additive	Remaining TH-2 (%)	yield of 61a (%)	ee of 61a (%)	yield of TH-1 (%)
1	Et <sub>3</sub> N [5 equiv.]	80	7	15	13
2	Et <sub>3</sub> N [5 equiv.] + Et <sub>3</sub> N·HCl [5 equiv.]	53	17	21	30
3	-	21	74	27	6
4	<b>60f</b> [4 equiv.] + Et <sub>3</sub> N [20 equiv.]	78	9	31	13

*Reaction conditions:* **TH-2** (0.025 mmol), Rh(cod)<sub>2</sub>OTf (2 mol%), JosiPhos J002-2 (2.2 mol%), additive, THF/TFE (2:1, 1.5 mL), 50 °C, 50 bar H<sub>2</sub>, 20 h. Conversion and *ee* determined by chiral GC.

The latter two experiments strongly indicate that neither **TH-1** nor **TH-2** are the intermediates leading to the highly enantioselective formation of **61a**. Since those were the only

prochiral tetrahydropyridines, the enantioselective hydrogenation must occur on a dihydropyridine intermediate which leads to the unidentified tetrahydropyridine (**TH-3** or **TH-4**), whose *ee* had been found to be very high (see the monitoring of the reaction over time, Figure 10).

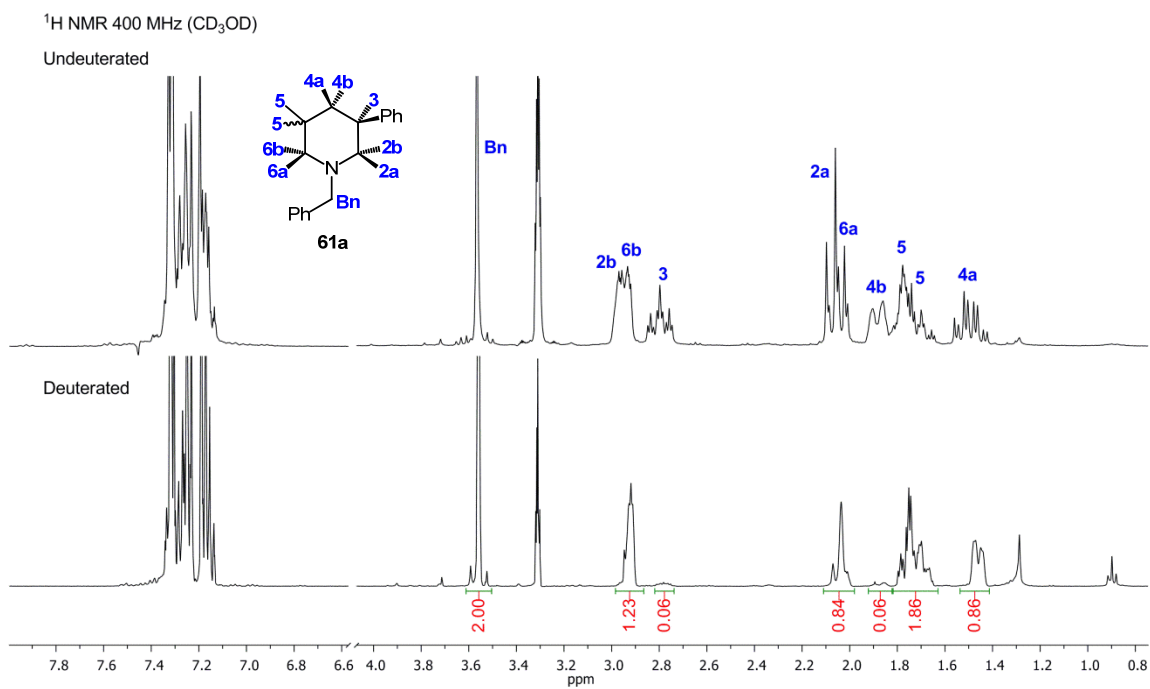
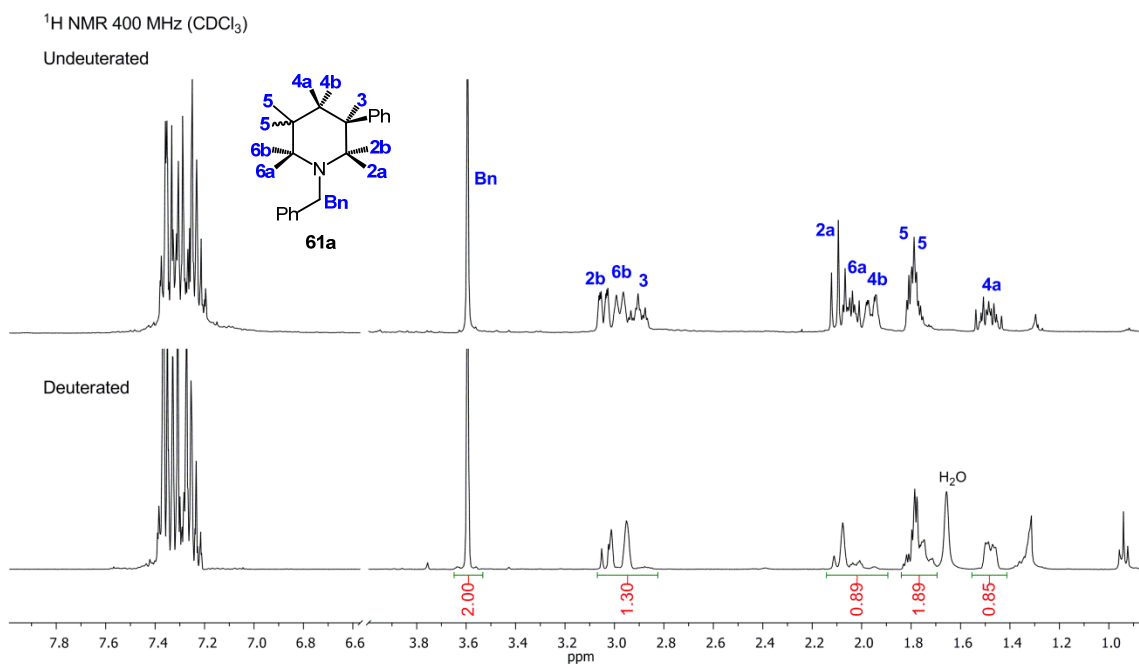
The plausible pathways for the hydrogenation of **60a** to **61a** are shown in Scheme 61. The first hydride addition could take place in any of the most electrophilic positions (C2, C4 and C6), to afford dihydropyridines **DH-1**, **DH-2** and **DH-3**, respectively. Unfortunately, these dihydropyridines are not observed experimentally. Their enantioselective hydrogenation to afford **TH-3** or **TH-4** might go through the reduction of an enamine double bond (**DH-3** → **TH-4** or **DH-2** → **TH-3**) or by reduction of the C3-C4 double bond (**DH-1** → **TH-3**).



**Scheme 61.** Plausible pathways for the hydrogenation of **60a** to **61a**.

To ascertain which of these pathways was occurring, an isotopic labeling experiment using  $D_2$  instead of  $H_2$  was performed. The deuteration pattern of **61a** was not easy to determine, since all hydrogen atoms in the piperidine ring are diastereotopic. To be able to ascertain the extent of deuterium incorporation in all positions it was necessary to record the  $^1H$  NMR in three different solvents ( $CDCl_3$  – Figure 14,  $CD_3OD$  – Figure 15 and toluene- $d_8$  – Figure 16). In each of these solvents, different protons were separated from the rest, allowing for an accurate integration.

Assignment of the chemical shift of each proton was done by multidimensional NMR analysis. Geminal protons were differentiated based on the anisotropy cone of C-C single bonds described in Chapter II.



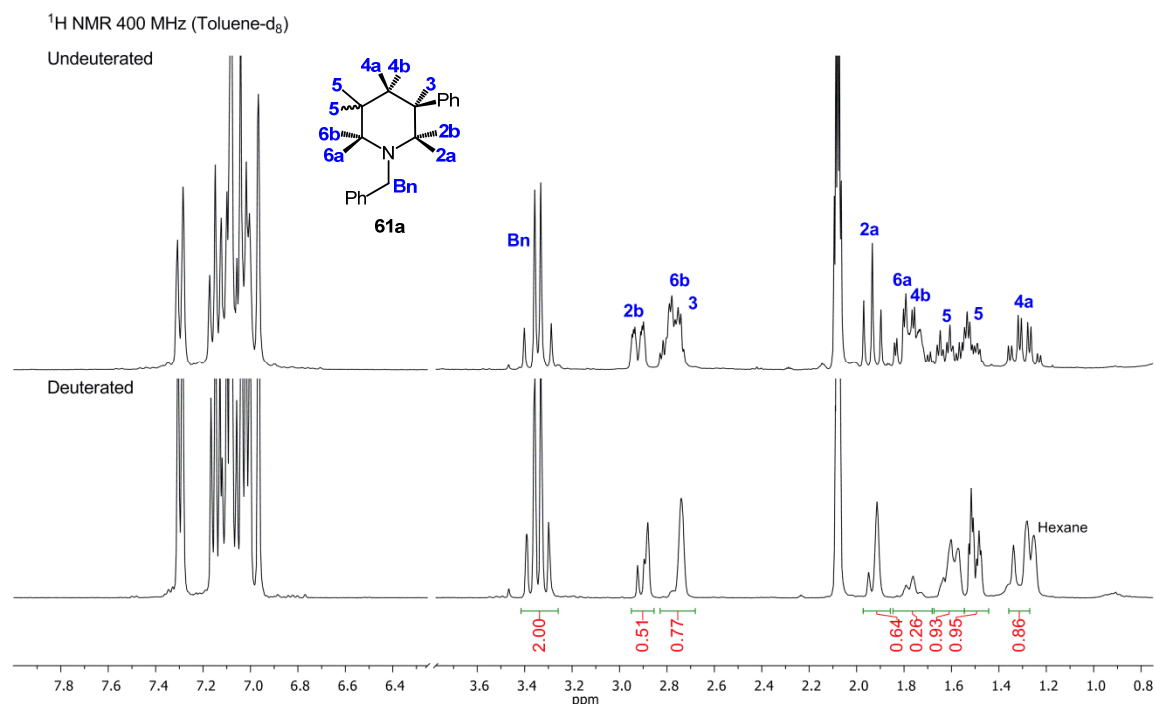


Figure 16. <sup>1</sup>H-NMR of **61a** and deuterated **61a** in toluene-d<sub>8</sub>.

Simple systems of equations with the integrals in the different solvents allowed for the calculation of the integral of overlapping signals in the deuterated sample:

$$\begin{cases} \text{CDCl}_3: & \text{H}_{2b} + \text{H}_{6b} + \text{H}_3 = 1.30 \\ \text{CD}_3\text{OD}: & \text{H}_{2b} + \text{H}_{6b} = 1.23 & \mathbf{H}_3 = 0.06 \\ \text{Tol-d}_8: & \text{H}_{6b} + \text{H}_3 = 0.77 & \mathbf{H}_{2b} = 0.51 & \mathbf{H}_{6b} = 0.72 \end{cases}$$

$$\begin{cases} \text{CDCl}_3: & \text{H}_{2a} + \text{H}_{6a} + \text{H}_{4b} = 0.89 \\ \text{CD}_3\text{OD}: & \text{H}_{2a} + \text{H}_{6a} = 0.84 & \mathbf{H}_{4b} = 0.06 \\ \text{Tol-d}_8: & \text{H}_{6a} + \text{H}_{4b} = 0.26 & \mathbf{H}_{2a} = 0.64 & \mathbf{H}_{6a} = 0.20 \end{cases}$$

$$\begin{cases} \text{CDCl}_3: & \text{H}_5 + \text{H}_{5'} = 1.89 \\ \text{CD}_3\text{OD}: & \text{H}_5 + \text{H}_{5'} = 1.86 \\ \text{Tol-d}_8: & \mathbf{H}_5 = 0.93 & \mathbf{H}_{5'} = 0.95 & \mathbf{H}_{4a} = 0.86 \end{cases}$$

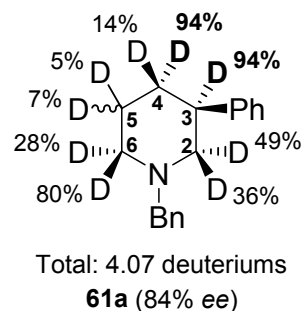
A summary of the chemical shifts of each proton in the different solvents can be found in Table 19, together with the integrals of the deuterated **61a**.

As expected, the deuteration pattern **61a** turned out to be quite complex. It has to be considered that different pathways might be taking place simultaneously leading to a final linear combination of different deuteration distributions. Despite this complexity, the analysis of the deuteration pattern provided some useful information. First and most important, two *syn*-arranged atoms of deuterium are incorporated at C3 and C4. According to the postulated pathways (Scheme 61), this can only originate from the hydrogenation of **TH-2** → **2a** or **DH-1** → **TH-3**. Since we have already shown that the hydrogenation **TH-2** is poorly enantioselective, the only reasonable pathway is a highly enantioselective hydrogenation of **DH-1**. This means that the

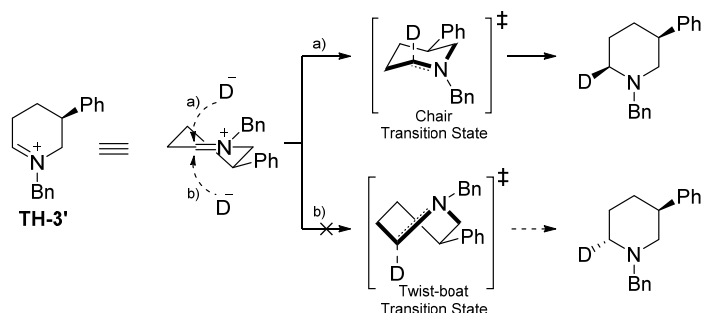
unidentified tetrahydropyridine is in fact **TH-3**. Second, the total number of deuterium atoms incorporated in **61a** is four and not five, as it might have been expected if all protons were coming from hydrogen gas. This implies that one hydrogen from the solvent is also incorporated (probably at C5, which is the least deuterated position). This incorporation might arise from the tautomerization of enamine **TH-3** to the corresponding iminium, prior to hydrogenation.

**Table 19.** Chemical shift of each proton in different solvents and NMR integrals of the deuterated **61a**.

H	$\delta$ (ppm) in CDCl <sub>3</sub>	$\delta$ (ppm) in CD <sub>3</sub> OD	$\delta$ (ppm) in toluene-d <sub>8</sub>	Integrals of deuterated <b>61a</b>
2a	2.09	2.06	1.93	0.64
2b	3.04	2.96	2.92	0.51
3	2.90	2.80	2.75	0.06
4a	1.48	1.49	1.29	0.86
4b	1.96	1.88	1.75	0.06
5	1.79	1.77	1.61	0.93
5'	1.79	1.70	1.53	0.95
6a	2.04	2.04	1.80	0.20
6b	2.98	2.93	2.79	0.72



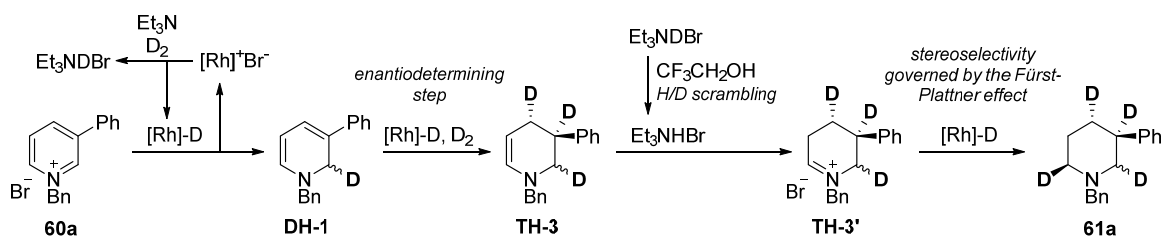
Third, it should be carefully analyzed the deuteration patterns in the two positions where the hydride addition is taking place, C2 and C6. While the deuterium incorporation in the two diastereotopic positions of C2 is quite similar (49% and 36%), in C6 that difference is much more remarkable (80% for the pro-*S* hydrogen and 28% for the pro-*R*). A possible explanation for it might be that, since the hydride addition to C2 takes place before the stereocenter is formed (**60a** → **DH-1**) it is only influenced by the chiral catalyst. Instead, when the hydride addition to C6 takes place the stereocenter is already formed (**TH-3** → **61a**), hence there is a remarkable substrate control also operating. Accordingly, the higher deuteration of the pro-*S* hydrogen in C6 can be explained by the Fürst-Plattner rule (also known as the trans-diaxial effect),<sup>73</sup> which predicts the stereoselective addition of nucleophiles to cyclohexenes (or similar) based on the stability of the transition state, i.e. a chair-like transition state will be more favored than the twist-boat one. In our specific case, a chair-like transition state is involved when the deuterium addition takes place from the phenyl substituent side.



**Scheme 62.** Fürst-Plattner effect governing the hydride addition to iminium **TH-3'**.

Taking into account all this data regarding the pathway leading to **61a**, a mechanism to explain the observed deuteration pattern was proposed (Scheme 63). The first hydride addition would take place in the C2 position leading to **DH-1**. The enantioselective hydrogenation of the

C3=C4 bond affords **TH-3**, which by catching a proton from the medium isomerizes to the iminium form **TH-3'**. In the last step, a hydride addition governed by the Fürst-Plattner effect furnishes piperidine **61a**.



**Scheme 63.** Proposed mechanism leading to the observed deuteration pattern in **61a**.

As previously discussed, the achievement of high enantioselectivities generally requires a secondary coordinating unit. A clear example of this is the Rh-catalyzed AH of enamides, where the carbonyl group chelates the rhodium center leading to an improved stereocontrol (Figure 17A).<sup>74</sup> In our case, the distance between the double bond that has to be enantioselectively hydrogenated and the nitrogen atom (the only possible coordinating group) is optimal for the formation of a 5-membered ring intermediate after the first hydride addition (Figure 17B). The release of Rh from complex **62** might take place via protonation of C4 through a  $\sigma$ -bond metathesis with  $\text{H}_2$  or via an oxidative addition-reductive elimination sequence.

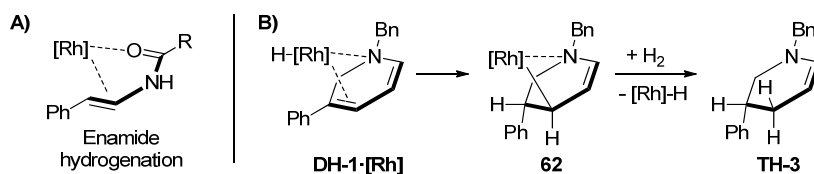
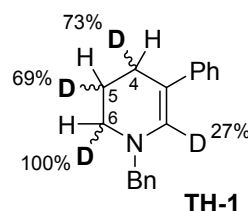


**Figure 17.** A) Secondary coordination on the Rh-catalyzed enantioselective hydrogenation of enamides. B) Proposed secondary coordination for the enantioselective hydrogenation of dihydropyridine **DH-1**.

In the isotopic labeling experiment with  $\text{D}_2$ , deuterated **TH-1** and **TH-2**<sup>†</sup> were also isolated and analyzed (see III.3 Experimental section for the NMR spectra). In the case of **TH-1** (Table 20), the more deuterated positions are C4, C5 and C6. According to it, the postulated pathway for the formation of **TH-1**[ $d_3$ ] would proceed via an initial hydride addition to C6 to afford dihydropyridine **DH-3**, and subsequent C4-C5 double bond hydrogenation (Scheme 64A).

**Table 20.** Chemical shift of each proton and NMR integrals of the deuterated **TH-1**.

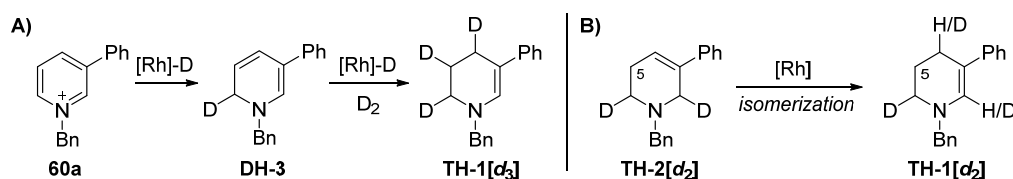
H	$\delta$ (ppm) in $\text{CDCl}_3$	Integrals of deuterated <b>TH-1</b>
2	6.75	0.73
4	2.45	1.27
5	2.02	1.31
6	3.00	0.98



<sup>†</sup> For clarity, the carbon numbering on the tetrahydropyridines follows the same numbering than the final piperidine **61a** and not the IUPAC rules.



However, the theoretical deuteration shown in **TH-1**[ $d_3$ ] (Scheme 64) does not perfectly correlate with the observed deuteration in Table 20. On the one hand, the unexpected deuteration at C2 might be explained by H/D scrambling between C2 and C4 due to a Rh-catalyzed allylamine-enamine isomerization.<sup>72</sup> Indeed, the sum of deuterium at C2 and C4 is equal to one (0.73 + 0.27). On the other hand, the rather low deuteration at the C5 position (0.69 instead of 1) could also be explained by the same mechanism. The isomerization of **TH-2**[ $d_2$ ], whose C4 position is not deuterated (*vide infra*), could afford **TH-1**[ $d_2$ ], which is also devoid of deuterium at C4 (Scheme 64B). Thus, a linear combination of **TH-1**[ $d_3$ ] and **TH-1**[ $d_2$ ] would make up for the observed deuteration at C4.



**Scheme 64.** A) Postulated formation of **TH-1**[ $d_3$ ] from **60a**. B) Postulated formation of **TH-1**[ $d_2$ ] from **TH-2**[ $d_2$ ].

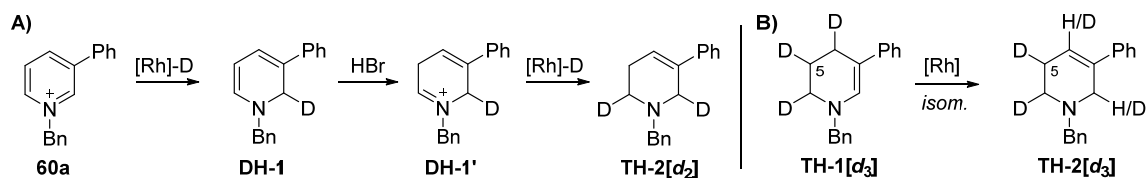
In the case of **TH-2** the most deuterated positions were C2 and C6 (Table 21). An initial hydride addition to C2 would afford **DH-1** that, after tautomerization to the iminium form (no deuteration in C5), would be reduced to **TH-2**[ $d_2$ ] (Scheme 65A).

**Table 21.** Chemical shift of each proton and NMR integrals of the deuterated **TH-2**.

H	$\delta$ (ppm) in $CDCl_3$	Integrals of deuterated <b>TH-2</b>
2	3.37	1.09
4	6.12	0.91
5	2.34	0.99
6	2.63	1.88

Chemical structure of **TH-2** with NMR integrals: C2 (12%), C4 (9%), C5 (100%), C6 (91%).

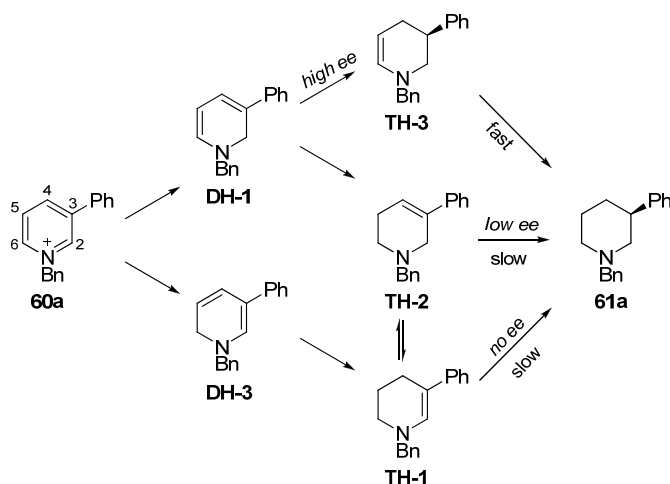
Similarly to what was observed for **TH-1**, there is an unexpected deuteration in C4, ascribable to the allylamine-enamine isomerization, and a small amount of deuteration in C5 which might arise from the isomerization of **TH-1**[ $d_3$ ] to **TH-2**[ $d_3$ ] (Scheme 65B).



**Scheme 65.** A) Postulated formation of **TH-2**[ $d_2$ ] from **60a**. B) Postulated formation of **TH-2**[ $d_3$ ] from **TH-1**[ $d_3$ ].

On the basis of this detailed study, a mechanism involving all different pathways investigated was proposed (Scheme 66). An initial hydride addition to C2 or C6 would afford dihydropyridines **DH-1** or **DH-3**, respectively. An enantioselective hydrogenation of the C3-C4 double bond in **DH-1** would lead to the highly enantioenriched tetrahydropyridine **TH-3**, which

would be relatively fast hydrogenated to **61a** via the corresponding iminium intermediate. Instead, the tautomerization of **DH-1** to the more activated iminium form would trigger a fast hydrogenation to tetrahydropyridine **TH-2**. The latter can either undergo a Rh-catalyzed allylamine-enamine isomerization or be very slowly hydrogenated to **61a** with a very low enantioselectivity. Simultaneously, the hydrogenation of the C4-C5 double bond of **DH-3** affords tetrahydropyridine **TH-1**, which can also undergo a Rh-catalyzed isomerization to **TH-2** or be non-enantioselectively hydrogenated to **61a**. The proposed mechanism does not exclude other transformations or intermediates that might be involved in the process.



**Scheme 66.** Proposed pathways involved in the AH of **60a** to **61a**. All represented steps involve Rh species.

### III.3 CONCLUSIONS

To conclude, the first highly enantioselective hydrogenation of 3-substituted pyridines has been successfully developed. The addition of a simple base, like  $\text{Et}_3\text{N}$ , remarkably improved the obtained yields and enantioselectivities with a Rh-Josiphos catalyst. Furthermore, an exhaustive mechanistic study shed some light on the main pathways governing the complex reaction network involved in the AH of these pyridinium salts. As initially postulated, the addition of a base retarded the enamine-iminium tautomerization on **TH-1**. However, the high enantioselectivities obtained did not arise from the enamine hydrogenation, but from an alternative pathway involving the AH of the dihydropyridine intermediate **DH-1**. The enamine intermediate **TH-1** resulted to be a side-product of the reaction that, under non-basic conditions, is readily hydrogenated to the final piperidine in a non-enantioselective fashion, thus eroding the final enantiomeric excess.

Although these results are still far from being amenable to industrial application, we hope that the better understanding of the system and its mechanism will contribute to the rational design of more efficient catalyst for the AH of 3-substituted pyridines.

### III.4 EXPERIMENTAL SECTION

Dry DCM and THF were obtained using an MBraun SPS system. Dry MeOH, EtOH, *i*PrOH and toluene (over molecular sieves in bottles with crown cap) were purchased from Sigma Aldrich and stored under nitrogen. 2,2,2-trifluoroethanol (TFE) was dried over molecular sieves. Commercially available reagents (from TCI Chemicals, ACROS, Sigma Aldrich, Strem) were used as received, without any further purification.

Flash column chromatography was performed using Grace Reveleris® X2 Flash Chromatography System (silica gel cartridges with particle size 40 µm). Gas chromatography was performed on an Agilent Technologies 7890A and Hewlett Packard 6890 instruments, equipped with a flame ionization detector, using respectively a chiral and an achiral capillary column. HPLC analysis were performed using a Waters HPLC with a dual λ absorbance detector working at 210 and 254 nm.

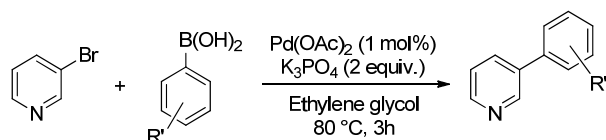
<sup>1</sup>H-NMR spectra were recorded using two different spectrometers operating at 400 or 500 MHz. Proton chemical shifts are reported in ppm (δ) with the solvent reference relative to tetramethylsilane (TMS) employed as the internal standard (CDCl<sub>3</sub> δ = 7.26 ppm; CD<sub>2</sub>Cl<sub>2</sub> δ = 5.32 ppm, CD<sub>3</sub>OD δ = 3.31 ppm, toluene-*d*<sub>8</sub> δ = 7.09, 7.01, 6.97 and 2.08). <sup>13</sup>C-NMR spectra were recorded on a 400 MHz spectrometer operating at 101 MHz, with complete proton decoupling. Carbon chemical shifts are reported in ppm (δ) relative to TMS with the respective solvent resonance as the internal standard (CDCl<sub>3</sub>, δ = 77.16 ppm, CD<sub>2</sub>Cl<sub>2</sub> δ = 53.84 ppm, CD<sub>3</sub>OD δ = 49.00 ppm). <sup>19</sup>F-NMR spectra were recorded on a 300 MHz spectrometer operating at 282 MHz, with complete proton decoupling. Fluorine chemical shifts are reported in ppm (δ) relative to external CFCl<sub>3</sub> at 0 ppm (positive values downfield). The following abbreviations are used to describe spin multiplicity: s = singlet, d = doublet, t = triplet, q = quartet, m = multiplet, dd = doublet-doublet, ddd = doublet-doublet-doublet, dt = doublet-triplet. Coupling constant values are given in Hz.

Optical rotation signs were determined on an automatic polarimeter with a 1 dm cell at the sodium D line (λ = 589 nm). High resolution mass spectra (HRMS) were performed on a Fourier Transform Ion Cyclotron Resonance (FT-ICR) Mass Spectrometer APEX II & Xmass software (Bruker Daltonics) – 4.7 T Magnet (Magnex) equipped with ESI source. Infrared spectra were recorded on a standard FT/IR spectrometer. *In situ* FTIR spectroscopy was performed with a Mettler Toledo ReactIR™ 15 system connected with optical fibers to an ATR Diamond probe inserted in the reactor. Multivariate data analysis was performed with iC IR Software (Mettler Toledo).

#### General procedure for the synthesis of 3-arylpyridines

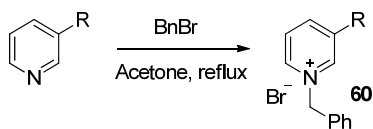
A mixture of 3-bromopyridine (1 ml, 9.9 mmol), the boronic acid (14.9 mmol, 1.5 equiv.), Pd(OAc)<sub>2</sub> (22 mg, 0.1 mmol), K<sub>3</sub>PO<sub>4</sub> (4.2 g, 19.8 mmol) and 75 mL of ethylene glycol were stirred at 80 °C for 5 h. Once the reaction was completed, the reaction mixture was poured into

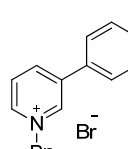
150 mL of brine and extracted with 150 mL of Et<sub>2</sub>O. NaOH (7.5 g) was added to the ethereal phase and the mixture was stirred for 15 min. Then it was poured into 150 mL of brine, the ethereal phase was again separated and stirred in the presence of NaOH (7.5 g). After 15 min more, the mixture was poured one last time into 150 mL of brine and the ethereal phase was separated, dried over Na<sub>2</sub>SO<sub>4</sub>, filtered and concentrated several times in the presence of MeOH. The obtained 3-arylpyridine was used in the next step without any further purification.

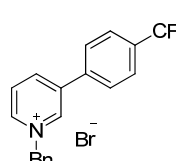


### General procedure for the benzylation of pyridines

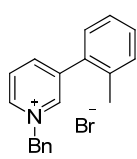
Pyridinium salts **60** were prepared according to known literature methods.<sup>16,60</sup> A mixture of 3-substituted pyridine (6.5 mmol), benzyl bromide (7.7 mmol, 1.2 equiv.) and 2.5 mL acetone were stirred under reflux temperature for 18-48h. If the product precipitated, it was filtered, washed several times with acetone and dried under high vacuum. If the product did not precipitate, the solvent was removed and the resulting sticky oil was recrystallized from MeOH/AcOEt (9:1). If the desired product could not be recrystallized, it was purified from the reaction mixture by column chromatography on silica gel using CH<sub>2</sub>Cl<sub>2</sub>/MeOH (30:1) to give the desired products (25-95%).



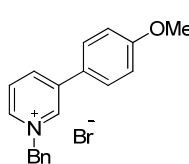
 **N-Benzyl-3-phenylpyridinium bromide (60a):** White solid; m.p. = 91 °C; <sup>1</sup>H NMR (400 MHz, CDCl<sub>3</sub>) δ 9.48 (s, 1H), 9.24 (d, <sup>3</sup>J(H,H) = 6.0 Hz, 1H), 8.52 (d, <sup>3</sup>J(H,H) = 8.0 Hz, 1H), 8.06 (dd, <sup>3</sup>J(H,H) = 8.0 Hz, <sup>3</sup>J(H,H) = 6.0 Hz, 1H), 7.78 (m, 2H), 7.63 (m, 2H), 7.59 – 7.46 (m, 3H), 7.46 – 7.38 (m, 3H), 6.27 (s, 2H); <sup>13</sup>C NMR (101 MHz, CDCl<sub>3</sub>) δ 142.9, 142.9, 142.5, 141.3, 133.4, 132.7, 130.6, 129.9, 129.9, 129.8, 129.6, 128.4, 127.8, 64.0; IR (film): ν = 3053.7, 2924.5, 1629.6, 1488.8, 1456.0, 1431.9, 1155.2 cm<sup>-1</sup>; HRMS (ESI<sup>+</sup>): m/z 246.12790 [M]<sup>+</sup> (calcd. for C<sub>18</sub>H<sub>16</sub>N<sub>1</sub>: 246.12773).

 **N-Benzyl-3-(4-(trifluoromethyl)phenyl)pyridinium bromide (60b):** White solid; m.p. = 170 °C; <sup>1</sup>H NMR (400 MHz, CD<sub>3</sub>OD) δ 9.59 (s, 1H), 9.07 (d, <sup>3</sup>J(H,H) = 6.1 Hz, 1H), 8.95 (d, <sup>3</sup>J(H,H) = 8.2 Hz, 1H), 8.22 (dd, <sup>3</sup>J(H,H) = 8.2 Hz, <sup>3</sup>J(H,H) = 6.1 Hz, 1H), 8.06 (d, <sup>3</sup>J(H,H) = 8.2 Hz, 2H), 7.92 (d, <sup>3</sup>J(H,H) = 8.2 Hz, 2H), 7.63 – 7.57 (m, 2H), 7.53 – 7.45 (m, 3H), 5.98 (s, 2H); <sup>13</sup>C NMR (101 MHz, CD<sub>3</sub>OD) δ 145.3, 144.7, 144.5, 141.4, 138.4, 134.6, 133.1 (q, <sup>2</sup>J(C,F) = 32.9 Hz), 131.1, 130.7, 130.3, 129.9, 129.7, 127.5 (q, <sup>3</sup>J(C,F) = 3.8 Hz), 124.0 (q, <sup>1</sup>J(C,F) = 271.8 Hz), 65.9; <sup>19</sup>F NMR (282 MHz, CD<sub>3</sub>OD) δ -64.7; IR (film): ν = 3042.2, 2956.3, 1629.6, 1497.5, 1456.0, 1406.8,

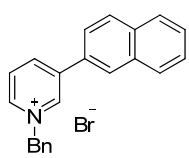
1326.8, 1170.6, 1123.3, 1075.1  $\text{cm}^{-1}$ ; HRMS (ESI+):  $m/z$  314.11468  $[\text{M}]^+$  (calcd. for  $\text{C}_{19}\text{H}_{15}\text{N}_1\text{F}_3$ : 314.11511).



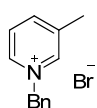
**N-Benzyl-3-(2-tolyl)pyridinium bromide (60c):** White solid; m.p. = 151 °C;  $^1\text{H}$  NMR (400 MHz,  $\text{CD}_3\text{OD}$ )  $\delta$  9.20 (t,  $^4J(\text{H,H}) = 1.7$  Hz, 1H), 9.11 (dt,  $^3J(\text{H,H}) = 6.1$  Hz,  $^4J(\text{H,H}) = 1.3$  Hz, 1H), 8.62 (ddd,  $^3J(\text{H,H}) = 8.0$  Hz,  $^4J(\text{H,H}) = 1.8$  Hz,  $^4J(\text{H,H}) = 1.2$  Hz, 1H), 8.20 (dd,  $^3J(\text{H,H}) = 7.8$  Hz,  $^3J(\text{H,H}) = 6.3$  Hz, 1H), 7.65 – 7.58 (m, 2H), 7.53 – 7.35 (m, 7H), 5.97 (s, 2H), 2.28 (s, 3H);  $^{13}\text{C}$  NMR (101 MHz,  $\text{CD}_3\text{OD}$ )  $\delta$  147.5, 145.6, 144.1, 143.8, 137.0, 135.1, 134.8, 132.2, 131.2, 131.1, 131.1, 130.7, 130.2, 129.4, 127.9, 65.8, 20.2; IR (film):  $\nu = 3023.8, 2949.6, 1626.7, 1485.9, 1456.0, 1273.8, 1153.2$   $\text{cm}^{-1}$ ; HRMS (ESI+):  $m/z$  260.14385  $[\text{M}]^+$  (calcd. for  $\text{C}_{19}\text{H}_{18}\text{N}_1$ : 260.14338).



**N-Benzyl-3-(4-methoxyphenyl)pyridinium bromide (60d):** Yellowish solid; m.p. = 178 °C;  $^1\text{H}$  NMR (400 MHz,  $\text{CD}_3\text{OD}$ )  $\delta$  9.46 (t,  $^4J(\text{H,H}) = 1.5$  Hz, 1H), 8.92 (dt,  $^3J(\text{H,H}) = 6.1$  Hz,  $^4J(\text{H,H}) = 1.1$  Hz, 1H), 8.80 (ddd,  $^3J(\text{H,H}) = 8.2$  Hz,  $^4J(\text{H,H}) = 1.9$  Hz,  $^4J(\text{H,H}) = 1.1$  Hz, 1H), 8.11 (dd,  $^3J(\text{H,H}) = 8.1$  Hz,  $^3J(\text{H,H}) = 6.1$  Hz, 1H), 7.84 – 7.79 (m, 2H), 7.63 – 7.58 (m, 2H), 7.50 – 7.43 (m, 3H), 7.14 – 7.09 (m, 2H), 5.96 (s, 2H), 3.86 (s, 3H);  $^{13}\text{C}$  NMR (101 MHz,  $\text{CD}_3\text{OD}$ )  $\delta$  163.2, 143.7, 143.2, 142.9, 142.7, 134.8, 131.0, 130.7, 130.2, 130.1, 129.6, 126.5, 116.2, 65.7, 56.1; IR (film):  $\nu = 3034.4, 2959.2, 2839.7, 1607.4, 1496.5, 1456.0, 1305.6, 1291.11, 1257.4, 1185.0, 1029.8, 1017.3$   $\text{cm}^{-1}$ ; HRMS (ESI+):  $m/z$  276.13858  $[\text{M}]^+$  (calcd. for  $\text{C}_{19}\text{H}_{18}\text{N}_1\text{O}_1$ : 276.13829).

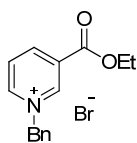


**N-Benzyl-3-(naphthalen-2-yl)pyridinium bromide (60e):** White solid; m.p. = 207 °C;  $^1\text{H}$  NMR (400 MHz,  $\text{CDCl}_3$ )  $\delta$  9.73 (s, 1H), 9.10 (d,  $^3J(\text{H,H}) = 5.8$  Hz, 1H), 8.61 (d,  $^3J(\text{H,H}) = 8.1$  Hz, 1H), 8.38 (s, 1H), 8.05 – 8.00 (m, 2H), 7.98 (d,  $^3J(\text{H,H}) = 8.8$  Hz, 1H), 7.87 – 7.79 (m, 2H), 7.63 (m, 2H), 7.60 – 7.52 (m, 2H), 7.45 – 7.38 (m, 3H), 6.26 (s, 2H);  $^{13}\text{C}$  NMR (101 MHz,  $\text{CDCl}_3$ )  $\delta$  143.0, 142.3, 142.2, 141.0, 133.8, 133.4, 129.9, 129.8, 129.7, 129.6, 129.5, 129.2, 128.2, 128.1, 127.9, 127.7, 127.2, 124.0, 64.0; IR (film):  $\nu = 3035.4, 2949.6, 1626.7, 1501.3, 1456.0, 1155.2$   $\text{cm}^{-1}$ ; HRMS (ESI+):  $m/z$  296.14378  $[\text{M}]^+$  (calcd. for  $\text{C}_{22}\text{H}_{18}\text{N}_1$ : 296.14338).



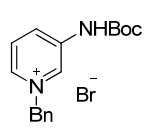
**N-Benzyl-3-methylpyridinium bromide (60f)**

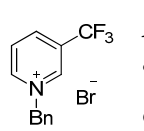
Known compound. Spectroscopic data are superimposable to those reported in the literature.<sup>75</sup>

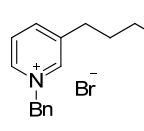


**N-Benzyl-3-(ethoxycarbonyl)pyridinium bromide (60g)**

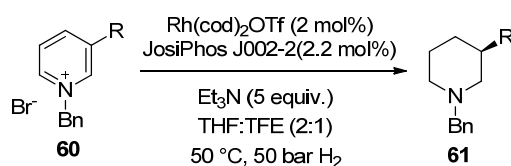
Known compound. Spectroscopic data are superimposable to those reported in the literature.<sup>76</sup>


**N-Benzyl-3-((*tert*-butoxycarbonyl)amino)pyridinium bromide (60h):** White solid; m.p. = 186 °C; <sup>1</sup>H NMR (400 MHz, CD<sub>3</sub>OD) δ 9.31 (s, 1H), 8.68 (d, <sup>3</sup>J(H,H) = 5.6 Hz, 1H), 8.33 (d, <sup>3</sup>J(H,H) = 8.7 Hz, 1H), 7.97 (dd, <sup>3</sup>J(H,H) = 8.6 Hz, <sup>3</sup>J(H,H) = 6.0 Hz, 1H), 7.56 – 7.43 (m, 5H), 5.82 (s, 2H), 1.53 (s, 9H); <sup>13</sup>C NMR (101 MHz, CD<sub>3</sub>OD) δ 153.9, 142.5, 139.0, 134.6, 134.4, 134.3, 131.0, 130.7, 130.2, 129.4, 83.2, 66.2, 28.4; IR (film): ν = 3093.3, 2980.5, 1725.0, 1630.5, 1551.5, 1507.1, 1248.7, 1156.1 cm<sup>-1</sup>; HRMS (ESI<sup>+</sup>): *m/z* 285.16038 [M]<sup>+</sup> (calcd. for C<sub>17</sub>H<sub>21</sub>N<sub>2</sub>O<sub>2</sub>: 285.15975).

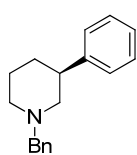

**N-Benzyl-3-(trifluoromethyl)pyridinium bromide (60i):** White solid; m.p. = 151 °C; <sup>1</sup>H NMR (400 MHz, CD<sub>3</sub>OD) δ 9.83 (s, 1H), 9.44 (d, <sup>3</sup>J(H,H) = 6.2 Hz, 1H), 9.05 (d, <sup>3</sup>J(H,H) = 8.2 Hz, 1H), 8.43 (dd, <sup>3</sup>J(H,H) = 7.6 Hz, <sup>3</sup>J(H,H) = 6.8 Hz, 1H), 7.74 – 7.65 (m, 2H), 7.54 – 7.43 (m, 3H), 6.13 (s, 2H); <sup>13</sup>C NMR (101 MHz, CD<sub>3</sub>OD) δ 149.5, 144.5 (q, <sup>3</sup>J(C,F) = 3.3 Hz), 144.3, 133.8, 132.0 (q, <sup>2</sup>J(C,F) = 36.4 Hz), 131.3, 130.8, 130.7, 130.7, 122.8 (q, <sup>1</sup>J(C,F) = 273.1 Hz), 66.3; <sup>19</sup>F NMR (282 MHz, CD<sub>3</sub>OD) δ -64.4; IR (film): ν = 3037.3, 2997.8, 2943.8, 1642.1, 1476.2, 1335.5, 1188.9, 1146.5, 1098.3 cm<sup>-1</sup>; HRMS (ESI<sup>+</sup>): *m/z* 238.08431 [M]<sup>+</sup> (calcd. for C<sub>13</sub>H<sub>11</sub>N<sub>1</sub>F<sub>3</sub>: 238.08381).


**N-Benzyl-3-butylpyridinium bromide (60j):** Colorless and viscous oil; <sup>1</sup>H NMR (400 MHz, CDCl<sub>3</sub>) δ 9.47 (s, <sup>3</sup>J(H,H) = 11.2 Hz, 1H), 9.42 (d, <sup>3</sup>J(H,H) = 6.1 Hz, 1H), 8.15 (d, <sup>3</sup>J(H,H) = 8.0 Hz, 1H), 7.92 (dd, <sup>3</sup>J(H,H) = 7.9 Hz, <sup>3</sup>J(H,H) = 6.2 Hz, 1H), 7.77 – 7.64 (m, 2H), 7.37 – 7.28 (m, 3H), 6.26 (s, 2H), 2.81 (d, <sup>3</sup>J(H,H) = 15.8 Hz, 2H), 1.62 (m, 2H), 1.31 (m, 2H), 0.87 (t, <sup>3</sup>J(H,H) = 7.3 Hz, 3H); <sup>13</sup>C NMR (101 MHz, CDCl<sub>3</sub>) δ 144.9, 144.4, 144.3, 142.5, 133.3, 129.9, 129.7, 129.6, 127.9, 63.8, 32.5, 32.3, 22.1, 13.7.; IR (film): ν = 3031.6, 2957.3, 2930.3, 2869.6, 1629.6, 1498.4, 1456.0, 1205.3, 1149.4 cm<sup>-1</sup>; HRMS (ESI<sup>+</sup>): *m/z* 226.15875 [M]<sup>+</sup> (calcd. for C<sub>16</sub>H<sub>20</sub>N<sub>1</sub>: 226.15903).

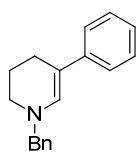
### General procedure for the asymmetric hydrogenation of pyridinium salts



Inside a glovebox, Rh(cod)<sub>2</sub>OTf (0.23 mg, 2 mol%) and JosiPhos J002-2 (0.30 mg, 2.2 mol%) were stirred for 1 h at 40 °C in 0.5 mL of THF. The solution was then transferred into a vial containing a mixture of **1** (0.025 mmol), Et<sub>3</sub>N (17.4 μL, 0.125 mmol, 5 equiv.) and dodecane (10 mg) in a solution of THF: TFE (1:1, 1 mL). The vial was capped and placed into a Premex 96er Multireaktor<sup>®</sup>. After flushing it 5 times with N<sub>2</sub> and 5 times with H<sub>2</sub>, it was pressurized to 50 bar of H<sub>2</sub> and stirred at 50 °C for 16 h. The yield and *ee* of the reaction were determined by GC or HPLC using dodecane as internal standard.

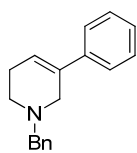


**(S)-(-)-N-Benzyl-3-phenylpiperidine (2a):**  $^1\text{H}$  NMR (400 MHz,  $\text{CDCl}_3$ )  $\delta$  7.41 – 7.18 (m, 10H), 3.59 (s, 2H), 3.05 (m, 1H), 3.01 – 2.86 (m, 2H), 2.14 – 2.00 (m, 2H), 2.00 – 1.92 (m, 1H), 1.83 – 1.73 (m, 2H), 1.48 (m, 1H);  $^{13}\text{C}$  NMR (101 MHz,  $\text{CDCl}_3$ )  $\delta$  145.0, 138.4, 129.4, 128.5, 128.3, 127.4, 127.1, 126.4, 63.7, 61.2, 53.9, 43.0, 31.8, 25.9.; IR (film):  $\nu$  = 3026.7, 2931.3, 2796.3, 1661.37, 1600.6, 1493.6, 1452.1, 756.0  $\text{cm}^{-1}$ ; HRMS (ESI+):  $m/z$  252.17515  $[\text{M}+\text{H}]^+$  (calcd. for  $\text{C}_{18}\text{H}_{22}\text{N}_1$ : 252.17468). Yield and enantiomeric excess determined by GC: CP-Chirasil-Dex CB (25m x 0.25mm, 0.25 $\mu\text{m}$ ); carrier: helium; gas flow: 2.7 bar; oven temperature: 150 °C for 8 min., 5 °C/min., 170 °C for 60 min.:  $t_{\text{R}}$  = 23.6 min.,  $t_{\text{S}}$  = 24.0 min. Absolute configuration assigned by comparison of the sign of the optical rotation with literature data.<sup>77</sup>



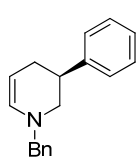
**N-Benzyl-5-phenyl-1,2,3,4-tetrahydropyridine (TH-1):**  $^1\text{H}$  NMR (400 MHz,  $\text{CDCl}_3$ )  $\delta$  7.41 – 7.25 (m, 9H), 7.07 (m, 1H), 6.75 (s, 1H), 4.19 (s, 2H), 3.00 (t,  $^3J(\text{H},\text{H})$  = 5.4 Hz, 2H), 2.45 (t,  $^3J(\text{H},\text{H})$  = 6.3 Hz, 2H), 2.02 (m, 2H);  $^{13}\text{C}$  NMR (101 MHz,  $\text{CDCl}_3$ )  $\delta$  141.9, 138.6, 134.2, 128.6, 128.4, 128.0, 127.4, 123.8, 122.5, 106.2, 59.9, 46.4, 23.3, 22.6; IR (film):  $\nu$  = 3026.7, 2924.5, 2838.7, 1673.9, 1631.5, 1593.9, 1493.6, 1450.2, 1360.5, 1175.4  $\text{cm}^{-1}$ ; HRMS (ESI+):  $m/z$  250.15924  $[\text{M}+\text{H}]^+$  (calcd. for  $\text{C}_{18}\text{H}_{20}\text{N}_1$ : 250.15903). Yield determined by GC: CP-Chirasil-Dex CB (25m x 0.25mm, 0.25 $\mu\text{m}$ ); carrier: helium; gas flow: 2.7 bar; oven temperature: 150 °C for 8 min., 5 °C/min., 170 °C for 60 min.:  $t$  = 46.8 min.

**TH-1** slowly decomposes to unknown products, even when stored at -20 °C.

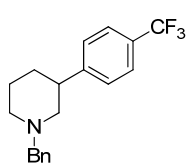


**N-Benzyl-5-phenyl-1,2,3,6-tetrahydropyridine (TH-2):**  $^1\text{H}$  NMR (400 MHz,  $\text{CDCl}_3$ )  $\delta$  7.44 – 7.18 (m, 10H), 6.12 (m, 1H), 3.71 (s, 2H), 3.37 (dd,  $^3J(\text{H},\text{H})$  = 4.3 Hz,  $^3J(\text{H},\text{H})$  = 2.4 Hz, 2H), 2.63 (t,  $^3J(\text{H},\text{H})$  = 5.7 Hz, 2H), 2.34 (m, 2H);  $^{13}\text{C}$  NMR (101 MHz,  $\text{CDCl}_3$ )  $\delta$  140.4, 138.4, 135.5, 129.3, 128.4, 127.2, 127.1, 125.1, 122.7, 63.0, 54.9, 49.3, 26.6; IR (film):  $\nu$  = 3026.7, 2908.1, 2799.2, 1947.8, 1868.7, 1807.9, 1741.4, 1599.7, 1493.6, 1453.1, 1122.4, 1047.2, 853.3  $\text{cm}^{-1}$ ; HRMS (ESI+):  $m/z$  250.15943  $[\text{M}+\text{H}]^+$  (calcd. for  $\text{C}_{18}\text{H}_{20}\text{N}_1$ : 250.15903). Yield determined by GC: CP-Chirasil-Dex CB (25m x 0.25mm, 0.25 $\mu\text{m}$ ); carrier: helium; gas flow: 2.7 bar; oven temperature: 150 °C for 8 min., 5 °C/min., 170 °C for 60 min.:  $t$  = 32.2 min.

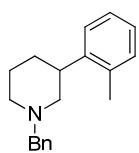
**TH-2** could be independently prepared by the following method:  $\text{NaBH}_4$  (2.5 mmol) was added to a solution of **60a** (326 mg, 1 mmol) in EtOH (5 mL) and stirred for 18 h at 50 °C. The reaction was then quenched with 15 mL of  $\text{H}_2\text{O}$  and extracted with DCM (3 x 15 mL). The organic phase was dried over  $\text{Na}_2\text{SO}_4$ , filtered and concentrated. Flash column chromatography with hexane:EtOAc (95:5) afforded the pure product (212 mg, 85% yield).



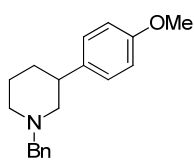
**(S)-N-Benzyl-3-phenyl-1,2,3,4-tetrahydropyridine (TH-3):** Not isolated. GC-MS: found molecular peak – 250 (expected  $m/z$  = 250). Yield and enantiomeric excess determined by GC: CP-Chirasil-Dex CB (25m x 0.25mm, 0.25 $\mu\text{m}$ ); carrier: helium; gas flow: 2.7 bar; oven temperature: 150 °C for 8 min., 5 °C/min., 170 °C for 60 min.:  $t_{\text{R}}$  = 27.8 min.,  $t_{\text{S}}$  = 28.2 min.



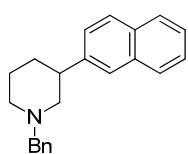
**(-)-N-Benzyl-3-(4-(trifluoromethyl)phenyl)piperidine (2b):**  $^1\text{H}$  NMR (400 MHz,  $\text{CDCl}_3$ )  $\delta$  7.54 (d,  $^3J(\text{H,H}) = 8.1$  Hz, 2H), 7.39 – 7.27 (m, 5H), 3.65 (s, 2H), 3.13 – 2.94 (m, 3H), 2.22 – 2.06 (m, 2H), 1.95 (m, 1H), 1.91 – 1.75 (m, 2H), 1.48 (m, 1H);  $^{13}\text{C}$  NMR (101 MHz,  $\text{CDCl}_3$ )  $\delta$  148.2, 129.7, 128.9 (q,  $^2J(\text{C,F}) = 32.6$  Hz), 128.6, 127.7, 125.5 (q,  $^3J(\text{C,F}) = 3.7$  Hz), 124.4 (q,  $^1J(\text{C,F}) = 271.9$  Hz), 63.3, 60.1, 53.5, 42.3, 31.3, 25.1;  $^{19}\text{F}$  NMR (282 MHz,  $\text{CDCl}_3$ )  $\delta$  -62.9; IR (film):  $\nu = 2931.3$ , 2852.2, 1639.2, 1619.9, 1326.8, 1164.8, 1122.4, 1069.3  $\text{cm}^{-1}$ ; HRMS (ESI+):  $m/z$  320.16290  $[\text{M}+\text{H}]^+$  (calcd. for  $\text{C}_{19}\text{H}_{21}\text{N}_1\text{F}_3$ : 320.16206). Yield and enantiomeric excess determined by GC: CP-Chirasil-Dex CB (25m x 0.25mm, 0.25 $\mu\text{m}$ ); carrier: helium; gas flow: 2.7 bar; oven temperature: 150  $^\circ\text{C}$  for 8 min., 5  $^\circ\text{C}/\text{min.}$ , 170  $^\circ\text{C}$  for 60 min.:  $t_{e1} = 24.8$  min.,  $t_{e2} = 25.4$  min.



**(-)-N-Benzyl-3-(2-tolyl)piperidine (2c):**  $^1\text{H}$  NMR (400 MHz,  $\text{CDCl}_3$ )  $\delta$  7.36 – 7.04 (m, 10H), 3.59 (d,  $^2J(\text{H,H}) = 13.1$  Hz, 1H), 3.52 (d,  $^2J(\text{H,H}) = 13.2$  Hz, 1H), 3.06 (m, 1H), 3.01 – 2.87 (m, 2H), 2.31 (s, 3H), 2.09 – 1.95 (m, 2H), 1.86 (m, 1H), 1.81 – 1.68 (m, 2H), 1.46 (m, 1H);  $^{13}\text{C}$  NMR (101 MHz,  $\text{CDCl}_3$ )  $\delta$  142.9, 137.8, 135.9, 130.5, 129.4, 128.3, 127.1, 126.1, 126.1, 125.8, 63.6, 60.2, 54.2, 38.6, 31.2, 26.1, 19.6.; IR (film):  $\nu = 3024.8$ , 2930.3, 2853.2, 2795.3, 1641.1, 1492.6, 1454.1, 1099.2, 753.1  $\text{cm}^{-1}$ ; HRMS (ESI+):  $m/z$  266.19038  $[\text{M}+\text{H}]^+$  (calcd. for  $\text{C}_{19}\text{H}_{24}\text{N}_1$ : 266.19033). Yield and enantiomeric excess determined by GC: CP-Chirasil-Dex CB (25m x 0.25mm, 0.25 $\mu\text{m}$ ); carrier: helium; gas flow: 2.7 bar; oven temperature: 150  $^\circ\text{C}$  for 8 min., 5  $^\circ\text{C}/\text{min.}$ , 170  $^\circ\text{C}$  for 60 min.:  $t_{e1} = 28.3$  min.,  $t_{e2} = 28.9$  min.



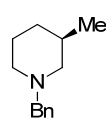
**(-)-N-Benzyl-3-(4-methoxyphenyl)piperidine (2d):**  $^1\text{H}$  NMR (400 MHz,  $\text{CDCl}_3$ )  $\delta$  7.36 – 7.20 (m, 6H), 7.13 (d,  $^3J(\text{H,H}) = 8.6$  Hz, 2H), 6.82 (d,  $^3J(\text{H,H}) = 8.6$  Hz, 2H), 3.78 (s, 3H), 3.54 (s, 2H), 3.02 – 2.87 (m, 2H), 2.79 (m, 1H), 2.05 – 1.93 (m, 2H), 1.90 (m, 1H), 1.79 – 1.68 (m, 2H), 1.41 (m, 1H);  $^{13}\text{C}$  NMR (101 MHz,  $\text{CDCl}_3$ )  $\delta$  158.1, 138.4, 137.2, 129.4, 128.3, 128.3, 127.1, 113.8, 63.7, 61.5, 55.4, 53.9, 42.2, 32.0, 25.9; IR (film):  $\nu = 2930.3$ , 1638.2, 1610.3, 1512.9, 1245.8, 1036.6  $\text{cm}^{-1}$ ; HRMS (ESI+):  $m/z$  282.18518  $[\text{M}+\text{H}]^+$  (calcd. for  $\text{C}_{19}\text{H}_{24}\text{N}_1\text{O}_1$ : 282.18524). Yield and enantiomeric excess determined by GC: CP-Chirasil-Dex CB (25m x 0.25mm, 0.25 $\mu\text{m}$ ); carrier: helium; gas flow: 2.7 bar; oven temperature: isotherm 170  $^\circ\text{C}$  for 60 min.:  $t_{e1} = 52.5$  min.,  $t_{e2} = 53.4$  min.



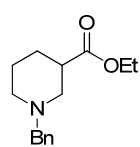
**(-)-N-Benzyl-3-(naphthalen-2-yl)piperidine (2e):**  $^1\text{H}$  NMR (400 MHz,  $\text{CDCl}_3$ )  $\delta$  7.82 – 7.71 (m, 3H), 7.66 (s, 1H), 7.48 – 7.20 (m, 8H), 3.58 (s, 2H), 3.13 – 2.90 (m, 3H), 2.16 (t,  $^3J(\text{H,H}) = 10.8$  Hz, 1H), 2.10 – 1.97 (m, 2H), 1.86 – 1.71 (m, 2H), 1.58 (m, 1H);  $^{13}\text{C}$  NMR (101 MHz,  $\text{CDCl}_3$ )  $\delta$  142.5, 138.4, 133.7, 132.4, 129.4, 128.3, 127.9, 127.7, 127.7, 127.1, 126.4, 126.0, 125.4, 125.4, 63.7, 61.1, 54.0, 43.1, 31.8, 25.9; IR (film):  $\nu = 3055.7$ , 2931.3, 2796.3, 1600.6, 1453.1, 1348.0, 1097.3, 816.7, 738.6  $\text{cm}^{-1}$ ; HRMS (ESI+):  $m/z$  302.19056  $[\text{M}+\text{H}]^+$  (calcd. for  $\text{C}_{22}\text{H}_{24}\text{N}_1$ : 302.19033). Yield determined by GC: HP-1 (30m x 0.32mm, 0.25 $\mu\text{m}$ ); carrier: helium; gas flow: 15.2 psi; oven temperature: 45  $^\circ\text{C}$  for 5 min., 20  $^\circ\text{C}/\text{min.}$ , 245  $^\circ\text{C}$  for 2 min.:  $t = 9.5$  min. Enantiomeric excess



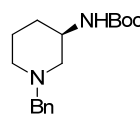
determined by HPLC: Chiralcel OD-H (250 x 4.6 mm); hexane/*i*PrOH (98:2); 0.4 mL/min:  $t_{e1}$  = 19.6 min.,  $t_{e2}$  = 22.8 min.



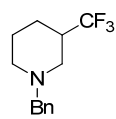
**(R)-(-)-N-Benzyl-3-methylpiperidine (2f).**<sup>78</sup> Absolute configuration assigned by comparison of the optical rotation with literature data.<sup>79</sup> Yield and enantiomeric excess determined by GC: CP-Chirasil-Dex CB (25m x 0.25mm, 0.25 $\mu$ m); carrier: hydrogen; gas flow: 1.0 bar; oven temperature: isotherm 105 °C for 40 min.:  $t_R$  = 29.8 min.,  $t_S$  = 30.7 min.



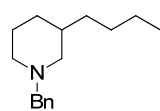
**Ethyl N-Benzylpiperidine-3-carboxylate (2g).**<sup>80</sup> Yield and enantiomeric excess determined by GC: CP-Chirasil-Dex CB (25m x 0.25mm, 0.25 $\mu$ m); carrier: hydrogen; gas flow: 1.0 bar; oven temperature: isotherm 140 °C for 50 min.:  $t_{e1}$  = 36.7 min.,  $t_{e2}$  = 37.3 min. Determination of the optical rotation was not possible due to the low conversion.



**tert-Butyl (R)-(+)-(N-benzylpiperidin-3-yl)carbamate (2h).**<sup>20</sup> Yield and enantiomeric excess determined by GC: CP-Chirasil-Dex CB (25m x 0.25mm, 0.25 $\mu$ m); carrier: hydrogen; gas flow: 1.0 bar; oven temperature: isotherm 170 °C for 40 min.:  $t_S$  = 26.4 min.,  $t_R$  = 27.7 min. Absolute configuration assigned by comparison of the sign of the optical rotation with literature data.<sup>81</sup>



**N-Benzyl-3-(trifluoromethyl)piperidine (2i):** <sup>1</sup>H NMR (400 MHz, CDCl<sub>3</sub>)  $\delta$  7.35 – 7.25 (m, 5H), 3.55 (d, <sup>2</sup>J(H,H) = 13.2 Hz, 1H), 3.51 (d, <sup>2</sup>J(H,H) = 13.2 Hz, 1H), 3.04 (m, 1H), 2.85 (m, 1H), 2.35 (m, 1H), 2.00 – 1.86 (m, 3H), 1.78 – 1.67 (m, 2H), 1.57 (m, 1H); <sup>13</sup>C NMR (101 MHz, CDCl<sub>3</sub>)  $\delta$  138.1, 129.1, 128.4, 127.3, 127.1 (q, <sup>1</sup>J(C,F) = 278.7 Hz), 63.4, 53.3, 52.4 (q, <sup>3</sup>J(C,F) = 3.0 Hz), 41.2 (q, <sup>2</sup>J(C,F) = 26.1 Hz), 24.3, 23.4 (q, <sup>2</sup>J(C,F) = 2.5 Hz); <sup>19</sup>F NMR (282 MHz, CDCl<sub>3</sub>)  $\delta$  -73.5; IR (film):  $\nu$  = 2947.7, 2925.5, 2855.1, 1455.0, 1335.5, 1258.3, 1185.0, 1118.5, 1090.6 cm<sup>-1</sup>; HRMS (ESI+):  $m/z$  244.13059 [M+H]<sup>+</sup> (calcd. for C<sub>13</sub>H<sub>17</sub>N<sub>1</sub>F<sub>3</sub>: 244.13076). Yield and enantiomeric excess determined by GC: CP-Chirasil-Dex CB (25m x 0.25mm, 0.25 $\mu$ m); carrier: hydrogen; gas flow: 1.0 bar; oven temperature: isotherm 105 °C for 40 min.:  $t_{e1}$  = 27.0 min.,  $t_{e2}$  = 27.8 min. Determination of the optical rotation was not possible due to the low conversion.



**(-)-N-Benzyl-3-butylpiperidine (2j):** <sup>1</sup>H NMR (400 MHz, CD<sub>2</sub>Cl<sub>2</sub>)  $\delta$  7.35 – 7.26 (m, 4H), 7.22 (m, 1H), 3.47 (d, <sup>2</sup>J(H,H) = 13.2 Hz, 1H), 3.41 (d, <sup>2</sup>J(H,H) = 13.2 Hz, 1H), 2.85 – 2.69 (m, 2H), 1.92 – 1.84 (m, 2H), 1.78 (m, 1H), 1.68 – 1.57 (m, 2H), 1.57 – 1.43 (m, 2H), 1.35 – 1.09 (m, 6H), 0.94 – 0.82 (m, 3H); <sup>13</sup>C NMR (101 MHz, CD<sub>2</sub>Cl<sub>2</sub>)  $\delta$  139.6, 129.5, 128.5, 127.2, 63.9, 61.1, 54.7, 36.6, 34.7, 312.5, 29.6, 26.0, 23.4, 14.3; IR (film):  $\nu$  = 2954.4, 2928.4, 2855.1, 2755.8, 1644.0, 1465.6, 1454.1, 1121.4, 736.7, 698.1 cm<sup>-1</sup>; HRMS (ESI+):  $m/z$  232.20661 [M+H]<sup>+</sup> (calcd. for C<sub>16</sub>H<sub>26</sub>N<sub>1</sub>: 232.20598). Yield and enantiomeric excess determined by GC: CP-Chirasil-Dex CB (25 m x 0.25mm, 0.25 $\mu$ m); carrier: hydrogen; gas flow: 1.0 bar; oven temperature: isotherm 125 °C for 55 min.:  $t_{e1}$  = 44.3 min.,  $t_{e2}$  = 45.1 min.

### Monitoring of the reaction over time by GC and NMR

Inside a glovebox, Rh(cod)<sub>2</sub>OTf (14.3 mg, 2 mol%) and JosiPhos J002-2 (18.2 mg, 2.2 mol%) were stirred for 1 h at 40 °C in 9 mL of THF. The solution was then transferred into a 50 mL EasyMax<sup>TM</sup> high pressure autoclave (Mettler Toledo) containing a mixture of **60a** (503.52 mg, 1.53 mmol), Et<sub>3</sub>N (1.068 mL, 7.65 mmol, 5 equiv.), dodecane (351.4 mg – as GC internal standard) and dimethyl terephthalate (151.24 mg – as NMR internal standard) in a solution of THF/TFE (1:1, 18 mL). The autoclave was closed and taken out of the glovebox. After flushing it 5 times with N<sub>2</sub>, it was pressurized to 50 bar of H<sub>2</sub> and stirred at 50 °C for 47 h with sampling at different times. All samples were analyzed by GC analysis with CP-Chirasil-Dex CB column and some by NMR (results shown in Table 22).

**Table 22.** Yield and *ee* of different species involved in the AH of **60a** to **61a**.

Time (h)	<b>60a</b> (%) <sup>[a]</sup>	<b>61a</b> (%) <sup>[b]</sup>	<i>ee</i> of <b>61a</b> (%) <sup>[b]</sup>	<b>TH-1</b> (%) <sup>[b]</sup>	<b>TH-2</b> (%) <sup>[b]</sup>	<b>TH-3</b> (%) <sup>[b]</sup>	<i>ee</i> of <b>TH-3</b> (%) <sup>[b]</sup>	Et <sub>3</sub> NH <sup>+</sup> (mmol) <sup>[a]</sup>
0	100	0	-	0	0	0	-	0
0,5	71	6	53	10	1	1	93	0,42
1	50	9	53	18	1	4	93	0,61
2	24	9	61	21	2	9	93	0,97
3,5	6	12	76	25	2	11	93	1,18
6,9	1	24	83	26	2	10	93	1,35
10	0	31	85	26	2	7	93	1,44
13,25		38	87	26	2	4	93	
17,1	0	43	86	25	2	2	93	1,53
23,1		48	85	25	2	1	93	
30		51	83	25	2	1	93	
47		55	79	24	1	1	93	

[a] Determined by NMR with dimethyl terephthalate as internal standard. [b] Determined by GC analysis with CP-Chirasil-Dex CB column with dodecane as internal standard. Positive values of *ee* correspond to *S* configuration.

### Monitoring of the reaction over time by *in situ* FTIR spectroscopy

Inside a glovebox, Rh(cod)<sub>2</sub>OTf (140.5 mg, 2 mol%) and JosiPhos J002-2 (179.0 mg, 2.2 mol%) were stirred for 1 h at 40 °C in 9 mL of THF. The solution was then transferred into a 50 mL EasyMax<sup>TM</sup> high pressure autoclave (Mettler Toledo) containing a mixture of **60a** (4.9 g, 15 mmol) and Et<sub>3</sub>N (9 mL, 64.5 mmol, 4.3 equiv.) in a solution of THF/TFE (1:1, 18 mL). The autoclave was closed and taken out of the glovebox and the IR probe was assembled. After flushing it 5 times with N<sub>2</sub>, it was pressurized to 40 bar of H<sub>2</sub> and stirred at 50 °C for 20 h. The spectral resolution for the FTIR acquisition was set to 4 cm<sup>-1</sup>, the number of scans to 256 and the measurement interval to one minute.

### General procedure for the hydrogenation of **TH-1** and **TH-2**

Inside a glovebox, Rh(cod)<sub>2</sub>OTf (0.23 mg, 2 mol%) and JosiPhos J002-2 (0.30 mg, 2.2 mol%) were stirred for 1 h at 40 °C in 0.5 mL of THF. The solution was then transferred into a vial containing a mixture of **TH-1** or **TH-2** (0.025 mmol) and the selected additive in a solution

of THF/TFE (1:1, 1 mL). The vial was capped and placed into a Premex 96er Multireaktor®. After flushing it 5 times with N<sub>2</sub> and 5 times with H<sub>2</sub>, it was pressurized to 50 bar of H<sub>2</sub> and stirred at 50 °C for 20 h. The conversion and *ee* of the reaction were determined by GC analysis with CP-Chirasil-Dex CB column.

### Isotopic labeling experiment

Inside a glovebox, Rh(cod)<sub>2</sub>OTf (14.3 mg, 2 mol%) and JosiPhos J002-2 (18.2 mg, 2.2 mol%) were stirred for 1 h at 40 °C in 9 mL of THF. The catalyst solution was transferred into a 50 mL autoclave containing a mixture of **60a** (500 mg, 1.53 mmol), Et<sub>3</sub>N (1.07 mL, 7.65 mmol) in 9 mL of THF and 9 mL of TFE. The autoclave was closed and taken out of the glovebox. After flushing it 5 times with N<sub>2</sub>, it was pressurized to 40 bar of D<sub>2</sub> and stirred at 50 °C for 20 h. After that time, the crude mixture was concentrated, the product was redissolved in DCM (30 mL) and washed with a saturated aqueous solution of Na<sub>2</sub>CO<sub>3</sub> (30 mL) and H<sub>2</sub>O (30 mL). The organic phase was dried over Na<sub>2</sub>SO<sub>4</sub>, filtered and concentrated under vacuum. Purification by column chromatography with hexane/EtOAc (99:1 to 95:5) afforded **TH-1** (76 mg, 0.31 mmol, 20% yield), **TH-2** (8 mg, 0.03 mmol, 2% yield) and **61a** (200 mg, 0.8 mmol, 52% yield).

- NMR spectra of deuterated **61a** can be found in section 3.2 *Results and discussion* (Figure 14, Figure 15, Figure 16).
- Deuterated NMR spectra of tetrahydropyridines **TH-1** and **TH-2** are shown below in Figure 18 and Figure 19.

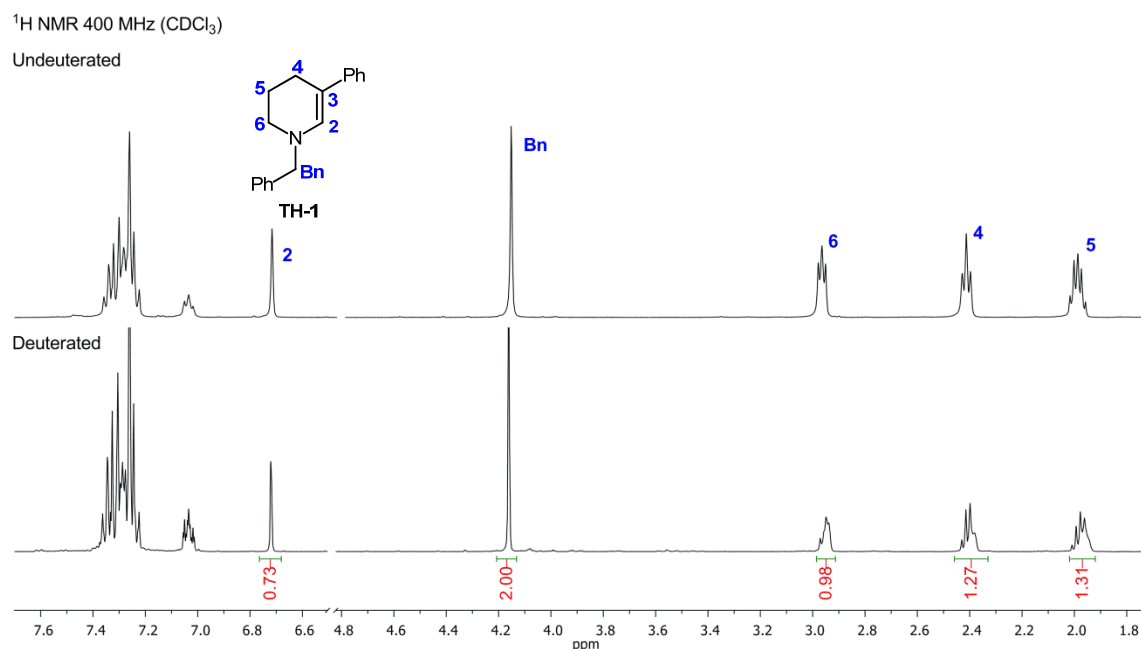


Figure 18. <sup>1</sup>H-NMR of **TH-1** and deuterated **TH-1** in CDCl<sub>3</sub>.

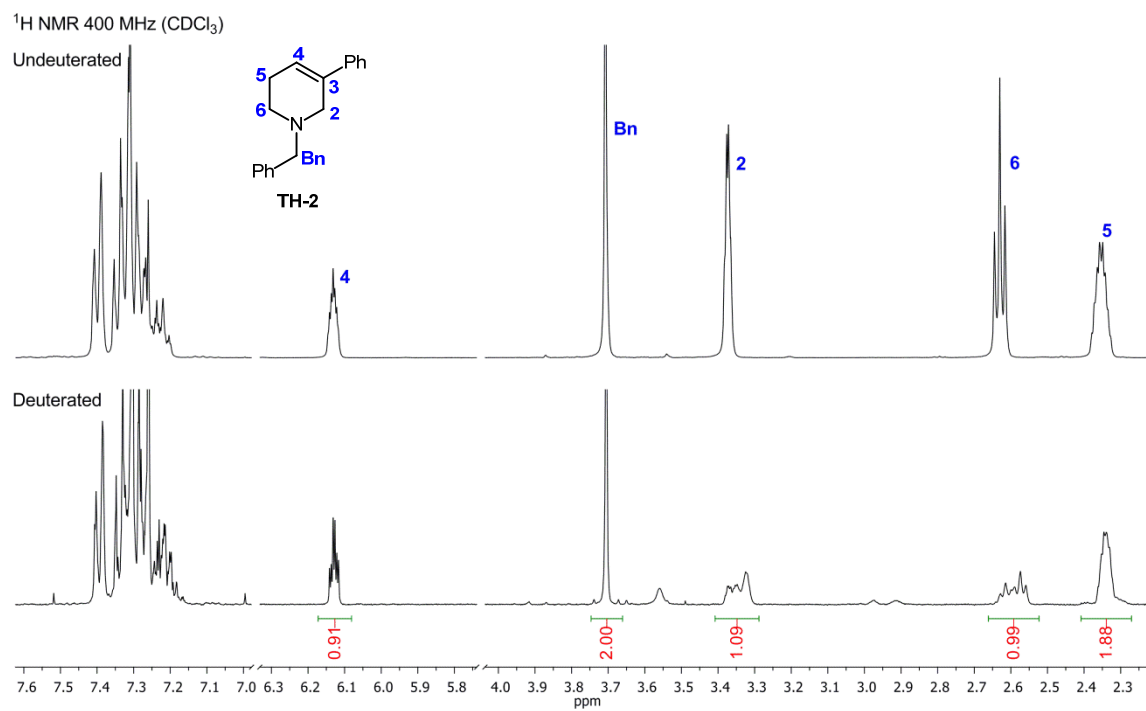


Figure 19. <sup>1</sup>H-NMR of TH-2 and deuterated TH-2 in CDCl<sub>3</sub>.

## REFERENCES

1. a) A. R. Katritzky, K. Jug, D. C. Oniciu, *Chem. Rev.* **2001**, *101*, 1421–1449. b) C. W. Bird, *Tetrahedron* **1992**, *48*, 335–340.
2. H.-U. Blaser, H. Hönl, M. Studer, C. Wedemeyer-Exl, *J. Mol. Catal. A: Chem.* **1999**, *139*, 253–257.
3. A. Lei, M. Chen, M. He, X. Zhang, *Eur. J. Org. Chem.* **2006**, *2006*, 4343–4347.
4. S. A. Raynor, J. M. Thomas, R. Raja, B. F. Johnson, R. G. Bell, M. D. Mantle, *Chem. Commun.* **2000**, 1925–1926.
5. L. Hegedűs, V. Háda, A. Tungler, T. Máthé, L. Szepesy, *Appl. Catal. A-Gen.* **2000**, *201*, 107–114.
6. a) N. Douja, M. Besson, P. Gallezot, C. Pinel, *J. Mol. Catal. A-Chem.* **2002**, *186*, 145–151. b) N. Douja, R. Malacea, M. Banciu, M. Besson, C. Pinel, *Tetrahedron Lett.* **2003**, *44*, 6991–6993.
7. F. Glorius, N. Spielkamp, S. Holle, R. Goddard, C. W. Lehmann, *Angew. Chem. Int. Ed.* **2004**, *43*, 2850–2852.
8. M. Studer, C. Wedemeyer-Exl, F. Spindler, H.-U. Blaser, *Monatsh. Chem.* **2000**, *131*, 1335–1343.
9. X.-B. Wang, W. Zeng, Y.-G. Zhou, *Tetrahedron Lett.* **2008**, *49*, 4922–4924.
10. a) W. Tang, Y. Sun, L. Xu, T. Wang, Q. Fan, K.-H. Lam, A. S. C. Chan, *Org. Biomol. Chem.* **2010**, *8*, 3464–3471. b) W.-J. Tang, J. Tan, L.-J. Xu, K.-H. Lam, Q.-H. Fan, A. S. Chan, *Adv. Synth. Catal.* **2010**, *352*, 1055–1062.
11. B. Balakrishna, J. L. Núñez-Rico, A. Vidal-Ferran, *Eur. J. Org. Chem.* **2015**, *2015*, 5293–5303.
12. For a review see: M. Ahamed, M. H. Todd, *Eur. J. Org. Chem.* **2010**, 5935–5942.
13. C. Y. Legault, A. B. Charette, *J. Am. Chem. Soc.* **2005**, *127*, 8966–8967.
14. A. Cadu, P. K. Upadhyay, P. G. Andersson, *Asian J. Org. Chem.* **2013**, *2*, 1061–1065.
15. S. G. Ruggeri, J. M. Hawkins, T. M. Makowski, J. L. Rutherford, F. J. Urban (Pfizer Products Inc.), WO 012953, **2007**.
16. Z.-S. Ye, M.-W. Chen, Q.-A. Chen, L. Shi, Y. Duan, Y.-G. Zhou, *Angew. Chem. Int. Ed.* **2012**, *51*, 10181–10184.
17. M. Chang, Y. Huang, S. Liu, Y. Chen, S. W. Krska, I. W. Davies, X. Zhang, *Angew. Chem. Int. Ed.* **2014**, *53*, 12761–12764.
18. Y. Kita, A. Iimuro, S. Hida, K. Mashima, *Chem. Lett.* **2014**, *43*, 284–286.
19. M.-W. Chen, Z.-S. Ye, Z.-P. Chen, B. Wu, Y.-G. Zhou, *Org. Chem. Front.* **2015**, *2*, 586–589.
20. J. Wu, W. Tang, A. Pettman, J. Xiao, *Adv. Synth. Catal.* **2013**, *355*, 35–40.
21. M. Rueping, A. P. Antonchick, *Angew. Chem. Int. Ed.* **2007**, *46*, 4562–4565.
22. Y. Liu, H. Du, *J. Am. Chem. Soc.* **2013**, *135*, 12968–12971.
23. a) *Dictionary of Alkaloids, 2nd edition* (Eds.: J. Buckingham, K. H. Baggaley, A. D. Roberts, L. F. Szabo), CRC Press, New York, **2010**. b) N. Neuss, M. N. Neuss, *The Alkaloids* (Eds.: A. Brossi, M. Suffness), Academic Press, San Diego, **1990**. c) F. Gueritte, J. Fahy, *Anticancer Agents from Natural Products* (Eds.: G. M. Cragg, D. G. I.

- Kingstom, D. J. Newman), CRC Press, Boca Raton, **2005**; 123. d) *Modern Alkaloids: Structure, Isolation, Synthesis and Biology* (Eds.: E. Fattorusso, O. Tagliatalata-Scafati), Wiley-VCH, Weinheim, **2008**.
24. a) J. L. Núñez-Rico, H. Fernández-Pérez, A. Vidal-Ferran, *Green Chemistry* **2014**, *16*, 1153–1157. b) A. Baeza, A. Pfaltz, *Chemistry* **2010**, *16*, 2036–2039.
25. a) R. Kuwano, K. Kaneda, T. Ito, K. Sato, T. Kurokawa, Y. Ito, *Org. Lett.* **2004**, *6*, 2213–2215. b) R. Kuwano, M. Kashiwabara, K. Sato, T. Ito, K. Kaneda, Y. Ito, *Tetrahedron Asymmetry* **2006**, *17*, 521–535. c) A. M. Maj, I. Suisse, C. Méliet, F. Agbossou-Niedercorn, *Tetrahedron Asymmetry* **2010**, *21*, 2010–2014. d) R. Kuwano, K. Sato, T. Kurokawa, D. Karube, Y. Ito, *J. Am. Chem. Soc.* **2000**, *122*, 7614–7615. e) N. Mršić, T. Jerphagnon, A. J. Minnaard, B. L. Feringa, J. G. de Vries, *Tetrahedron Asymmetry* **2010**, *21*, 7–10.
26. R. Kuwano, M. Kashiwabara, *Org. Lett.* **2006**, *8*, 2653–2655.
27. a) D.-S. Wang, Q.-A. Chen, W. Li, C.-B. Yu, Y.-G. Zhou, X. Zhang, *J. Am. Chem. Soc.* **2010**, *132*, 8909–8911. b) Y. Duan, L. Li, M.-W. Chen, C.-B. Yu, H.-J. Fan, Y.-G. Zhou, *J. Am. Chem. Soc.* **2014**, *136*, 7688–7700. c) D.-S. Wang, J. Tang, Y.-G. Zhou, M.-W. Chen, C.-B. Yu, Y. Duan, G.-F. Jiang, *Chem. Sci.* **2011**, *2*, 803–806. d) Y. Duan, M.-W. Chen, Z.-S. Ye, D.-S. Wang, Q.-A. Chen, Y.-G. Zhou, *Chem.-Eur. J.* **2011**, *17*, 7193–7197. e) Y. Duan, M.-W. Chen, Q.-A. Chen, C.-B. Yu, Y.-G. Zhou, *Org. Biomol. Chem.* **2012**, *10*, 1235–1238. f) C. Li, J. Chen, G. Fu, D. Liu, Y. Liu, W. Zhang, *Tetrahedron* **2013**, *69*, 6839–6844.
28. V. Háda, A. Tungler, L. Szepeszy, *Appl. Catal A- Gen* **2001**, *210*, 165–171.
29. R. Kuwano, M. Kashiwabara, M. Ohsumi, H. Kusano, *J. Am. Chem. Soc.* **2008**, *130*, 808–809.
30. D.-S. Wang, Z.-S. Ye, Q.-A. Chen, Y.-G. Zhou, C.-B. Yu, H.-J. Fan, Y. Duan, *J. Am. Chem. Soc.* **2011**, *133*, 8866–8869.
31. a) M. Fantin, M. Marti, Y. P. Auberson, M. Morari, *J. Neurochem.* **2007**, *103*, 2200–2211. b) R. E. TenBrink, W. B. Im, V. H. Sethy, A. H. Tang, D. B. Carter, *J. Med. Chem.* **1994**, *37*, 758–768. c) S. Li, X. Tian, D. M. Hartley, L. A. Feig, *J. Neurosci.* **2006**, *26*, 1721–1729. d) K. Torisu, K. Kobayashi, M. Iwahashi, Y. Nakai, T. Onoda, T. Nagase, I. Sugimoto, Y. Okada, R. Matsumoto, F. Nanbu, S. Ohuchi-da, H. Nakai, M. Toda, *Bioorg. Med. Chem.* **2004**, *12*, 5361–5378. e) A. Wang, C. P. Prouty, P. D. Pelton, M. Yong, K. T. Demarest, W. V. Murray, G.-H. Kuo, *Bioorg. Med. Chem. Lett.* **2010**, *20*, 1432–1435. f) D. Bouzard, *Antibiotics and Antiviral Compounds* (Eds.: K. Korhn, H. A. Rirst, H. Maag), VCH, Weinheim, **1993**.
32. a) T. Nagano, A. Iimuro, R. Schwenk, T. Ohshima, Y. Kita, A. Togni, K. Mashima, *Chem.-Eur. J.* **2012**, *18*, 11578–11592. b) W. Tang, L. Xu, Q.-H. Fan, J. Wang, B. Fan, Z. Zhou, K.-H. Lam, A. S. C. Chan, *Angew. Chem. Int. Ed.* **2009**, *48*, 9135–9138. c) N. Mršić, T. Jerphagnon, A. J. Minnaard, B. L. Feringa, J. G. de Vries, *Adv. Synth. Catal.* **2009**, *351*, 2549–2552. d) D. Cartigny, F. Berhal, T. Nagano, P. Phansavath, T. Ayad, J.-P. Genêt, T. Ohshima, K. Mashima, V. Ratovelomanana-Vidal, *J. Org. Chem.* **2012**, *77*, 4544–4556. e) C. Bianchini, P. Barbaro, G. Scapacci, *J. Organomet. Chem.* **2001**, *621*, 26–33. f) C. Bianchini, P. Barbaro, G. Scapacci, E. Farnetti, M. Graziani, *Organometallics* **1998**, *17*, 3308–3310. g) L. Qiu, F. Y. Kwong, J. Wu, W. H. Lam, S. Chan, W.-Y. Yu, Y.-M. Li, R. Guo, Z. Zhou, A. S. Chan, *J. Am. Chem. Soc.* **2006**, *128*, 5955–5965. h) D. Cartigny, T. Nagano, T. Ayad, J.-P. Genêt, T. Ohshima, K. Mashima, V. Ratovelomanana-Vidal, *Adv. Synth. Catal.* **2010**, *352*, 1886–1891.
33. a) N. Arai, Y. Saruwatari, K. Isobe, T. Ohkuma, *Adv. Synth. Catal.* **2013**, *355*, 2769–2774. b) J. P. Henschke, M. J. Burk, C. G. Malan, D. Herzberg, J. A. Peterson, A. J. Wildsmith, C. J. Cobley, G. Casy, *Adv. Synth. Catal.* **2003**, *345*, 300–307. c) C. J. Cobley, J. P. Henschke, *Adv. Synth. Catal.* **2003**, *345*, 195–201.
34. S. Fleischer, S. Zhou, S. Werkmeister, K. Junge, M. Beller, *Chem.-Eur. J.* **2013**, *19*, 4997–5003.

35. a) Z. Zhang, H. Du, *Angew. Chem. Int. Ed.* **2015**, *54*, 623–626. b) M. Rueping, F. Tato, F. Schoepke, others, *Chem.-Eur. J.* **2010**, *16*, 2688–2691.
36. Q.-A. Chen, D.-S. Wang, Y.-G. Zhou, Y. Duan, H.-J. Fan, Y. Yang, Z. Zhang, *J. Am. Chem. Soc.* **2011**, *133*, 6126–6129.
37. Q.-A. Chen, K. Gao, Y. Duan, Z.-S. Ye, L. Shi, Y. Yang, Y.-G. Zhou, *J. Am. Chem. Soc.* **2012**, *134*, 2442–2448.
38. Y. Kita, K. Higashida, K. Yamaji, A. Iimuro, K. Mashima, *Chem. Commun.* **2015**, *51*, 4380–4382.
39. a) A. Mitchinson, A. Nadin, *J. Chem. Soc., Perkin Trans. 1*, **2000**, 2862–2892. b) J. D. Scott, R. M. Williams, *Chem. Rev.* **2002**, *102*, 1669–1730. c) C. S. Schneider, K. H. Weber, H. Daniel, W. D. Bechtel, K. Boeke-Kuhn, *J. Med. Chem.* **1984**, *27*, 1150–1155.
40. a) S.-M. Lu, Y.-Q. Wang, X.-W. Han, Y.-G. Zhou, *Angew. Chem. Int. Ed.* **2006**, *45*, 2260–2263. b) L. Shi, Z.-S. Ye, L.-L. Cao, R.-N. Guo, Y. Hu, Y.-G. Zhou, *Angew. Chem. Int. Ed.* **2012**, *51*, 8286–8289. c) Z.-S. Ye, R.-N. Guo, X.-F. Cai, M.-W. Chen, L. Shi, Y.-G. Zhou, *Angew. Chem. Int. Ed.* **2013**, *52*, 3685–3689. d) R.-N. Guo, X.-F. Cai, L. Shi, Z.-S. Ye, M.-W. Chen, Y.-G. Zhou, *Chem. Commun.* **2013**, *49*, 8537–8539. e) A. Iimuro, K. Yamaji, S. Kandula, T. Nagano, Y. Kita, K. Mashima, *Angew. Chem. Int. Ed.* **2013**, *52*, 2046–2050. f) Y. Kita, K. Yamaji, K. Higashida, K. Sathaiah, A. Iimuro, K. Mashima, *Chem.-Eur. J.* **2015**, *21*, 1915–1927.
41. Z.-Y. Ding, T. Wang, Y.-M. He, F. Chen, H.-F. Zhou, Q.-H. Fan, Q. Guo, A. S. Chan, *Adv. Synth. Catal.* **2013**, *355*, 3727–3735.
42. a) A. J. Minnaard, B. L. Feringa, L. Lefort, J. G. de Vries, *Acc. Chem. Res.* **2007**, *40*, 1267–1277. b) J.-H. Xie, S.-F. Zhu, Q.-L. Zhou, *Chem. Rev.* **2011**, *111*, 1713–1760; c) J. H. Xie, S.-F. Zhu, Q.-L. Zhou, *Chem. Soc. Rev.* **2012**, *41*, 4126–4139.
43. a) J. D. Keay, *Comprehensive Organic Synthesis* (Eds.: B. M. Trost, I. Fleming), Pergamon, Oxford, **1991**, 579. b) *Comprehensive Natural Products Chemistry* (Eds.: D. H. R. Barton, K. Nakanishi, O. Meth-Cohn) Elsevier, Oxford, **1999**.
44. a) W.-B. Wang, S.-M. Lu, P.-Y. Yang, X.-W. Han, Y.-G. Zhou, *J. Am. Chem. Soc.* **2003**, *125*, 10536–10537. b) S.-M. Lu, X.-W. Han, Y.-G. Zhou, *Adv. Synth. Catal.* **2004**, *346*, 909–912. c) L. Xu, K. H. Lam, J. Ji, J. Wu, Q.-H. Fan, W.-H. Lo, A. S. C. Chan, *Chem. Commun.* **2005**, 1390–1392. d) K. H. Lam, L. Xu, L. Feng, Q.-H. Fan, F. L. Lam, W. Lo, A. S. Chan, *Adv. Synth. Catal.* **2005**, *347*, 1755–1758. e) T. Yamagata, H. Tadaoka, M. Nagata, T. Hirao, Y. Kataoka, V. Ratovelomanana-Vidal, J. P. Genet, K. Mashima, *Organometallics* **2006**, *25*, 2505–2513. f) M. T. Reetz, X. Li, *Chem. Commun.* **2006**, 2159–2160. g) S. H. Chan, K. H. Lam, Y.-M. Li, L. Xu, W. Tang, F. L. Lam, W. H. Lo, W. Y. Yu, Q. Fan, A. S. Chan, *Tetrahedron Asymmetry* **2007**, *18*, 2625–2631. h) Z.-J. Wang, G.-J. Deng, Y. Li, Y.-M. He, W.-J. Tang, Q.-H. Fan, *Org. Lett.* **2007**, *9*, 1243–1246. i) W.-J. Tang, S.-F. Zhu, L.-J. Xu, Q.-L. Zhou, Q.-H. Fan, H.-F. Zhou, K. Lam, A. S. C. Chan, *Chem. Commun.* **2007**, 613–615. j) J.-P. Genet, K. Mashima, V. Ratovelomanana-Vidal, *Synlett* **2007**, 2743–2747. k) M. Jahjah, M. Alame, S. Pellet-Rostaing, M. Lemaire, *Tetrahedron Asymmetry* **2007**, *18*, 2305–2312. l) X.-B. Wang, Y.-G. Zhou, *J. Org. Chem.* **2008**, *73*, 5640–5642. m) S.-M. Lu, C. Bolm, *Adv. Synth. Catal.* **2008**, *350*, 1101–1105. n) Z.-W. Li, T.-L. Wang, Y.-M. He, Z.-J. Wang, Q.-H. Fan, J. Pan, L.-J. Xu, *Org. Lett.* **2008**, *10*, 5265–5268. o) N. Mršić, L. Lefort, J. A. Boogers, A. J. Minnaard, B. L. Feringa, J. G. de Vries, *Adv. Synth. Catal.* **2008**, *350*, 1081–1089. p) H. Tadaoka, D. Cartigny, T. Nagano, T. Gosavi, T. Ayad, J.-P. Genêt, T. Ohshima, V. Ratovelomanana-Vidal, K. Mashima, *Chem.-Eur. J.* **2009**, *15*, 9990–9994. q) M. Eggenstein, A. Thomas, J. Theuerkauf, G. Franciò, W. Leitner, *Adv. Synth. Catal.* **2009**, *351*, 725–732. r) F.-R. Gou, W. Li, X. Zhang, Y.-M. Liang, *Adv. Synth. Catal.* **2010**, *352*, 2441–2444. s) J. L. Núñez-Rico, H. Fernández-Pérez, J. Benet-Buchholz, A. Vidal-Ferran, *Organometallics* **2010**, *29*, 6627–6631. t) D.-S. Wang, Y.-G. Zhou, *Tetrahedron Lett.* **2010**, *51*, 3014–3017. u) D.-S. Wang, J. Zhou, D.-W. Wang, Y.-L. Guo, Y.-G. Zhou, *Tetrahedron Lett.* **2010**, *51*, 525–528. v) M. Rubio, A. Pizzano, *Molecules* **2010**, *15*, 7732–7741. w)

- M. Rueping, R. M. Koenigs, *Chem. Commun.* **2011**, 47, 304–306. x) Z.-P. Chen, Z.-S. Ye, M.-W. Chen, Y.-G. Zhou, *Synthesis* **2013**, 45, 3239–3244. y) A. M. Maj, I. Suisse, C. Hardouin, F. Agbossou-Niedercorn, *Tetrahedron* **2013**, 69, 9322–9328. z) S. E. Lyubimov, D. V. Ozolin, P. Y. Ivanov, A. Melman, V. S. Velezheva, V. A. Davankov, *Chirality* **2014**, 26, 56–60.
45. a) D.-W. Wang, X.-B. Wang, D.-S. Wang, S.-M. Lu, Y.-G. Zhou, Y.-X. Li, *J. Org. Chem.* **2009**, 74, 2780–2787. b) X.-F. Cai, R.-N. Guo, M.-W. Chen, L. Shi, Y.-G. Zhou, *Chem.-Eur. J.* **2014**, 20, 7245–7248. c) J. John, C. Wilson-Konderka, C. Metallinos, *Adv. Synth. Catal.* **2015**, 357, 2071–2081.
46. X.-F. Cai, W.-X. Huang, Z.-P. Chen, Y.-G. Zhou, *Chem. Commun.* **2014**, 50, 9588–9590.
47. a) H. Zhou, Z. Li, Z. Wang, T. Wang, L. Xu, Y. He, Q.-H. Fan, J. Pan, L. Gu, A. S. C. Chan, *Angew. Chem. Int. Ed.* **2008**, 47, 8464–8467. b) Z.-J. Wang, H.-F. Zhou, T.-L. Wang, Y.-M. He, Q.-H. Fan, *Green Chem.* **2009**, 11, 767–769. c) T. Wang, L.-G. Zhuo, Z. Li, F. Chen, Z. Ding, Y. He, Q.-H. Fan, J. Xiang, Z.-X. Yu, A. S. C. Chan, *J. Am. Chem. Soc.* **2011**, 133, 9878–9891. d) Z. Yang, F. Chen, Y.-M. He, N. Yang, Q.-H. Fan, *Catal. Sci. Technol.* **2014**, 4, 2887–2890.
48. a) D.-W. Wang, W. Zeng, Y.-G. Zhou, *Tetrahedron Asymmetry* **2007**, 18, 1103–1107. b) D.-S. Wang, Y.-G. Zhou, *Tetrahedron Lett.* **2010**, 51, 3014–3017.
49. V. Parekh, J. A. Ramsden, M. Wills, *Tetrahedron Asymmetry* **2010**, 21, 1549–1556.
50. C. Wang, C. Li, X. Wu, A. Pettman, J. Xiao, *Angew. Chem. Int. Ed.* **2009**, 48, 6524–6528.
51. a) V. Sumerin, K. Chernichenko, M. Nieger, M. Leskelä, B. Rieger, T. Repo, *Adv. Synth. Catal.* **2011**, 353, 2093–2110. b) Z. Zhang, H. Du, *Org. Lett.* **2015**, 17, 2816–2819.
52. a) M. Rueping, A. P. Antonchick, T. Theissmann, *Angew. Chem. Int. Ed.* **2006**, 45, 3683–3686. b) Q.-S. Guo, D.-M. Du, J. Xu, *Angew. Chem. Int. Ed.* **2008**, 47, 759–762. c) M. Rueping, T. Theissmann, S. Raja, J. W. Bats, *Adv. Synth. Catal.* **2008**, 350, 1001–1006. d) M. Rueping, T. Theissmann, *Chem. Sci.* **2010**, 1, 473–476. e) M. Rueping, L. Hubener, *Synlett* **2011**, 2011, 1243–1246. f) X.-F. Tu, L.-Z. Gong, *Angew. Chem. Int. Ed.* **2012**, 51, 11346–11349. g) X.-F. Cai, M.-W. Chen, Z.-S. Ye, R.-N. Guo, L. Shi, Y.-Q. Li, Y.-G. Zhou, *Chem. Asian J.* **2013**, 8, 1381–1385. h) R.-N. Guo, Z.-P. Chen, X.-F. Cai, Y.-G. Zhou, *Synthesis* **2014**, 46, 2751–2756. i) X.-F. Cai, R.-N. Guo, G.-S. Feng, B. Wu, Y.-G. Zhou, *Org. Lett.* **2014**, 16, 2680–3. j) M.-W. Chen, X.-F. Cai, Z.-P. Chen, L. Shi, Y.-G. Zhou, *Chem. Commun.* **2014**, 50, 12526–12529. k) A. A. Desai, Y. Guan, A. L. Odom, S. Majumder, W. D. Wulff, *Tetrahedron Lett.* **2015**, 56, 3481–3485. l) G. V. More, B. M. Bhanage, *Tetrahedron Asymmetry* **2015**, 26, 1174–1179.
53. a) J. Kobayashi, F. Kanda, M. Ishibashi, H. Shigemori, *J. Org. Chem.* **1991**, 56, 4574–4576. b) I. Ohtani, R. E. Moore, M. T. C. Runnegar, *J. Am. Chem. Soc.* **1992**, 114, 7941–7942. c) L. A. McDonald, L. R. Barbieri, G. T. Carter, E. Lenoy, J. Lotvin, P. J. Petersen, M. M. Siegel, G. Singh, R. T. Williamson, *J. Am. Chem. Soc.* **2002**, 124, 10260–10261. d) F. Reyes, R. Fernández, A. Rodríguez, A. Francesch, S. Taboada, C. Ávila, C. Cuevas, *Tetrahedron* **2008**, 64, 5119–5123. e) J. M. Pastor, M. Salvador, M. Argandoña, V. Bernal, M. Reina-Bueno, L. N. Csonka, J. L. Iborra, C. Vargas, J. J. Nieto, M. Cánovas, *Biotechnol. Adv.* **2010**, 28, 782–801.
54. R. Kuwano, Y. Hashiguchi, R. Ikeda, K. Ishizuka, *Angew. Chem. Int. Ed.* **2015**, 54, 2393–2396.
55. a) G. Erre, S. Enthaler, K. Junge, S. Gladiali, M. Beller, *Coord. Chem. Rev.* **2008**, 252, 471–491. b) M. van den Berg, B. L. Feringa, A. J. Minnaard, *The Handbook of Homogeneous Hydrogenation, Chapter 28* (Eds.: J. G. de Vries, C. J. Elsevier), Wiley-VCH, Weinheim, **2007**, 995–1027. c) D. J. Ager, A. H. M. de Vries, J. G. de Vries, *Platinum Met. Rev.* **2006**, 50, 54–63. d) J. G. de Vries, *Handbook of Chiral Chemicals, 2nd Edition* (Ed. D. J. Ager), CRC Press, Boca Raton, **2005**, 269–286. e) I. V. Komarov, A. Börner, *Angew. Chem. Int. Ed.* **2001**, 40, 1197–1200. f) T. Jerphagnon, J.-L. Renaud, C. Bruneau, *Tetrahedron Asymmetry* **2004**, 15, 2101–2111.



56. a) J. G. de Vries, L. Lefort, *Chem. Eur. J.* **2006**, *12*, 4722–4734. b) L. Lefort, J. A. F. Boogers, A. H. M. de Vries, J. G. de Vries, *Org. Lett.* **2004**, *6*, 1733–1735.
57. a) N. Mršić, L. Panella, A. J. Minnaard, B. L. Feringa, J. G. de Vries, *Tetrahedron Asymmetry* **2011**, *22*, 36–39. b) A. J. Minnaard, B. L. Feringa, L. Lefort, J. G. De Vries, *Acc. Chem. Res.* **2007**, *40*, 1267–1277. c) R. Hoen, T. Tiemersma-Wegman, B. Procuranti, L. Lefort, J. G. de Vries, A. J. Minnaard, B. L. Feringa, *Org. Biomol. Chem.* **2007**, *5*, 267–275. d) R. Hoen, J. A. F. Boogers, H. Bernsmann, A. J. Minnaard, A. Meetsma, T. D. Tiemersma-Wegman, A. H. M. de Vries, J. G. de Vries, B. L. Feringa, *Angew. Chem. Int. Ed.* **2005**, *44*, 4209–4212. e) M. T. Reetz, G. Mehler, *Tetrahedron Lett.* **2003**, *44*, 4593–4596.
58. a) Y. N. C. Chan, D. Meyer, J. A. Osborn, *J. Chem. Soc., Chem. Commun.* **1990**, 869–871. b) Y. N. C. Chan, J. A. Osborn, *J. Am. Chem. Soc.* **1990**, *112*, 9400–9401.
59. a) A. G. Cook, C. A. Schering, P. A. Campbell, S. S. Hayes, *Tetrahedron Lett.* **2005**, *46*, 5451–5454. b) A. W. Gregory, A. Chambers, A. Hawkins, P. Jakubec, D. J. Dixon, *Chem. Eur. J.* **2015**, *21*, 111–114.
60. a) M. J. Rashkin, M. L. Waters, *J. Am. Chem. Soc.* **2002**, *124*, 1860–1861. b) C. K. Bradsher, T. W. G. Solomons, *J. Am. Chem. Soc.* **1959**, *81*, 2550–2552.
61. C. B. Martin, B. O. Patrick, A. Cammers-Goodwin *J. Org. Chem.*, **1999**, *64*, 7807–7812.
62. X.-H. Yang, J.-H. Xie, W.-P. Liu, Q.-L. Zhou, *Angew. Chem. Int. Ed.* **2013**, *52*, 7833–7836.
63. N. A. Grayson, W. D. Bowen, K. C. Rice, *Heterocycles* **1992**, *34*, 2281–2292.
64. A. Liljeblad, H.-M. Kavenius, P. Tähtinen, L. T. Kanerva, *Tetrahedron Asymmetry* **2007**, *18*, 181–191.
65. a) M. Amat, O. Lozano, C. Escolano, E. Molins, J. Bosch, *J. Org. Chem.* **2007**, *72*, 4431–4439. b) M. Amat, N. Llor, J. Hidalgo, C. Escolano, J. Bosch, *J. Org. Chem.* **2003**, *68*, 1919–1928. c) M. Amat, E. Brunaccini, B. Checa, M. Perez, N. R. Llor, J. Bosch, *Org. Lett.* **2009**, *11*, 4370–4373. d) Y. Nakamura, A. M. Burke, S. Kotani, J. W. Ziller, S. D. Rychnovsky, *Org. Lett.* **2009**, *12*, 72–75. e) D. Gnecco, A. M. Lumbreras, J. L. Teran, A. Galindo, J. R. Juarez, M. L. Orea, A. Castro, R. G. Enriquez, W. F. Reynolds, *Heterocycles* **2009**, *78*, 2589–2594.
66. a) T. X. Metro, D. G. Pardo, J. Cossy, *J. Org. Chem.* **2007**, *72*, 6556–6561. b) J. Cossy, C. Dumas, D. G. Pardo, *Eur. J. Org. Chem.* **1999**, 1693–1699. c) J. Cossy, O. Mirguet, D. G. Pardo, *Synlett* **2001**, 1575–1577. d) S. B. D. Jarvis, A. B. Charette, *Org. Lett.* **2011**, *13*, 3830–3833.
67. a) J. J. Verendel, T. Zhou, J.-Q. Li, A. Paptchikhine, O. Lebedev, P. G. Andersson, *J. Am. Chem. Soc.* **2010**, *132*, 8880–8881. b) M. Renom-Carrasco, P. Gajewski, L. Pignataro, J. G. de Vries, U. Piarulli, C. Gennari, L. Lefort, *Adv. Synth. Catal.* **2015**, *357*, 2223–2228.
68. J. Wysocki, C. Schleppehorst, F. Glorius, *Synlett* **2015**, *26*, 1557–1562.
69. a) V. I. Tararov, R. Kadyrov, T. H. Riermeier, J. Holz, A. Börner, *Tetrahedron Lett.* **2000**, *41*, 2351–2355. b) G.-H. Hou, J.-H. Xie, P.-C. Yan, Q.-L. Zhou, *J. Am. Chem. Soc.* **2009**, *131*, 1366–1367. c) Z.-J. Wang, H.-F. Zhou, T.-L. Wang, Y.-M. He, Q.-H. Fan, *Green Chem.* **2009**, *11*, 767–769. d) N. E. Lee, S. L. Buchwald, *J. Am. Chem. Soc.* **1994**, *116*, 5985–5986.
70. a) L. A. Oro, D. Carmona, *The Handbook of Homogeneous Hydrogenation, Chapter I* (Eds.: J.G. de Vries, C.J. Elsevier), Wiley-VCH, Weinheim, **2007**, 3–30. b) S. Enthaler, G. Erre, K. Junge, J. Holz, A. Börner, E. Alberico, I. Nieddu, S. Gladiali, M. Beller, *Org. Process Res. Dev.* **2007**, *11*, 568–577. c) H. Bernsmann, M. van den Berg, R. Hoen, A. J. Minnaard, G. Mehler, M. T. Reetz, J. G. De Vries, B. L. Feringa, *J. Org. Chem.* **2005**, *70*, 943–951. d) Y. Liu, K. Ding, *J. Am. Chem. Soc.* **2005**, *127*, 10488–10489. e) A. Ohashi, S. Kikuchi, M. Yasutake, T. Imamoto, *Eur. J. Org. Chem.* **2002**, *2002*, 2535–2546. f) Y. J. Zhang, J. H. Park, S. Lee, *Tetrahedron Asymmetry* **2004**, *15*, 2209–2212. g) D. Peña, A. J. Minnaard, J. G. de Vries, B. L. Feringa, *J. Am. Chem. Soc.* **2002**, *124*, 14552–14553.

- h) D. J. Wallace, K. R. Campos, C. S. Shultz, A. Klapars, D. Zewge, B. R. Crump, B. D. Phenix, J. C. McWilliams, S. Krska, Y. Sun, et al., *Org. Process Res. Dev.* **2009**, *13*, 84–90. i) W. Tang, S. Wu, X. Zhang, *J. Am. Chem. Soc.* **2003**, *125*, 9570–9571. j) Y.-G. Zhou, W. Tang, W.-B. Wang, W. Li, X. Zhang, *J. Am. Chem. Soc.* **2002**, *124*, 4952–4953. k) F. W. Patureau, C. Worch, M. A. Siegler, A. L. Spek, C. Bolm, J. N. Reek, *Adv. Synth. Catal.* **2012**, *354*, 59–64. l) P. Dupau, C. Bruneau, P. H. Dixneuf, *Adv. Synth. Catal.* **2001**, *343*, 331–334.
71. A. Togni, C. Breutel, A. Schnyder, F. Spindler, H. Landert, A. Tijani, *J. Am. Chem. Soc.* **1994**, *116*, 4062–4066.
72. S. Otsuka, K. Tani, T. Yamagata, S. Akutagawa, H. Kumobayashi, M. Yagi (Takasago Perfumery Co., Ltd.) EP 0068506 A1, **1983**.
73. Fürst, P. A. Plattner, *Helv. Chim. Acta* **1949**, *32*, 275–283.
74. a) D. Heller, R. Kadyrov, *Tetrahedron Asymmetry* **1996**, *7*, 3025–3035. b) A. Fabrello, A. Bachelier, M. Urrutigoity, P. Kalck, *Coord. Chem. Rev.* **2010**, *254*, 273–287. c) I. D. Gridnev, N. Higashi, K. Asakura, T. Imamoto, *J. Am. Chem. Soc.* **2000**, *122*, 7183–7194. d) I. D. Gridnev, T. Imamoto, G. Hoge, M. Kouchi, H. Takahashi, *J. Am. Chem. Soc.* **2008**, *130*, 2560–2572. e) T. Imamoto, K. Tamura, Z. Zhang, Y. Horiuchi, M. Sugiya, K. Yoshida, A. Yanagisawa, I. D. Gridnev, *J. Am. Chem. Soc.* **2012**, *134*, 1754–1769.
75. X. M. Zhang, F. G. Bordwell, M. V. D. Puy, H.E. Fried, *J. Org. Chem.* **1993**, *58*, 3060–3066.
76. C. Baumert, M. Günthel, S. Krawczyk, M. Hemmer, T. Wersig, A. Langner, J. Molnár, H. Lage, A. Hilgeroth, *Bioorg. Med. Chem.* **2013**, *21*, 166–177.
77. G. Bettoni, C. Franchini, F. Morlacchi, N. Tangari, V. Tortorella, *J. Org. Chem.*, **1976**, *41*, 2780–2782.
78. D. Crich, S. Neelamkavil, *Org. Lett.* **2002**, *4*, 2573–2575.
79. G. Bettoni, E. Duranti, V. Tortorella, *Gazzetta Chimica Italiana* **1972**, *102*, 189–204.
80. S. H. Lee, D. S. Im, C. S. Cheong, B. Y. Chung, *Heterocycles* **1999**, *51*, 1913–1919.
81. M. Joerres, I. Schiffrers, I. Atodiresei, C. Bolm, *Organic Letters* **2012**, *14*, 4518–4521.

Part B.

# Tandem Olefin Metathesis – Asymmetric (Transfer) Hydrogenation

**Abstract:**

An overview on the state of the art of tandem olefin metathesis followed by hydrogenation or transfer hydrogenation is presented in Chapter IV. The disclosed mechanistic studies on the transformation of Ru complexes involved in olefin metathesis into Ru hydride species active in hydrogenation are also summarized. In Chapters V and VI, the asymmetric version of these tandem protocols is investigated and the successful development of a tandem olefin metathesis–asymmetric hydrogenation and a tandem olefin metathesis–asymmetric transfer hydrogenation are described, respectively.



# CHAPTER IV.

## OVERVIEW ON THE TANDEM OLEFIN METATHESIS – (TRANSFER) HYDROGENATION

---

Over the last few decades, plenty of synthetic methodologies have been developed which allowed for more selective, efficient and green transformations. However, pharmaceutical drug molecules are of great complexity and long multi-step syntheses are required for their preparation. Practically, this means that large amounts of reagents, solvents and energy are required, which then produce big quantities of waste.<sup>1</sup> For this reason, the research in synthetic methodologies has been focusing more and more into developing one-pot processes, trying to mimic the efficiency of biological systems.<sup>2</sup> These processes do not require the isolation of the intermediates, thus considerably reducing the large amount of solvent used to perform the reactions and the purification steps. When metal-catalyzed processes are involved, one-pot sequential processes may also allow reusing the same metal for more than one reaction. Furthermore, there is no loss of yield arising from the purification of intermediates. Overall, one-pot methodologies save time, money, energy and considerably reduce the amount of waste when compared to their stepwise counterparts.

Due to the rapid progress of this field, the term to define a reaction like cascade, domino, tandem and sequential catalysis has been used interchangeably to describe different processes.<sup>3</sup> Fogg *et al.*, in their review on the taxonomy of tandem catalysis, proposed a clear classification for all the one-pot processes involving multiple catalytic events. According to it, tandem catalysis describes “coupled catalyses in which sequential transformation of the substrate occurs via two (or more) mechanistically distinct processes”.<sup>3</sup> This definition rules out similar concepts like domino or cascade catalysis, where the sequential transformations are effected via the same mechanism. Tandem catalysis can be divided in three subcategories: orthogonal, auto-tandem and assisted catalysis. Orthogonal catalysis implies the use of two catalysts, both present at the beginning of the reaction, which catalyze two consecutive transformations on the initial substrate (Figure 1A). In auto-tandem catalysis processes, instead, only one catalyst precursor is used, which is able to catalyze two consecutive reactions via different mechanisms, interacting differently with the various species present (Figure 1B). Finally, in assisted tandem catalysis

processes, the initial catalyst, which performs the first reaction, is converted into new species able to catalyze the second transformation upon addition of a reagent or a change in the reaction conditions (Figure 1C).

Apart from the workup efficiency, inherent in all one-pot reactions, assisted tandem catalysis processes have several advantages: (i) efficiency in catalyst utilization, (ii) no interaction between the two catalysts –as they do not coexist– and (iii) possibility to optimize the conditions for the two catalytic cycles independently. Although the development of this technology is still in early stages, it has already been widely explored in tandem catalytic processes involving olefin metathesis. Some of the reactions that have been used in tandem with Ru-carbene-catalyzed olefin metathesis catalysts include: Kharasch additions, oxidations, hydrogenations, cyclopropanations, isomerizations, cycloadditions, Wittig olefinations and intramolecular hydroarylations.<sup>4</sup>

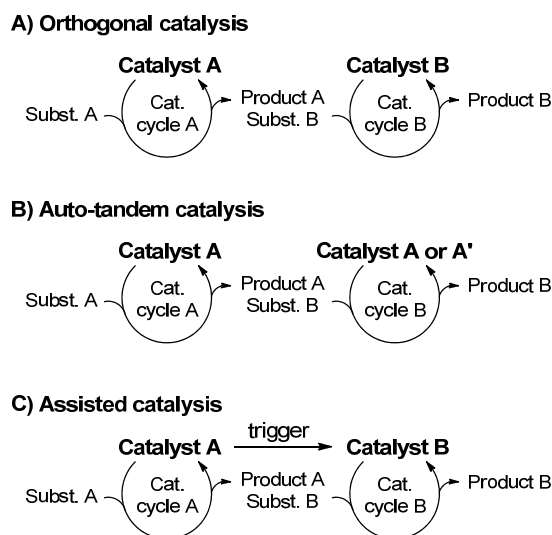
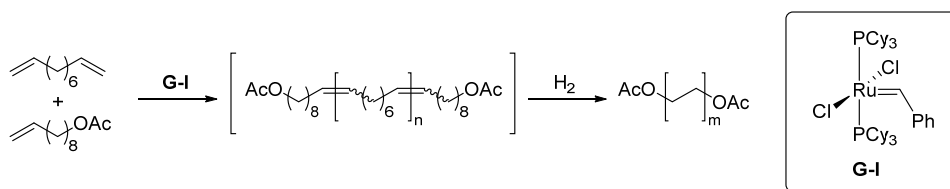


**Figure 1.** Classification of tandem catalysis processes.

This introduction will focus on assisted tandem olefin metathesis–hydrogenation and olefin metathesis–transfer hydrogenation, as those are the subject of investigation in the second part of this thesis.

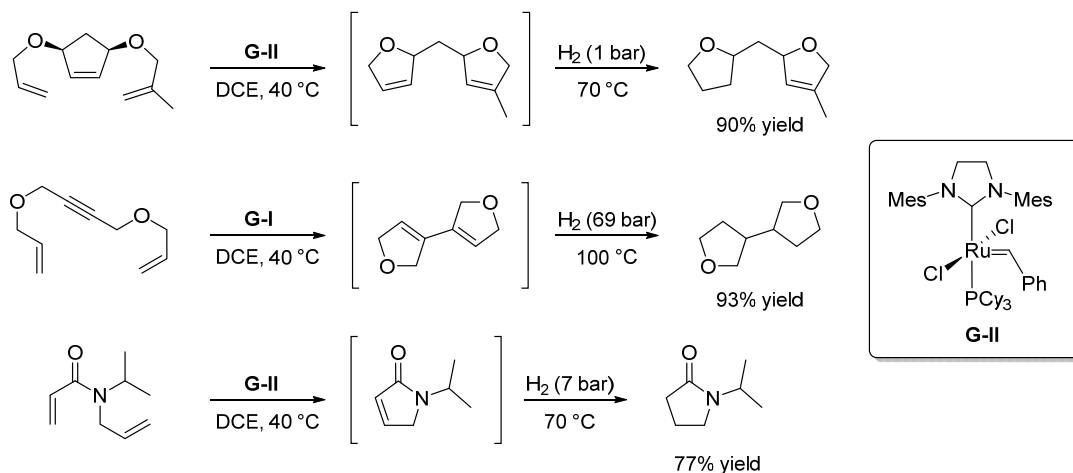
## IV.1 TANDEM OLEFIN METATHESIS–HYDROGENATION

The first uses of tandem olefin metathesis–hydrogenation were in the production of saturated polymers (Scheme 1).<sup>5</sup> After the metathesis step, upon treatment with H<sub>2</sub> the Ru present in the reaction mixture was able to catalyze the double bond hydrogenation. Grubbs and co-workers proposed that the addition of H<sub>2</sub> to 1<sup>st</sup> generation Grubbs catalyst (**G-I**) was leading to the formation of the [RuHCl(H<sub>2</sub>)(PCy<sub>3</sub>)<sub>2</sub>] complex,<sup>5c</sup> which was already known to be an effective hydrogenation pre-catalyst.<sup>6</sup>



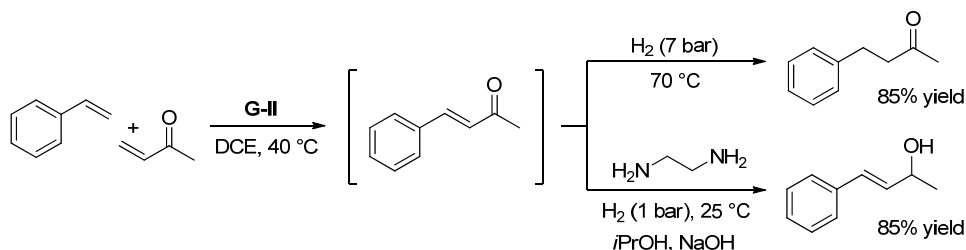
**Scheme 1.** Tandem olefin metathesis–hydrogenation applied in the field of polymers.

Soon after, Grubbs and co-workers extended this process to the synthesis of small molecules (Scheme 2).<sup>7</sup> Using either 1<sup>st</sup> generation (**G-I**) or 2<sup>nd</sup> generation (**G-II**) Grubbs catalysts, they demonstrated with several examples the viability of this tandem process and expanded it to transfer hydrogenation and transfer dehydrogenation of alcohols (see Section IV.2).



**Scheme 2.** Examples of tandem olefin metathesis–hydrogenation.

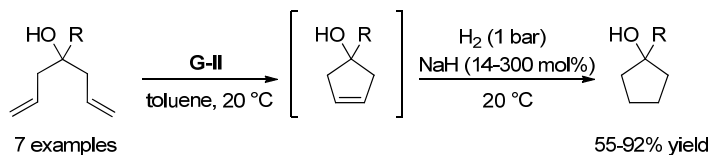
In this same publication, there is an interesting example where the selectivity of the Ru hydrogenation catalyst is modulated by addition of ethylenediamine, which might be acting as a ligand (Scheme 3). After the cross metathesis of styrene with methyl vinyl ketone, if the system is pressurized with hydrogen and warmed up to 70 °C, the double bond is selectively hydrogenated. Instead, if ethylenediamine is added, also in presence of *i*PrOH, NaOH and H<sub>2</sub>, the carbonyl group is hydrogenated selectively. This was the only example in the literature where a ligand was used to modulate the hydrogenation step of this tandem protocol, and it became the inspiration for our investigations in this second part of my thesis.



**Scheme 3.** Catalyst selectivity modulated by addition of ethylenediamine.

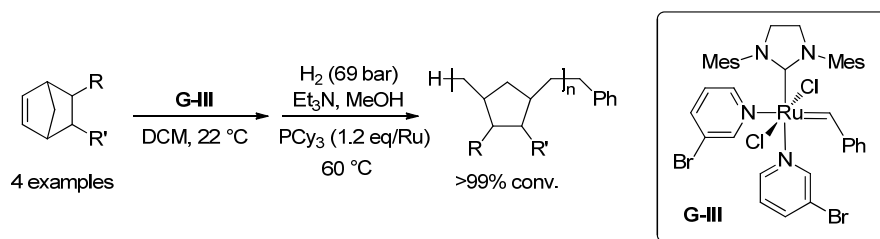
Since then, tandem olefin metathesis–hydrogenation processes have found plenty of applications in chemical synthesis. Schmidt and Pohler disclosed a milder protocol for the conversion of **G-II** into an effective hydrogenation catalyst.<sup>8</sup> To avoid the use of elevated

pressures and temperature, Ru hydride species were formed *in situ* by addition of an inorganic hydride (NaH) and the hydrogenation was run at 20 °C and under 1 bar of H<sub>2</sub>. Applying this methodology, they carried out the ring-closing metathesis (RCM)–hydrogenation of different diallyl carbinols (Scheme 4).



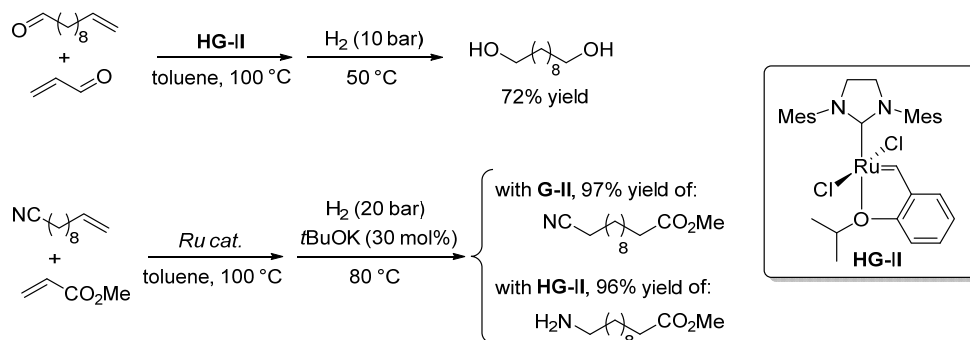
**Scheme 4.** RCM–hydrogenation of different diallyl carbinols.

In the effort to expand this technology to other Grubbs catalysts, Fogg and co-workers reported the tandem ring-opening metathesis polymerization–hydrogenation with 3<sup>rd</sup> generation Grubbs catalyst (**G-III**).<sup>9</sup> This catalyst, one of the fastest-initiating ruthenium catalyst known (measured to be >4000 faster to initiate than **G-II**), is commonly used in ROMP as it provides narrow polydispersity.<sup>10</sup> Initially, the hydrogenation step led to very poor yields. Fogg proposed that the lack of stabilizing phosphines in this catalyst might make it very unstable under hydrogenation conditions. Thus, the addition of PCy<sub>3</sub> (1.2 equivalents/Ru) prior to the hydrogenation step proved very effective, achieving full hydrogenation in all examples (Scheme 5).



**Scheme 5.** Tandem ROMP–hydrogenation with **G-III**.

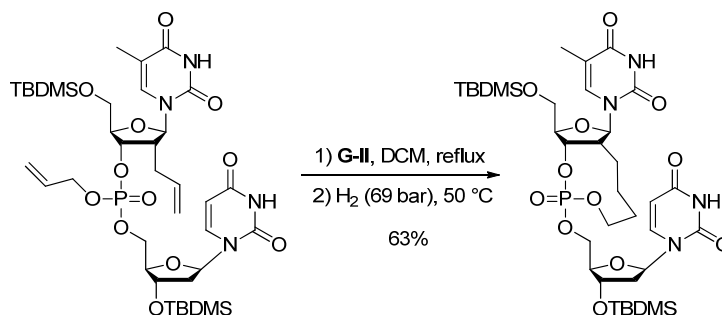
Miao *et al.* employed the same protocol to synthesize different saturated linear diols<sup>11</sup> and aminoesters<sup>12</sup> –important polymer monomers– via cross-metathesis (CM)–hydrogenation, using 2<sup>nd</sup> generation Hoveyda-Grubbs catalyst (**HG-II**). It is remarkable the observed difference in selectivity when employing **G-II** or **HG-II** since the former, unlike the latter, is able to hydrogenate the double bond without reducing the nitrile to amine (Scheme 6).



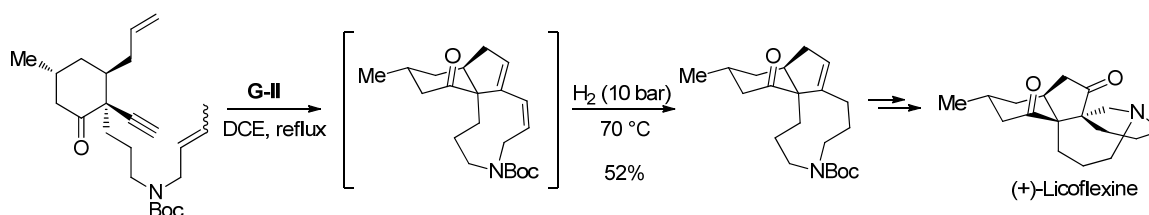
**Scheme 6.** CM–hydrogenation for the synthesis of saturated linear diols and aminoesters.



This technology has also been applied as intermediate step for the synthesis of other relevant molecules, such as cyclic dinucleotides (Scheme 7),<sup>13</sup> peptidomimetics<sup>14</sup> and biologically active compounds (Scheme 8).<sup>15</sup>



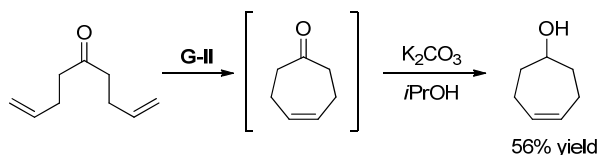
**Scheme 7.** Example of RCM–hydrogenation for the synthesis of a cyclic nucleotide.



**Scheme 8.** Example of RCM–hydrogenation for the synthesis of an intermediate in the total synthesis of (+)-Licoflexine.

## IV.2 TANDEM OLEFIN METATHESIS–TRANSFER HYDROGENATION

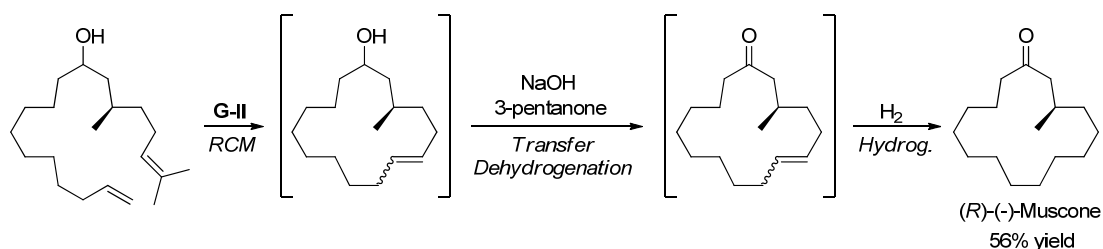
Transfer hydrogenation (TH) is defined as the process of addition of hydrogen to a molecule from a source different than H<sub>2</sub>. Grubbs and co-workers were the first to show that Ru olefin metathesis catalysts **G-I** and **G-II** could be also transformed into efficient transfer hydrogenation catalysts.<sup>7</sup> After an initial RCM step, the addition of a base (K<sub>2</sub>CO<sub>3</sub> or NaOH) and *i*PrOH selectively afforded the reduction of the carbonyl group without affecting the C=C double bond (Scheme 9). Analogously, the dehydrogenation of alcohols could be performed using 3-pentanone as solvent. Employing the latter methodology, and with a subsequent hydrogenation of the C–C double bond, they achieved the one-pot synthesis of (*R*)-(-)-Muscone (Scheme 10).



**Scheme 9.** Example of a tandem olefin metathesis–TH.

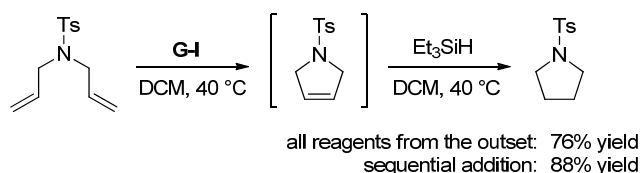
This report had been so far the only one describing a tandem olefin metathesis–TH of ketones. Surprisingly, although it has been reported that ruthenium complexes are not particularly efficient in promoting the hydrogen transfer towards olefins and alkynes,<sup>16</sup> all later

publications have been focused in the TH of C=C bonds. The published methodologies differ in the hydrogen source and in the mode of generating the Ru hydride species.



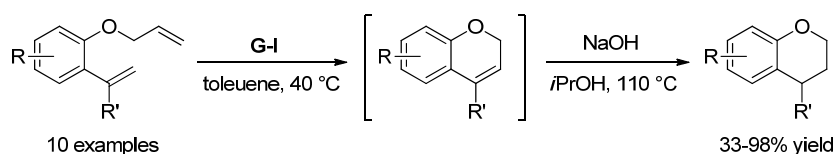
**Scheme 10.** Example of three Ru-catalyzed steps in tandem.

The first report on the TH of alkenes using a Ru olefin metathesis catalysts was disclosed by Menozzi *et al.*<sup>17</sup> They initially demonstrated that the combination of triethylsilane and **G-I** was able to effect the reduction of C=C bonds. The proposed mechanism consisted of a Ru-catalyzed stepwise addition of two hydrides, originating from the triethylsilane, to the double bond, generating disilane as by-product. When trying to establish the tandem protocol for the olefin metathesis–TH, they realized that the presence of triethylsilane was not affecting the metathetic activity of the Ru complex. Thus, it was possible to perform the tandem reaction with all the reagents present from the outset. However, when performing the same reaction with sequential additions of the carbene catalyst followed by the alkylsilane, the yield was slightly improved (Scheme 11).

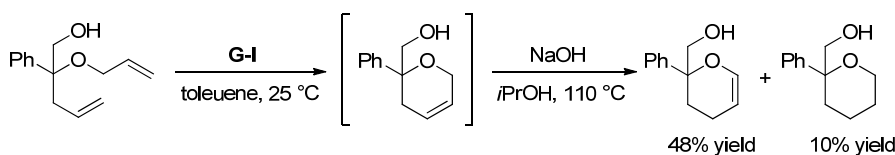


**Scheme 11.** Tandem RCM–TH of olefins using Et<sub>3</sub>SiH as hydrogen source.

Schmidt *et al.* disclosed the use of **G-I** for the RCM–TH of 2-(allyloxy)styrenes to give different chromane derivatives.<sup>18</sup> Employing similar conditions to those used by Grubbs and co-workers for the TH of ketones (NaOH and *i*PrOH),<sup>7</sup> they were able to hydrogenate C=C double bonds (Scheme 12). However, when this methodology was applied to non-benzofused substrates, the hydrogenation proceeded much slower and isomerization took place preferentially (Scheme 13).<sup>19</sup>

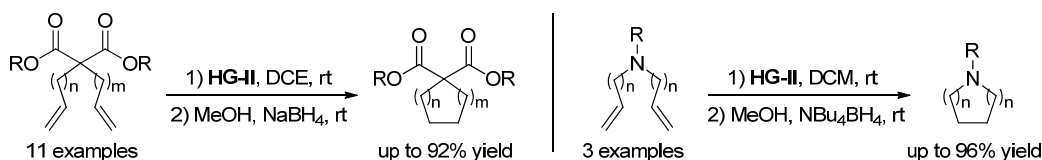


**Scheme 12.** Synthesis of chromanes by tandem RCM–TH.



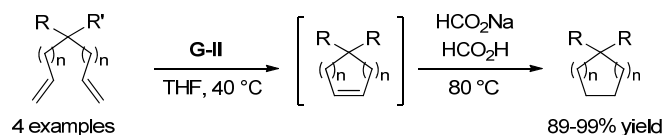
**Scheme 13.** Attempt to synthesize tetrahydropyran derivatives by tandem RCM–TH.

Connolly *et al.* recently found that the addition NaBH<sub>4</sub> and an alcohol to a Ru olefin metathesis catalyst was inducing the reduction of C=C bonds.<sup>20</sup> In this case, the use of MeOH as co-solvent was crucial for the formation of Ru species able to efficiently transfer hydrogen from NaBH<sub>4</sub> to the substrate. From these findings they developed a tandem protocol for the RCM–TH (Scheme 14). Obviously, under these conditions, any group susceptible to be reduced by NaBH<sub>4</sub> was also hydrogenated (e.g. ketones, aldehydes).

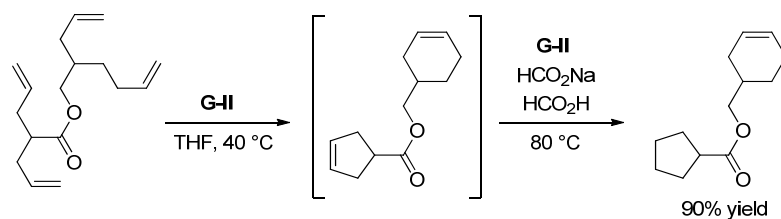


**Scheme 14.** Tandem RCM–TH of alkenes using borohydrides as hydrogen source.

The most recent report of a tandem RCM–TH of alkenes was disclosed by Grela and co-workers.<sup>21</sup> In this approach, **G-II** is converted into Ru hydride species by addition of sodium formate and formic acid, which also serves as a source of hydrogen (Scheme 15). During a substrate scope investigation, it was observed that trisubstituted alkenes were hydrogenated slower than disubstituted. Moreover, differently sized unsaturated rings were hydrogenated with different rates. While cyclopentene and cycloheptene derivatives were smoothly hydrogenated, the hydrogenation of cyclohexene rings was about two orders of magnitude slower. Taking advantage of this situation, they showed the possibility of a selective hydrogenation, although an additional amount of **G-II** had to be added before the hydrogenation step (Scheme 16).



**Scheme 15.** Tandem RCM–TH of alkenes using formic acid as hydrogen source.



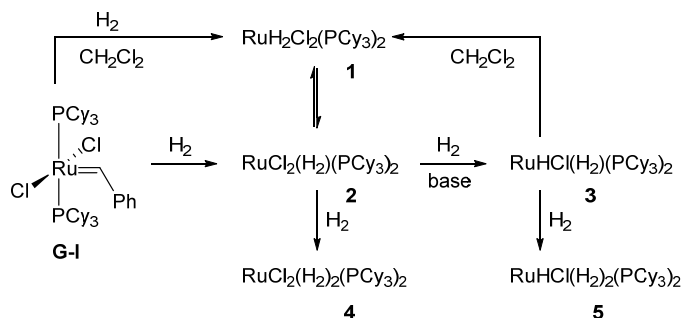
**Scheme 16.** Selective TH of cycloalkenes after RCM.

### IV.3 MECHANISTIC STUDIES

During these years of development of the tandem olefin metathesis–(transfer) hydrogenation protocols, many efforts have also been put into understanding the mechanism of formation of the active species and the role of the different additives used (e.g. bases or alcohols).

The first study on the reaction of **G-I** with H<sub>2</sub> in different conditions was performed by Fogg and co-workers (Scheme 17).<sup>22</sup> Hydrogenolysis of the ruthenium carbene in chlorinated solvents

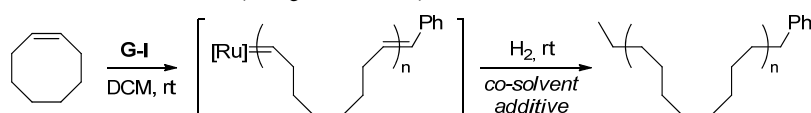
affords the Ru(IV) dihydride species **1**. Instead, with non-chlorinated solvents, complex **2** is formed preferentially, although it is in equilibrium with its tautomeric form **1**. Addition of a base abstracts HCl leading to the Ru(II) hydride species **3**, which is assumed to be the one entering into the catalytic cycle. Coordination of a second molecule of H<sub>2</sub> can lead to the formation of complexes **4** and **5**.



**Scheme 17.** Different Ru species formed by hydrogenolysis of **G-I** under different conditions.

In a later publication, Fogg and co-workers demonstrated the great influence of solvents and additives to form different Ru hydride species featuring various levels of efficiency in hydrogenation.<sup>23</sup> After ROMP of octene with **G-I** in DCM, the subsequent hydrogenation was performed in different conditions (Table 1). The Ru species **1**, formed exclusively in DCM, gave very low conversions even at high pressures of H<sub>2</sub> (Table 1, entry 1). When THF was used as co-solvent, the equilibrium was displaced to the formation of **2**, which proved to be much more active in hydrogenation, but only at high pressures (entries 2 and 3). In presence of a base (entry 4), the Ru species **3** was formed, which showed high efficiency in the reduction step. Surprisingly, the addition of MeOH as co-solvent strongly accelerated the hydrogenation rate (entry 5) and with addition of Et<sub>3</sub>N full conversion was achieved under only 1 bar of H<sub>2</sub> at 60 °C (entry 6). In the latter case, the already known hydrogenation catalyst [RuHCl(CO)(PCy<sub>3</sub>)<sub>2</sub>] (**6**), which might have been formed by decarbonylation of methanol, was identified as the active species. However, although decarbonylation cannot occur with *i*PrOH, its use also increased the reaction rate (entry 7), thus suggesting an additional role of the alcohol.

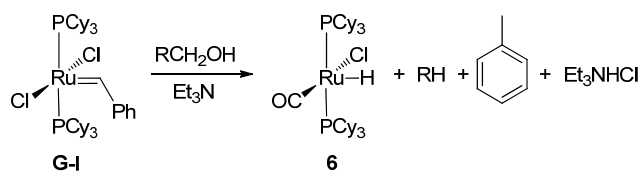
**Table 1.** ROMP-hydrogenation of cyclooctene in DCM.



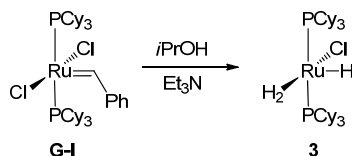
#	co-solvent	additive	pH <sub>2</sub> (bar)	time (h)	conv. (%)
1	-	-	69	24	32
2	75% THF	-	69	24	>99
3	75% THF	-	7	24	9
4	-	Et <sub>3</sub> N	7	24	85
5	20% MeOH	-	7	4	83
6	20% MeOH	Et <sub>3</sub> N	1	24	>99 <sup>a</sup>
7	20% <i>i</i> PrOH	-	7	4	54

a) Hydrogenation at 60 °C.

Complementary conclusions were drawn by Dinger and Mol when investigating the conversion of **G-I** to the Ru species **6** in absence of H<sub>2</sub>.<sup>24</sup> When **G-I** was reacted with an excess of a primary alcohol in toluene at 70 °C for 2 days, compound **6** was obtained. These findings were also reported by Grubbs and co-workers.<sup>25</sup> However, when secondary alcohols or water were used, no reaction was observed. Addition of a base (organic or inorganic) greatly increased the rate of formation and the yield of **6** in presence of primary alcohols (Scheme 18). Although a general mechanism could not be proposed, it was shown that the base was facilitating the abstraction of HCl (triethylamine hydrochloride was isolated) and that the carbonyl ligand was originating by decarbonylation of the primary alcohol (1-<sup>13</sup>C-labeled ethanol was used to prove it). In this case, toluene, the product of hydrogenation of the benzylidene moiety, and the decarbonylated primary alcohol were also detected. Nolan and co-workers later proved that the reaction of **G-I** with secondary alcohols and Et<sub>3</sub>N did not lead to the hydridocarbonyl species **6**, but to the Ru-dihydrogen complex **3** (Scheme 19).<sup>26</sup>

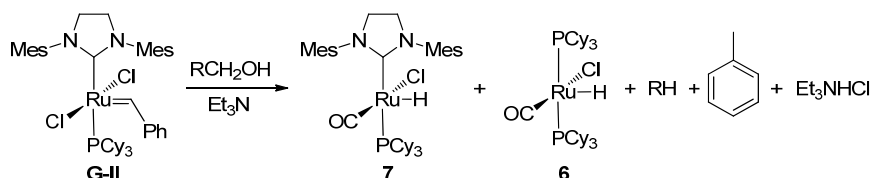


**Scheme 18.** Conversion of **G-I** to Ru species **6** and observed by-products.



**Scheme 19.** Reaction of **G-I** with secondary alcohols and base to give Ru species **3**.

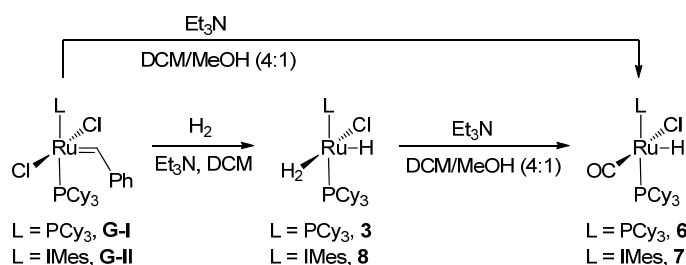
Simultaneously, Dinger and Mol also studied the reaction of **G-II** with primary alcohols and bases (Scheme 20).<sup>27</sup> The resulting reaction mixture turned out to be more complicated than when **G-I** had been used. The expected hydridocarbonyl Ru complex **7** was indeed formed along with decarbonylated alcohol and toluene. In addition, complex **6** was also formed by exchange of the NHC ligand (IMes) for PCy<sub>3</sub>, but unfortunately the possibly formed bis-carbene complex arising from the PCy<sub>3</sub>/IMes scrambling could not be unambiguously identified. Comparable results were obtained by Banti and Mol<sup>28</sup> when reacting a complex analogous of **G-II** bearing SIPr instead of SIMes as the NHC ligand.



**Scheme 20.** Conversion of **G-II** to Ru species **7** and **6** and observed by-products.

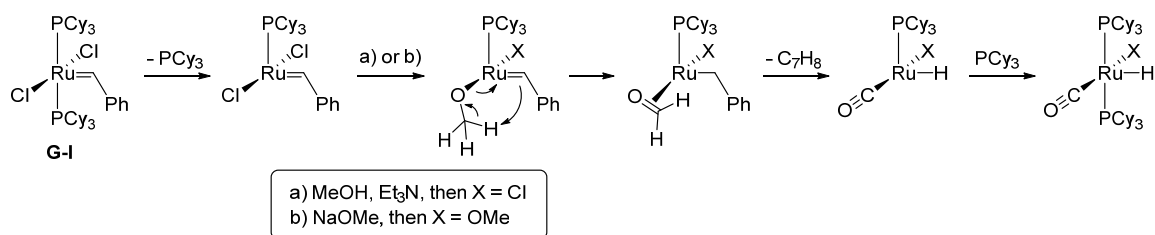
As observed in all these reports, Ru hydridocarbonyl complexes, highly active in hydrogenation, can be formed by reaction of **G-I** or **G-II** with a primary alcohol and a base, in the presence or in the absence of H<sub>2</sub>. The increasing number of applications of these complexes in

tandem olefin metathesis–hydrogenation required a better understanding of which is the most efficient path for the formation of the active hydrogenation species. For this reason, Fogg and co-workers undertook investigations on both hydrogenolysis and methanolysis processes of **G-I** and **G-II**.<sup>29</sup> The competition studies were based on the two different paths already described to obtain the Ru hydridocarbonyl complexes **6** and **7** (Scheme 21). A first path involves an initial hydrogenolysis, in presence of hydrogen to give the dihydrogen complexes **3** and **8**, followed by decarbonylation of methanol. The second path is a direct methanolysis of the Ru benzylidene complexes to afford the final hydridocarbonyl complexes in one step. Analyzing the rate of reaction of the different paths and the speciation, it was concluded that for **G-I** the most efficient route is the two-steps hydrogenolysis–carbonylation. Direct methanolysis of **G-I** is much slower and decomposition therefore competes. Instead, for **G-II** the one-step protocol is much more efficient. This is due to the susceptibility of dihydrogen complex **8** to disproportionate into bis-phosphine and bis-carbene complexes  $-\text{[RuHCl(H}_2\text{)(PCy}_3\text{)}_2\text{]}$  and  $[\text{RuHCl(H}_2\text{)(IMes)}_2\text{}]$ , respectively.



**Scheme 21.** Possible paths for the conversion of **G-I** and **G-II** to the corresponding hydridocarbonyl species.

Mechanisms for the formation of this type of hydridocarbonyl species have been proposed by Dinger and Mol,<sup>24</sup> when using MeOH and Et<sub>3</sub>N, and by Fogg and co-workers,<sup>30</sup> using NaOMe in MeOH. At room temperature, the PCy<sub>3</sub> ligand in **G-I** is labile enough to allow the insertion of MeOH or NaOMe. This dissociative pathway had been demonstrated when the hydrogenation of **G-I** and **G-II** was inhibited by addition of PCy<sub>3</sub> and enhanced by HBF<sub>4</sub> (a phosphine scavenger).<sup>29</sup> Then, a proton transfer from the methoxide to the benzylidene leads to the Ru-formaldehyde complex. By dehydrogenation of formaldehyde, the carbonyl group is formed with liberation of the benzyl group as toluene. Final re-coordination of PCy<sub>3</sub> renders the hydridocarbonyl species. The facile β-elimination from methoxide makes the proposed mechanism possible, in contrast to what is observed when using *tert*-butoxide<sup>31</sup> or phenoxides,<sup>32</sup> which form stable Ru-bis(alkoxides).



**Scheme 22.** Proposed mechanism for the formation of Ru-hydridocarbonyl species from **G-I**.

An analogous mechanistic study for similar Ru-carbene catalysts was reported by Nolan and co-workers, which reinforces the one previously described.<sup>26</sup> The same mechanism is also proposed for **G-II**, but without the initial decoordination of the phosphine, since it has been observed that it is much slower than in 1<sup>st</sup> generation catalysts.





# CHAPTER V.

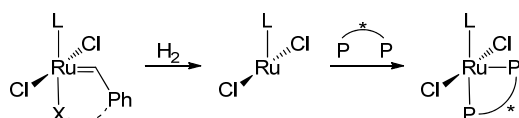
## TANDEM OLEFIN METATHESIS – ASYMMETRIC HYDROGENATION

---

### V.1 INTRODUCTION

Inspired by the findings of Grubbs and co-workers,<sup>7</sup> where the hydrogenation selectivity of Grubbs 2<sup>nd</sup> generation catalyst (**G-II**) after a metathesis step was modulated by addition of ethylenediamine (probably acting as ligand), we wondered if it would be possible to use a chiral ligand instead. In this way, it might be possible to convert a Grubbs catalyst into an asymmetric hydrogenation (AH) catalyst.

As shown in the reported mechanistic studies, under hydrogenolysis conditions the benzyldiene moiety attached to the Ru center is hydrogenated out leaving free coordination sites, where eventually a chiral ligand could coordinate.



**Scheme 23.** Simplified concept for the formation of a chiral hydrogenation Ru catalyst from a Grubbs catalyst.

This concept could be later applied to a tandem protocol, in which the chiral ligand would be added after the metathesis step and before the addition of H<sub>2</sub>. However, this approach could be risky considering that at the end of a metathesis step the original Grubbs catalyst is no longer present. Instead, new Ru species originating from the metathesis of the Ru-benzyldiene with other alkenes and from the decomposition of the metathesis catalyst are coexisting in solution.<sup>33,34</sup> The addition of a chiral ligand to that mixture, under hydrogen pressure, might lead to different complexes containing or not containing the chiral ligand and showing diverse efficiencies in AH.

## V.2 RESULTS AND DISCUSSION

Among the different commercially available Ru olefin metathesis catalysts (Figure 2), we selected Hoveyda-Grubbs 2<sup>nd</sup> generation catalyst (**HG-II**), since it does not contain any phosphine which could compete with the added ligand leading to the formation of achiral hydrogenation catalysts.

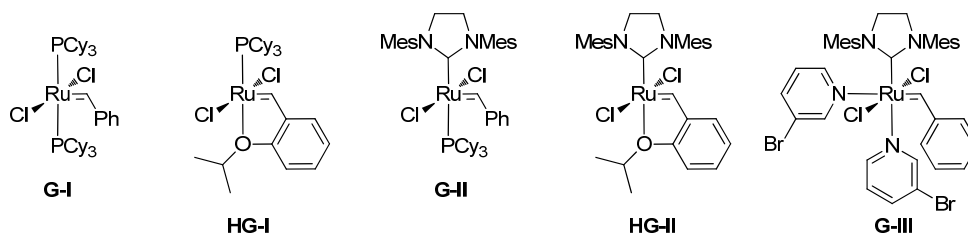
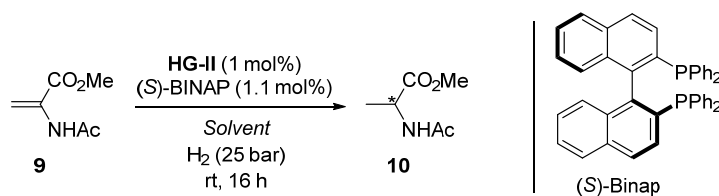


**Figure 2.** Commercially available Ru olefin metathesis catalysts.

For the initial attempts, the enantioselective hydrogenation of methyl 2-acetamidoacrylate (**9**) was attempted using **HG-II** in combination with (*S*)-BINAP as chiral ligand. In THF or DCM, the conversion of **9** to methyl 2-acetamidopropanoate (**10**) was almost zero, either in the presence or in the absence of ligand (Table 2, entries 1-4). As reported by Fogg and co-workers,<sup>9,23,35</sup> the presence of alcohols can enhance the activity of Grubbs catalysts in hydrogenation. Indeed, the same experiments carried out with (*S*)-BINAP in DCM/MeOH 1:4 or THF/MeOH 1:4 led to full conversion (entries 5-6). Even more gratifying was the significant enantioselectivity obtained in both cases, suggesting that a Ru-BINAP complex active in hydrogenation had formed.

**Table 2.** AH with **HG-II** and (*S*)-BINAP.



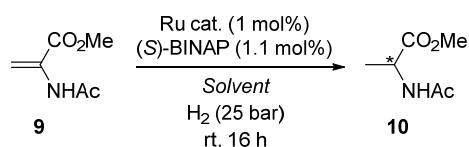
#	Ligand	Solvent	Conv. (%)	ee (%)
1	none	DCM	2	0
2	none	THF	0	0
3	( <i>S</i> )-BINAP	DCM	2	0
4	( <i>S</i> )-BINAP	THF	0	0
5	( <i>S</i> )-BINAP	DCM/MeOH 1:4	100	59
6	( <i>S</i> )-BINAP	THF/MeOH 1:4	100	61
7	none	DCM/MeOH 1:4	15	0
8	none	THF/MeOH 1:4	16	0
9 <sup>[a]</sup>	none	DCM/MeOH 1:4	29	0
10 <sup>[a]</sup>	( <i>S</i> )-BINAP	DCM/MeOH 1:4	35	4

Reaction conditions: **9** (1 mmol), **HG-II** (1 mol %), (*S*)-BINAP (1.1 mol %), H<sub>2</sub> (25 bar), solvent (5 mL), 16 h, rt. Conversion and ee determined by chiral GC. [a] 3 equiv. Et<sub>3</sub>N relative to Ru.

In the absence of ligand (entries 7-8) the activity of the catalyst was significantly reduced, which indicates that the hydrogenation was ligand-accelerated. In fact, this is the most desirable situation, since the enantioselective catalyst is much more active than the non-enantioselective one, and thus the erosion of the *ee* due to the activity of the non-enantioselective catalyst is minimized. Fogg already observed this effect<sup>9</sup> when, by adding PCy<sub>3</sub> after the metathesis step, the activity in hydrogenation of the **G-III** precursor was substantially improved, most probably by stabilizing the resting state of the catalyst. Et<sub>3</sub>N was also reported to be beneficial for the formation of active hydrogenation species.<sup>9,23,35</sup> However, this additive did not give any positive effect in our case (entries 9-10).

To ascertain whether the ligand-acceleration observed for **HG-II** was also acting when using other catalyst precursors, the hydrogenation of **9** was carried out with different commercially available ruthenium olefin metathesis catalysts in DCM/MeOH 1:4 (Table 3, entries 1-6). The same trend was observed with **G-III**, but not with **G-II**, which led to full conversion but no *ee*, either in presence or absence of BINAP.

**Table 3.** Ligand-acceleration effect in the hydrogenation of methyl acetamidoacrylate with different ruthenium catalysts.



#	Ru cat.	Ligand	Solvent	Conv. (%)	<i>ee</i> (%)
1	<b>G-II</b>	none	DCM/MeOH 1:4	100	0
2	<b>G-II</b>	( <i>S</i> )-BINAP	DCM/MeOH 1:4	100	0
3	<b>HG-II</b>	none	DCM/MeOH 1:4	15	0
4	<b>HG-II</b>	( <i>S</i> )-BINAP	DCM/MeOH 1:4	100	58
5	<b>G-III</b>	none	DCM/MeOH 1:4	39	0
6	<b>G-III</b>	( <i>S</i> )-BINAP	DCM/MeOH 1:4	72	26
7	<b>G-I</b>	none	THF/ <i>i</i> PrOH 1:4	13	0
8	<b>G-I</b>	( <i>S</i> )-BINAP	THF/ <i>i</i> PrOH 1:4	100	82
9	<b>HG-I</b>	none	THF/ <i>i</i> PrOH 1:4	99	0
10	<b>HG-I</b>	( <i>S</i> )-BINAP	THF/ <i>i</i> PrOH 1:4	100	72
11	<b>G-II</b>	none	THF/ <i>i</i> PrOH 1:4	59	0
12	<b>G-II</b>	( <i>S</i> )-BINAP	THF/ <i>i</i> PrOH 1:4	93	40
13	<b>HG-II</b>	none	THF/ <i>i</i> PrOH 1:4	7	0
14	<b>HG-II</b>	( <i>S</i> )-BINAP	THF/ <i>i</i> PrOH 1:4	65	83
15	<b>G-III</b>	none	THF/ <i>i</i> PrOH 1:4	4	0
16	<b>G-III</b>	( <i>S</i> )-BINAP	THF/ <i>i</i> PrOH 1:4	17	70

*Reaction conditions:* **9** (1 mmol), Ru catalyst (1 mol %), (*S*)-BINAP (1.1 mol %), H<sub>2</sub> (25 bar), solvent (5 mL), 16 h, rt. Conversion and *ee* determined by chiral GC.

When the solvent mixture THF/*i*PrOH was used (entries 7-16), the same effect was observed for all tested catalyst precursors. Even in the case where the reaction is completed in

absence of ligand (entry 9), the kinetic profile (Figure 3) shows a much faster reaction rate in presence of the ligand. While without ligand the reaction takes 16 h to be completed, in the presence of (*S*)-BINAP the reaction is finished in about 6 h.

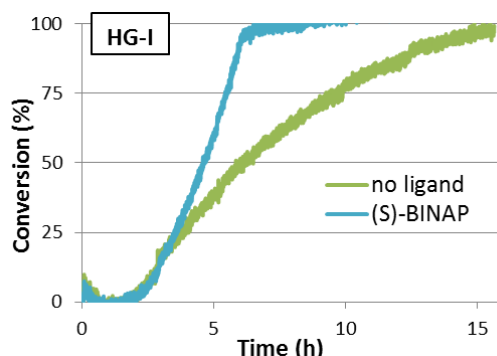
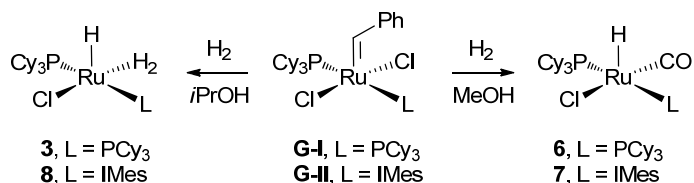


**Figure 3.** Kinetic profiles (conv. vs time) of entries 9 and 10 from Table 3, derived from hydrogen consumption measurements.

The reactions proved much faster when MeOH was used as alcoholic solvent, but more enantioselective in the presence of *i*PrOH. These differences might be attributed to the formation of different active species. Actually, carbonyl complexes (such as **6** and **7**, Scheme 24), which are formed by dehydrogenation of methanol, proved to be much more robust and active in hydrogenation than **3** or **8**,<sup>36</sup> which would be formed in presence of a secondary alcohol like *i*PrOH.<sup>23-28</sup> However, the presence of a strongly coordinating CO ligand would prevent the coordination of a bisphosphine ligand, thus leading to lower *ee*'s.



**Scheme 24.** Formation of Ru-hydride species upon addition of hydrogen to **G-I** and **G-II**.

Analyzing the reaction rate profiles, derived from hydrogen consumption measurements, with different Ru olefin metathesis catalysts and (*S*)-BINAP in THF/*i*PrOH 1:4, some observations can be made (Figure 4). First of all, induction times (ranging from a few minutes to almost 4 h) follow the trend **G-III** < **G-I**  $\approx$  **HG-I** < **G-II**  $\approx$  **HG-II**. This is the same trend followed by the initiation rates of these complexes in the metathesis reaction.<sup>33</sup> The phosphines of the 1<sup>st</sup> generation catalysts are quite labile, being the dissociation rate slightly faster in the case of **G-I** as it contains two equivalent phosphines which can be dissociated. With respect to **G-II**, although one might expect a fast dissociation of the phosphine due to the large *trans*-effect of the NHC ligand, it was demonstrated by Grubbs *et al.* that the dissociation of the phosphine is extremely slow compared to **G-I**.<sup>37</sup> Actually, mechanistic studies have shown that, while the activation of 1<sup>st</sup> generation catalysts goes via the dissociation of the phosphine, with 2<sup>nd</sup> generation catalysts this dissociation does not take place, making the whole process slower.<sup>26,30,33</sup> For **HG-II** an initiation rate similar to that of **G-II** is reported.<sup>38</sup> Finally, **G-III** is known to be one of the fastest-initiating catalysts,<sup>10a</sup> thus being the catalyst with the shortest induction time. The

similar trend on the activation of the catalysts suggests that the hydrogenation of the benzylidene moiety and the initiation of the metathesis reaction might follow a similar mechanism.

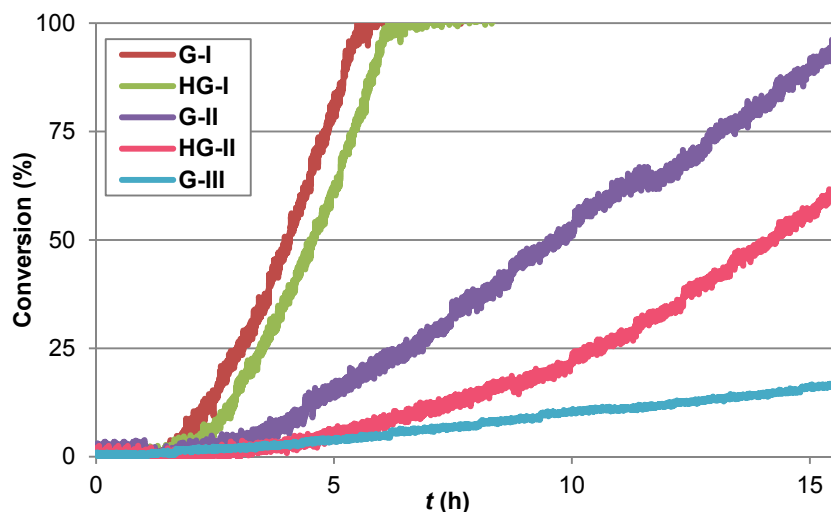


**Figure 4.** Kinetic profiles (conv. vs time) derived from hydrogen consumption measurements in the hydrogenation of methyl acetamidoacrylate with different ruthenium catalysts (corresponding to entries 8, 10, 12, 14 and 16 from Table 3). Reaction conditions: **9** (1 mmol), Ru catalyst (1 mol %), (*S*)-BINAP (1.1 mol %), H<sub>2</sub> (25 bar), THF/*i*PrOH 1:4 (5 ml), 16 h, rt.

Additional relevant information that can be extracted from Figure 4 is the reaction rates (slope of the curves). The 1<sup>st</sup> generation catalysts have parallel slopes, this denoting the same reaction rate and hence, with high probability, the same active species involved in hydrogenation. In the case of the 2<sup>nd</sup> generation catalysts, although the slope of **HG-II** increases with time, indicating that more active species are being generated as the reaction proceeds, it eventually gets constant and parallel to that of **G-II**, again suggesting that most likely the same active species are involved. The case of **G-III** is a bit more surprising, because from an NHC-containing catalyst we would expect similar active species and similar reaction rates to those of the 2<sup>nd</sup> generation catalysts, but instead it is remarkably lower. The explanation for this observation might be in the study from Fogg *et al.* where they found out that **G-III**, although it is very fast hydrogenated, decomposes under hydrogenation conditions, thus generating negligible amounts of hydride species.<sup>9</sup>

It is well known that the solvent plays a crucial role in AH.<sup>39</sup> As we have already observed, it is even more so in our case, where the solvent can determine the nature of the active hydrogenation species and their rate of formation. Therefore, employing the most enantioselective catalyst found so far (**HG-II**), we continued the study by carrying out a solvent screening with mixtures of THF or DCM with different amounts of MeOH or *i*PrOH (Figure 5).

For all solvent mixtures, the addition of an alcoholic solvent led to higher activities and, almost in all cases, higher enantioselectivities. The induction periods, ranging from 1 to 10 hours, and the reaction rates appeared to be also highly dependent on the solvent system. In DCM/MeOH 4:1 (Figure 5A), poor activity and no enantioselectivity was observed. Instead,

when the alcoholic solvent was increased all the way up to pure MeOH, full conversion was obtained without important differences in the reaction rates and enantioselectivities. The same was true in mixtures DCM/*i*PrOH (Figure 5B), even when using only 20% alcohol. However, in these cases the activity was overall lower, with longer induction times and lower rates, but with higher enantiomeric excesses (82% in DCM/*i*PrOH vs 60% in DCM/MeOH). A very different behavior was observed in THF (Figure 5C and D). The reaction rates increased considerably with the amount of alcohol and the enantiomeric excesses varied significantly with the different solvent ratios, but in an opposite manner depending on the alcohol employed. Thus, the highest enantioselectivities were obtained in THF/MeOH 4:1 (89% *ee*) and in DCM/*i*PrOH 1:4 (83% *ee*).

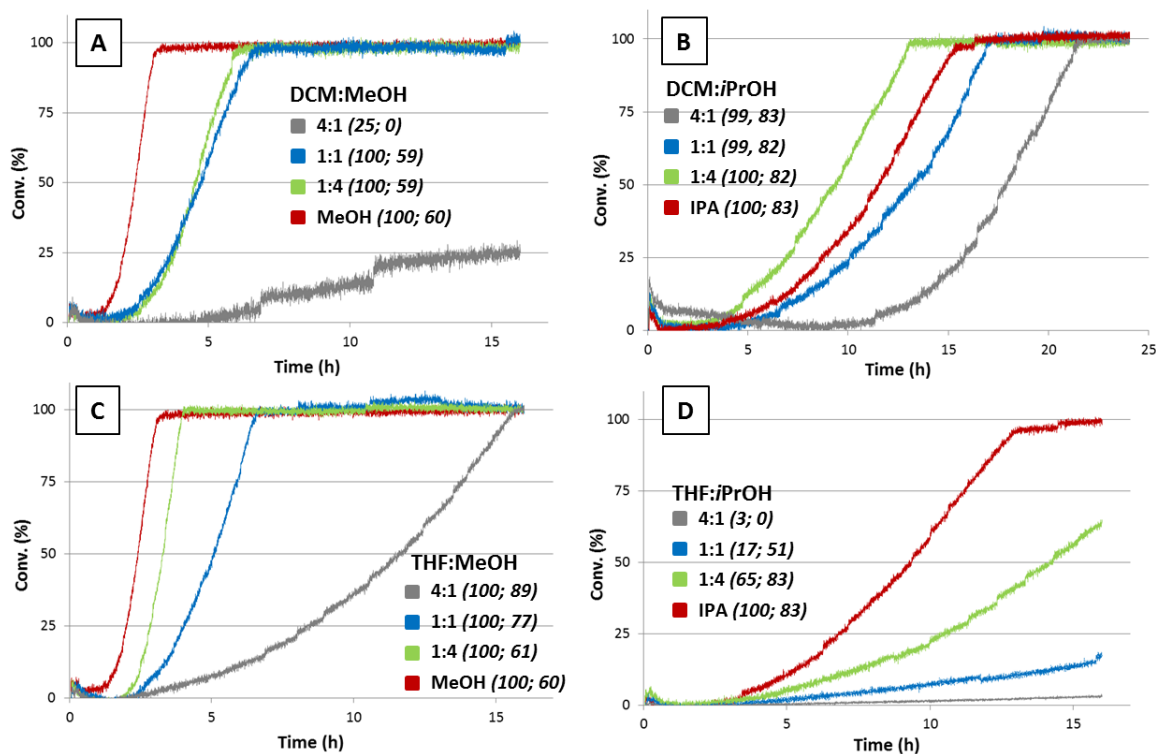


**Figure 5.** AH of **9** with **HG-II**/*(S)*-BINAP in different solvent mixtures. The kinetic profiles (conv. vs time) are derived from hydrogen consumption measurement (in parenthesis, the conversion and *ee* at the end of the reaction are reported). *Reaction conditions:* **9** (1 mmol), Ru-catalyst (1 mol %), *(S)*-BINAP (1.1 mol %), H<sub>2</sub> (25 bar), solvent (5 mL), rt. Conversion and *ee* determined by chiral GC.

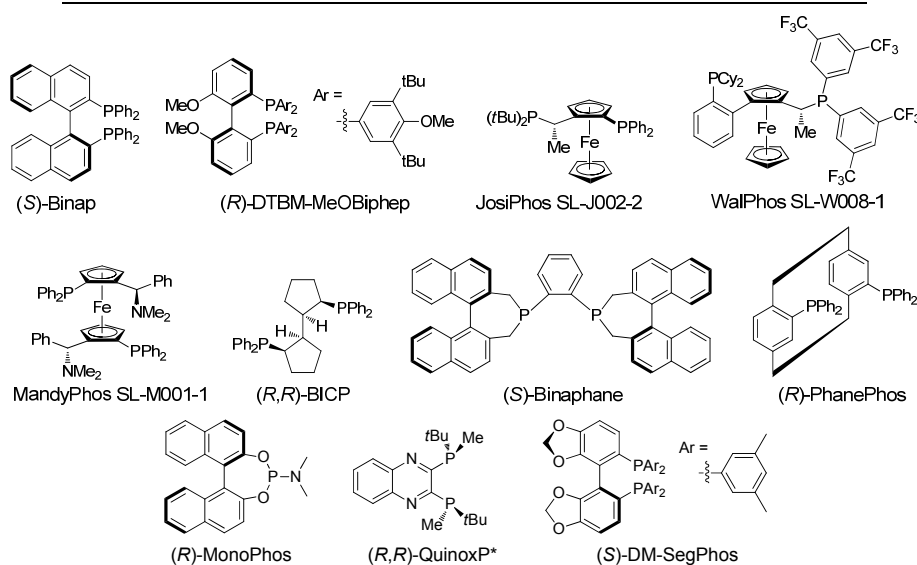
A detailed understanding of the molecular processes that take place in the different solvent combinations is difficult. The nature of the solvent influences the formation of the active hydrogenation species, its activity and its enantioselectivity. Although the effects governing the overall catalytic performance are difficult to deconvolute, several observations can be made. First, the induction periods observed are dependent on the rate of alcoholysis and/or hydrogenolysis towards active hydrogenation species. This transformation seems to occur more readily when using MeOH as alcoholic solvent than with *i*PrOH, indicating that the former is more efficient in the alcoholysis of **HG-II**. Second, for the slower reactions (generally the ones with a lesser amount of alcohol), the rate of hydrogenation increases with time, indicating that some

additional active species are being formed during the course of the reaction. In contrast, at higher ratios of alcohol, the reaction profiles resemble zero order kinetics, which suggests that **HG-II** undergoes a rapid and complete transformation to the active hydrogenation species before significant hydrogenation takes place. Third, the remarkable variation of the enantiomeric excess with different amounts of THF, compared to the little influence that DCM has on it, might be ascribed to the known ability of THF to bind ruthenium, thus modulating its performance.

A screening with a variety of monodentate and bidentate ligands showed that actually (*S*)-BINAP is the best performing in both solvent mixtures (Table 4). The ferrocene derivative MandyPhos SL-M001-1 also showed promising enantioselectivities.

**Table 4.** Ligand screening for the AH of **9** with **HG-II**.

#	Ligand	DCM/ <i>i</i> PrOH 1:4		THF/MeOH 4:1	
		Conv. (%)	<i>ee</i> (%)	Conv. (%)	<i>ee</i> (%)
1	( <i>S</i> )-BINAP	100	82	100	89
2	( <i>R</i> )-DTBM-MeOBiphep	40	60	28	21
3	Josiphos SL-J002-2	100	66	100	66
4	WalPhos SL-W008-1	21	8	27	9
5	MandyPhos SL-M001-1	100	72	100	81
6	( <i>R,R</i> )-BICP	11	0	11	0
7	( <i>S</i> )-Binaphane	15	5	27	0
8	( <i>S</i> )-PhanePhos	12	8	18	7
9	( <i>R</i> )-MonoPhos	4	58	2	22
10	( <i>R,R</i> )-QuinoxP*	45	0	70	0
11	( <i>R</i> )-DM-SegPhos	100	58	73	59



*Reaction conditions:* **9** (1 mmol), **HG-II** (1 mol %), ligand (1.1 mol % for bidentate, 2.2 mol% for monodentate), H<sub>2</sub> (50 bar), solvent (5 mL), 16 h, rt. Conversion and *ee* determined by chiral GC.

In an effort to determine the nature of the active hydrogenation catalyst, the alcoholysis of **HG-II** with (*S*)-BINAP in THF-*d*<sub>8</sub>:CD<sub>3</sub>OD (4:1) or CD<sub>2</sub>Cl<sub>2</sub>:*i*PrOH-*d*<sub>8</sub> (1:1) was followed by <sup>1</sup>H

NMR, but no changes were observed after 2 days stirring at room temperature. When the same mixture was submitted to 50 bar of H<sub>2</sub> at room temperature for 18 h, again no change was appreciable (Figure 6B). The latter experiments were repeated in presence of 2 equivalents of methyl 2-acetamidoacrylate **9** (Figure 6C). Product **10** was obtained with full conversion and different enantioselectivities (85% and 77% *ee* respectively) depending on the solvent mixture. Surprisingly, the only observed change by NMR was the quantitative disappearance of **9** and the appearance of **10**. All signals corresponding to **HG-II** and (*S*)-BINAP were still present in the same amount than at the beginning of the reaction. No signal of a possible coordination of (*S*)-BINAP with Ru was observed by <sup>31</sup>P NMR either.

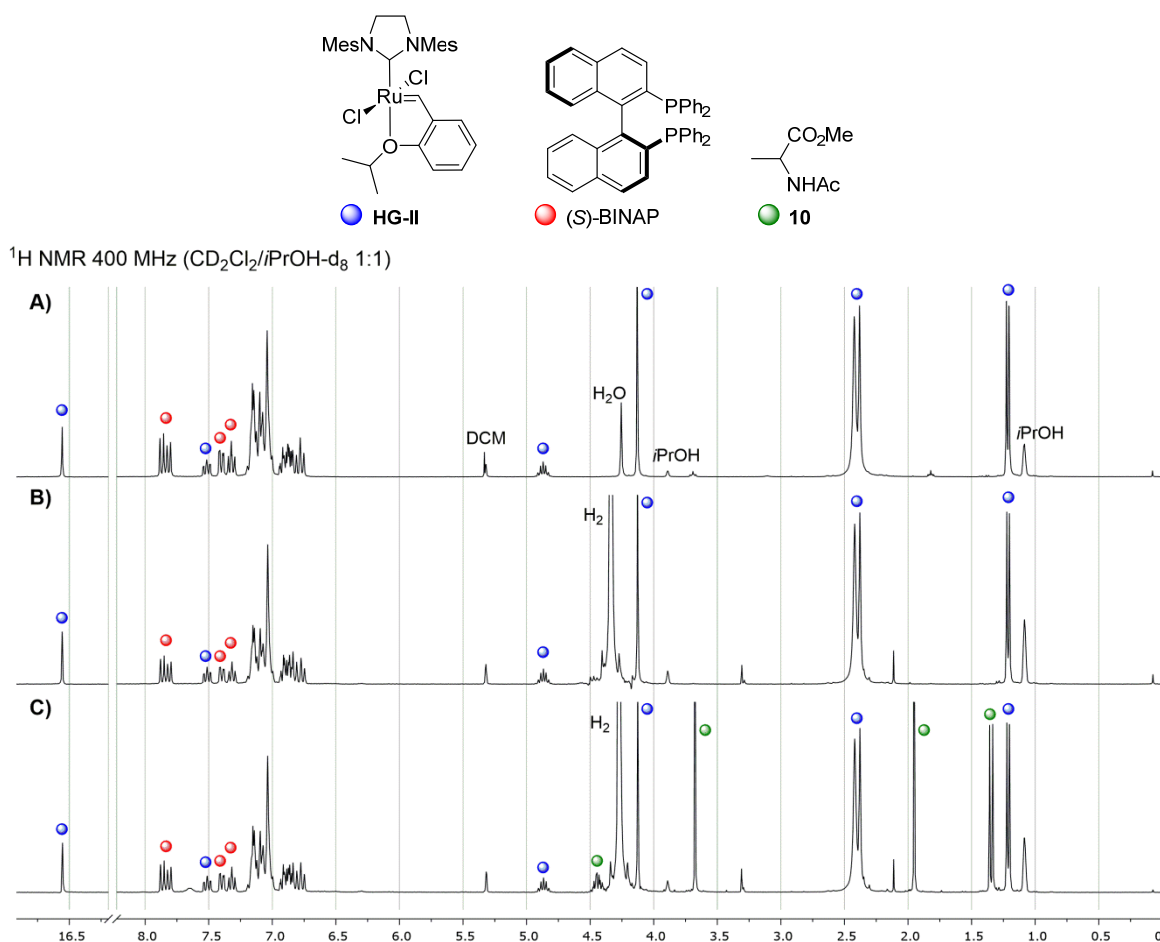


**Figure 6.** <sup>1</sup>H NMR in CD<sub>2</sub>Cl<sub>2</sub>/*i*PrOH-*d*<sub>8</sub> of: A) **HG-II** + (*S*)-BINAP; B) **HG-II** + (*S*)-BINAP stirred for 18 h at room temperature under 50 bar of H<sub>2</sub>; C) **HG-II** + (*S*)-BINAP + **9** stirred for 18 h at room temperature under 50 bar of H<sub>2</sub>

Although most mechanistic studies use a base for the activation of the catalyst – which in our case proved detrimental for the reaction – Fogg and co-workers reported that **G-I** could be converted into Ru-hydride species by hydrogenation of its benzylidene moiety in the absence of a base.<sup>22,23</sup> Hence, we decided to try the same experiments with another NHC-containing catalyst, in this case **G-II** (Figure 7). After stirring it in presence of one equivalent of (*S*)-BINAP under 50 bar of H<sub>2</sub> we could observe that the integral of the benzylidene proton ( $\delta = 19.44$  ppm) decreased *ca.* 35% compared to the NHC or PCy<sub>3</sub> protons. Moreover, a hydride peak appeared as a singlet



at  $\delta = -6.13$  ppm, which could be correlated with other small peaks that appeared in the aromatic region. The multiplicity of this peak indicates that no phosphorus is attached to the Ru center (also confirmed by  $^{31}\text{P}$  NMR), thus suggesting that, although these species might be involved in the overall process, they are not the enantioselective ones. The slow conversion to Ru-hydride species had been already reported by Fogg, when the hydrogenolysis of **G-II** in presence of  $\text{Et}_3\text{N}$  at 69 bar of  $\text{H}_2$  was not completed after 24 hours.<sup>29</sup> Thus, we could expect **HG-II** to be even less reactive, due to the chelation of the isopropoxy group attached to the benzylidene moiety.

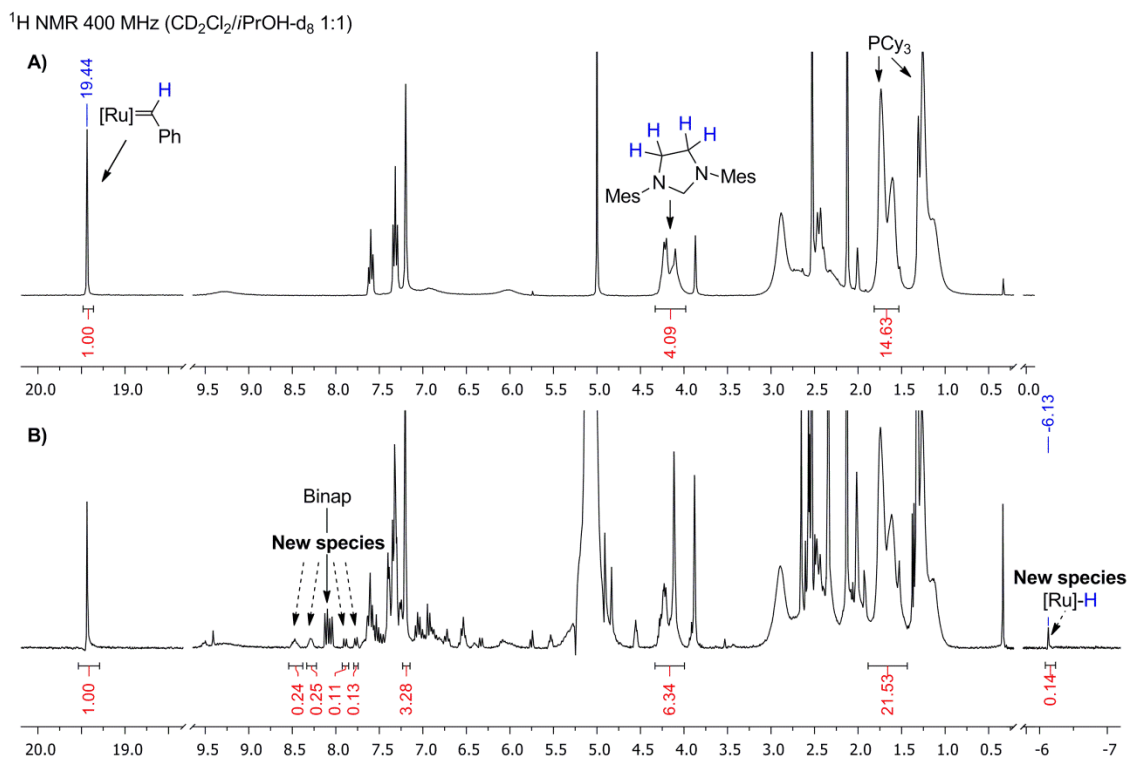


**Figure 7.**  $^1\text{H}$  NMR in  $\text{CD}_2\text{Cl}_2/i\text{PrOH-}d_8$  of: A) **G-II**; B) **G-II** + (S)-BINAP stirred for 18 h at room temperature under 50 bar of  $\text{H}_2$ .

The experiments performed with **HG-II** were also injected in the GC-MS, but no extra information could be obtained. Furthermore, ESI-MS analysis of the crude mixtures, before and after hydrogenation, showed several peaks corresponding to Ru species, but none of them could be identified as a Ru-BINAP complex.

Besides all these inconclusive experiments, the hydrogenation of **9** in the optimized conditions proceeds with up to 89% *ee*. Thus, only two explanations can be given for the lack of evidences in the mechanistic studies: (i) not observable traces of **HG-II** are hydrogenated to afford highly active Ru-BINAP hydride species or (ii) the hydrogenation proceeds via an unknown mechanism that does not involve the hydrogenation of the benzylidene moiety and where **HG-II** regenerates when the catalytic cycle is finished, as it is observed at the end of the reaction without any change.

Two other prochiral substrates, methyl 2-acetamidocinnamate (**11**) and dimethyl itaconate (**13**), were tested under the optimized conditions in the two solvent mixtures. Using **11** as substrate led to almost no conversion and no enantiomeric excess (Table 5, entries 1 and 2). Even trying to optimize the conditions on a ligand screening, no good results were achieved, being the best ligands those shown in Table 5, entries 3 and 4. Instead for substrate **13**, acceptable results were obtained in DCM/*i*PrOH but not in THF/MeOH (Table 6, entries 1 and 2). A Ru precursor and ligand screening allowed improving the results, achieving up to 86% *ee* with full conversion (Table 6, entry 3). Since we had observed that different combinations of Ru precursors and ligands can form more efficient catalysts, a large screening was also performed with **9**. Gratifyingly, it was found that the combination of **HG-I**, **G-I** or **G-III** with MandyPhos SL-M001-1 achieved enantioselectivities up to 93% *ee* (Table 7, entries 3-5). These results just demonstrated something that is well-known in the AH field, i.e. that every substrate requires its own optimization.

**Table 5.** Selected results from a large screening on the AH of **11**.

#	Ru cat.	Ligand	Solvent	Conv. (%)	<i>ee</i> (%)
1	<b>HG-II</b>	( <i>S</i> )-BINAP	DCM: <i>i</i> PrOH 1:4	7	0
2	<b>HG-II</b>	( <i>S</i> )-BINAP	THF/MeOH 4:1	3	0
3	<b>HG-II</b>	( <i>R</i> )-DM-SegPhos	THF/MeOH 4:1	31	62
4	<b>HG-II</b>	Josiphos SL-J002-2	DCM/ <i>i</i> PrOH 1:4	99	26

**Table 6.** Selected results from a large screening on the AH of **13**.

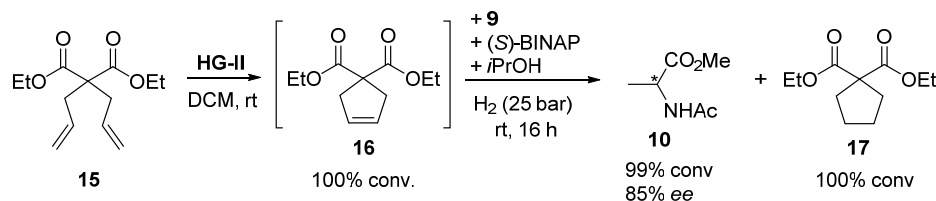
#	Ru cat.	Ligand	Solvent	Conv. (%)	<i>ee</i> (%)
1	<b>HG-II</b>	( <i>S</i> )-BINAP	DCM/ <i>i</i> PrOH 1:4	66	85
2	<b>HG-II</b>	( <i>S</i> )-BINAP	THF/MeOH 4:1	83	20
3	<b>HG-I</b>	( <i>R</i> )-DM-SegPhos	THF/ <i>i</i> PrOH 1:4	100	86
4	<b>G-II</b>	( <i>R</i> )-DM-SegPhos	THF/ <i>i</i> PrOH 1:4	100	70

**Table 7.** Selected results from a large screening on the AH of **9**.

#	Ru cat.	Ligand	Solvent	Conv. (%)	<i>ee</i> (%)
1	<b>HG-II</b>	( <i>S</i> )-BINAP	DCM/ <i>i</i> PrOH 1:4	100	82
2	<b>HG-II</b>	( <i>S</i> )-BINAP	THF/MeOH 4:1	100	89
3	<b>G-I</b>	MandyPhos SL-M001-1	THF/ <i>i</i> PrOH 1:4	100	92
4	<b>HG-I</b>	MandyPhos SL-M001-1	THF/ <i>i</i> PrOH 1:4	100	92
5	<b>G-III</b>	MandyPhos SL-M001-1	THF/ <i>i</i> PrOH 1:4	100	93

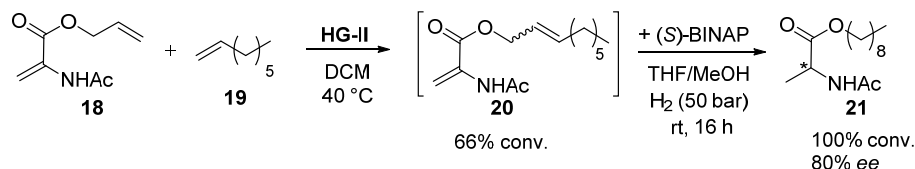
Having demonstrated that Ru olefin metathesis catalysts can be converted into efficient asymmetric hydrogenation catalysts, we decided to test whether the same transformation could be effectively performed after a metathesis step. As commented before, this might be challenging due to the different Ru species present in solution after a metathesis step, but also because the different Ru-carbene species, originating from the reaction with different alkenes, are known to greatly differ in the initiation rate of the metathesis reaction.<sup>33</sup>

To this purpose, diethyl diallylmalonate (**15**) was selected as metathesis substrate. After performing the ring-closing metathesis (RCM) of **15** with **HG-II** in DCM, we added the prochiral substrate **9**, (*S*)-BINAP and the alcohol to the reaction mixture and pressurized it to 25 bar of H<sub>2</sub> (Scheme 25). Gratifyingly, product **10** was formed with the same conversion and enantiomeric excess (99% conv. and 85% *ee*) that had been obtained without the previous metathesis step. Besides that, diethyl cyclopent-3-ene-1,1-dicarboxylate (**16**) was also fully hydrogenated to the corresponding saturated cyclopentane **17**.



**Scheme 25.** Proof of concept for the tandem metathesis–AH. *Reaction conditions:* metathesis: **15** (1 mmol), **HG-II** (1 mol%), DCM (1 mL), 15 min, rt; hydrogenation: **9** (1 mmol), (*S*)-BINAP (1.1 mol %), H<sub>2</sub> (25 bar), *i*PrOH (4 mL), 16 h, rt. Conversion and *ee* determined by chiral GC.

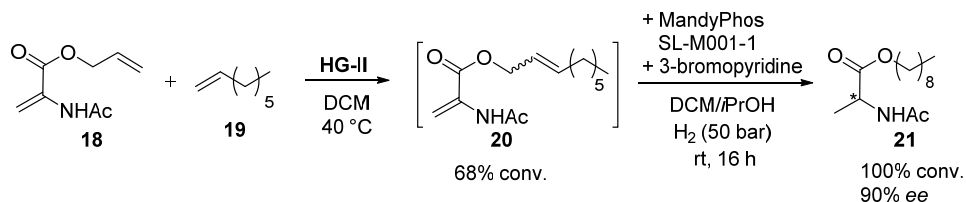
Since methyl 2-acetamidoacrylate (**9**) is not active in cross-metathesis with the known Ru catalysts, a modified version had to be synthesized to be able to carry out the metathesis reaction and the asymmetric hydrogenation on the same molecule. With this aim, allyl 2-acetamidoacrylate (**18**) was engineered by reaction of 2-acetamidoacrylic acid and allyl bromide. This substrate was submitted to cross-metathesis (CM) with an excess of 1-octene (**19**). Despite not having completely optimized the CM, the subsequent AH of **20** led quantitatively to the fully hydrogenated nonyl 2-acetamidoacrylate (**21**) with 80% *ee* (Scheme 26), thus demonstrating the concept. The non-metathesized **18** was also completely hydrogenated to propyl acetylalaninate (**22**) with 71% *ee*.



**Scheme 26.** Tandem metathesis–AH of **18**. *Reaction conditions:* metathesis: **18** (0.15 mmol), **19** (100 equivalents), **HG-II** (5 mol%), DCM (1.5 mL), 40 °C, 5.5 h; hydrogenation: (*S*)-BINAP (5.5 mol %), H<sub>2</sub> (50 bar), THF/MeOH 4:1 (2 mL), 16 h, rt. Conversion and *ee* determined by chiral GC.

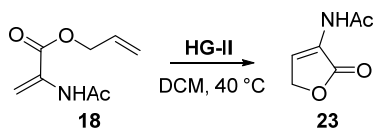
Considering that the highest enantioselectivities for the AH of **9** had been obtained with **G-III** and MandyPhos SL-M001-1 (Table 7, entry 5) we tried those conditions in the described

tandem reaction, but very low conversions were obtained in the cross-metathesis step. Thus, since the main difference between **G-III** and **HG-II** is the presence of 3-bromopyridine ligands in the former (Figure 2), we attempted the AH with **HG-II** and 3-bromopyridine derivative as additive. Indeed, after the CM with **HG-II** and subsequent AH with MandyPhos SL-M001-1 as ligand and 3-bromopyridine as additive, product **21** was obtained with an overall 68% conversion and 90% *ee* (Scheme 27).



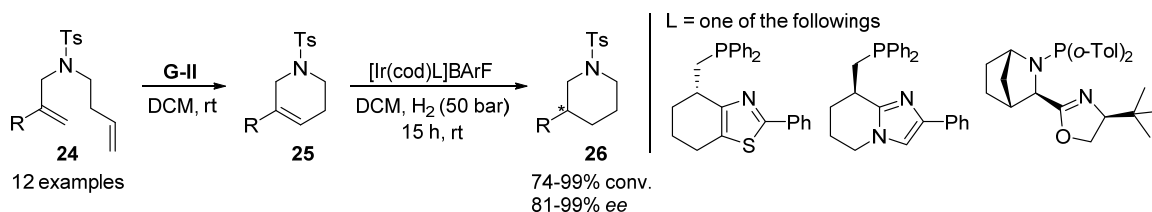
**Scheme 27.** Optimized tandem metathesis–AH of **18**. *Reaction conditions:* metathesis: **18** (0.05 mmol), **19** (100 equivalents), **HG-II** (5 mol%), DCM (1.5 mL), 40 °C, 5.5 h; hydrogenation: MandyPhos SL-M001-1 (5.5 mol %), 3-bromopyridine (30 mol%), H<sub>2</sub> (50 bar), DCM/*i*PrOH 1:4 (2 mL), 16 h, rt. Conversion and *ee* determined by chiral GC.

During the cross-metathesis of **18** a side product was always formed with *ca.* 18% conversion. After isolation and characterization by NMR it was identified as the RCM product **23**. Surprisingly, this compound was not hydrogenated in the following hydrogenation step.



**Scheme 28.** RCM product of **18**.

Finally, we decided to focus on an example where the prochiral olefin was the one formed by metathesis. To do so, we took inspiration on a recent publication by Andersson and co-workers.<sup>40</sup> There, the synthesis of 3-substituted piperidines **26** via RCM of **24**, isolation of the tetrahydropyridine intermediate **25** and AH of the formed alkene with an Ir chiral complex is reported (Scheme 29).



**Scheme 29.** Synthesis of 3-substituted piperidines by RCM and subsequent Ir-catalyzed enantioselective hydrogenation, reported by Andersson and co-workers.

Substrate **24a** (R = Me) was selected to apply our one-pot tandem protocol. Large screenings of different solvent mixtures, Ru olefin metathesis catalysts and ligands led to the final optimized conditions. As a matter of example, one of the screenings is shown in Figure 8. (*R*)-DTBM-MeOBiphep gave good conversions in almost all solvents but very poor enantioselectivities. The contrary was observed with MandyPhos SL-M001-1, which gave high

enantioselectivities but poor activities. Gratifyingly, the combination of **G-II** with (*S*)-PhanePhos in DCM/*i*PrOH 1:1 gave the best combination of conversion and enantioselectivity (87% conv. and 86% *ee*), demonstrating once more that each substrate requires a particular optimization.

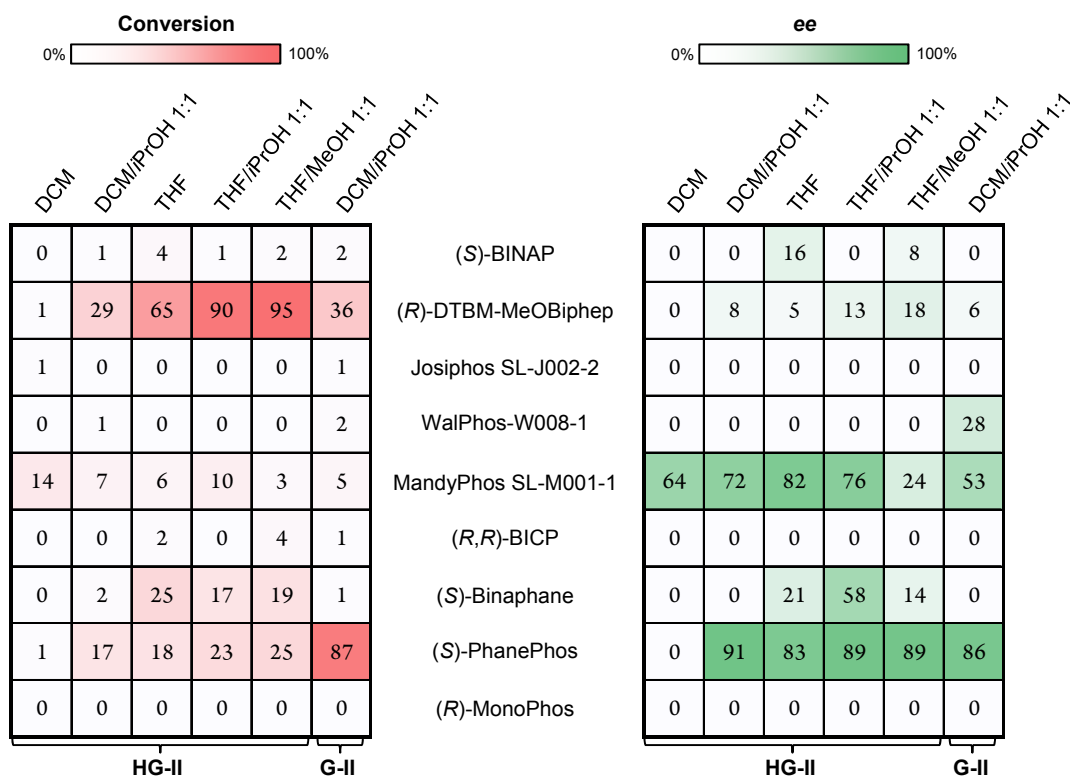
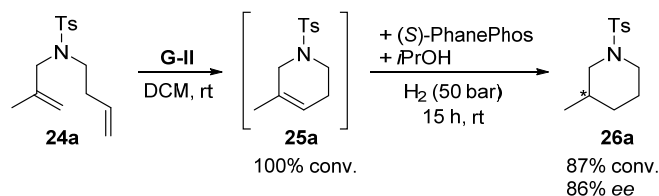


**Figure 8.** Screening of solvents, ligands and Ru catalysts for the AH of **25** to **26**.

Thus, the optimized AH protocol together with the RCM step, already optimized by Andersson and co-workers, led to *N*-tosyl-3-methylpiperidine (**26a**) in an overall 87% conversion and 86% *ee* from **24a** (Scheme 30).



**Scheme 30.** Tandem RCM–AH of **24a**. Reaction conditions: metathesis: **24a** (0.07 mmol), **G-II** (5 mol%), DCM (0.2 mL), 40 °C, 15 min; hydrogenation: (*S*)-PhanePhos (5.5 mol %), DCM (0.3 mL), *i*PrOH (0.5 mL), H<sub>2</sub> (50 bar), 16 h, rt. Conversion and *ee* determined by chiral GC.

### V.3 CONCLUSIONS

Our goal to demonstrate that the reactivity of a Ru olefin metathesis catalyst can be modulated under hydrogenation conditions by addition of a ligand has been reached: different Ru catalysts have been transformed into efficient AH catalysts, achieving *ee*'s up to 93% in the hydrogenation of methyl 2-acetamidoacrylate. Recent experiments also showed that, in some

cases, the enantioselectivity can be improved by reducing the H<sub>2</sub> pressure, leaving place for further improvements. Efforts have also been put in determining the active species responsible for the hydrogenation, but unfortunately no conclusive results could be obtained, leaving the door open for deeper investigations in this area.

The possibility to perform a tandem metathesis–AH has also been demonstrated for the first time. This allows an expensive metal like Ru to efficiently catalyze two consecutive reactions. Remarkably, high enantioselectivities were obtained from the mixture of Ru species present at the end of the metathesis reaction. In fact, practitioners in the field of AH usually take care of using very pure metal precursors, due to the high sensitivity of these reactions. However, this is not essential as long as the enantioselective species are much more active than the non-enantioselective ones. Considering the latest developments in the Ru-based metathesis to form tri- and tetrasubstituted prochiral olefins,<sup>41</sup> we hope that this methodology could be applied to a great number of substrates. Furthermore, we have demonstrated that this technology can be used for an alternative synthesis of 3-substitued piperidines, thus complementing the one presented in Chapter III, by tandem RCM–AH.

## V.4 EXPERIMENTAL SECTION

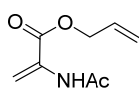
Dry DCM and THF were obtained from MBraun SPS system. Dry MeOH, *i*PrOH, DMF and acetonitrile (over molecular sieves in bottles with crown cap) were purchased from Sigma Aldrich and stored under nitrogen. Commercially available reagents (from TCI Chemicals, ACROS, Sigma Aldrich, Strem) were used as received, without any further purification. (*Z*)-methyl 2-acetamido-3-phenylacrylate (**11**) was synthesized according to the procedure described by Merlic *et al.*<sup>42</sup> *N*-(but-3-en-1-yl)-4-methyl-*N*-(2-methylallyl)benzenesulfonamide (**24a**) and 5-methyl-1-tosyl-1,2,3,6-tetrahydropyridine (**25a**) were synthesized according to the procedure described by Andersson *et al.*<sup>40</sup>

The reactions were monitored by analytical thin-layer chromatography (TLC) using silica gel 60 F254 pre-coated glass plates (0.25 mm thickness). Visualization was accomplished by irradiation with a UV lamp and/or staining with a potassium permanganate alkaline solution. Flash column chromatography was performed using Grace Reveleris® X2 Flash Chromatography System (silica gel cartridges with particle size 40 μm). Gas chromatography was performed on an Agilent Technologies 7890A and Hewlett Packard 6890 instruments, equipped with a flame ionization detector, using respectively a chiral and an achiral capillary column. Mass analysis was performed using a Hewlett Packard 6890 instrument coupled with a mass spectrometer.

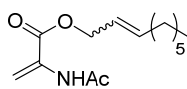
<sup>1</sup>H-NMR spectra were recorded on a spectrometer operating at 300 MHz. Proton chemical shifts are reported in ppm (δ) with the solvent reference relative to tetramethylsilane (TMS) employed as the internal standard (CDCl<sub>3</sub> δ = 7.26 ppm; CD<sub>2</sub>Cl<sub>2</sub> δ = 5.32 ppm, *i*PrOH-*d*<sub>8</sub> δ = 1.10, 3.89, 5.27[H<sub>2</sub>O] ppm). <sup>13</sup>C-NMR spectra were recorded on a 300 MHz spectrometer

operating at 75 MHz, with complete proton decoupling. Carbon chemical shifts are reported in ppm ( $\delta$ ) relative to TMS with the respective solvent resonance as the internal standard ( $\text{CDCl}_3$ ,  $\delta = 77.2$  ppm;  $\text{CD}_2\text{Cl}_2$   $\delta = 54.0$  ppm). The following abbreviations are used to describe spin multiplicity: s = singlet, d = doublet, t = triplet, q = quartet, m = multiplet, bs = broad signal, dd = doublet-doublet, td = triplet-doublet, ddd = doublet-doublet-doublet. Coupling constant values are given in Hz.

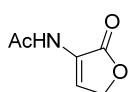
### Synthesis of new compounds



**Allyl 2-acetamidoacrylate (18):** Allyl bromide (2.6 mL, 30 mmol) was added to a solution of 2-acetamidoacrylic acid (2.6 g, 20 mmol) and  $\text{K}_2\text{CO}_3$  (3.3 g, 24 mmol) in 200 mL of DMF. The reaction mixture was stirred overnight at room temperature. After that, it was diluted with EtOAc (400 mL) and extracted with water (2 x 400 mL), 2 M HCl (1 x 400 mL) and brine (2 x 400 mL). The collected organic extracts were dried over anhydrous  $\text{MgSO}_4$  and concentrated under reduced pressure. After purification by column chromatography with heptane/EtOAc (95:5 to 85:15), allyl 2-acetamidoacrylate (3.2 g, 95 %) was obtained as a colorless oil.  $^1\text{H}$  NMR (300 MHz,  $\text{CDCl}_3$ )  $\delta$  7.73 (bs, 1H), 6.61 (s, 1H), 5.95 (m, 1H), 5.93 (s, 1H), 5.37 (ddd,  $^3J(\text{H,H}) = 17.1$  Hz,  $^2J(\text{H,H}) = 2.5$  Hz,  $^4J(\text{H,H}) = 1.2$  Hz, 1H), 5.30 (ddd,  $^3J(\text{H,H}) = 10.2$  Hz,  $^2J(\text{H,H}) = 2.5$  Hz,  $^4J(\text{H,H}) = 1.2$  Hz, 1H), 4.73 (dt,  $^3J(\text{H,H}) = 5.7$  Hz,  $^4J(\text{H,H}) = 1.2$  Hz, 2H), 2.13 (s, 3H);  $^{13}\text{C}$  NMR (75 MHz,  $\text{CDCl}_3$ )  $\delta$  168.9, 164.0, 131.4, 131.0, 119.2, 108.9, 66.8, 24.8; GC-MS: found molecular peak – 169 (expected 169).



**Non-2-en-1-yl 2-acetamidoacrylate (20):** In a nitrogen filled mBraun glovebox, to a solution of Hoveyda-Grubbs 2<sup>nd</sup> Generation catalyst (19 mg, 0.03 mmol, 5 mol%) in DCM (0.3 mL), a mixture of allyl 2-acetamidoacrylate (102 mg, 0.6 mmol) and 1-octene (60 mmol, 100 equiv.) in DCM (0.5 mL) was added. The vial was capped with a PTFE septum, pierced with a needle and stirred at 40°C for 5.5 hours. After purification by column chromatography with heptane/EtOAc (100:0 to 95:5), non-2-en-1-yl 2-acetamidoacrylate (99 mg, 0.39 mmol, 65% yield, 9:1 of *E/Z* ratio) was obtained.  $^1\text{H}$  NMR (300 MHz,  $\text{CD}_2\text{Cl}_2$ )  $\delta$  7.68 (bs, 1H), 6.43 (s, 1H), 5.76 (m, 1H), 5.75 (s, 1H), 5.52 (m, 1H), 4.69 (dd,  $^3J(\text{H,H}) = 6.8$  Hz,  $^4J(\text{H,H}) = 1.2$  Hz, 0.2H (*Z*)-isomer), 4.57 (dd,  $^3J(\text{H,H}) = 6.5$  Hz,  $^4J(\text{H,H}) = 1.1$  Hz, 1.8H (*E*)-isomer), 2.00 (s, 3H), 1.98 (m, 2H), 1.23 (m, 8H), 0.79 (t,  $J = 6.7$  Hz, 3H);  $^{13}\text{C}$  NMR for *E*-isomer (75 MHz,  $\text{CD}_2\text{Cl}_2$ )  $\delta$  169.2, 164.4, 138.1, 132.1, 123.5, 108.0, 67.4, 32.8, 32.2, 29.4, 29.3, 25.0, 23.2, 14.4;  $^{13}\text{C}$  NMR for *Z*-isomer (75 MHz,  $\text{CD}_2\text{Cl}_2$ )  $\delta$  169.2, 164.5, 137.0, 132.1, 123.0, 108.1, 62.4, 32.3, 30.0, 29.4, 28.2, 25.0, 23.2, 14.4; GC-MS: found molecular peak – 253 (expected 253).



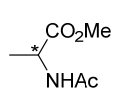
**N-(2-Oxo-2,5-dihydrofuran-3-yl)acetamide (23):** obtained as a by-product of the previously described cross-metathesis (18% yield).  $^1\text{H}$  NMR (300 MHz,  $\text{CD}_2\text{Cl}_2$ )  $\delta$  7.73 (bs, 1H), 7.40 (t,  $J = 2.1$  Hz, 1H), 4.80 (d,  $J = 2.1$  Hz, 2H), 2.07 (s, 3H);  $^{13}\text{C}$  NMR (75 MHz,  $\text{CD}_2\text{Cl}_2$ )  $\delta$  171.0, 169.6, 126.4, 126.2, 71.3, 24.2; GC-MS: found molecular peak – 141 (expected 141).

## General procedure for the asymmetric hydrogenation

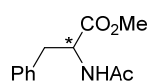
**Using Biotage® Endeavor™** - equipped with eight parallel autoclaves and allowing monitoring hydrogen consumption in real time. The substrate (1 mmol), metal complex (1 mol%) and ligand (1.1 mol%) were weighed in glass vials and placed in the reactor under a flow of N<sub>2</sub>. THF or DCM were added, followed by the selected alcohol (*i*PrOH or MeOH), to a total volume of 5 mL. The system was purged five times with 3 bar of N<sub>2</sub> and five times with 10 bar of H<sub>2</sub>. The reactions were stirred for 16 hours under 25 bar of H<sub>2</sub> at room temperature and then analyzed by GC for conversion and *ee* determination. This procedure was used for all the hydrogenations of 2-acetamido-acrylic acid methyl ester (**9**), methyl 2-acetamidocinnamate (**11**) and dimethyl itaconate (**13**).

**Using Premex 96er Multireaktor®** - autoclave allowing performing up to 96 reactions in parallel. In a N<sub>2</sub> filled mBraun glovebox, the ligand in solution (0.825 μmol in 200 μL of DCM, 1.1 mol%) were dispensed into 5 mL vials using Zinsser LISSY® Automated Liquid Handling Platform. The solvent was left for evaporation during 4h. A solution of the substrate (75 μmol in 100 μL in DCM or THF) and the metal complex (0.75 μmol in 150 μL in DCM or THF, 1 mol%) were added. The the selected alcohol was added to the vials in the selected amount. After capping with a PTFE septum, the vials were removed from the glovebox and placed in the Premex A96 Multireaktor®. The system was purged three times with 10 bar of N<sub>2</sub> and three times with 10 bar of H<sub>2</sub>. The reactions were stirred overnight under 50 bar of H<sub>2</sub> at room temperature. The reactions mixtures were analyzed by GC for conversion and *ee* determination. This procedure was used for large screenings.

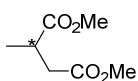
**Preparation of the racemates.** The substrate (0.15 mmol) in DCM (1 mL) was added to a vial with palladium on carbon (0.015 mmol) and placed into Premex 96er Multireaktor®. The system was purged five times with 10 bar of N<sub>2</sub> and five times with 10 bar of H<sub>2</sub>. The reactions were stirred for 16 hours under 50 bar of H<sub>2</sub> at room temperature. After filtration through a short pad of Celite®, the samples were analyzed by GC.



**Methyl acetylalaninate (10):**<sup>43</sup> Conversion and enantiomeric excess determined by GC: CP-Chirasil-Dex CB (25m x 0.25mm, 0.25μm); carrier: helium; gas flow: 2.7 bar; oven temperature: 115 °C for 7 min.; *t*<sub>9</sub> = 2.8 min.; *t*<sub>e1</sub> = 3.3 min.; *t*<sub>e2</sub> = 3.4 min.



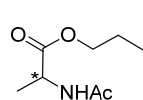
**Methyl 2-acetamido-3-phenylpropanoate (12):**<sup>44</sup> Conversion and enantiomeric excess determined by GC: CP-Chirasil-Dex CB (25m x 0.25mm, 0.25μm); carrier: helium; gas flow: 2.7 bar; oven temperature: 150 °C for 14 min., 15 °C/min. to 190 °C; *t*<sub>e1</sub> = 13.0 min.; *t*<sub>e2</sub> = 13.4 min.; *t*<sub>11</sub> = 18.2 min.



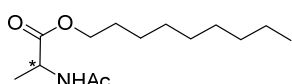
**Dimethyl 2-methylsuccinate (14):**<sup>45</sup> Conversion and enantiomeric excess determined by GC: Astec® Chiraldex® G-TA (30m x 0.25mm, 0.12 μm); carrier: helium; gas flow: 1.0 bar; oven temperature: 85 °C for 22 min., 10 °C/min. to 165



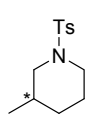
°C:  $t_{e1} = 20.4$  min.;  $t_{e2} = 21.1$  min.;  $t_{13} = 25.4$  min.



**Propyl acetylalaninate (22):**  $^1\text{H}$  NMR (300 MHz,  $\text{CDCl}_3$ )  $\delta$  6.11 (bs, 1H), 4.58 (m, 1H), 4.10 (t,  $^3J(\text{H,H}) = 6.5$  Hz, 2H), 2.01 (s, 3H), 1.67 (m, 2H), 1.40 (d,  $^3J(\text{H,H}) = 7.1$  Hz, 3H), 0.94 (t,  $^3J(\text{H,H}) = 7.4$  Hz, 3H);  $^{13}\text{C}$  NMR (75 MHz,  $\text{CDCl}_3$ )  $\delta$  173.7, 169.9, 67.4, 48.5, 23.6, 22.3, 19.1, 10.7; GC-MS: found molecular peak – 173 (expected 173). Conversion and enantiomeric excess determined by GC: CP-Chirasil-Dex CB (25m x 0.25mm, 0.25 $\mu\text{m}$ ); carrier: helium; gas flow: 2.7 bar; oven temperature: 120 °C for 10 min.:  $t_{18} = 6.0$  min.,  $t_{e1} = 6.6$  min.,  $t_{e2} = 6.8$  min.

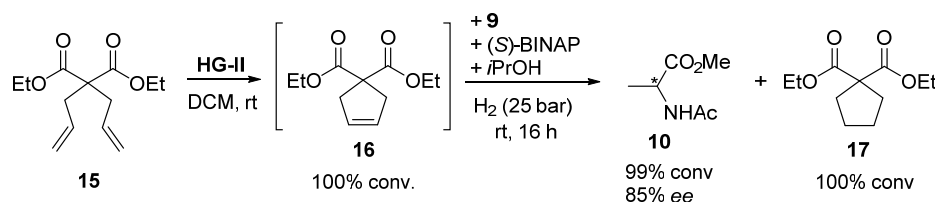


**Nonyl 2-acetamidopropanoate (21):**  $^1\text{H}$  NMR (300 MHz,  $\text{CDCl}_3$ )  $\delta$  6.15 (bs, 1H), 4.56 (m, 1H), 4.10 (m, 2H), 2.01 (s, 3H), 1.63 (m, 2H), 1.39 (d,  $^3J(\text{H,H}) = 7.2$  Hz, 3H), 1.36 – 1.21 (m, 12H), 0.87 (t,  $^3J(\text{H,H}) = 6.7$  Hz, 3H);  $^{13}\text{C}$  NMR (75 MHz,  $\text{CDCl}_3$ )  $\delta$  173.4, 169.8, 77.2, 65.8, 48.3, 32.0, 29.6, 29.3, 29.3, 28.6, 25.9, 23.3, 22.8, 18.8, 14.2; GC-MS: found molecular peak – 257 (expected 257). Conversion and enantiomeric excess determined by GC: CP-Chirasil-Dex CB (25m x 0.25mm, 0.25 $\mu\text{m}$ ); carrier: helium; gas flow: 2.7 bar; oven temperature: 140 °C for 50 min., 20 °C/min to 190 °C:  $t_{(Z)-20} = 46.6$  min.;  $t_{e1} = 48.1$  min.;  $t_{e2} = 49.1$  min.;  $t_{(E)-20} = 51.1$  min.



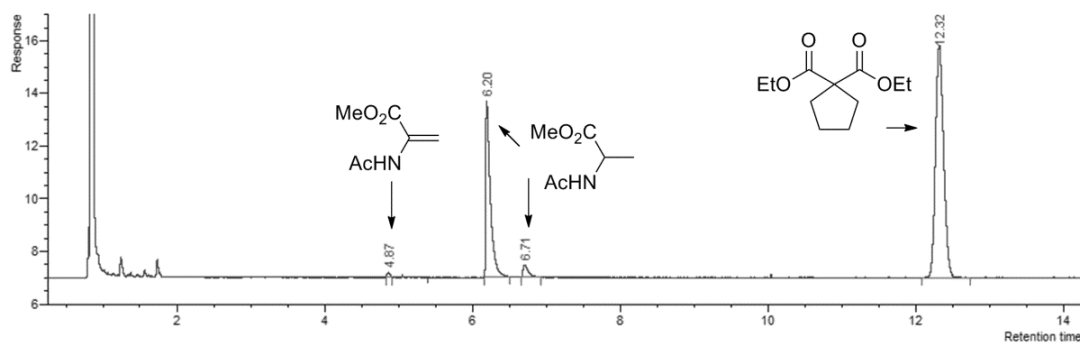
**3-methyl-1-tosylpiperidine (26a):**<sup>40</sup> Conversion and enantiomeric excess determined by GC: CP-Chirasil-Dex CB (25m x 0.25mm, 0.25 $\mu\text{m}$ ); carrier: helium; gas flow: 2.7 bar; oven temperature: 160 °C for 30.5 min, gradient 20 °C/min, 180 °C for 3 min.:  $t_{e1} = 29.3$  min.;  $t_{e2} = 30.0$  min.;  $t_{2sa} = 32.8$  min.

### Procedure for the proof of concept of the tandem metathesis–AH

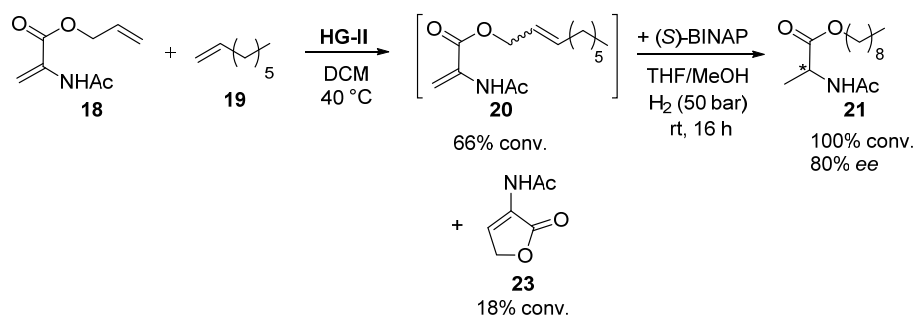


In a  $\text{N}_2$  filled mBraun glovebox, a solution of **HG-II** (6.27 mg, 0.01 mmol) in DCM (1 mL) was added to diethyl diallylmalonate (1 mmol, 240 mg). The reaction mixture was stirred in an open glass vial for 15 min. Analysis by GC confirmed that the RCM of the substrate was complete. The vial was placed in the Biotage® Endeavor™ under flow of  $\text{N}_2$ . **9** (143 mg, 1 mmol), (S)-BINAP (6.9 mg, 0.011 mmol) and *i*PrOH (4 mL) were added. The system was purged five times with 3 bar of  $\text{N}_2$  and five times with 10 bar of  $\text{H}_2$ . The reactions mixture was stirred for 16 h under 25 bar of  $\text{H}_2$  at room temperature.

Conversion and enantiomeric excess determined by GC: CP-Chirasil-Dex CB (25m x 0.25mm, 0.25 $\mu\text{m}$ ); carrier: helium; gas flow: 2.7 bar; oven temperature: 105 °C for 10 min., 5 °C/min. to 125 °C:  $t_9 = 4.9$  min.;  $t_{10} = 6.2$  and 6.7 min.;  $t_{17} = 12.3$  min.



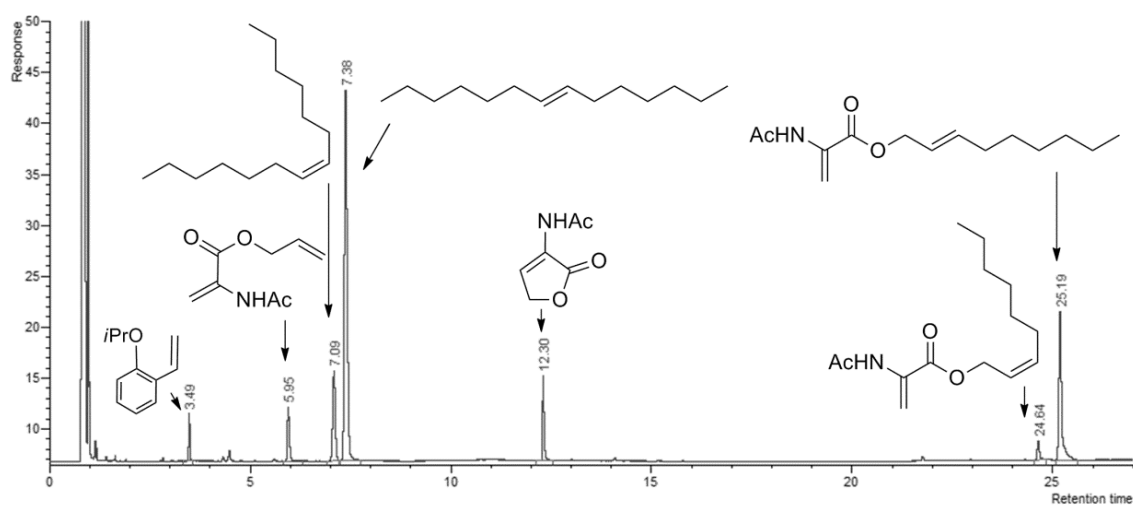
### Procedure for tandem metathesis–AH of **18**



#### Step I: Cross-metathesis

In a  $N_2$  filled mBraun glovebox, in a 5 mL vial, **HG-II** (0.0075 mmol, 5 mol%) was dissolved in DCM (1.0 mL). A mixture of **18** (0.15 mmol) and 1-octene **19** (15 mmol, 100 eq) in DCM (0.5 mL) was added. The vial was capped with a PTFE septum, pierced with a needle and stirred at 40 °C for 5.5 hours (until full solvent evaporation).

Conversion determined by GC: CP-Chirasil-Dex CB (25m x 0.25mm, 0.25 $\mu$ m); carrier: helium; gas flow: 2.7 bar; oven temperature: 120 °C for 10 min., 30 °C/min., 150 °C for 10 min., 30 °C/min, 180 °C for 5 min:  $t_{18}$  = 6.0 min.;  $t_{(Z)\text{-tetradec-7-ene}}$  = 7.1 min.;  $t_{(E)\text{-tetradec-7-ene}}$  = 7.4 min.;  $t_{23}$  = 12.3 min.;  $t_{(Z)\text{-20}}$  = 24.7 min.,  $t_{(E)\text{-20}}$  = 25.2 min.

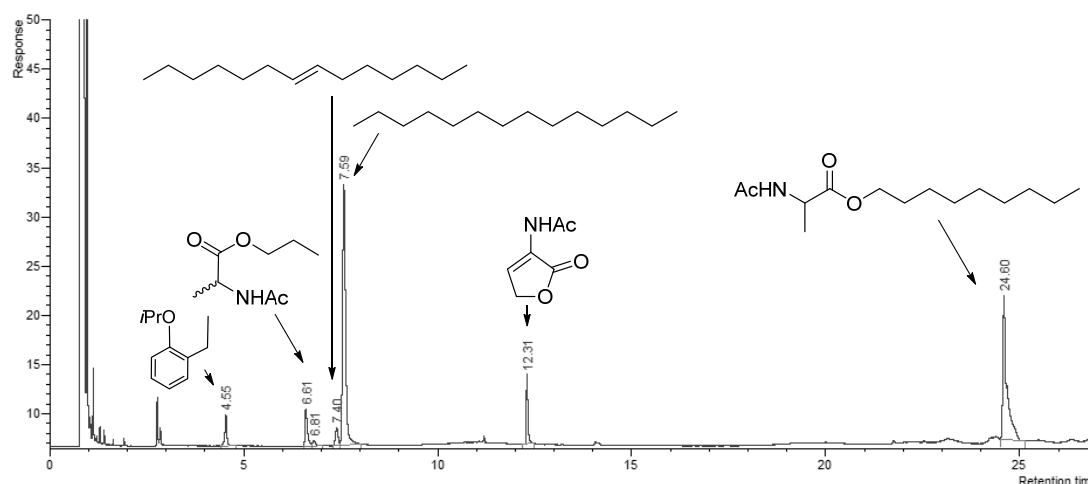
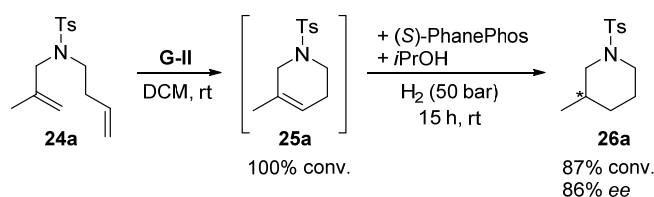


*Step II: Asymmetric hydrogenation*

To the vial from step I, a solution of (*S*)-BINAP (0.083 mmol, 5.5 mol%) in THF (1.6 mL) was added followed by MeOH (0.4 mL). After recapping with a PTFE septum, the vial was removed from the glovebox and placed in the Premex 96er Multireaktor<sup>®</sup>. The system was purged three times with 10 bar of N<sub>2</sub> and three times with 10 bar of H<sub>2</sub>. The reactions were stirred overnight under 50 bar of H<sub>2</sub> at room temperature.

Conversion and enantiomeric excess determined by GC: CP-Chirasil-Dex CB (25m x 0.25mm, 0.25μm); carrier: helium; gas flow: 2.7 bar; oven temperature: 120 °C for 10 min., 30 °C/min., 150 °C for 10 min, 30 °C/min, 180 °C for 5 min:  $t_{22} = 6.6$  and  $6.8$  min.;  $t_{(E)\text{-tetradec-7-ene}} = 7.4$  min.;  $t_{\text{tetradecane}} = 7.6$  min.;  $t_{23} = 12.3$  min.;  $t_{21} = 24.6$  min. (no separation of the enantiomers)

Enantiomeric excess of **21**: CP-Chirasil-Dex CB (25m x 0.25mm, 0.25μm); carrier: helium; gas flow: 2.7 bar; oven temperature: 140 °C for 50 min., 20 °C/min to 190 °C:  $t_{21} = 48.1$  and  $49.1$  min.

**High-throughput screening for the tandem metathesis–AH of **24a*****Step I: RCM*

In a N<sub>2</sub> filled mBraun glovebox, to a 20 mL vial with **24a** (2.87 mmol) a solution of Grubbs catalyst (0.144 mmol - 5 mol %) in 6.5 mL of solvent (DCM or THF) was added. The vial was capped with a PTFE septum, pierced with a needle and stirred for 15 min at 26 °C. A sample was analyzed by GC, confirming that the reaction was complete:

Conversion determined by GC: Agilent J&W HP-1 (30m x 0.32mm, 0.25 $\mu$ m); carrier: helium; gas flow: 2.7 bar; oven temperature: 150°C, 10 °C/min. to 250°C:  $t_{24a}$  = 6.9 min.;  $t_{25a}$  = 7.4 min.

*Step II: Asymmetric hydrogenation*

Using Zinsser LISSY® Automated Liquid Handling Platform, the solution of **25a** with the Ru catalyst (170  $\mu$ L containing 0.07 mmol of **25a** and 0.0035 mmol of Ru) was dispensed to 5 mL vials containing a chiral ligand solution (330  $\mu$ L, 0.0039 mmol, 5.5 mol %). Alcohols (0.5 mL of methanol or propan-2-ol) were added. After capping with a PTFE septum, the vials were removed from the glovebox and placed in the Premex 96er Multireaktor®. The system was purged three times with 10 bar of N<sub>2</sub> and three times with 10 bar of H<sub>2</sub>. The reactions were stirred overnight under 50 bar of H<sub>2</sub> at room temperature.

Conversion and enantiomeric excess determined by GC: CP-Chirasil-Dex CB (25m x 0.25mm, 0.25 $\mu$ m); carrier: helium; gas flow: 2.7 bar; oven temperature: 160 °C for 30.5 min, gradient 20 °C/min, 180 °C for 3 min.:  $t_{24a}$  = 29.3 and 30.0 min.;  $t_{25a}$  = 32.8 min.

# CHAPTER VI.

## TANDEM OLEFIN METATHESIS – ASYMMETRIC TRANSFER HYDROGENATION

---

### VI.1 INTRODUCTION

Having demonstrated that Ru olefin metathesis catalyst can be converted into efficient asymmetric hydrogenation catalyst by addition of a chiral ligand (Chapter V), we decided to expand this concept to transfer hydrogenation reactions.

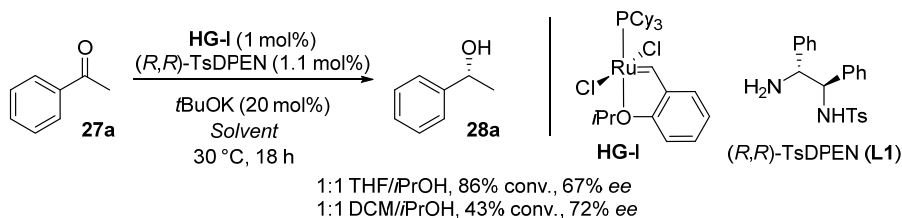
Transfer hydrogenation refers to reactions where the hydrogen added to a molecule originates from a non-H<sub>2</sub> source. This methodology is a good alternative to direct hydrogenation for a series of reasons: (i) it does not require the use of hazardous pressurized H<sub>2</sub> and specific experimental setups; (ii) the hydrogen donors are readily available, inexpensive and easy to handle; (iii) the dehydrogenated compound can be recycled.<sup>46</sup>

As discussed in Chapter IV, Grubbs and co-workers already demonstrated the possibility of a tandem metathesis–transfer hydrogenation of carbonyl groups,<sup>7</sup> but later publications have been mainly focused in the transfer hydrogenation of C=C bonds.<sup>17-21</sup> In our case, we decided to focus on the enantioselective reduction of prochiral ketones. A tandem protocol of this kind would allow for an olefin metathesis followed by the asymmetric transfer hydrogenation (ATH) of a carbonyl group present in the molecule, employing only one Ru source.

### VI.2 RESULTS AND DISCUSSION

Initially we explored the viability of converting a Ru olefin metathesis catalyst into an ATH catalyst. To do so, we took inspiration from the seminal work of Noyori and co-workers in the ATH of ketones with Ru catalysts.<sup>47</sup> We selected acetophenone (**27a**) as model substrate, **HG-I** as Ru precursor, (*R,R*)-TsDPEN (**L1**) as chiral ligand, *t*BuOK as base to activate the catalyst and *i*PrOH as the hydrogen donor. Since the final goal was to apply this methodology after a metathesis step, two co-solvents suitable for this reaction were chosen, THF and DCM. Gratifyingly, the initial tests already achieved good conversions and moderate enantioselectivities. Similar enantiomeric excesses were obtained, 67% and 72% respectively,

suggesting that the same active species are present in solution, but higher activities were observed in THF (Scheme 31). When the same experiment was performed with **HG-II**, only poor activities (less than 15% conversion) and low enantioselectivities (less than 9% *ee*) were obtained.



**Scheme 31.** Initial tests on the ATH of acetophenone (**27a**) with **HG-I**.

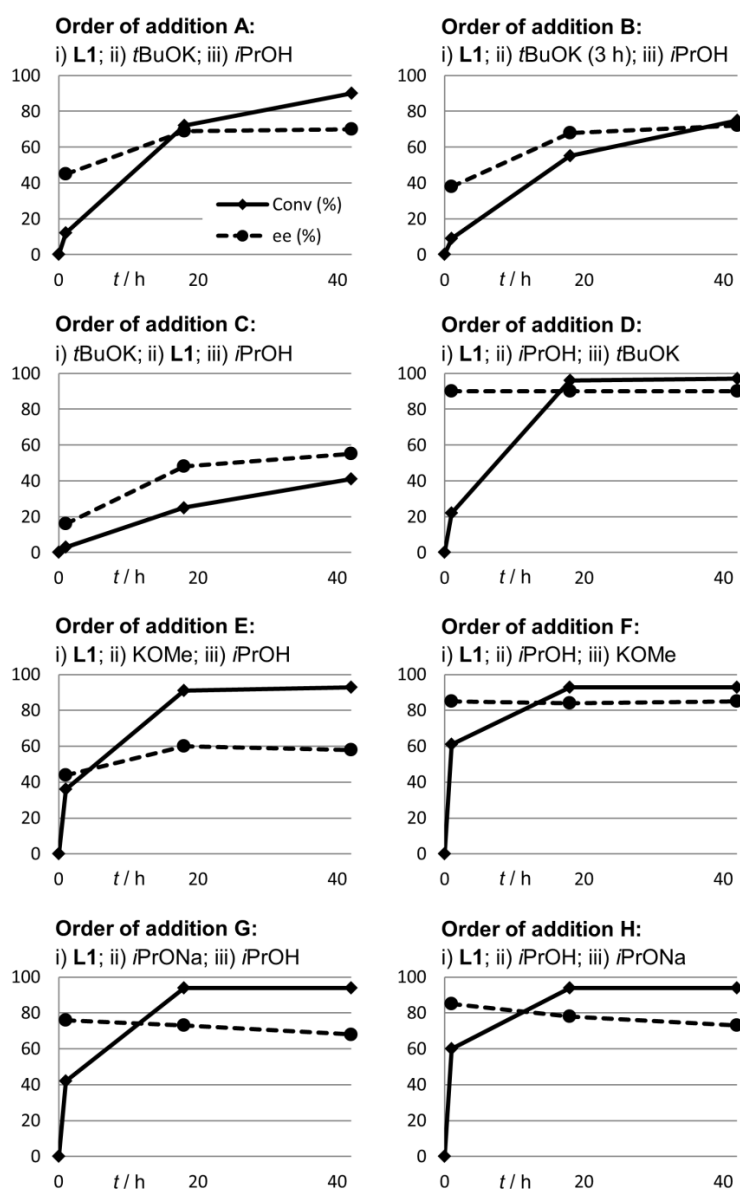


**Figure 9.** Conversion and *ee* vs time for the ATH of **27a**. **27a** and **HG-I** were mixed in THF and the other components were subsequently added in the order shown on top of each graph (stirring 5 min between each addition unless otherwise stated). Reaction conditions: **27a** (0.1 mmol), **HG-I** (1 mol%), THF (1 mL), **L1** (1.1 mol%), base (20 mol%), *i*PrOH (1 mL), 30 °C, 18 h. Conversion and *ee* determined by chiral GC.

When the reaction was monitored over time, we found out that the enantiomeric excess was increasing during the first 18 h (Figure 9A, order of addition used in the initial tests). This observation led us to think that probably a more enantioselective species than the initial one(s) was being formed during the course of the reaction. Thus, we first tried to stir the catalyst for longer in presence of the base before the addition of *i*PrOH (Figure 9B), but this was only detrimental for the activity. Furthermore, when adding the base before the ligand, both the activity and the enantioselectivity were negatively affected (Figure 9C). From these experiments we concluded that addition of *i*PrOH was the responsible of the formation of highly enantioselective species, most probably by reaction with *tert*-butoxide to give isopropoxide. Hence, when *t*BuOK was added the latest (Figure 9D), 1-phenylethanol (**28a**) was obtained with 96% conversion and 90% *ee* and, importantly, the enantiomeric excess remained constant during all the reaction course. Surprisingly, no erosion of the *ee* was observed even after 40 h of reaction, in contrast to what is observed with these types of reactions as a result of the reversibility of this transformation.<sup>47a,48</sup> When KOMe was employed instead of *t*BuOK, the same behavior was observed regarding the order of addition of base and *i*PrOH (Figure 9E and F). In contrast, when *i*PrONa was employed, a high *ee* was observed from the beginning of the reaction independently of the order of addition (Figure 9G and H). Remarkably, the latter reactions showed a slow erosion of the *ee* with time, possibly due to a cation effect (Na *vs* K) already reported in previous studies.<sup>49</sup> All these experiments together point towards a Ru-isopropoxide species as the responsible for the high enantiomeric excesses obtained or as the intermediate towards it. Actually, the remarkably stable 14-electron species  $[(PCy_3)(tBuO)_2Ru=CHPh]$  has been isolated and characterized by Grubbs and co-workers by reaction of **G-I** with an excess of *t*BuOK.<sup>31</sup> An analogue of this compound is what we might be forming when we add the *t*BuOK before the *i*PrOH.

To try to get further insight into the active species responsible for the obtained enantioselectivity we undertook some NMR and GC-MS studies under the optimized reaction conditions (Figure 9D). **HG-I** and TsDPEN were dissolved in THF-*d*<sub>8</sub>:*i*PrOH-*d*<sub>8</sub> (1:1), and NMR spectra were recorded before adding the *t*BuOK and after stirring the mixture with the base for 5 h. In the <sup>31</sup>P NMR (Figure 10), the singlet at  $\delta = 56.1$  ppm, corresponding to the Ru(PCy<sub>3</sub>), disappeared after addition of the base. Besides, some new species formed: two singlets at  $\delta = 47.3$  and 6.2 ppm corresponding to O=PCy<sub>3</sub> and free PCy<sub>3</sub>, respectively, and more interesting, two 1:1:1 triplets at  $\delta = 56.8$  and 56.2 ppm, in a ratio 3:1. These triplets correspond to RuD(PCy<sub>3</sub>) species, both with a <sup>2</sup>J<sub>P,D</sub> = 7.7 Hz. Consistently with the latter signals, the <sup>1</sup>H NMR (Figure 11) showed two doublets at  $\delta = -7.4$  and  $-7.5$  ppm (with a <sup>2</sup>J<sub>H,P</sub> = 52 Hz) in a ratio 3:1, corresponding to the same species but with hydrogen instead of deuterium, RuH(PCy<sub>3</sub>). In this case the intensity is very low, since these species are formed with the residual undeuterated *i*PrOH. Knowing that <sup>2</sup>J<sub>H,P</sub> coupling constants follow a Karplus-like equation,<sup>50</sup> the value of 52 Hz suggests a disposition of the hydride in between *cis* (10-25 Hz) and *trans* (>100 Hz) with respect to the phosphine. Two more singlets, corresponding to RuH species without any phosphine coordinated, are also observed at  $\delta = -5.0$  and  $-6.2$  ppm. It is remarkable the high *ee* obtained with

this system if we consider the mixture of hydride species observed by NMR. This suggests that one enantioselective Ru species bearing the TsDPEN ligand is much more active than the other species present in solution.

$^{31}\text{P}$  NMR 202.5 MHz (THF- $d_8$ )  
before addition of *t*BuOK

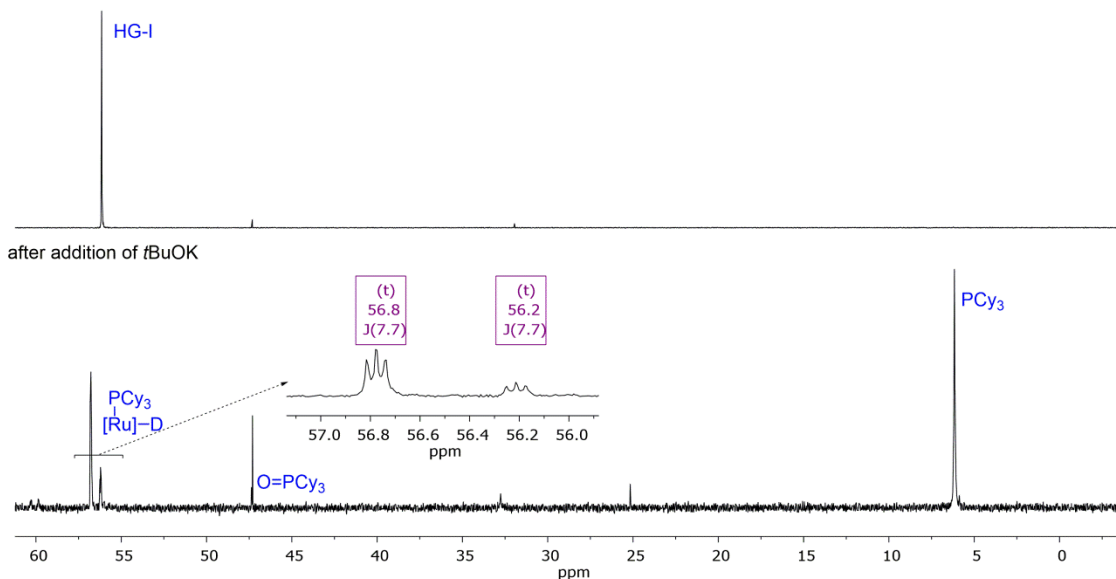


**Figure 10.** Comparison of the  $^{31}\text{P}$  NMR before and after the addition of *t*BuOK (15 equiv.) to a solution of **HG-I** (5 mg) and TsDPEN (1.1 equiv.) in THF- $d_8$ :*i*PrOH- $d_8$  (1:1, 1 mL).

$^1\text{H}$  NMR 500 MHz (THF- $d_8$ )  
before addition of *t*BuOK

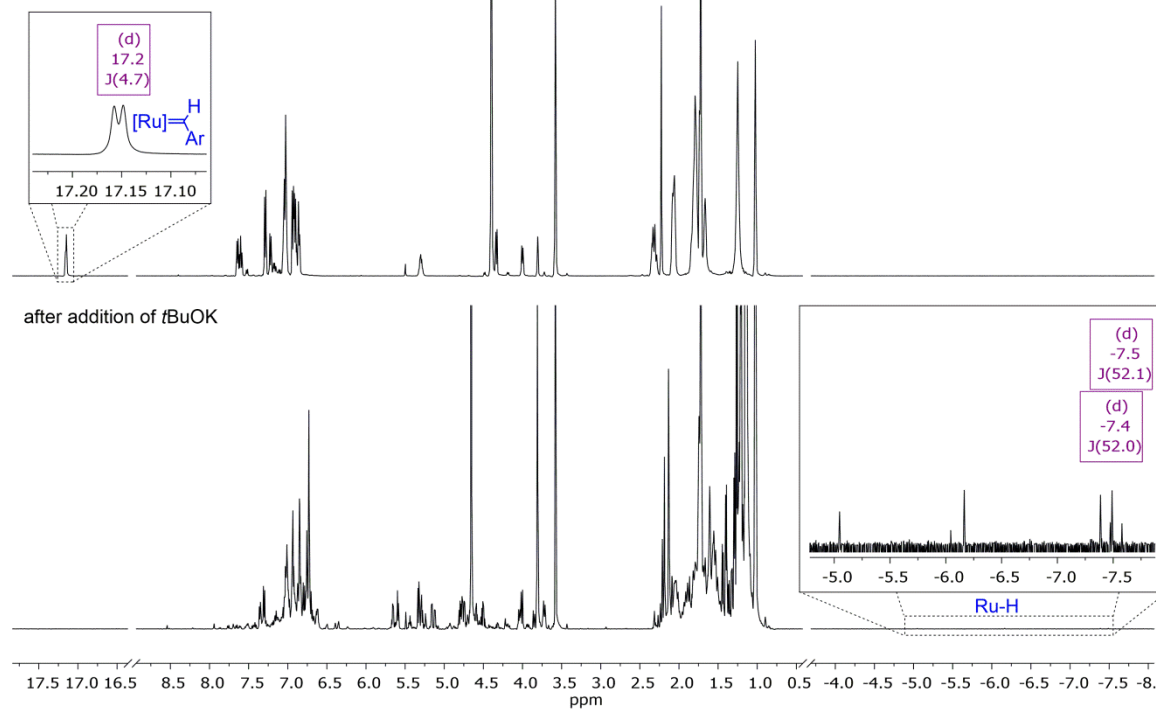
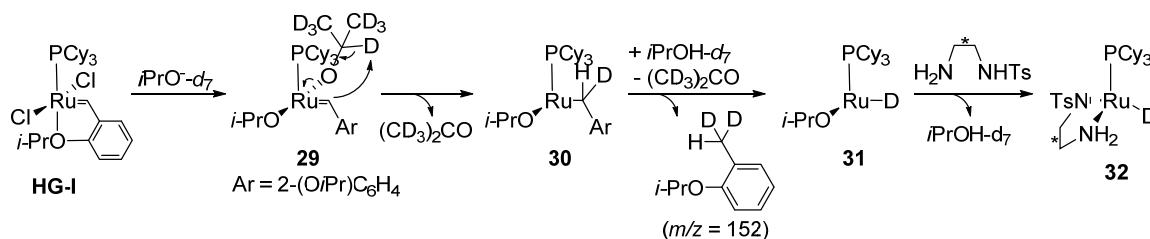


**Figure 11.** Comparison of the  $^1\text{H}$  NMR before and after the addition of *t*BuOK (15 equiv.) to a solution of **HG-I** (5 mg) and TsDPEN (1.1 equiv.) in THF- $d_8$ :*i*PrOH- $d_8$  (1:1, 1 mL).



Furthermore, the benzylidene proton at  $\delta = 17.2$  ppm completely disappeared after the addition of *t*BuOK. All these data are consistent with the alcoholysis of Grubbs catalysts and the concomitant formation of Ru hydrides, which has been previously reported.<sup>24,27,29,30</sup> When the same sample was injected in the GC-MS, a peak corresponding to *o*-isopropoxytoluene-*d*<sub>2</sub> ( $m/z = 152$ ) was detected and, as expected, when the experiment was performed with non-deuterated solvents, undeuterated *o*-isopropoxytoluene ( $m/z = 150$ ) was detected instead. This confirms that the benzylidene moiety is hydrogenated out after dehydrogenation of *i*PrOH, as shown in Scheme 32. Initially the chlorides would be exchanged by isopropoxide<sup>30</sup> and subsequent partial hydrogenation of the benzylidene moiety with concomitant release of acetone would afford complex **30**. Then, dehydrogenation of another molecule of *i*PrOH would complete the hydrogenation of the benzylidene moiety releasing *o*-isopropoxytoluene and forming hydride species **31**, which might be able to accommodate the TsDPEN ligand.



**Scheme 32.** Proposed mechanism for the hydrogenation of the benzylidene moiety and for chelation of the TsDPEN ligand.

Interesting was also the deuteration pattern observed on PCy<sub>3</sub>. When non-deuterated PCy<sub>3</sub> was injected in the GC-MS, the mass spectra showed three main fragments with  $m/z = 280$ , 198 and 117 corresponding to PCy<sub>3</sub><sup>+</sup>, PHCy<sub>2</sub><sup>+</sup> and PH<sub>3</sub>Cy<sup>+</sup>, respectively (see Figure 12). However, when the reaction was performed in deuterated solvents PCy<sub>3</sub>-*d*<sub>9</sub> was found instead and, according to the fragmentation peaks ( $m/z = 289$ , 204 and 120) each cyclohexyl contained exactly three deuterium atoms (Figure 12). Indeed, the same trend is observed for O=PCy<sub>3</sub> and O=PCy<sub>3</sub>-*d*<sub>9</sub>

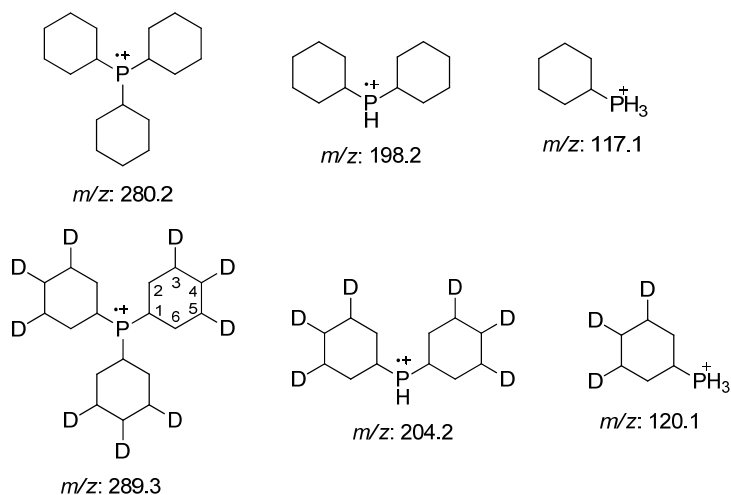
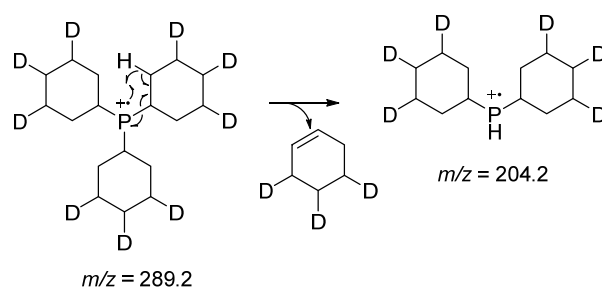


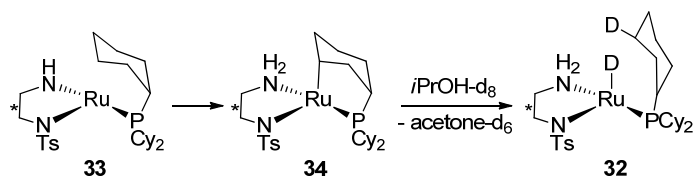
**Figure 12.** Main peaks observed in the GC-MS fragmentation for PCy<sub>3</sub> and PCy<sub>3</sub>-*d*<sub>9</sub>

The deuterium incorporation on the cyclohexyl ring presumably takes place in the 3-, 4- and 5-positions, otherwise the deuterium would be transferred to the phosphorus atom during the fragmentation process, according to the proposed fragmentation pathway (Scheme 33).<sup>51</sup>



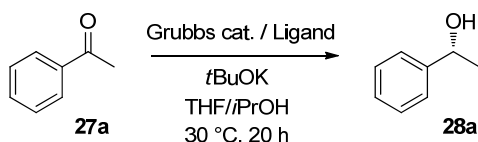
**Scheme 33.** Proposed fragmentation pathway for  $\text{PCy}_3\text{-d}_6$ .

We propose that this deuteration takes place via a C-H activation forming stable 5- and 6-membered metallacycles with the 3-, 4- and 5-positions of the cyclohexyl ring, as shown in Scheme 34. In fact, a chelation like the one of complex **34**, have been reported also by Cheung *et al* with similar complexes.<sup>52</sup>

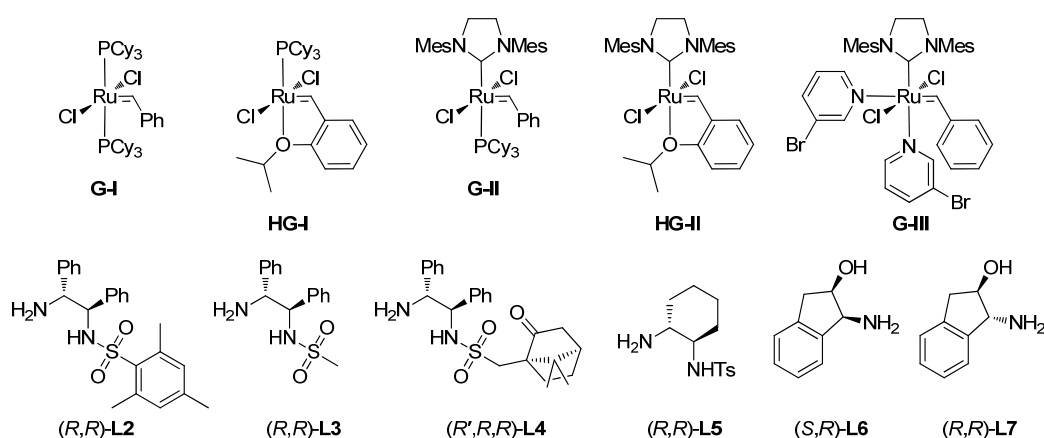


**Scheme 34.** Proposed pathway for the deuteration of the cyclohexyl rings.

Simultaneously to this mechanistic study, the ATH of **27a** was further optimized (Table 8). As expected, when no base was added, no conversion was obtained (Table 8, entry 1), and at least 20 equivalents of base compared to Ru had to be used to achieve some conversion (entries 2-5). Different ratios of THF/*i*PrOH were also explored, finding that a higher amount of *i*PrOH increased the activity (entry 6) and a higher amount of THF slightly increased the *ee* but decreased the activity (entry 7). The most common commercially available Ru olefin metathesis catalyst were also tested and, surprisingly, only the 1<sup>st</sup> generation catalyst achieved good results (entries 6 and 8), while NHC-containing catalysts led to conversions under 10% (entries 9-11). Finally, a ligand screening was performed (entries 12-17), making evident the great dependence of both activity and enantioselectivity from small variations on the ligand structure. The only ligand with a performance comparable to that one of (*R,R*)-TsDPEN (**L1**) was the (*R,R*)-camphorsulfonyl-DPEN (**L4**).

**Table 8.** Optimization of the reaction conditions on the ATH of **27a**.

#	Ru cat.	Ligand	<i>t</i> BuOK	THF/ <i>i</i> PrOH	Conv. (%)	<i>ee</i> (%)
1	HG-I	L1	-	1:1	0	-
2	HG-I	L1	5	1:1	0	-
3	HG-I	L1	10	1:1	0	-
4	HG-I	L1	20	1:1	86	93
5	HG-I	L1	40	1:1	95	92
6	HG-I	L1	20	1:3	97	93
7	HG-I	L1	20	3:1	56	96
8	G-I	L1	20	1:3	96	95
9	HG-II	L1	20	1:3	4	10
10	G-II	L1	20	1:3	8	86
11	G-III	L1	20	1:3	4	30
12	HG-I	L2	20	1:3	53	62
13	HG-I	L3	20	1:3	96	88
14	HG-I	L4	20	1:3	92	94
15	HG-I	L5	20	1:3	97	78
16	HG-I	L6	20	1:3	67	64
17	HG-I	L7	20	1:3	34	-5



*Reaction conditions:* **27a** (0.1 mmol), Ru catalyst (1 mol%), ligand (1.1 mol%), THF/*i*PrOH (2 mL), *t*BuOK, 30 °C, 18 h. Conversion and *ee* determined by chiral GC.

Surprised by the negative results obtained with 2<sup>nd</sup> generation catalysts, we performed a series of experiments to try to form an active enantioselective species from **G-II** (Table 9). The highest enantioselectivities were obtained with isopropoxide (entries 1 and 3), but with very low activities. When pre-stirring the catalyst with *t*BuOK (entry 2), again a very ineffective catalyst was obtained. Instead, when using methoxide the activity increased substantially, probably due to the formation of active Ru carbonyl species, but unfortunately the obtained enantioselectivities were very low (entries 4 and 5). Finally, to assess whether the lack of activity in the standard conditions was due to a lack of stability of the formed complex, as Fogg had reported for **G-III**,<sup>9</sup>

we added one equivalent of PCy<sub>3</sub>, and in fact the activity increased, but the enantioselectivity dropped considerably.

**Table 9.** Attempts to convert **G-II** into a highly active and enantioselective ATH catalyst.

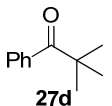
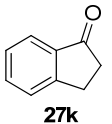
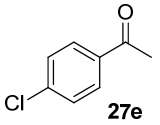
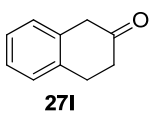
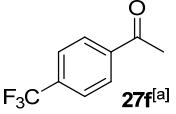
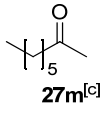
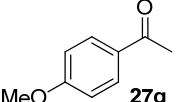
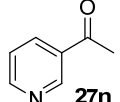
#	Penultimate reagent added <sup>[a]</sup>	Last reagent added <sup>[a]</sup>	Conv. (%)	ee (%)
1	<i>i</i> PrOH	<i>t</i> BuOK	8	86
2	<i>t</i> BuOK	<i>i</i> PrOH	30	24
3	<i>i</i> PrOK <sup>[b]</sup>	<i>i</i> PrOH	16	77
4	NaOMe	<i>i</i> PrOH	57	20
5	KOMe	<i>i</i> PrOH	33	10
6	<i>i</i> PrOH + PCy <sub>3</sub> <sup>[c]</sup>	<i>t</i> BuOK	47	37

*Reaction conditions:* **27a** (0.1 mmol), Ru catalyst (1 mol%), ligand (1.1 mol%), THF/*i*PrOH (2 mL), *t*BuOK, 30 °C, 18 h. Conversion and *ee* determined by chiral GC. [a] Between the penultimate reagent added and the last one, the solution was stirred for 3 h at 30 °C. [b] A 0.5 M solution of *t*BuOK in *i*PrOH was used. [c] 1 equivalent of PCy<sub>3</sub> compared to Ru.

With the optimized conditions and, unfortunately, without being able to effectively convert NHC-containing Ru precursors in ATH catalysts, we set to validate the system with a substrate screening employing **HG-I** and (*R,R*)-TsDPEN (Table 10). Very bulky alkyl groups were not well tolerated, decreasing substantially the activity and the enantioselectivity (entries 2-4). The presence of *ortho*-substituents in the aromatic ring produced the same effect (entry 8). The best conversions were achieved with electron-deficient acetophenones (entries 5 and 6), while the electron-rich ones only led to good conversions (entry 7). 2-Acetonaphthone as well as aromatic cyclic ketones (entries 9-11) were reduced with *ee*'s up to 97%. Unfortunately, more challenging substrates such as 3-acetylpyridine (entry 14) or alkyl ketones (entries 12 and 13) led to poor or no conversion and low *ee*. In general, the obtained results are quite close to those reported with the Noyori catalyst.<sup>47</sup>

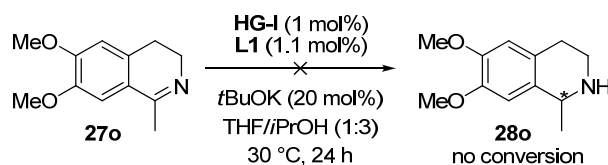
**Table 10.** Substrate scope for the ATH with **HG-I** and (*R,R*)-TsDPEN.

#	Substrate	Conv. (%) ee (%)	#	Substrate	Conv. (%) ee (%)
1		97 93, <i>R</i>	8		0 n.d.
2		84 90, <i>R</i>	9		96 95, <i>R</i>
3		27 33, <i>R</i>	10		60 97, <i>R</i>

4		36 17, R	11		43 93, R
5		99 80, R	12		4 n.d.
6		100 73, R	13		45 30, R
7		73 85, R	14		0 n.d.

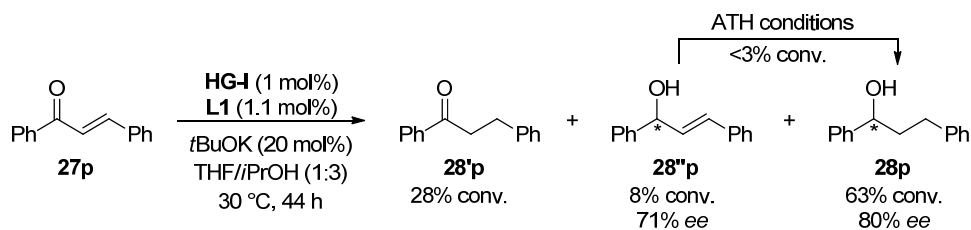
Reaction conditions: **27** (0.1 mmol), **HG-I** (1 mol%), (*R,R*)-**L1** (1.1 mol%), THF/*i*PrOH (1:3, 2 mL), *t*BuOK (20 mol%), 30 °C, 20 h. Conversion and *ee* determined by chiral GC. n.d.= not determined. [a] 40 equivalents of base compared to the catalyst. [b] Reaction run for 44 h. [c] Reaction run for 90 h.

The reduction of the imine **27o** was also attempted, but unfortunately no conversion was obtained under the optimized conditions (Scheme 35).



Scheme 35. Attempt for the ATH of imine **27o**.

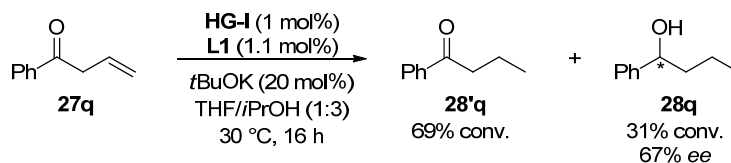
We then tested the possibility to hydrogenate  $\alpha,\beta$ -unsaturated ketones. When *trans*-chalcone (**27p**) was submitted to the optimized ATH conditions, three different products were obtained (Scheme 36), the main product being the fully reduced alcohol **28p** with 80% *ee*. To assess which of the two partially hydrogenated products was the intermediate towards **28p**, the commercially available alcohol **28''p** was submitted to ATH conditions, but almost no conversion was observed. This suggests that, while simple double bonds are unreactive under these conditions, double bonds conjugated with ketones are readily hydrogenated. Thus, the formation of **28p** goes via intermediate **28'p**.



Scheme 36. ATH of *trans*-chalcone **27p**.

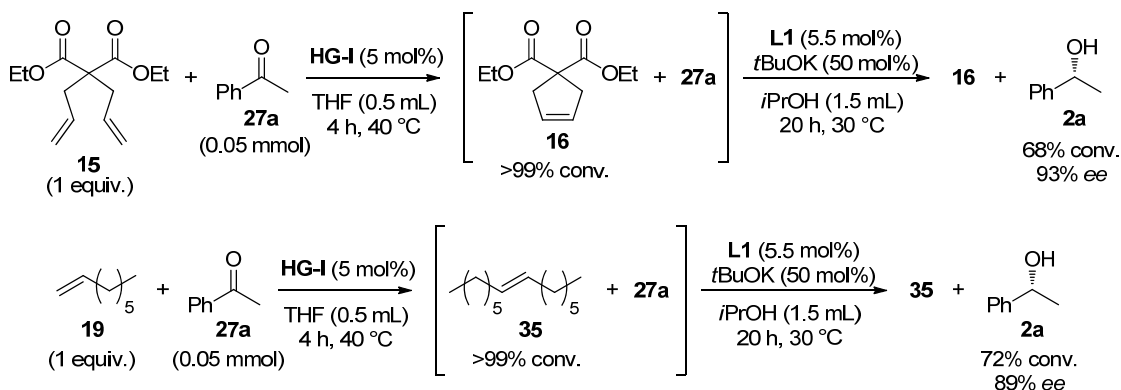
The last substrate tested was the  $\beta,\gamma$ -unsaturated ketone **27q**, and also in this case the double bond was hydrogenated faster than the ketone. Since we have observed that isolated double bonds are not hydrogenated with this system, we proposed that a base-catalyzed isomerization of

the double bond would produce the  $\alpha,\beta$ -unsaturated ketone<sup>53</sup> which would be then readily hydrogenated to **28'q**, and a subsequent ketone reduction would render alcohol **28q**.



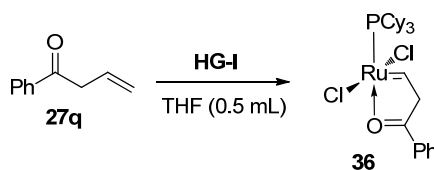
**Scheme 37.** ATH of 1-phenylbut-3-en-1-one (**27q**).

Once demonstrated that 1<sup>st</sup> generation Ru olefin metathesis catalyst can be converted into efficient ATH catalysts by addition of a chiral ligand, *i*PrOH and a base, we undertook investigations towards a tandem olefin metathesis–ATH protocol. The first thing to test was whether the Ru complex could be converted into an ATH catalyst after having performed a metathesis step. To this purpose, we carried out in parallel the ring-closing metathesis (RCM) of diethyl 2,2-diallylmalonate (**15**) and the homo-metathesis of 1-octene (**19**) in presence of acetophenone (**27a**). After checking by GC that the metathesis reaction had been completed, the ligand, *i*PrOH and *t*BuOK were added in this order. After 20 h of reaction, (*R*)-1-phenylethanol was obtained with moderate conversions and excellent enantioselectivities, 93% and 89% *ee* respectively (Scheme 38). It is also remarkable that the double bonds generated by metathesis remained unchanged after the ATH step.



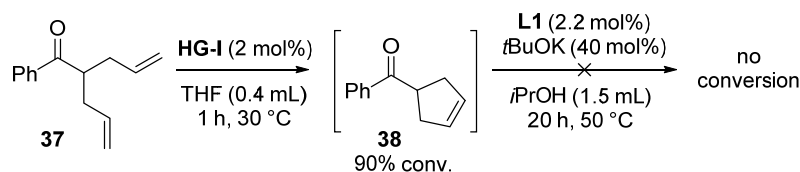
**Scheme 38.** Proof of concept for the tandem olefin metathesis–ATH.

Encouraged by the obtained results, we undertook the search of a substrate that could undergo both the metathesis reaction and the ATH. The  $\beta,\gamma$ -unsaturated ketone **27q** was the first choice, but when the metathesis reaction was attempted no conversion was obtained, independently of the cross-metathesis partner. This was probably due to the stable chelating alkylidene complex formed with these kinds of substrates after the first metathesis cycle (Scheme 39).<sup>54</sup>



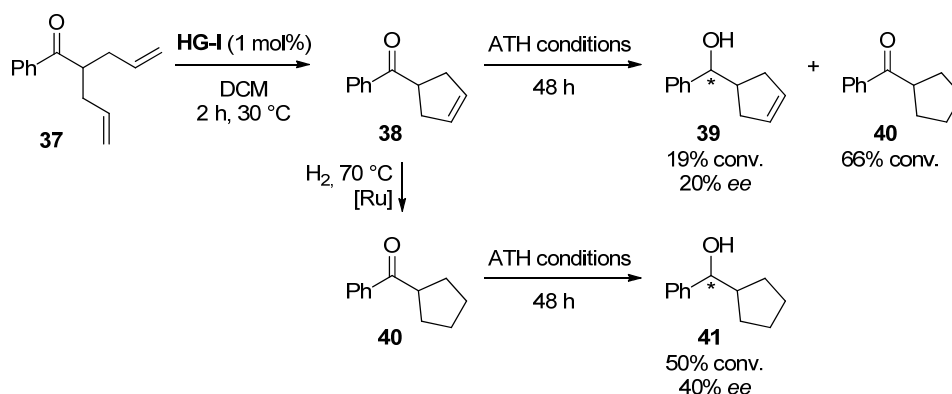
**Scheme 39.** Chelating alkylidene Ru-complex formed by reaction of  $\beta,\gamma$ -unsaturated ketones and **HG-I**.

The second substrate synthesized was the diallyl ketone **37**. In this case the RCM proceeded smoothly, but when the ATH was attempted no carbonyl reduction was observed (Scheme 40).



**Scheme 40.** Attempt of tandem RCM–ATH of **37**.

Surprised by this lack of activity we tried to find a possible cause. The metathesis reaction was repeated and, before starting the ATH step, acetophenone (**27a**) was added to the reaction mixture. After 4 h of hydrogenation, (*R*)-1-phenylethanol was observed with 10% conversion and 77% *ee*, proving that the catalyst was still active, although less than usual. To check if the problem was arising from the substrate, ketones **38** and **40** were synthesized and isolated (Scheme 41). When these two were submitted to the standard ATH conditions, results comparable to those obtained with 2-methyl-1-phenylpropan-1-one (**27c**) were observed. Then, the only possible explanation for the lack of activity might be the conjunction of a not very active catalyst, formed after the RCM step, with a sterically hindered substrate, challenging for this system.

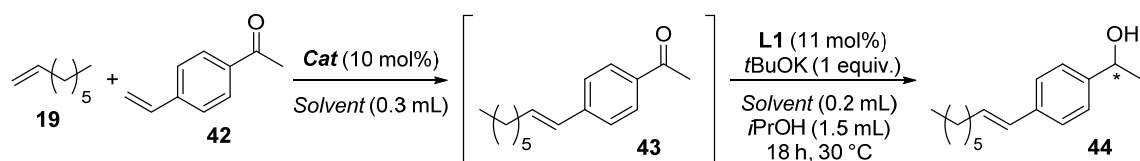


**Scheme 41.** Attempts to hydrogenate ketones **38** and **40** with the optimized ATH conditions.

After trying different substrates with olefins in the alkyl part of the ketone without much success, it was decided to attach the olefin to the aromatic moiety, thus 4-vinylacetophenone (**42**) was selected as substrate. Although electron-poor styrenes are known to be sluggish in metathesis with 1<sup>st</sup> generation Grubbs catalysts (type II olefin in Chatterjee/Grubbs nomenclature),<sup>55</sup> we expected that the distance between the double bond and the ketone would make the ATH step easier. 1-octene was selected as a cross-metathesis partner and the tandem metathesis–ATH was carried out in different solvents and with **G-I** or **HG-I** as catalysts (Table 11, entries 1-6). **HG-I** performed much better than **G-I** and, while the best *ee* was obtained in toluene (entry 4), the best overall conversion was achieved in DCM (entry 5). Performing the metathesis reaction in toluene at 50 °C, instead of 40 °C, led to a higher overall yield but a lower enantioselectivity (entry 7). When 2,2-dichloroethane was used instead of DCM, the temperature of the metathesis step could be risen to 50 °C, which proved beneficial for the conversion (entry 8). Moreover, in the ATH step a good conversion (60%) and the highest

enantiomeric excess (87% *ee*) were obtained. The remaining 4-vinylacetophenone (**42**) was hydrogenated to 1-(4-vinylphenyl)ethan-1-ol (**45**) with 79% conversion and 90% *ee*.

**Table 11.** Tandem cross metathesis–ATH of 4-vinylacetophenone (**37**) with 1-octene.



#	Solvent	Metathesis		ATH	
		Conditions	Conv. (%)	Conv. (%)	<i>ee</i> (%)
1	toluene	<b>G-I</b> , 40 °C, 4h	39	12	24
2	DCM	<b>G-I</b> , 40 °C, 4h	18	10	35
3	THF	<b>G-I</b> , 40 °C, 4h	38	50	19
4	toluene	<b>HG-I</b> , 40 °C, 4h	30	26	73
5	DCM	<b>HG-I</b> , 40 °C, 4h	38	74	54
6	THF	<b>HG-I</b> , 40 °C, 4h	18	23	64
7	toluene	<b>HG-I</b> , 50 °C, 5h	42	54	48
8	2,2-dichloroethane	<b>HG-I</b> , 50 °C, 5h	46	60	87

Reaction conditions: Metathesis: **42** (0.05 mmol), **19** (0.15 mmol), Ru cat. (10 mol%), solvent (0.3 mL); ATH: (*R,R*)-**L1** (11 mol%), solvent (0.3 mL), *i*PrOH (1.5 mL), *t*BuOK (20 mol%), 30 °C, 18 h. Conversion and *ee* determined by chiral GC.

## VI.3 CONCLUSIONS

In this chapter, it has been demonstrated that 1<sup>st</sup> generation Ru olefin metathesis catalyst can be converted into efficient and highly enantioselective asymmetric transfer hydrogenation catalysts, achieving enantioselectivities up to 97% *ee*. However, NHC-containing complexes did not prove suitable for this transformation. It has also been shown that a tandem olefin metathesis–ATH protocol is possible and a selective carbonyl hydrogenation can be obtained in some cases. We believe that the orthogonal reactivity shown by this system might be of interest for the synthetic community, especially in the field of high-throughput synthesis. Furthermore, the multiple uses of a precious metal such as ruthenium discloses new prospects towards a more efficient and sustainable use of this expensive and scarce metal.

## VI.4 EXPERIMENTAL SECTION

Dry DCM and THF were obtained from MBraun SPS system. Dry MeOH, *i*PrOH and 1,2-dichloroethane (over molecular sieves in bottles with crown cap) were purchased from Sigma Aldrich and stored under nitrogen. Commercially available reagents (from TCI Chemicals, ACROS, Sigma Aldrich, Strem) were used as received, without any further purification. 1-(4-vinylphenyl)ethanone (**42**) was synthesized according to the procedure described by Littke *et*

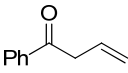


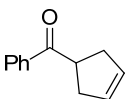
*al.*<sup>56</sup> 2-allyl-1-phenylpent-4-en-1-one (**37**) was synthesized according to the procedure described by Pandey *et al.*<sup>57</sup>

The reactions were monitored by analytical thin-layer chromatography (TLC) using silica gel 60 F254 pre-coated glass plates (0.25 mm thickness). Visualization was accomplished by irradiation with a UV lamp and/or staining with a potassium permanganate alkaline solution. Flash column chromatography was performed using Grace Reveleris® X2 Flash Chromatography System (silica gel cartridges with particle size 40 µm). Gas chromatography was performed on an Agilent Technologies 7890A and Hewlett Packard 6890 instruments, equipped with a flame ionization detector, using respectively a chiral and an achiral capillary column. Infrared spectra were recorded on a standard FT/IR spectrometer. High resolution mass spectra (HRMS) were performed on a Fourier Transform Ion Cyclotron Resonance (FT-ICR) Mass Spectrometer APEX II & Xmass software (Bruker Daltonics) – 4.7 T Magnet (MagneX) equipped with ESI source, available at CIGA (Centro Interdipartimentale Grandi Apparecchiature) c/o Università degli Studi di Milano.

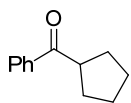
<sup>1</sup>H-NMR spectra were recorded in two different a spectrometer operating at 400 or 500 MHz. Proton chemical shifts are reported in ppm (δ) with the solvent reference relative to tetramethylsilane (TMS) employed as the internal standard (CDCl<sub>3</sub> δ = 7.26 ppm; THF-d<sub>8</sub>, δ = 1.72 and 3.58 ppm). <sup>13</sup>C-NMR spectra were recorded on a 400 MHz spectrometer operating at 100 MHz, with complete proton decoupling. Carbon chemical shifts are reported in ppm (δ) relative to TMS with the respective solvent resonance as the internal standard (CDCl<sub>3</sub>, δ = 77.2 ppm). <sup>31</sup>P-NMR spectra were recorded on a 500 MHz spectrometer operating at 202.5 MHz, with complete proton decoupling. <sup>31</sup>P-NMR chemical shifts are reported in ppm (δ) relative to external H<sub>3</sub>PO<sub>4</sub> (85% in H<sub>2</sub>O) at 0 ppm (positive values downfield). The following abbreviations are used to describe spin multiplicity: s = singlet, d = doublet, t = triplet, q = quartet, m = multiplet, bs = broad signal, td = triplet-doublet. Coupling constant values are given in Hz.

### Synthesis of substrates and characterization of new compounds

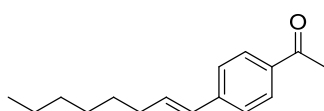
 **1-phenylbut-3-en-1-one (27q):** 1-phenylbut-3-en-1-ol (0.75 g, 5 mmol) was dissolved in DCM (25 mL) and cooled down to 0 °C. Dess-Martin periodinane (2.5 g, 6 mmol) was added and the mixture was stirred for 2 h at room temperature. After that time, a saturated aqueous solution of NaHCO<sub>3</sub>/Na<sub>2</sub>S<sub>2</sub>O<sub>3</sub> (1:1, 20 mL) was added and the resulting mixture stirred for 30 min. The organic layer was separated and washed once more with the same saturated solution (20 mL) and then with brine (20 mL). The organic extracts were dried with MgSO<sub>4</sub>, filtered and concentrated. The reaction was purified by column chromatography (Heptane:EtOAc 20:1). Known compound. Spectroscopic data are superimposable to those reported in the literature.<sup>58</sup>

 **Cyclopent-3-en-1-yl(phenyl)methanone (38):** 2-allyl-1-phenylpent-4-en-1-one **37** (150 mg, 0.75 mmol), **HG-I** (1 mol%) and DCM (2 mL) were stirred for 2 h at 30 °C. After this time, **38** was quantitatively obtained as observed by NMR.<sup>59</sup> Half of

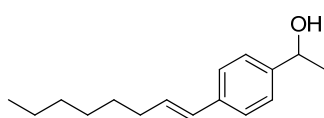
it was used for the synthesis of **40** and the other half was purified by filtration through a short pad of silica.



**Cyclopentyl(phenyl)methanone (40)**: the reaction crude from the synthesis of **38**, with the Ru catalyst still inside, was submitted to hydrogenation at 70 °C and 50 bar of H<sub>2</sub> for 16 h. The product was purified by filtration through a short pad of silica and identified as **40**.<sup>21</sup>



**(E)-1-(4-(oct-1-en-1-yl)phenyl)ethanone (43)**: In a 5 ml vial, Grubbs-Hoveyda 1<sup>st</sup> generation (30 mg, 0.05 mmol) was added to a mixture of 1-(4-vinylphenyl)ethanone (150 mg, 1.02 mmol) and 1-octene (482  $\mu$ l, 3.07 mmol) in 1,2-dichloroethane (2 ml). The reaction was stirred at 50 °C for 18 h. The reaction was concentrated and purified by column chromatography (Hexane:EtOAc 50:1) to obtain 138 mg (0.6 mmol, 59% yield) of **7-CM** as a colorless oil. <sup>1</sup>H NMR (400 MHz, CDCl<sub>3</sub>)  $\delta$  7.89 (d, <sup>3</sup>J(H,H) = 8.3 Hz, 2H), 7.41 (d, <sup>3</sup>J(H,H) = 8.3 Hz, 2H), 6.45 – 6.36 (m, 2H), 2.58 (s, 3H), 2.24 (m, 2H), 1.48 (m, 2H), 1.40 – 1.24 (m, 6H), 0.90 (t, <sup>3</sup>J(H,H) = 6.8 Hz, 3H); <sup>13</sup>C NMR (100 MHz, CDCl<sub>3</sub>)  $\delta$  197.70, 142.81, 135.49, 134.71, 129.02, 128.86, 126.02, 33.31, 31.83, 29.23, 29.04, 26.65, 22.73, 14.21; IR (film):  $\nu$  = 3027.7, 3001.7, 2956.3, 2925.5, 2854.1, 1681.6, 1601.6, 1357.6, 1267.0, 1180.2, 965.2, 854.3 cm<sup>-1</sup>; HRMS (ESI+):  $m/z$  253.15694 [M + Na]<sup>+</sup> (calcd. for C<sub>16</sub>H<sub>22</sub>O<sub>1</sub>Na: 253.15629).

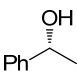


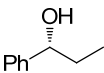
**(±,E)-1-(4-(oct-1-en-1-yl)phenyl)ethanol (44)**: NaBH<sub>4</sub> (68 mg, 1.8 mmol) was added to a solution of **7-CM** (138 mg, 0.60 mmol) and CeCl<sub>3</sub>·7H<sub>2</sub>O (313 mg, 0.84 mmol) in MeOH (5 ml) at 0 °C and the solution was stirred for 3 h at room temperature. After this time, the reaction was quenched with a saturated aqueous solution of NH<sub>4</sub>Cl (5 ml) and extracted with DCM (3 x 10ml). The organic phases were dried over Na<sub>2</sub>SO<sub>4</sub>, filtered and concentrated, to render 132 mg (0.57mmol, 95% yield) of **8** as colorless oil. <sup>1</sup>H NMR (400 MHz, CDCl<sub>3</sub>)  $\delta$  7.36 – 7.27 (m, 4H), 6.37 (d, <sup>3</sup>J(H,H) = 15.8 Hz, 1H), 6.22 (dt, <sup>3</sup>J(H,H) = 15.8, 6.8 Hz, 1H), 4.87 (q, <sup>3</sup>J(H,H) = 6.4 Hz, 1H), 2.21 (q, <sup>3</sup>J(H,H) = 6.8 Hz, 2H), 1.81 (bs, 1H), 1.49 (d, <sup>3</sup>J(H,H) = 6.5 Hz, 3H), 1.47 (m, 2H), 1.40 – 1.28 (m, 6H), 0.90 (t, <sup>3</sup>J(H,H) = 6.8 Hz, 3H); <sup>13</sup>C NMR (100 MHz, CDCl<sub>3</sub>)  $\delta$  144.44, 137.52, 131.45, 129.46, 126.18, 125.70, 70.37, 33.19, 31.90, 29.50, 29.04, 25.17, 22.77, 14.22; IR (film):  $\nu$  = 3352.6, 3022.9, 2957.3, 2924.5, 2853.2, 1453.1, 1086.7, 964.2 cm<sup>-1</sup>; HRMS (ESI+):  $m/z$  255.17260 [M + Na]<sup>+</sup> (calcd. for C<sub>16</sub>H<sub>24</sub>O<sub>1</sub>Na: 255.17194).

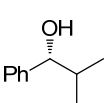
### General procedure for the ATH

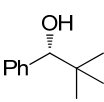
Substrate (0.1 mmol), metal complex (0.001 mmol, 1 mol%) and ligand (0.0011 mmol, 1.1 mol%) were dissolved in THF (0.5 ml) and *i*PrOH (1.5 ml) inside a nitrogen filled mBraun glovebox. After stirring the solution for 5 min, *t*BuOK (0.02 mmol, 20 mol%) was added and the reaction was stirred for 20 h at 30 °C. After this time, the reaction was analyzed by GC or HPLC for conversion and *ee* determination.

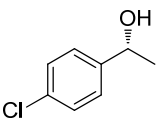
Products' absolute configurations were assigned by comparison of the sign of the optical rotation with literature data.

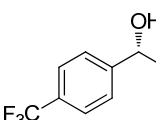
 **(R)-1-Phenylethanol (28a):**<sup>60</sup> Conversion and *ee* determined by GC: CP-Chirasil-Dex CB, 0.25  $\mu\text{m}$ ; diameter = 0.25 mm; length = 25 m; carrier: helium; gas flow: 2.7 bar; oven temperature: 120 °C for 10 min:  $t_{\text{substrate}} = 3.5$  min;  $t_R = 6.9$  min;  $t_S = 7.5$  min.

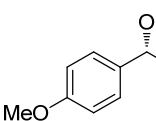
 **(R)-1-Phenylpropan-1-ol (28b):**<sup>60</sup> Conversion and *ee* determined by GC: CP-Chirasil-Dex CB (25m x 0.25mm, 0.25 $\mu\text{m}$ ); carrier: helium; gas flow: 2.7 bar; oven temperature: 120 °C for 10 min:  $t_{\text{substrate}} = 3.7$  min;  $t_R = 8.2$  min;  $t_S = 8.7$  min.

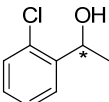
 **(R)-2-Methyl-1-phenylpropan-1-ol (28c):**<sup>61</sup> Conversion and *ee* determined by GC: CP-Chirasil-Dex CB (25m x 0.25mm, 0.25 $\mu\text{m}$ ); carrier: helium; gas flow: 2.7 bar; oven temperature: 120 °C for 15 min:  $t_{\text{substrate}} = 4.0$  min;  $t_R = 11.7$  min;  $t_S = 12$  min.

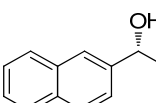
 **(R)-2,2-Dimethyl-1-phenylpropan-1-ol (28d):**<sup>60</sup> Conversion and *ee* determined by GC: CP-Chirasil-Dex CB (25m x 0.25mm, 0.25 $\mu\text{m}$ ); carrier: helium; gas flow: 2.7 bar; oven temperature: 120 °C for 20 min:  $t_{\text{substrate}} = 4.5$  min;  $t_S = 15.6$  min;  $t_R = 16.0$  min.

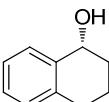
 **(R)-1-(4-Chlorophenyl)ethanol (28e):**<sup>62</sup> Conversion and *ee* determined by GC: CP-Chirasil-Dex CB (25m x 0.25mm, 0.25 $\mu\text{m}$ ); carrier: helium; gas flow: 2.7 bar; oven temperature: 120 °C for 25 min:  $t_{\text{substrate}} = 6.3$  min;  $t_R = 17.3$  min;  $t_S = 20.6$  min.

 **(R)-1-(4-(Trifluoromethyl)phenyl)ethanol (28f):**<sup>60</sup> Conversion and *ee* determined by GC: CP-Chirasil-Dex CB (25m x 0.25mm, 0.25 $\mu\text{m}$ ); carrier: helium; gas flow: 2.7 bar; oven temperature: 120 °C for 10 min:  $t_{\text{substrate}} = 2.7$  min;  $t_R = 7.7$  min;  $t_S = 9.3$  min.

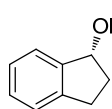
 **(R)-1-(4-Methoxyphenyl)ethanol (28g):**<sup>60</sup> Conversion and *ee* determined by GC: CP-Chirasil-Dex CB (25m x 0.25mm, 0.25 $\mu\text{m}$ ); carrier: helium; gas flow: 2.7 bar; oven temperature: 120 °C for 20 min:  $t_{\text{substrate}} = 10.8$  min;  $t_R = 16.7$  min;  $t_S = 18.3$  min.

 **1-(2-Chlorophenyl)ethanol (28h):**<sup>63</sup> Conversion determined by GC: CP-Chirasil-Dex CB (25m x 0.25mm, 0.25 $\mu\text{m}$ ); carrier: helium; gas flow: 2.7 bar; oven temperature: 120 °C for 15 min:  $t_{\text{substrate}} = 6.6$  min;  $t_{R+S} = 11.7$  min.

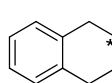
 **(R)-1-(Naphthalen-1-yl)ethanol (28i):**<sup>61</sup> Conversion and *ee* determined by GC: CP-Chirasil-Dex CB (25m x 0.25mm, 0.25 $\mu\text{m}$ ); carrier: helium; gas flow: 2.7 bar; oven temperature: 140 °C for 30 min:  $t_{\text{substrate}} = 13.9$  min;  $t_R = 25.8$  min;  $t_S = 28.0$  min.

 **(R)-1,2,3,4-Tetrahydronaphthalen-1-ol (28j):**<sup>60</sup> Conversion and *ee* determined by GC: CP-Chirasil-Dex CB (25m x 0.25mm, 0.25 $\mu\text{m}$ ); carrier: helium; gas flow: 2.7

bar; oven temperature: 130 °C for 17 min:  $t_{\text{substrate}} = 8.1$  min;  $t_{\text{S}} = 13.6$  min;  $t_{\text{R}} = 14.3$  min.



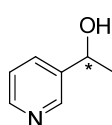
**(R)-2,3-Dihydro-1H-inden-1-ol (28k):**<sup>64</sup> Conversion and *ee* determined by GC: CP-Chirasil-Dex CB (25m x 0.25mm, 0.25 $\mu$ m); carrier: helium; gas flow: 2.7 bar; oven temperature: 130 °C for 10 min:  $t_{\text{substrate}} = 5.1$  min;  $t_{\text{S}} = 7$  min;  $t_{\text{R}} = 7.2$  min.



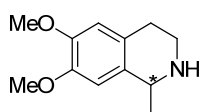
**1,2,3,4-Tetrahydronaphthalen-2-ol (28l):**<sup>65</sup> The product was derivatized as acetate before conversion and *ee* determination by GC: MEGADEX DACTBS $\beta$ , diacetyl-*tert*-butylsilyl- $\beta$ -cyclodextrin (25m x 0.25mm, 0.25  $\mu$ m); carrier: hydrogen; inlet pressure: 1 bar; oven temperature: 110 °C for 40 min:  $t_{\text{e1}} = 29.3$  min;  $t_{\text{e2}} = 30.3$  min;  $t_{\text{substrate}} = 35.1$  min.



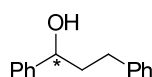
**(R)-2-Octanol (28m):**<sup>66</sup> Conversion and *ee* determined by GC: CP-Chirasil-Dex CB (25m x 0.25mm, 0.25 $\mu$ m); carrier: helium; gas flow: 2.7 bar; oven temperature: 80 °C for 25 min:  $t_{\text{substrate}} = 9.4$  min;  $t_{\text{S}} = 21.1$  min;  $t_{\text{R}} = 21.4$  min.



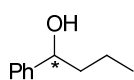
**1-(Pyridin-3-yl)ethanol (28n):**<sup>67</sup> Conversion determined by GC: MEGADEX DACTBS $\beta$ , diacetyl-*tert*-butylsilyl- $\beta$ -cyclodextrin (25m x 0.25mm, 0.25  $\mu$ m); carrier: hydrogen; inlet pressure: 1 bar; oven temperature: 130 °C for 15 min:  $t_{\text{substrate}} = 3.4$  min;  $t_{\text{R+S}} = 12.0$  min.



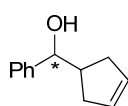
**6,7-Dimethoxy-1-methyl-1,2,3,4-tetrahydroisoquinoline (28o):**<sup>68</sup> Conv. and *ee* determined by HPLC: CHIRALPAK IB-3 (150 x 4.6 mm, 3  $\mu$ m), 254 nm, 40 °C, isocratic Heptane/*i*PrOH/DEA 95:5:0.05, 1.3 mL/min:  $t_{\text{substrate}} = 14.3$  min;  $t_{\text{S}} = 22.0$  min;  $t_{\text{R}} = 24.3$  min.



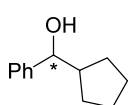
**1,3-Diphenylpropan-1-ol (28p):**<sup>69</sup> Conversion and *ee* determined by HPLC: CHIRALCEL OD-H (150 x 4.6 mm, 3  $\mu$ m), 215 nm, isocratic Heptane/*i*PrOH 90:10, 1 mL/min:  $t_{\text{substrate}} = 13.3$  min;  $t_{\text{e1}} = 20.1$  min;  $t_{\text{e2}} = 23.3$  min.



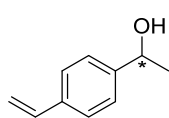
**1-Phenylbutan-1-ol (28q):**<sup>70</sup> Conversion and *ee* determined by GC: CP-Chirasil-Dex CB (25m x 0.25mm, 0.25 $\mu$ m); carrier: helium; gas flow: 2.7 bar; oven temperature: 130 °C for 10 min:  $t_{\text{substrate}} = 3.5$  min;  $t_{\text{e1}} = 7.0$  min;  $t_{\text{e2}} = 7.1$  min. A77



**Cyclopent-3-en-1-yl(phenyl)methanol (39):**<sup>59</sup> Conversion and *ee* determined by GC: CP-Chirasil-Dex CB (25m x 0.25mm, 0.25 $\mu$ m); carrier: helium; gas flow: 2.7 bar; oven temperature: 130 °C for 10 min:  $t_{\text{substrate}} = 12.6$  min;  $t_{\text{e1}} = 26.5$  min;  $t_{\text{e2}} = 27.0$  min.

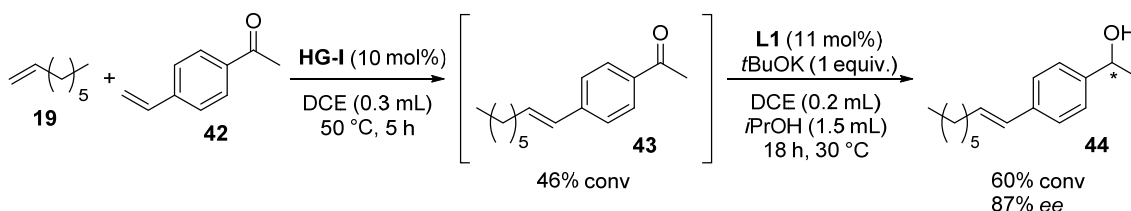


**Cyclopentyl(phenyl)methanol (41):**<sup>71</sup> Conversion and *ee* determined by GC: CP-Chirasil-Dex CB (25m x 0.25mm, 0.25 $\mu$ m); carrier: helium; gas flow: 2.7 bar; oven temperature: 130 °C for 10 min:  $t_{\text{substrate}} = 12.3$  min;  $t_{\text{e1}} = 28.0$  min;  $t_{\text{e2}} = 28.5$  min.



**1-(4-vinylphenyl)ethan-1-ol (45):**<sup>72</sup> Conversion and *ee* determined by GC: CP-Chirasil-Dex CB (25m x 0.25mm, 0.25 $\mu$ m); carrier: helium; gas flow: 2.7 bar; oven temperature: 120 °C for 10 min, gradient 30 °C/min, 150 °C for 1 min:  $t_{e1}$  = 11.7 min,  $t_{e2}$  = 12.1 min.

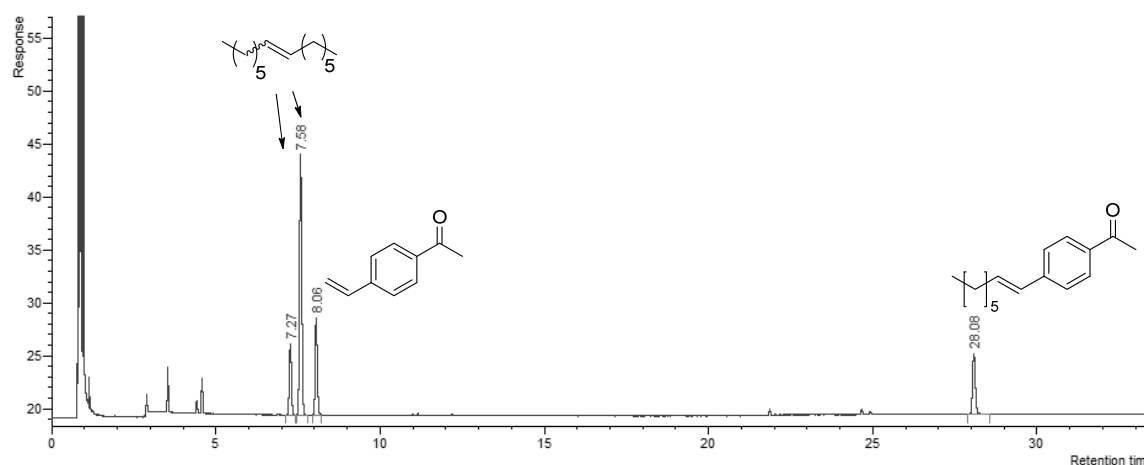
### Procedure for the tandem metathesis-ATH



#### Step I: RCM

In a nitrogen filled mBraun glovebox, a solution of **HG-I** (3.0 mg, 0.005 mmol) in 2,2-dichloroethane (0.3 mL) was added to 1-octene (16.8 mg, 0.15 mmol) and 1-(4-vinylphenyl)ethanone (7.3 mg, 0.05 mmol). The reaction mixture was stirred in an open glass vial for 5 h at 50 °C. The conversion to the cross-metathesis product was analyzed by GC.

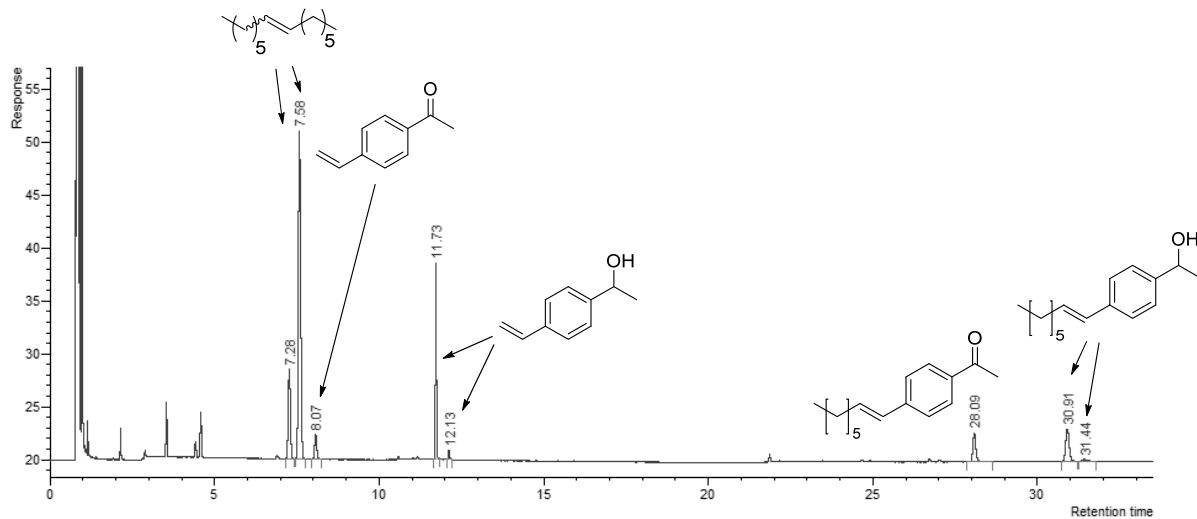
Conversion determined by GC: CP-Chirasil-Dex CB (25m x 0.25mm, 0.25 $\mu$ m); carrier: helium; gas flow: 2.7 bar; oven temperature: 120 °C for 10 min, gradient 30 °C/min, 150 °C for 10 min, gradient 30 °C/min, 180 °C for 15 min:  $t_{(Z)\text{-tetradec-7-ene}}$  = 7.3 min.;  $t_{(E)\text{-tetradec-7-ene}}$  = 7.6 min.;  $t_{42}$  = 8.1 min.;  $t_{43}$  = 28.1 min.



#### Step II: Asymmetric hydrogenation

(*R,R*)-TsDPEN (2.0 mg, 0.0055 mmol), 2,2-dichloroethane (0.2 ml), *i*PrOH (1.5 mL) and *t*BuOK (5.6 mg, 0.05 mmol) were added in this order. The vial was closed and stirred for 18 h at 30 °C.

Conversion and *ee* determined by GC: CP-Chirasil-Dex CB (25m x 0.25mm, 0.25 $\mu$ m); carrier: helium; gas flow: 2.7 bar; oven temperature: 120 °C for 10 min, gradient 30 °C/min, 150 °C for 10 min, gradient 30°C/min, 180 °C for 15 min:  $t_{(Z)\text{-tetradec-7-ene}} = 7.3$  min.;  $t_{(E)\text{-tetradec-7-ene}} = 7.6$  min.;  $t_{42} = 8.1$  min.;  $t_{1\text{-(4-vinylphenyl)ethan-1-ol}} = 11.7/12.1$  min.;  $t_{43} = 28.1$  min.;  $t_{44} = 30.9/31.4$  min.;



## REFERENCES

1. R. A. Sheldon, *Chem. Commun.* **2008**, 44, 3352–3365.
2. K. C. Nicolaou, D. J. Edmonds, P. G. Bulger, *Angew. Chem. Int. Ed.* **2006**, 45, 7134–7186.
3. D. E. Fogg, E. N. dos Santos, *Coord. Chem. Rev.* **2004**, 248, 2365–2379.
4. a) B. Schmidt, *Pure Appl. Chem.* **2006**, 78, 469–476. b) V. Dragutan, I. Dragutan, *J. Organomet. Chem.* **2006**, 691, 5129–5147. c) S. Kotha, S. Misra, G. Sreevani, B. V. Babu, *Curr. Org. Chem.* **2013**, 17, 2776–2795. d) B. Alcaide, P. Almendros, A. Luna, *Chem. Rev.* **2009**, 109, 3817–3858.
5. a) J. McLain, S. D. Arthur, E. Hauptman, J. Feldman, W. A. Nugent, L. K. Johnson, S. Mecking, M. Brookhart, *Polym. Mater. Sci. Eng.* **1997**, 76, 246–247. b) M. D. Watson, K. B. Wagener, *Macromolecules* **2000**, 33, 3196–3201. c) C. W. Bielawski, J. Louie, R. H. Grubbs, *J. Am. Chem. Soc.* **2000**, 122, 12872–12873.
6. R. P. Beatty, R. A. Paciello (E. I. Du Pont de Nemours and Company), U.S. Patent 5554778, **1996**.
7. J. Louie, C. W. Bielawski, R. H. Grubbs, *J. Am. Chem. Soc.* **2001**, 123, 11312–11313.
8. B. Schmidt, M. Pohler, *Org. Biomol. Chem.* **2003**, 1, 2512–2517.
9. K. D. Camm, N. M. Castro, Y. Liu, P. Czechura, J. L. Snelgrove, D. E. Fogg, *J. Am. Chem. Soc.* **2007**, 129, 4168–4169.
10. a) J. A. Love, J. P. Morgan, T. M. Trnka, R. H. Grubbs, *Angew. Chem. Int. Ed.* **2002**, 41, 4035–4037. b) T.-L. Choi, R. H. Grubbs, *Angew. Chem. Int. Ed.* **2003**, 42, 1743–1746.
11. X. Miao, C. Fischmeister, C. Bruneau, P. H. Dixneuf, *ChemSusChem* **2009**, 2, 542–545.
12. X. Miao, C. Fischmeister, C. Bruneau, P. H. Dixneuf, J.-L. Dubois, J.-L. Couturier, *ChemSusChem* **2012**, 5, 1410–1414. b) X. Miao, C. Fischmeister, P. H. Dixneuf, C. Bruneau, J.-L. Dubois, J.-L. Couturier, *Green Chem.* **2012**, 14, 2179–2183.
13. a) P. Børsting, K. E. Nielsen, P. Nielsen, *Org. Biomol. Chem.* **2005**, 3, 2183–2190. b) P. Børsting, P. Nielsen, *Chem. Commun.* **2002**, 2140–2141. P. Børsting, M. Freitag, P. Nielsen, *Tetrahedron* **2004**, 60, 10955–10966.
14. A. N. Whelan, J. Elaridi, R. J. Mulder, A. J. Robinson, W. R. Jackson, *Can. J. Chem.* **2005**, 83, 875–881.
15. a) A. Fürstner, A. Leitner, *Angew. Chem. Int. Ed.* **2003**, 42, 308–311. b) A. V. Statsuk, D. Liu, S. A. Kozmin, *J. Am. Chem. Soc.* **2004**, 126, 9546–9547. c) P. A. Evans, D. K. Leahy, W. J. Andrews, D. Uraguchi, *Angew. Chem. Int. Ed.* **2004**, 43, 4788–4791. d) J. Ramharter, H. Weinstabl, J. Mulzer *J. Am. Chem. Soc.* **2010**, 132, 14338–14339. e) T. E. La Cruz, S. D. Rychnovsky, *J. Org. Chem.* **2007**, 72, 2602–2611. f) L. J. Van Orden, B. D. Patterson, S. D. Rychnovsky, *J. Org. Chem.* **2007**, 72, 5784–5793.
16. a) R. H. Morris, Ruthenium and Osmium. In *The Handbook of Homogenous Hydrogenation* (Eds.: J. G. De Vries, C. J. Elsevier ) Wiley-VCH, Weinheim **2007**, 1, 45. b) S. Horn, M. Albrecht, *Chem. Commun.* **2011**, 47, 8802–8804. c) A. A. Poeylout-Palena, S. A. Testero, E. G. Mata, *Chem. Commun.* **2011**, 47, 1565–1567. d) T. D. Nixon, M. K. Whittlesey, J. M. J. Williams, *Tetrahedron Lett.* **2011**, 52, 6652–6654.
17. C. Menozzi, P. I. Dalko, J. Cossy, *Synlett* **2005**, 2449–2452.

18. B. Schmidt, S. Krehl, V. Sotelo-Meza, *Synthesis* **2012**, 1603–1613.
19. B. Schmidt, *J. Org. Chem.* **2004**, *69*, 7672–7687.
20. T. Connolly, Z. Wang, M. A. Walker, I. M. McDonald, K. M. Peese, *Org. Lett.* **2014**, *16*, 4444–4447.
21. G. K. Zieliński, C. Samojłowicz, T. Wdowik, K. Grela, *Org. Biomol. Chem.* **2015**, *13*, 2684–2688.
22. S. D. Drouin, G. P. Yap, D. E. Fogg, *Inorg. Chem.* **2000**, *39*, 5412–5414.
23. S. D. Drouin, F. Zamanian, D. E. Fogg, *Organometallics* **2001**, *20*, 5495–5497.
24. M. B. Dinger, J. C. Mol, *Organometallics* **2003**, *22*, 1089–1095.
25. T. M. Trnka, J. P. Morgan, M. S. Sanford, T. E. Wilhelm, M. Scholl, T.-L. Choi, S. Ding, M. W. Day, R. H. Grubbs, *J. Am. Chem. Soc.* **2003**, *125*, 2546–2558.
26. S. Manzini, A. Poater, D. J. Nelson, L. Cavallo, A. M. Z. Slawin, S. P. Nolan, *Angew. Chem. Int. Ed.* **2014**, *53*, 8995–8999.
27. M. B. Dinger, J. C. Mol, *Eur. J. Inorg. Chem.* **2003**, *2003*, 2827–2833.
28. D. Banti, J. C. Mol, *J. Organomet. Chem.* **2004**, *689*, 3113–3116.
29. N. J. Beach, K. D. Camm, D. E. Fogg, *Organometallics* **2010**, *29*, 5450–5455.
30. N. J. Beach, J. A. Lummiss, J. M. Bates, D. E. Fogg, *Organometallics* **2012**, *31*, 2349–2356.
31. M. S. Sanford, L. M. Henling, M. W. Day, R. H. Grubbs, *Angew. Chem. Int. Ed.* **2000**, *39*, 3451–3453.
32. a) J. C. Conrad, D. Amoroso, P. Czechura, G. P. A. Yap, D. E. Fogg, *Organometallics* **2003**, *22*, 3634–3636. b) J. N. Coalter, J. C. Bollinger, O. Eisenstein, K. G. Caulton, *New J. Chem.* **2000**, *24*, 925–927. c) S. R. Caskey, M. H. Stewart, Y. J. Ahn, M. J. A. Johnson, J. W. Kampf, *Organometallics* **2005**, *24*, 6074–6076.
33. M. S. Sanford, J. A. Love, R. H. Grubbs, *J. Am. Chem. Soc.* **2001**, *123*, 6543–6554.
34. a) S. H. Hong, A. G. Wenzel, T. T. Salguero, M. W. Day, R. H. Grubbs, *J. Am. Chem. Soc.* **2007**, *129*, 7961–7968. b) M. Ulman, R. H. Grubbs, *J. Org. Chem.* **1999**, *64*, 7202–7207. c) W. J. van Rensburg, P. J. Steynberg, W. H. Meyer, M. M. Kirk, G. S. Forman, *J. Am. Chem. Soc.* **2004**, *126*, 14332–14333. d) D. Amoroso, G. P. A. Yap, D. E. Fogg, *Organometallics* **2002**, *21*, 3335–3343. e) D. Amoroso, G. P. A. Yap, D. E. Fogg, *Can. J. Chem.* **2001**, *79*, 958–963. f) D. Bourgeois, A. Pancrazi, S. P. Nolan, J. Prunet, *J. Organomet. Chem.* **2002**, *643-644*, 247–252. g) S. H. Hong, M. W. Day, R. H. Grubbs, *J. Am. Chem. Soc.* **2004**, *126*, 7414–7415. h) G. C. Vougioukalakis, R. H. Grubbs, *Chem. Rev.* **2010**, *110*, 1746–1787. i) M. B. Herbert, Y. Lan, B. K. Keitz, P. Liu, K. Endo, M. W. Day, K. N. Houk, R. H. Grubbs, *J. Am. Chem. Soc.* **2012**, *134*, 7861–7866.
35. D. E. Fogg, D. Amoroso, S. D. Drouin, J. Snelgrove, J. Conrad, F. Zamanian, *J. Mol. Catal. A: Chem.* **2002**, *190*, 177–184.
36. a) Rowley, C. N.; Foucault, H. M.; Woo, T. K.; Fogg, D. E. *Organometallics* **2008**, *27*, 1661–1663. b) Beach, N. J.; Blacquiere, J. M.; Drouin, S. D.; Fogg, D. E. *Organometallics* **2009**, *28*, 441–447.
37. Sanford, M. S.; Ulman, M.; Grubbs, R. H. *J. Am. Chem. Soc.* **2001**, *123*, 749–750.
38. *Handbook of Metathesis: Catalyst Development and Mechanism, Volume 1* (Eds.: R. H. Grubbs, A. G. Wenzel) John Wiley & Sons, **2015**.
39. a) N. Haddad, B. Qu, S. Rodriguez, L. van der Veen, D. C. Reeves, N. C. Gonnella, H. Lee, N. Grinberg, S. Ma, D. Krishnamurthy, T. Wunberg, C. H. Senanayake, *Tetrahedron Lett.* **2011**, *52*, 3718–3722. b) U. Berens, C.



- Fischer, R. Selke, *Tetrahedron Asymmetry* **1995**, 6, 1105–1108. c) A. Wolfson, I. F. J. Vankelecoma, D. Geresh, P. A. Jacobs, *J. Mol. Catal. A-Chem.* **2003**, 198, 39–45. d) E. V. Starodubtseva, O. V. Turova, M. G. Vinogradov, L. S. Gorshkova, V. A. Ferapontov, *Russ. Chem. Bull., Int. Ed.*, **2007**, 56, 552–554.
40. J. J. Verendel, T. Zhou, J. Li, A. Paptchikhine, O. Lebedev, P. G. Andersson, *J. Am. Chem. Soc.* **2010**, 132, 8880–8881.
41. a) T. Vorfalt, S. Leuthäuser, H. Plenio, *Angew. Chem. Int. Ed.* **2009**, 48, 5191–5194. b) I. C. Stewart, T. Ung, A. A. Pletnev, J. M. Berlin, R. H. Grubbs, Y. Schrodi, *Org. Lett.* **2007**, 9, 1589–1592. c) Y. Liang, R. Raju, T. Le, C. D. Taylor, A. R. Howell, *Tetrahedron Lett.* **2009**, 50, 1020–1022. d) D. Rost, M. Porta, S. Gessler, S. Blechert, *Tetrahedron Lett.* **2008**, 49, 5968–5971. e) X. Elias, R. Pleixats, M. W. C. Man, J. J. E. Moreau, *Adv. Synth. Catal.* **2007**, 349, 1701–1713. f) A. Fürstner, O. R. Thiel, L. Ackermann, H.-J. Schanz, S. P. Nolan, *J. Org. Chem.* **2000**, 65, 2204–2207. g) S.-M. Paek, *Molecules* **2012**, 17, 3348–3358.
42. C. A. Merlic, M. F. Semmelhack, *J. Organomet. Chem.* **1990**, 391, C23–C27.
43. C. Stueckler, C. K. Winkler, M. Hall, B. Hauer, M. Bonnekessel, K. Zangger, K. Faber, *Adv. Synth. Catal.* **2011**, 353, 1169–1173.
44. N. Khiar, R. Navas, B. Suárez, E. Álvarez, I. Fernández, *Org. Lett.* **2008**, 10, 3697–3700.
45. L. Yu, Z. Wang, J. Wu, S. Tu, K. Ding, *Angew. Chem. Int. Ed.* **2010**, 49, 3627–3630.
46. D. Wang, D. Astruc, *Chem. Rev.* **2015**, 115, 6621–6686.
47. a) S. Hashiguchi, A. Fujii, J. Takehara, T. Ikariya, R. Noyori, *J. Am. Chem. Soc.*, **1995**, 117, 7562–7563. b) R. Noyori, S. Hashiguchi, *Acc. Chem. Res.*, **1997**, 30, 97–102.
48. Y. Jiang, Q. Jiang, X. Zhang, *J. Am. Chem. Soc.*, **1998**, 120, 3817–3818.
49. a) R. Hartmann, P. Chen, *Angew. Chem. Int. Ed.*, **2001**, 40, 3581–3585. b) J.-H. Xie, S. Liu, X.-H. Huo, X. Cheng, H.-F. Duan, B.-M. Fan, L.-X. Wang, Q.-L. Zhou, *J. Org. Chem.*, **2005**, 70, 2967–2973. c) P. Västilä, A. B. Zaitsev, J. Wettergren, T. Privalov, H. Adolfsson, *Chem. Eur. J.*, **2006**, 12, 3218–3225.
50. *Phosphorus-31 NMR Spectroscopy*. (Ed. Olaf Köhl), Springer-Verlag Berlin Heidelberg, **2008**.
51. R. G. Kostyanovsky, V. G. Plekhano, *Org. Mass Spectrom.* **1972**, 6, 1183–1198.
52. W.-M. Cheung, W.-H. Chiu, X.-Y. Yi, Q.-F. Zhang, I. D. Williams, W.-H. Leun, *Organometallics* **2010**, 29, 1981–1984.
53. E. N. Eccott, R. P. Linstead, *J. Chem. Soc.* **1930**, 905–919.
54. *Olefin Metathesis Theory and Practice*. Chapter 2.2. (Ed. K. Grela), John Wiley & Sons, Inc., Hoboken, NY, **2014**.
55. A. K. Chatterjee, T.-L. Choi, D. P. Sanders, R. H. Grubbs, *J. Am. Chem. Soc.*, **2003**, 125, 11360–11370.
56. A. F. Littke, L. Schwarz, G. C. Fu *J. Am. Chem. Soc.* **2002**, 124, 6343–6348.
57. G. Pandey, B. B. V. S. Sekhar, *J. Org. Chem.* **1992**, 57, 4019–4023.
58. K. Moriyama, M. Takemura, H. Togo, *J. Org. Chem.* **2014**, 79, 6094–6104

59. T. Wdowik, C. Samojlowicz, M. Jawiczuk, M. Malinska, K. Wozniak, K. Grela, *Chem. Commun.* **2013**, 49, 674–676.
60. F. Jiang, K. Yuan, M. Achard, C. Bruneau *Chem. Eur. J.* **2013**, 19, 10343–10352.
61. S. W. Krabbe, M. A. Hatcher, R. K. Bowman, M. B. Mitchell, M. S. McClure, J. S. Johnson, *Org. Lett.* **2013**, 15, 4560–4563.
62. D. R. Li, A. He, J. R. Falck *Org. Lett.* **2010**, 12, 1756–1759.
63. D. Lowicki, A. Bezlada, J. Mlynarski, *Adv. Synth. Catal.* **2014**, 356, 591–595.
64. S. Abbina, S. Bian, C. Oian, G. Du, *ACS Catal.* **2013**, 3, 678–684.
65. P. Vitale, F. M. Perna, M. G. Perrone, A. Scilimati, *Tetrahedron: Asymmetry* **2011**, 22, 1985–1993.
66. L. Ren, T. Xu, R. He, Z. Jiang, H. Zhou, P. Wei, *Tetrahedron: Asymmetry* **2013**, 24, 249–253.
67. S. Rodriguez, B. Qu, K. R. Fandrick, F. Buono, N. Haddad, Y. Xu, M. A. Herbage, X. Zeng, S. Ma, N. Grinberg, H. Lee, Z. S. Han, N. K. Yee, C. H. Senanayake, *Adv. Synth. Catal.* **2014**, 356, 301–307.
68. X. Li, D. Leonori, N. S. Sheikh, I. Coldham, *Chem. Eur. J.* **2013**, 19, 7724–7730.
69. M. Lamani, G. S. Ravikumara, K. R. Prabhu, *Adv. Synth. Catal.* **2012**, 354, 1437–1442.
70. C. Guyon, E. Metay, N. Duguet, M. Lemaire, *Eur. J. Org. Chem.* **2013**, 24, 5439–5444.
71. A. Orjales, R. Mosquera, A. Toledo, M. C. Pumar, N. Garcia, L. Cortizo, L. Labeaga, A. Innerarity, *J. Med. Chem.* **2003**, 46, 5512–5532.
72. F. J. Barrios, B. C. Springer, D. A. Colby, *Org. Lett.* **2013**, 15, 3082–3085.

# Summary

In Part A of this thesis we focused on developing new methods for the asymmetric hydrogenation (AH) of pyridines, due to the fact that chiral piperidines are ubiquitous motifs in many natural products and biologically active compounds. AH represents a versatile, clean and atom economic methodology and, since many protocols exist for the preparation of substituted pyridines, this technology is foreseen as the most efficient for the synthesis of chiral piperidines.

We first explored the AH of 2-substituted pyridinium salts with iridium complexes: a high-throughput screening of chiral phosphoramidites and their combinations with achiral phosphines allowed to individuate a phosphine/phosphoramidite complex ensuring full conversions and enantioselectivities of up to 82% *ee*. Using this catalytic system, a mechanistic study was performed, which shed light into the elementary steps towards the formation of the chiral piperidines and showed that the stereogenic carbon is not formed until the last hydrogenation step.

We next investigated the AH of 3-substituted pyridinium salts, which are much more challenging substrates. By means of a Rh-Josiphos complex and the addition of Et<sub>3</sub>N, different substrates were hydrogenated with up to 50% yield and 90% *ee*. The mechanistic study of this system was more complex, as different paths involving a number of dihydropyridines and tetrahydropyridines were identified towards the formation of the final piperidine. Among them, only one was producing the final piperidine with high enantioselectivity and the main side-pathway, which was leading to a racemic piperidine, was found to be halted by the addition of the base.

In Part B of the thesis, the possibility of converting Ru olefin metathesis catalysts into AH and asymmetric transfer hydrogenation (ATH) catalysts was explored. Many systems had been disclosed in the last years for the tandem metathesis–AH or ATH, but for none of them an asymmetric version had been reported. When Ru olefin metathesis catalysts were pressurized under H<sub>2</sub> in the presence of a chiral diphosphine ligand and an alcoholic solvent, chiral Ru complexes formed, promoting the AH of methyl 2-acetamidoacrylate with up to 93% *ee*. Additionally, when 1<sup>st</sup> generation Grubbs catalyst were treated with a base in the presence of a

chiral diamine ligand and *i*PrOH, a chiral catalyst was obtained, which promoted the ATH of aromatic ketones with up to 97% *ee*.

These two protocols for the conversion of Ru olefin metathesis catalysts into AH and ATH catalysts, respectively, were also implemented “one-pot” after an initial metathesis step. In the first case, a tandem ring-closing metathesis-AH protocol for the synthesis of 3-methyl-*N*-tosylpiperidine with 86% *ee* was developed. In the second, the cross metathesis of 4-vinylacetophenone followed by ketone ATH was achieved in one pot with 87% *ee*.

Although it is clear that these technologies still need further development and optimization, we believe that the advances presented on the AH of pyridines and the tandem metathesis–AH/ATH protocols will broaden the understanding of these fields and open new lines of investigation.

# List of Publications

- *Assisted Tandem Catalysis: Metathesis Followed by Asymmetric Hydrogenation from a Single Ruthenium Source.* M. Renom-Carrasco, P. Gajewski, L. Pignataro, J. G. de Vries, U. Piarulli, C. Gennari, L. Lefort, *Adv. Synth. Catal.* **2015**, *10*, 2223–2228.

In this thesis, research from this paper is presented under copyright license with John Wiley and Sons – license number 3790221226550 from 15<sup>th</sup> January 2016.

- *Asymmetric Transfer Hydrogenation of Ketones with modified Grubbs Metathesis Catalysts: On the Way to a Tandem Process.* M. Renom-Carrasco, P. Gajewski, L. Pignataro, J. G. de Vries, U. Piarulli, C. Gennari, L. Lefort, *Adv. Synth. Catal.* **2016**, DOI: 10.1002/adsc.201500933, *in press*.
- *Chiral (Cyclopentadienone)iron Complexes for the Catalytic Asymmetric Hydrogenation of Ketones.* P. Gajewski, M. Renom-Carrasco, S. Vailati Facchini, L. Pignataro, L. Lefort, J. G. de Vries, R. Ferraccioli, A. Forni, U. Piarulli, C. Gennari, *Eur. J. Org. Chem.* **2015**, 1887–1893.
- *Synthesis of (R)-BINOL-Derived (Cyclopentadienone)iron Complexes and Their Application in the Catalytic Asymmetric Hydrogenation of Ketones.* P. Gajewski, M. Renom-Carrasco, S. Vailati Facchini, L. Pignataro, L. Lefort, J. G. de Vries, R. Ferraccioli, U. Piarulli, C. Gennari, *Eur. J. Org. Chem.* **2015**, 5526–5536.



# Acknowledgements

Now the most difficult part ... Actually I am happy because I am closing a stage, but, on the other hand, there will be people that I will not see as often as I would like to. Everything I can say here will be little, but every one of you knows what I think. So I will try to do it fast, as painless as possible and trying to not forget anybody – fingers crossed.

First of all, my most sincere gratitude to Prof. Gennari, for giving me the opportunity to work in your group and for your interest in the correct development of the projects. This experience allowed me not only to learn all the chemistry previously detailed, but also to meet all the amazing people that will be mentioned next. Prof. de Vries, thanks for sharing your knowledge so easily, in such a close way, and for the great restaurants you showed us in Maastricht. Dr. Lefort, thanks for your enthusiasm in the projects and for the blackboard discussions about chemistry, I really learned A LOT! Not to forget the nice and funny stories during a good dinner or with your IPA (not isopropanol) in hand. Sincerely, I had a great time there! Dr. Pignataro, apart from your infinite patience, that I will always admire, thanks for your jokes and humor, your funny stories, your counsels in chemistry, but above all, for the time you find for every single person in this group, it is extremely helpful. Prof. Piarulli, thanks for your contribution to these projects and for the good mood you always have.

Also a special mention is required for Piotr, soon Dr. Gajewski, with who I shared all these 3 years from the distance. It's been a pleasure to work with you, to discuss about chemistry and a lot of other things, but especially for all the trips, beers and meals together. I am sure we will keep on having more from time to time.

My stage in Milan has been just extraordinary; I would have never imagined finding such a great group of people abroad. Seriously guys, *mi mancherai un sacco* ... Albe, you've been there since the first day, helping me in all imaginable situations and, as you said one day, making sure I was never feeling alone, thanks man, having a person like you there is the best I could have ever wished. Simone, also you are always there, ready to help whenever somebody needs it, even your humor is needed sometimes! Mattia, my young padawan :P, we have spent a lot of hours together, inside and outside the lab, cooking, laughing, drinking... we know each other too well

now. I will miss the deep conversations with you, but also the stupid ones that nobody understood. Giulio, you are really a great guy, always in for everything, always happy, relaxed, easy to speak with, a great travel companion and a great host! And what to say about the five recently *laureati*? Ari, I am very happy to have spent so much time with you traveling, enjoying funny moments and having deep life conversations. Simona, the most gentile and kind person ever, with good gestures for everybody, but also able to party hard and enjoy good moments traveling. Daniele, my catalyst mate, the most clever and tidy guy that there will be in the catalyst lab for a long time, but also great as a person outside the lab. Fra and Rob, this group would have not been complete without you. You are great cooks and even better persons. Sofia, we did not work a lot together, but we had good moments when we did. André, it's been a very positive surprise meeting you, always well predisposed to do things – we still have some football matches pending. Paula, la galleguina, te deixo al mando! Enséñales cómo se hacen las cosas! Y, aunque te chinche un poco, ha sido un placer compartir estos meses contigo. Laura, it's been also a pleasure meeting you, I will never forget the Hungarian dinner. Marco and Cinzia, I hope you will continue the good atmosphere present in this group. Dennis, a serious German from outside, but a clever, funny and nice person inside. Alice, I'd have liked to have more time to know you better, but I am sure you will be an important piece in this group, keep on being so nice. Thanks also to other people that's been around, Iliana, Stefania, Leila...

Paolo, I was very lucky to meet you randomly in the Netherlands, you've been an amazing friend and I am sure we will keep on repeating these parties, beers and trips during the coming years. The first one to visit Emelie, the best Swedish ever, I will miss the good moments with you guys. Here I must include other great people with who I came across during my time in Milan: David, Ida, Nelleke, Babak and many others, thanks to all of you.

The time spent in Maastricht would not have been the same without the people from there. Mike, the moments in the lab were always a lot easier and funnier with you there, but I must say I learnt a lot from you, and that will stay always with me. Elena, you've been helping me a lot since the first day we met and you continued even now via Skype, I have no words to say how much I appreciate that. Joanne and Christine, you have been fantastic colleagues during the time we worked together, I learned also a lot from you. I would like to thank also the rest of people I met at DSM: Gerard, Lavinia, Paul, Ruben, Michèle, Andre, Alejandro, Karin and Harold (thanks for all the times you took me with you to climb). Not to forget all the people from MaasSAC, you were my disconnection zone, thanks.

To all of you, who live abroad, I am sure we will meet in other places and different situations. Good luck with all your future projects and goals. This experience would have never been the same without you all.

Em veig en la necessitat de fer extensible aquest agraïment als que van ser els meus jefes a la UAB: Ramón i Félix, gràcies per haver entès que això podia ser una gran oportunitat per mi, tot va ser molt més fàcil amb el vostre suport. També donar gràcies a en Jordi Cervelló, en Pau Bayón i



en Pere de March per engrescar-me i recolzar-me en aquesta decisió que no va ser gens fàcil, però que ha resultat ser un gran regal.

I evidentment, el més profund agraïment als que des dels laboratoris 453 i 457 heu estat sempre allà. Després del regal que em vau fer el dia que vaig marxar em sento en deute, i ni amb el que escrigués aquí podria pagar-ho, però espero poder anar-vos-ho tornant mica en mica amb els anys que ens queden per davant. Gràcies per els mails, Skypes, missatges i trobades durant aquests anys que he estat fora, gràcies de veritat: Marta, Nurie, Cris, Arnauet, Bea, Gladis, Toni, Rosa, Mireia, Laura, Guille, Silvia, Xin, Yuan, Meri, Roser, Javi, Èric, Fran, Adrià... ja tinc ganes de tornar a estar per allà amb vosaltres!

També gràcies a tots aquells que han estat amb mi tots aquests anys, siguin els de música, els de Terrassa, els del poble, els de l'institut o els que coneixo des que som petits i em segueixen venint a visitar allà on sóc. I per descomptat a la meva família, als que estan encara aquí i als que m'hagués agradat que em veiessin acabant el meu doctorat, gràcies.

Un dels agraïments especials va per la Núria, crec que t'ho he dit milers de vegades, però res d'això hagués estat igual sense tu. Ets la persona que em fa feliç cada dia, amb qui comparteixo el que em passa a diari, però que a sobre ets capaç de sacrificar el teu temps per venir allà on sóc i fer-te amic dels meus amics i descobrir món amb mi. No podria haver escollit una companya de viatge millor per tot el que ens queda per davant. Gràcies de tot cor.

El segon agraïment especial i últim és evidentment per als meus pares. Sou els principals responsables de que sigui qui sóc, d'haver conegut tota aquesta gent i d'haver-me fet ser la persona més feliç d'aquest món. Sempre m'heu donat suport en tot el que he volgut fer, m'heu ajudat en tot i més i sempre amb un somriure a la cara. No podria haver demanat un pares millors, intentaré anar-vos tornant tot el que heu fet per mi. No tinc paraules per agrair-vos aquests 27 anys de vida.

Moltes gràcies a tots! Thank you all! Grazie a tutti!





